Pratt & Whitney/Boeing Engine Validation of Noise Reduction Concepts
Final Report for NASA Contract NAS3-97144, Phase 1

Douglas C. Mathews and Larry A. Bock
United Technologies Corporation, Pratt & Whitney, East Hartford, Connecticut

Gerald W. Bielak, R.P. Dougherty, John W. Premo, and Dan F. Scharpf
Boeing Commercial Airplane Group, Seattle, Washington

Jia Yu
Goodrich Aerostructures, Chula Vista, California

NASA STI Program . . . in Profile

Since its founding, NASA has been dedicated to the advancement of aeronautics and space science. The NASA Scientific and Technical Information (STI) program plays a key part in helping NASA maintain this important role.

The NASA STI Program operates under the auspices of the Agency Chief Information Officer. It collects, organizes, provides for archiving, and disseminates NASA's STI. The NASA STI program provides access to the NASA Aeronautics and Space Database and its public interface, the NASA Technical Reports Server, thus providing one of the largest collections of aeronautical and space science STI in the world. Results are published in both non-NASA channels and by NASA in the NASA STI Report Series, which includes the following report types:

- TECHNICAL PUBLICATION. Reports of completed research or a major significant phase of research that present the results of NASA programs and include extensive data or theoretical analysis. Includes compilations of significant scientific and technical data and information deemed to be of continuing reference value. NASA counterpart of peer-reviewed formal professional papers but has less stringent limitations on manuscript length and extent of graphic presentations.

- TECHNICAL MEMORANDUM. Scientific and technical findings that are preliminary or of specialized interest, e.g., quick release reports, working papers, and bibliographies that contain minimal annotation. Does not contain extensive analysis.

- CONTRACTOR REPORT. Scientific and technical findings by NASA-sponsored contractors and grantees.

- CONFERENCE PUBLICATION. Collected papers from scientific and technical conferences, symposia, seminars, or other meetings sponsored or cosponsored by NASA.

- SPECIAL PUBLICATION. Scientific, technical, or historical information from NASA programs, projects, and missions, often concerned with subjects having substantial public interest.

- TECHNICAL TRANSLATION. English-language translations of foreign scientific and technical material pertinent to NASA's mission.

Specialized services also include creating custom thesauri, building customized databases, organizing and publishing research results.

For more information about the NASA STI program, see the following:

- Access the NASA STI program home page at *http://www.sti.nasa.gov*

- E-mail your question to *help@sti.nasa.gov*

- Fax your question to the NASA STI Information Desk at 443–757–5803

- Phone the NASA STI Information Desk at 443–757–5802

- Write to:
  STI Information Desk
  NASA Center for AeroSpace Information
  7115 Standard Drive
  Hanover, MD 21076–1320

Pratt & Whitney/Boeing Engine Validation of Noise Reduction Concepts
Final Report for NASA Contract NAS3-97144, Phase 1

Douglas C. Mathews and Larry A. Bock
United Technologies Corporation, Pratt & Whitney, East Hartford, Connecticut

Gerald W. Bielak, R.P. Dougherty, John W. Premo, and Dan F. Scharpf
Boeing Commercial Airplane Group, Seattle, Washington

Jia Yu
Goodrich Aerostructures, Chula Vista, California

National Aeronautics and
Space Administration

Glenn Research Center
Cleveland, Ohio 44135

Acknowledgments

Level of Review: This material has been technically reviewed by expert reviewer(s).

Available from

Forward

This report presents results of the work completed in Phase 1 of the Engine Validation of Noise Reduction Concepts (EVNRC) contract. The purpose of the program was to validate, through engine testing, advanced noise reduction concepts aimed at reducing engine noise up to 6 EPNdB and improving nacelle suppression by 50 percent relative to 1992 technology. Phase 2 of the program is currently near completion and upon its conclusion will be summarized in a separate report.

Summary

The EVNRC program was authorized by NASA in August 1997 to validate, through engine testing, noise reduction concepts and technologies that have evolved during the AST program. A team comprised of members from NASA, Pratt & Whitney, Boeing and Goodrich Aerostructures (formerly Rohr) participated in bringing together the new hardware, software, test equipment and support personnel necessary to complete Phase I of these tests on a PW 4098 engine, the latest and largest of P&W's 4000 series engines. Testing was conducted at P&W's Florida Test Facility on outdoor stand C-11 which is configured and instrumented to FAA noise measurement and data quality standards.

The major noise reduction concepts tested in this phase consisted of:

1. A new Boeing inlet featuring a scarfed design where the lower lip (keel) extends forward of the upper lip (crown) so that noise directivity is changed. This inlet also incorporates advanced triple layer liner treatment covering the entire internal surface from the mating flange of the engine's front fan case forward to the inlet highlight without any hardwall splices and patches.
2. Advanced noise liner treatment developed by Goodrich for the engine's front fan case. The treatment consisted of a 2-in. deep DDOF hybrid linear liner with a removable laser drilled polyurethane film bonded to the perforated face sheet. Removing the polyurethane allowed testing of a lower acoustical resistance liner than with the polyurethane installed.
3. By applying tape over various areas of the noise treatment, hardwall engine surfaces were simulated for testing purposes.

The major results of the testing were:

1. The new Boeing inlet with the advanced treatment in the front fan case showed a 2 to 4 EPNdB reduction in inlet fan noise at approach and cutback powers, compared to the production configuration. Approximately 80 percent dB nacelle suppression improvement was observed at approach power and 50 percent dB suppression improvement at cutback power.
2. A significant blade passing frequency (BPF) tone was measured with the scarf inlet, preventing an additional 1 EPNdB in noise reduction.
3. The BPF tone was found to be associated with the Boeing scarf inlet and was due to a flow separation problem at the crown location. This flow separation caused vortices to be shed into the fan. CFD calculations indicate that this separated flow will be eliminated with forward motion.
4. Noise treatment splices (joints) near the fan can produce large noise penalties of up to 4 EPNdB depending on the number and width of the splices.
5. Boeing's RDIFF predictions for tone and broadband lining attenuation generally were within 15 percent of the measured data in the direct radiation field but only within about 50 percent in the diffraction dominated field (aft of 70°). The very high frequency (8 to 10 kHz) attenuation by the lining was not accurately predicted.
6. Boeing's phased array of 198 Kulite microphones mounted in the Inflow Control Device (ICD), effectively showed that at approach power the inlet noise of the PW4098 has a strong contribution from the low compressor. Fan blade passage tones and broadband fan noise are also important. The inlet lip lining was very effective in attenuating buzzsaw noise at low spinning orders.

Contents

Pratt & Whitney/Boeing Engine Validation of Noise Reduction Concepts
Final Report for NASA Contract NAS3-97144, Phase 1

Douglas C. Mathews and Larry A. Bock
United Technologies Corporation
Pratt & Whitney
East Hartford, Connecticut 06108

Gerald W. Bielak, R.P. Dougherty, John W. Premo, and Dan F. Scharpf
Boeing Commercial Airplane Group
Seattle, Washington 98124

Jia Yu
Goodrich Aerostructures
Chula Vista, California 91910

1.0   Introduction

1.1   Background

Major airports in the world's air transportation systems face a serious problem in providing greater capacity to meet the ever increasing demands of air travel. This problem could be relieved if airports are allowed to increase their operating time, now restricted by curfews and by relaxing present limits on takeoffs and landings. The key operational issue in extending the present curfews is noise.

In response to these increasing restrictive noise regulations, NASA has launched a program to validate through engine testing, noise reduction concepts and technologies that have evolved from the Advanced Subsonic Technologies (AST) Noise Reduction Program. The goal of this AST program was to develop and validate technology that reduces engine noise and improves nacelle suppression effectiveness relative to 1992 technology. Contract NAS3-97144 titled "Engine Validation of Noise Reduction Concepts" (EVNRC) was awarded to P&W on August 12, 1997 to conduct full scale noise reduction tests in two Phases on a PW4098 engine. The following Section 1.2 provides a brief description of the overall program. The remainder of this report provides a detailed documentation of Phase I of the program.

1.2   EVNRC Program Description

The EVNRC program is a highly teamed effort involving NASA, Pratt & Whitney (P&W), Boeing, and Goodrich (formerly Rohr). The program duration was from August 1997 through September 2001 and consisted of two phases. The two phases correspond to separate noise test programs in late 1998, and mid-2001 and were conducted with P&W's latest and largest turbofan engine, the PW4098. This engine, which powers growth versions of Boeing's 777 aircraft, has a 112.9-in. diameter fan and generates a rated thrust of 98,000 lb. The tests were planned to validate in full-scale a number of advanced noise reduction concepts and to demonstrate compliance with the engine noise reduction goals and nacelle aeroacoustic goals of the Advanced Subsonic Technology Program.

The program encompasses a very wide range of noise reduction technology such as:

- Advanced noise reduction treatment in a novel Boeing inlet
- Advanced noise reduction treatment in P&W's engine cases
- Low noise, cut on fan exit guide vanes
- Primary jet nozzle with acoustic lining to attenuate turbine noise

The potential noise reduction from the technologies tested in this program was estimated to be in the 2 to 4 EPNdB range at each condition, relative to the baseline PW4098 engine. Relative to 1992 technology, noise reductions of up to 6 EPNdB in engine noise were expected, and nacelle suppression was expected to be improved by at least 50 percent.

This program offers high potential for technology transfer to commercial product lines. Reduced noise will be an internationally competitive issue, and this program is focused on technologies with a high probability of cost effective transition into the marketplace for new applications, as well as for retrofit or incorporation into today's production engines. Specific and direct beneficiaries of the technology demonstrated in this proposed program will be the GP7000, the new engine being developed jointly by a P&W/General Electric (GE) Engine Alliance for installation into Boeing's nacelle for the new Boeing 747MD (Major Derivative) stretched aircraft. The program output will also be applicable to the remainder of Boeing's nacelle product line, to the entire PW4000 engine family, to P&W's new PW6000 mid-thrust engine, and to P&W's future Advance Ducted Propulsor (ADP) family of engines, as well as other manufacturer product lines.

The program cost has been reduced because of the hardware sharing of team members. Boeing supplied the novel low noise inlet, valued at $1.5 million for the program, at no cost. Pratt & Whitney supplied the PW4098 engine and aft nacelle. Noise tests were conducted in conjunction with other planned P&W engine tests to reduce cost. Use of the P&W world-class outdoor C-11 test facilities in Florida, configured and instrumented to FAA noise measurement and data quality standards, also reduced costs.

Phase I has been completed and the purpose of this report is to document the content and results of that Phase. Phase 2 tests have been completed and data analysis is near completion. Results from Phase 2 will be reported separately.

1.2.1 Phase 1

The work of Phase I was broken into seven subtasks, described as follows:

1.2.1.1 Subtask 1.1.1—Concept Selection and Acoustic Design

The noise concepts that were defined by P&W and Boeing in the contract proposal were finalized in this subtask. In addition Goodrich was chosen as the supplier for the sound treatment liner material. The noise concepts selected were:

Boeing's Ideal Inlet:
- An extended lower lip (scarfing) for noise shielding and noise redirection.
- Advanced liner design and construction that features triple layer broadband acoustic lining with minimum splice widths.
- Treatment that extends upstream beyond the inlet throat and highlight.
- Circumferentially uniform liner close to the fan.
- No probes and associated hardwalled patches.

P&W's Engine Fan Case Treatment:
- A modified forward fan containment case that allowed testing of the current production liner, a hardwalled liner, and the new advanced linear double layer liner supplied by Goodrich, with only two circumferential segments separated by narrow hard wall splices.
- A design to minimize both community and interior buzzsaw noises.

These concepts are described more completely in Section 2.0 with diagrams and pictures.

1.2.1.2 Subtask 1.1.2—Mechanical Design

This subtask provided for the development of working drawings suitable for the fabrication of the modified engine fan case hardware. Detailed design work for the Boeing inlet was completed prior to the contract.

1.2.1.3 Subtask 1.1.3—Fabrication

The fabrication subtask funded construction of the modified engine fan case and two spoolpieces, one spoolpiece incorporating the production Bill of Material (BOM) liner material and the other the advanced Goodrich liner material.

1.2.1.4 Subtask 1.1.4—Boeing Subcontract

This subtask provided for Boeing's participation to provide overall engineering support and consultation for the Phase I program including concept selection, test configuration selection, instrumentation system installation and operation during testing, data analysis, test results and reporting.

1.2.1.5 Subtask 1.1.5—Testing

The testing subtask covered costs associated with full scale PW4098 engine testing at P&W's C-11 Stand Acoustic Test Facility at West Palm Beach, Florida. Test costs were reduced by combining (piggy-backing) the NASA funded tests with P&W funded PW4098 FAA Noise Certification Tests.

1.2.1.6 Subtask 1.1.6—Data Analysis

This subtask provided for the analysis of data collected during the testing subtask.

1.2.1.7 Subtask 1.1.7—Documentation

The parts of program documentation including preliminary test plans, design reviews with NASA, final test plans, design reports, data reviews with NASA, and final reports are covered by this subtask.

1.2.2 Phase 2

The work of Phase 2 was also broken into the same seven subtasks as described for Phase 1. The concepts chosen for testing in Phase 2 consisted of the Phase 1 concepts plus the following:

- Boeing's scarf inlet fitted with a bellmouth lip instead of a flight lip.
- A cut on, 28 vane fan exit guide vane system.
- Fan blade number increased from 22 to 24 blades.
- Acoustically treated primary jet exhaust nozzle and plug.

2.0 Noise Reduction Concepts and Hardware

2.1 Boeing Inlet

2.1.1 Scarf Inlet Design Objectives

Figure 1 summarizes the design objectives for the PW4098 demonstrator scarf inlet. The results of an earlier model scale scarf inlet test conducted at Boeing led to the decision to target a 15° scarf angle. It was desired to try to maximize the noise benefit of the scarf inlet by maximizing the scarf angle and at the same time push the comfort zone of the aerodynamics community while retaining a reasonable probability of meeting their requirements when tested. It was thought that a 15° scarf would meet this objective. Propulsion aerodynamics experts were concerned about inlet recovery, fan face flow distortion and high angle of attack separation. External aerodynamics for cruise performance was also an issue because the propulsion concerns affected the lip design on the external cowl as well as internally. For the design

- Scarf angle 15° for noise reduction.
- Acceptable inlet aerodynamics.
- Use flight lip-lining, radiation, aero design.
- Acoustic lining from highlight to fan face.
- Minimum splices and hardwall patches.
- Use advanced acoustic lining--triple layer.
- Advanced fan case lining.

Figure 1.—Demonstrator scarf design objectives.

study, the engine outer cowl and internal fan case geometry were fixed so that the scarf geometry would have to fare into these lines in an aerodynamically satisfactory manner.

It was desired to use a flight lip on the inlet for the static test rather than a bellmouth lip that is usually used for static engine noise testing. The purpose of the bellmouth lip is to match the internal inlet flow more closely to flight by reducing the high lip wall flow Mach number that occurs with a flight lip in static test. The lip design is a major aerodynamics issue with the scarf inlet and is strongly interdependent on the inlet length and scarf angle. Boeing wanted to insure that these interdependencies were considered for this design as they would be for a product design. Also, it is known that the lip shape affects the sound radiation directivity. Since the purpose of the scarf shape is to change the radiation directivity a bellmouth lip could confound the interpretation of the test results. Unfortunately the wall Mach number increase associated with the flight lip in the static condition may also affect the radiation. It was felt that this would be a secondary affect at the approach engine power condition but there was concern about the high power conditions.

A major acoustic objective was to acoustically treat the entire internal surface of the inlet and fan case from the fan rub strip to the inlet highlight without any hardwall splices and patches. Today's production inlets have no acoustic treatment on 30 to 50 percent of the internal inlet surface because of de-icing, concerns about boundary layer growth near the inlet throat, panel seams and structural reinforcement. Fully treating all surfaces of the scarf inlet would allow these hardwall surfaces to be simulated by taping over the lining to measure their acoustic importance. In addition it was decided to use advanced concept triple layer acoustic linings within the inlet. It was realized that the surface curvatures within the inlet would make building a triple layer lining with minimal splices a challenge but Boeing's Wichita manufacturing personnel believed it could be done for a static test inlet.

2.1.2   Internal Aerodynamics Design

2.1.2.1   Lines

Scarf inlet contours along the crown and keel are compared with the PW4098 production inlet contours in Figure 2. Two scarf inlet designs are represented. One is for the 15° objective and the second is a biplanar design with a 15° scarf on the bottom of the inlet and a smaller 12° scarf on the top, for a net 13° scarf angle. The biplanar scarf design was necessitated by the results of a Navier Stokes computer internal flow simulation of the 15° design. The Navier Stokes (NS) calculations were run for final confirmation of the inlet design iterations which were done using potential flow codes for max engine power inlet mass flows.
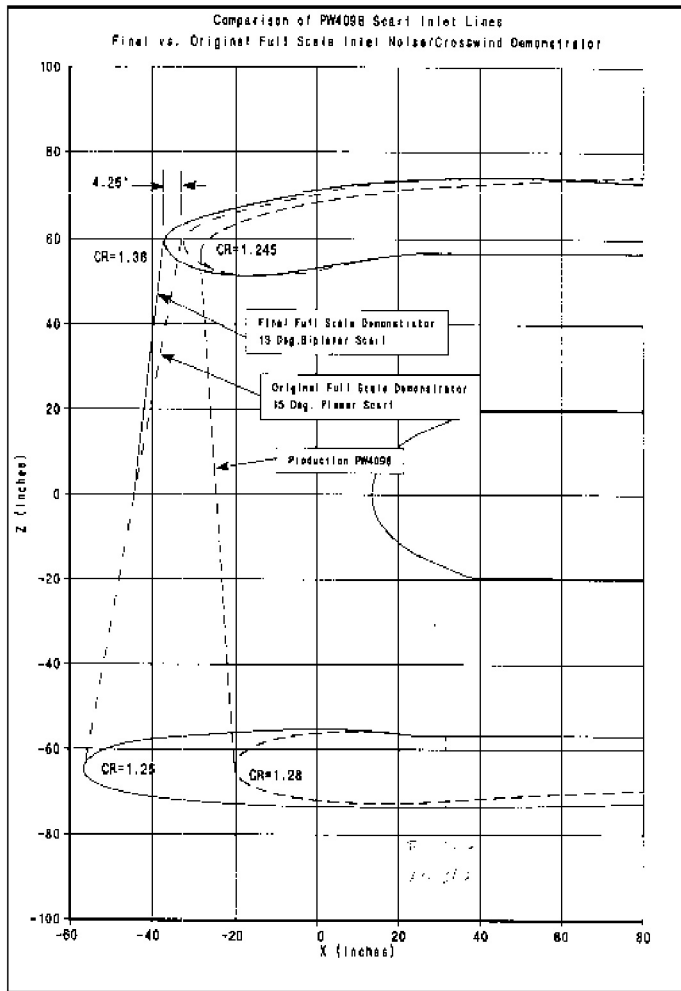
Figure 2.—Comparison of production and scarf inlet contours.

2.1.2.2 Distortion

The Navier Stokes (NS) results for the three inlets represented in Figure 2 are shown in Figure 3. For max power static operation, the Navier Stokes calculation predicted that the 15° scarf inlet would result in flow separation near the inlet crown and an associated distortion at the fan face. While it is expected that the separation would clean up with forward motion, it was determined that it may reduce the useful life of the fan blades given the amount of time the engines are run at high power with the airplane at rest. In addition, a calculation of the acoustic effect of the distortion concluded that it would generate a high fan tone noise level. The biplanar concept was therefore invented as a simple way to maintain much of the tooling that had been built by the time the NS results were completed and to solve the distortion problem.

Figure 3 shows that the NS calculation for the biplanar scarf predicted a much smaller distortion at the fan face at max power. The minimal distortion predicted at high engine power for the biplanar scarf led to the expectation that the distortion would totally disappear at approach engine power and perhaps cutback engine power as well so that distortion related fan tone generation would not be a serious problem. NS simulations for these engine powers were not done because of the high cost of these calculations.

Production inlet	15° scarf	13° biplanar scarf
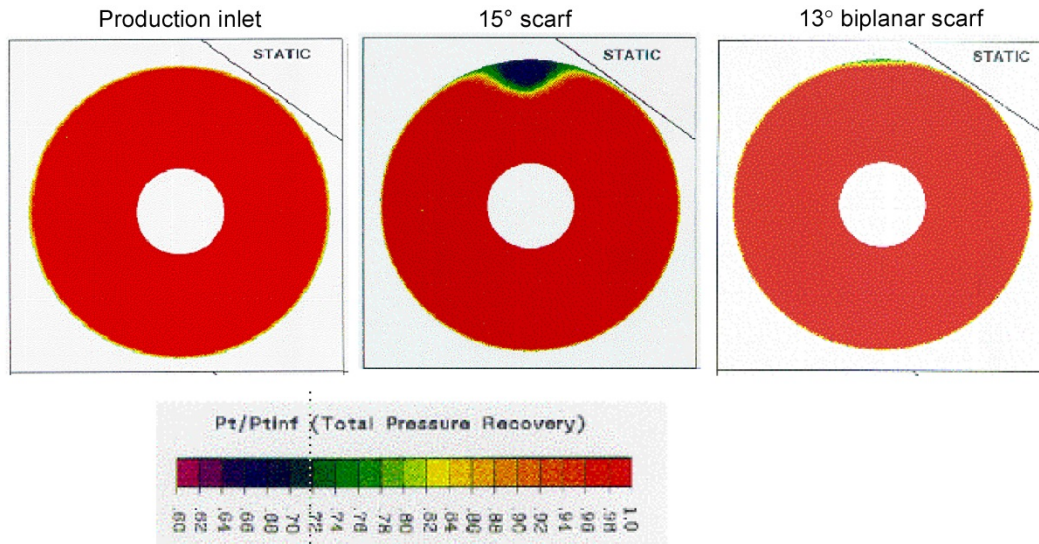
Figure 3.—Navier Stokes simulation—fan face distortion, PW4098, max power.

2.1.2.3   Mach Number Contours and Boundary Layer Thickness

Wall Mach number contours were calculated at approach, cutback and takeoff engine powers with a 3D potential flow code for the 13° biplanar scarf. The lower power calculations were not part of the design process and were not done until after manufacturing of the inlet had begun. The calculations were done for the crown (0°), mid line (90°) and keel (180°) of the inlet. For comparison the contours were calculated for both static operation (noise test situation) and flight. The results of these calculations are shown in Figure 4. The most striking feature of these results is the difference between static and flight. The "sink" flow turning around the inlet lip at the static condition results in very high Mach numbers near the inlet lip. The entire lip flow is supersonic at takeoff and the crown is supersonic at cutback. In flight this turning is reduced significantly and the Mach numbers are much lower. The supersonic flow in the inlet was of concern since it will have an effect on the propagation of noise and not be representative of flight. It was felt that the higher subsonic speed flow would not be a significant problem at the approach power condition but cutback and takeoff were of concern.

Figure 5 shows estimates of the fan face boundary layer thickness at the same azimuth angles for which the axial Mach number contours shown above were calculated. These calculations were done with a 3D boundary layer code. It is seen that the static boundary layer thickness at the crown, in particular, is much larger than for the flight condition. The thickness increase also increases with engine power. The azimuth spatial definition of the boundary layer thickening at the crown was not determined.
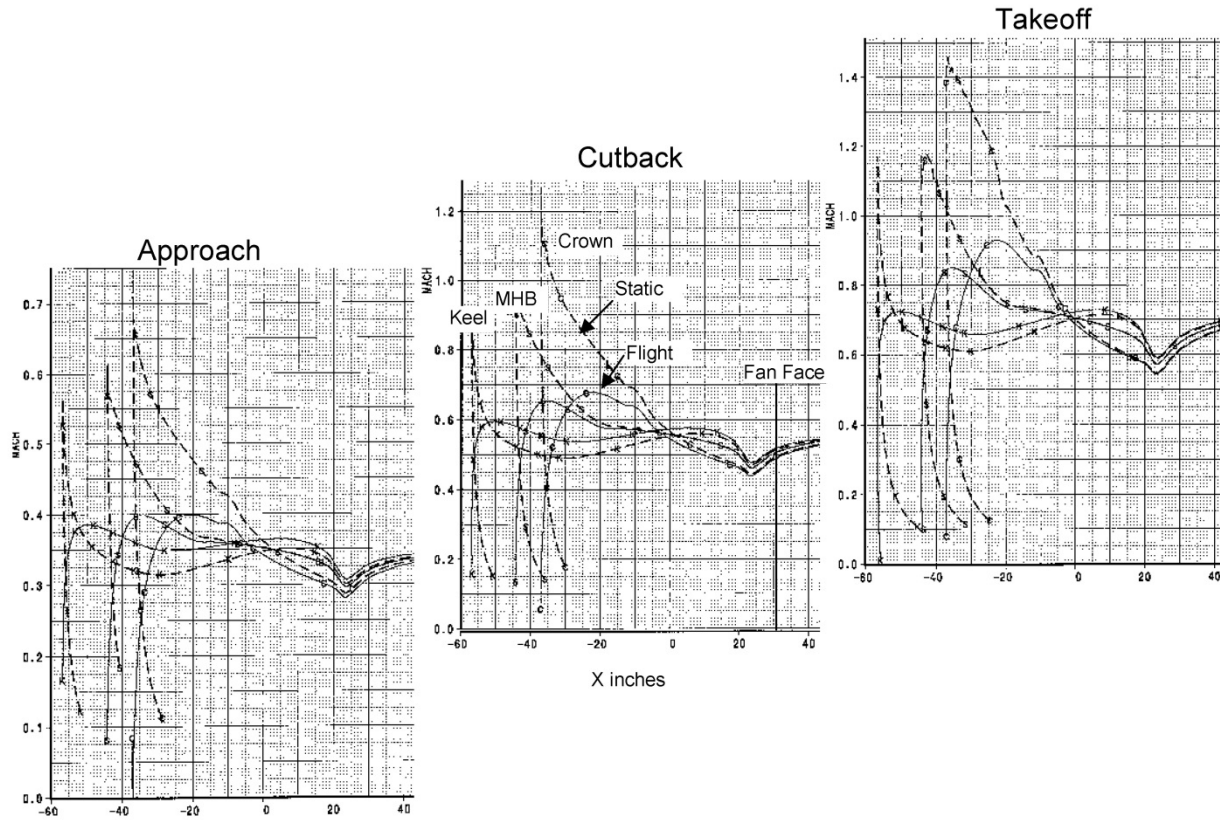
Figure 4.—Wall Mach number profiles for PW4098 demonstrator scarf inlet.
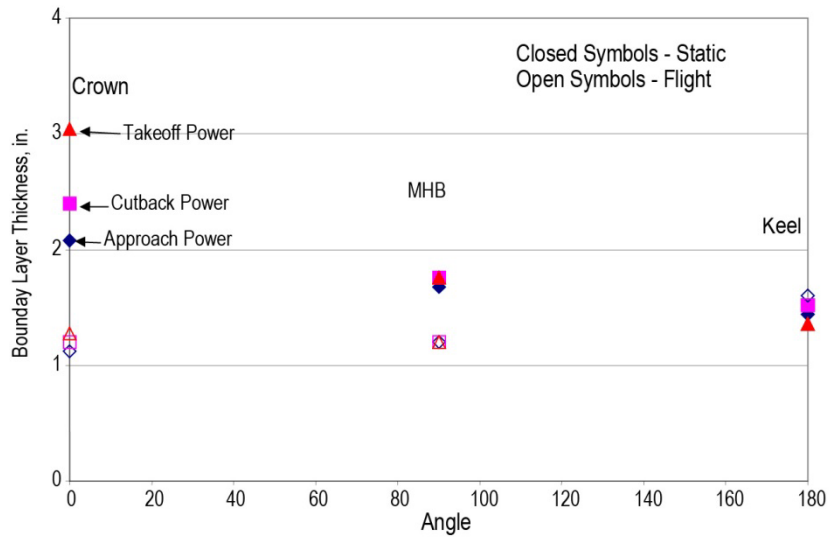
Figure 5.—Fan face boundary layer thickness, scarf inlet, static versus flight.

2.1.3　Scarf Inlet Pressurization Test

The inlet pressurization test was used to evaluate the potential sources of BPF tone due to leakage of air through the inlet liner. Covering the access holes with aluminum plates and applying RTV on all of the seams sealed the rear bulkhead of the inlet. The inlet was filled with shop air to a pressure of 2 psig and inspected for leaks. Small leaks were found in the bulkhead, and in the inlet where the inlet-probe plug was installed. Air passage through these leaks was barely perceptible by touch, and hence was not considered to be a contributor to the generation of the BPF tone.

2.1.4　Contour Confirmation

2.1.4.1　Lip Contour

Measurements were made to verify the lip contour of the inlet using templates placed at the crown, ±90° from the crown and at the keel. Measurements were made from the inlet highlight back 27 in. into the inlet every 0.5 in. Nearly 90 percent of the measurements were within 40 mil of the specified contour with a maximum deviation of 85 mil. This was considered to be within necessary tolerance.

2.1.4.2　"A" Flange Contour

An inlet template (Figure 6) was used to verify the circular uniformity of the inlet at the attach flange. The template was used with a "banana gauge" in order to quantify the deviations. Since the template only covered 90° of the inlet circumference, it was moved around the inlet at 45° intervals, while the gap between the template and inlet wall was measured every 5° relative to the template center. The template was designed with "feet" at each end in order to provide a gap between the template and the inlet. This also created a different reference for each measurement location. Because of this, no absolute measurement of the circumferential variation was possible by this technique.

Figure 7 shows the measurements from the template for the scarf inlet. Measurements were taken with the inlet de-pressurized and on the ground. By following a particular line style (solid or dashed) the variation can be seen as though the template were placed end-to end with no overlap. Differences between the solid and dashed curves provide some indication as to the variations in gap due to the different reference heights for each template location. The average measurement at each angular position is shown in Figure 8. A regular or periodic variation in inlet radius was not evident from these measurements.
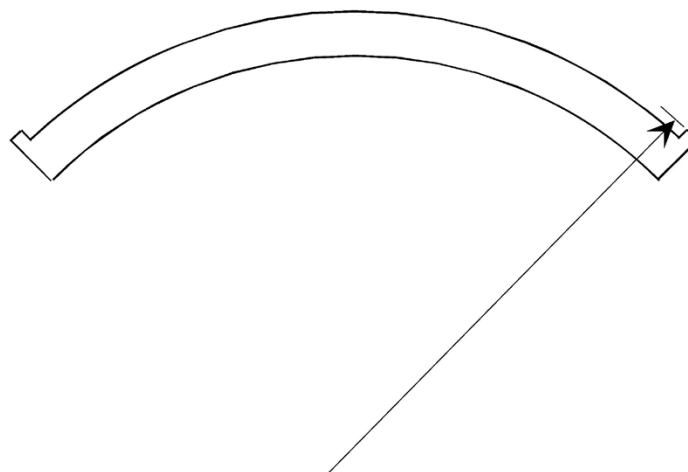
Figure 6.—Inlet template used to measure circumferential uniformity at the attach flange.
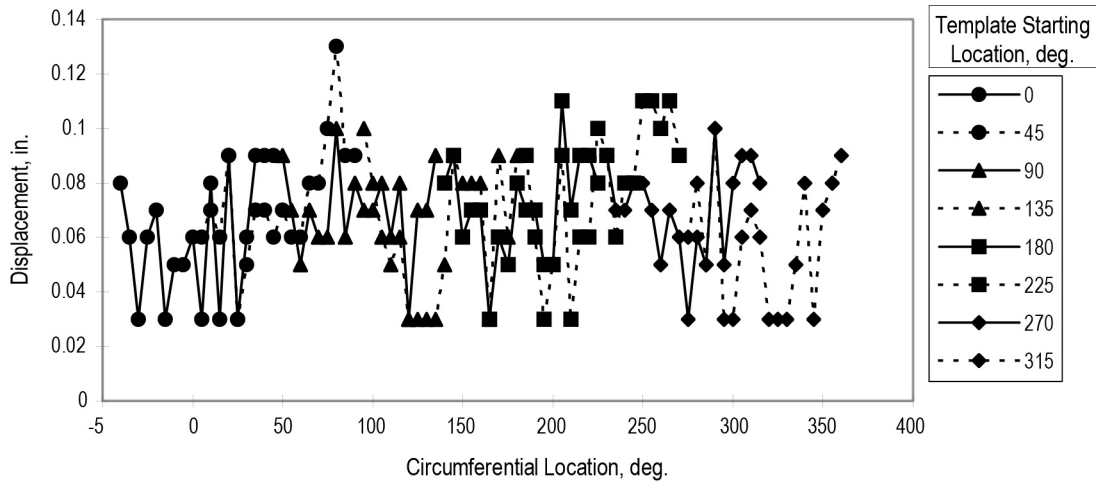
Figure 7.—Measured variations of the gap between the template and the scarf inlet at the attach flange.
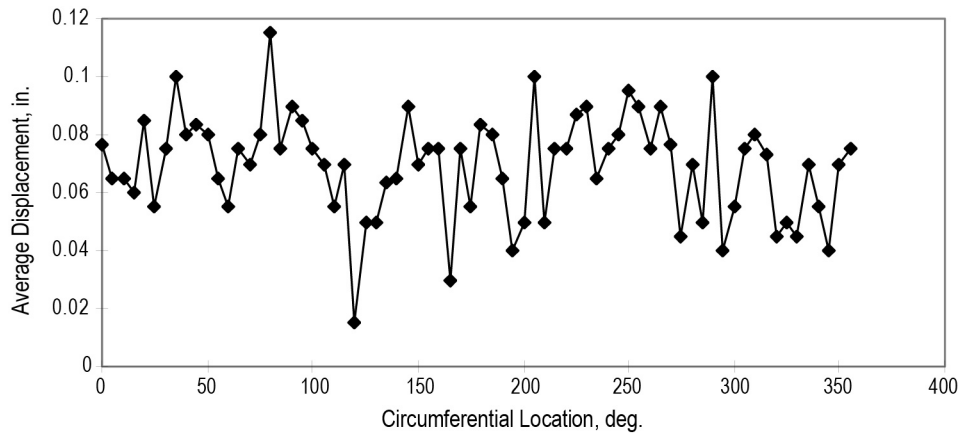
Figure 8.—Averaged variations of the gap between the template and the scarf inlet at the attach flange.

A Fourier decomposition of the average, template-measured displacements is shown in Figure 9. The mode numbers represent physical distortions of the inlet with a circumferential period equal to the mode number; e.g., an $n = 4$ mode implies that a four-lobe distortion of the circumference exists around the inlet. This type of physical distortion would create local steady distortions in the inlet boundary layer that could interact with the fan blades causing a BPF tone. The effect of this physical distortion may also be amplified when the inlet is attached to the fan case if the fan case is also not perfectly uniform. Figure 9 suggests that there are no dominant distortion modes.

Since relative measurements were used instead of absolute measurements, a numerical study was conducted to determine the error associated with using relative measurements to calculate distortion orders. Figure 10 shows the mode amplitudes for a 100-point pseudo-random distortion, which was analyzed in a manner similar to the physical measurements. Figure 10 shows the resulting mean and 95 percent confidence error for this study. The conclusion is that using relative measurements allows an accurate assessment of the higher distortion orders, but large errors exist at the lower distortion orders.
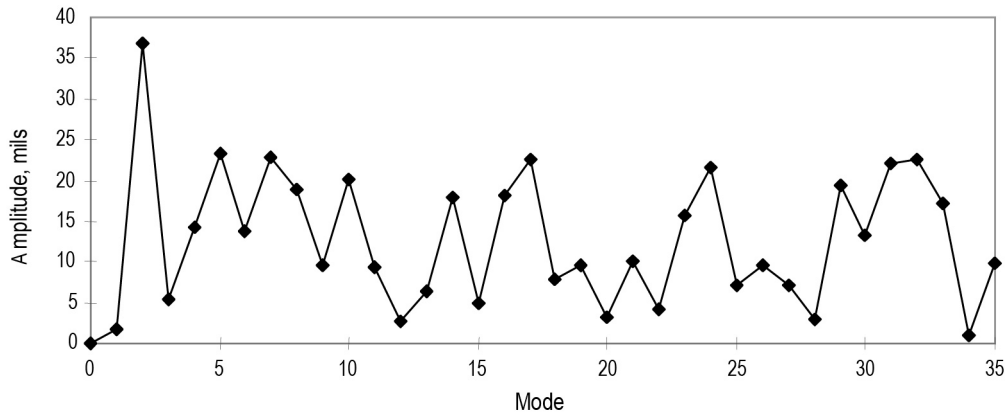
Figure 9.—Fourier decomposition of the averaged variations of the gap between the template and the scarf inlet at the attach flange.
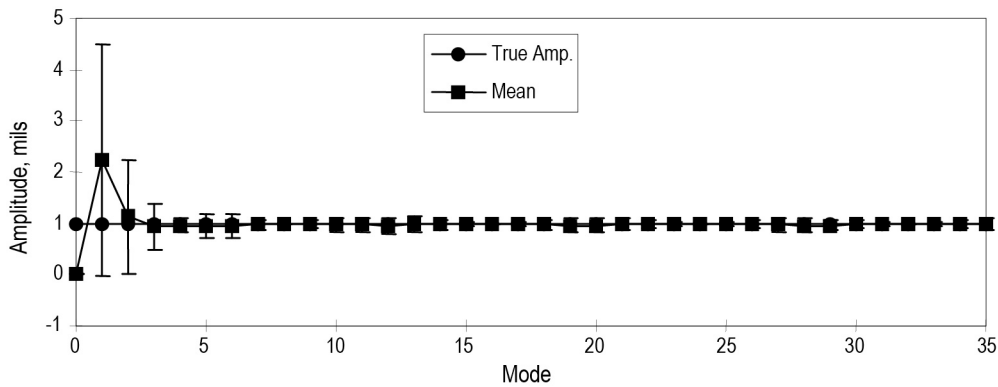
Figure 10.—Numerical experiment showing error associated with using relative measurements.

When the inlet was mounted on the production fan case on the engine, measurements were made of the fit of the inlet to the case. The size of the internal wall step from the inlet to the fan case was measured at 5° intervals around the entire inlet. The results of these measurements are shown in Figure 11(a), positive indicating a downward step from the inlet to the fan case. A step of approximately 0.1 in was found on the top part of the inlet. This step was smoothed to some degree at the test site with silicon adhesive. The Fourier components of the contour variations are also shown in Figure 11(b). A flow distortion associated with this shape variation would not be a significant cause of fan tone noise since the maximum modal amplitudes are in the lowest order components. Also the 0.1 in step is small compared to the 2 to 3 in. boundary layer thickness in the crown region so it is probably insignificant for broadband noise generation as well.
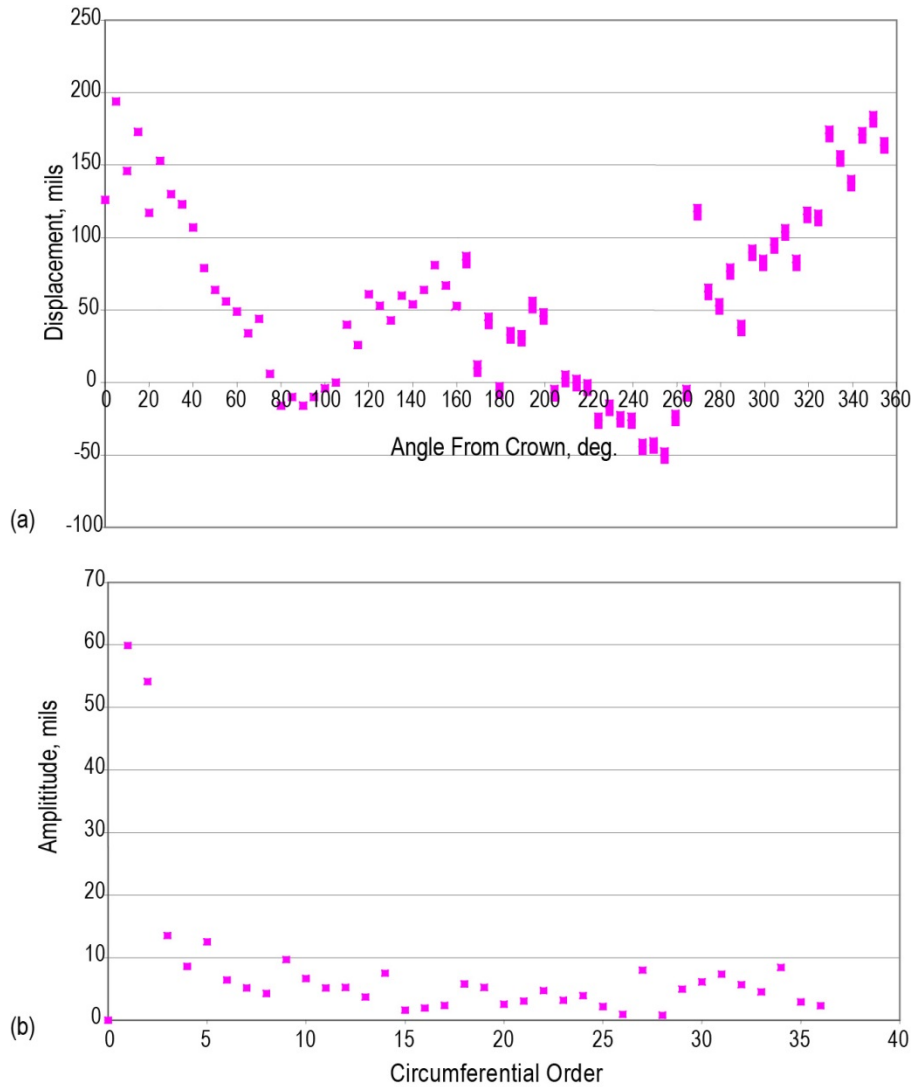
Figure 11.—(a) Displacement of inlet at "A" flange relative to engine fan
case, and (b) Scarf "A" flange displacement spectrum

2.1.5   Acoustic Linings

Three different acoustic lining designs were built for the scarf inlet and two designs were used for the advanced forward fan spool. Figure 12 shows schematics of these designs and where in the inlet they were used. Triple layer liners were used for the inlet and double layer liners used for the fan case spool. (Liner information for the P&W/Goodrich fan case is discussed in more detail in Section 2.3.) Liners with smaller open area face sheets were used in the regions of the inlet with higher Mach numbers. This was done to reduce "self-noise" generated as the high-speed air passed over the lining orifices. The diffuser lining was designed to an impedance of (2.6, –0.5) at the approach condition. Figure 13 shows the predicted acoustic impedances of the inlet liners at the approach and cutback conditions. The high grazing flow Mach numbers at the lip, together with the smaller open area of the lip liner face sheet, results in the relatively high acoustic resistances predicted for the lip liner and, to a lesser extent, for the forward

diffuser liner. The impedances at cutback engine power were a fall out of the designs of the liners that were optimized for the approach condition. The design target impedances for the approach and cutback conditions are shown for reference. A study was done optimizing the liners for the cutback condition with the approach power impedance then being a fall out. These liners were significantly inferior to the liners designed for approach when both conditions are considered.

Figure 14 shows the predicted impedances of the advanced fan case spool liners which are discussed in more detail in Section 2.3. Two sets of impedances are shown for each engine power condition. The higher resistances were obtained by placing a layer of 7.2 percent open area perforated polyurethane tape over the 32 percent open area punched aluminum face sheet of the liner. The tape is approximately 15 mil thick with 5 mil diameter holes. The spool piece liner was designed to have only two hardwall 0.1 in. splices, one at the top and one at the bottom of the spool. In actuality the splices were about 0.375 in. wide.
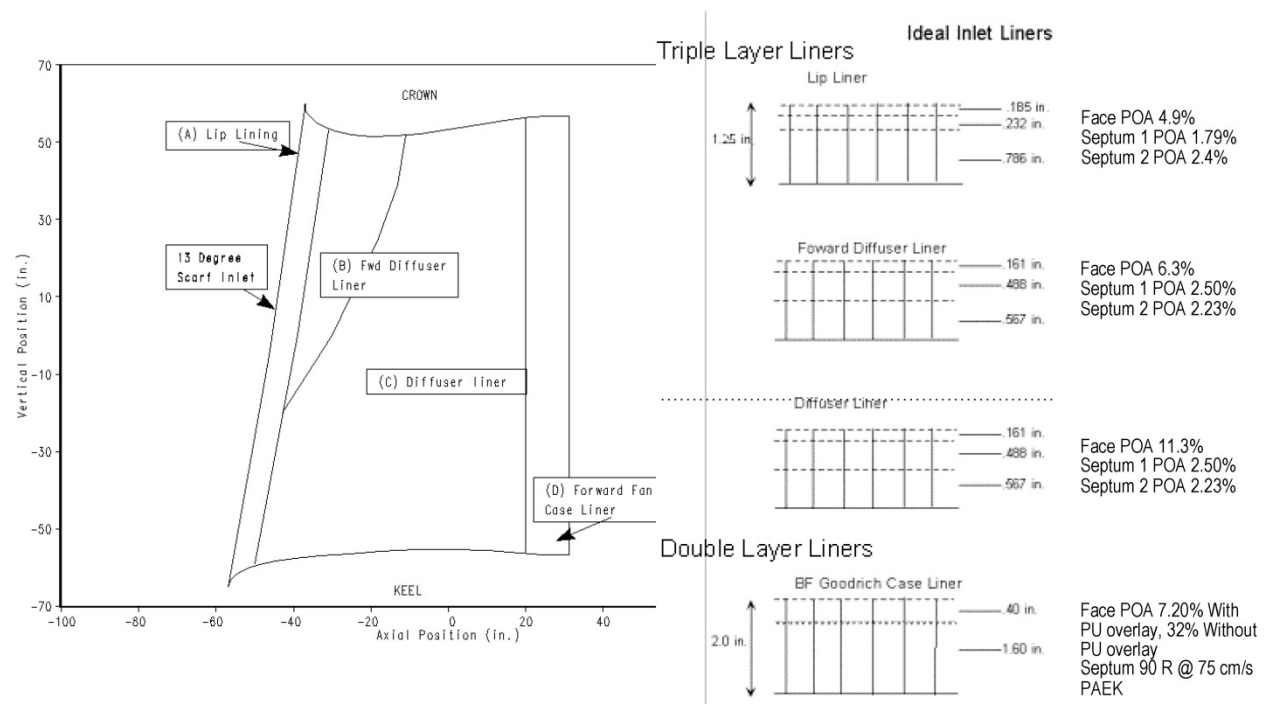
Figure 12.—Acoustic lining details.
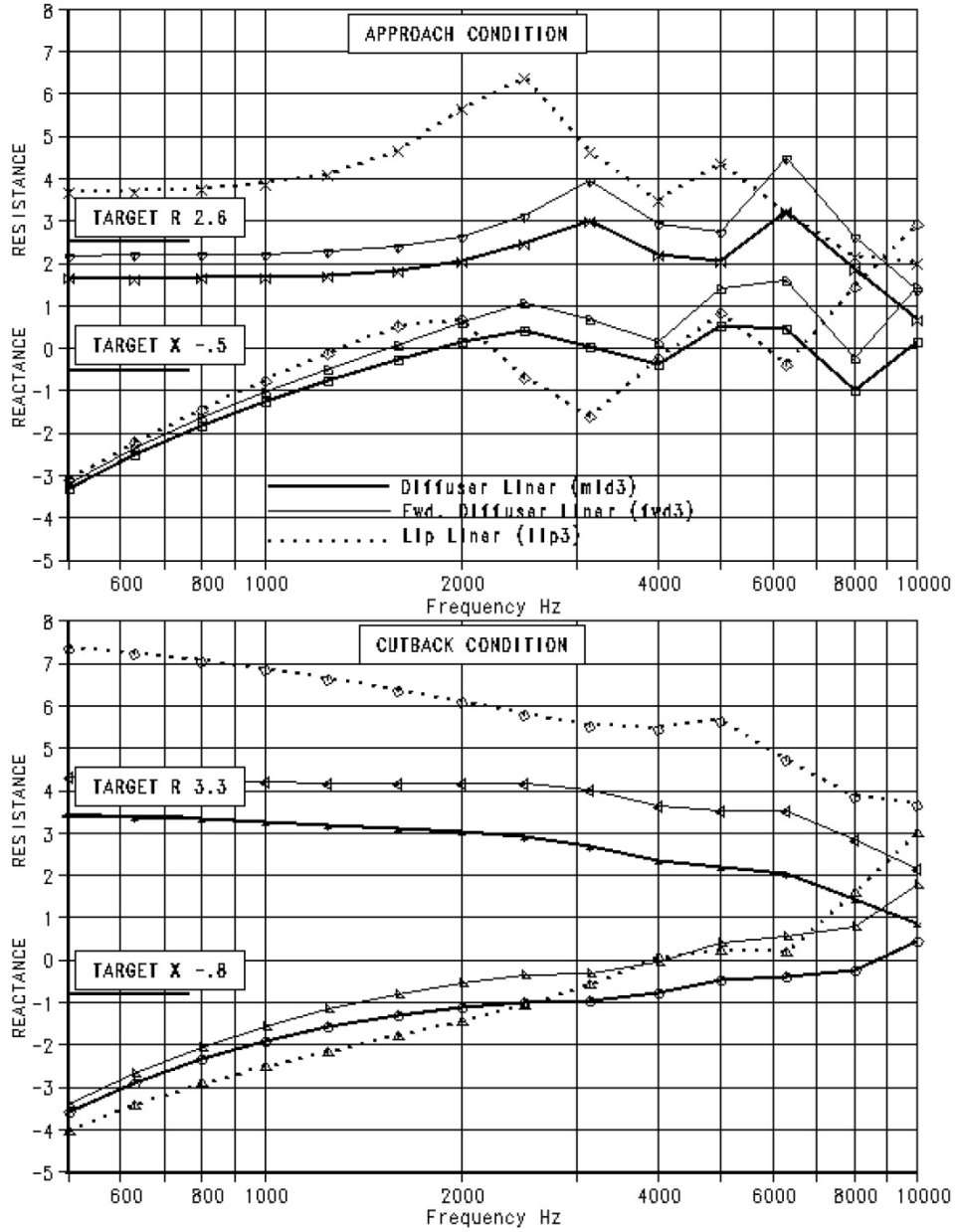
Figure 13.—Predicted impedance spectra of specified scarf inlet linings.
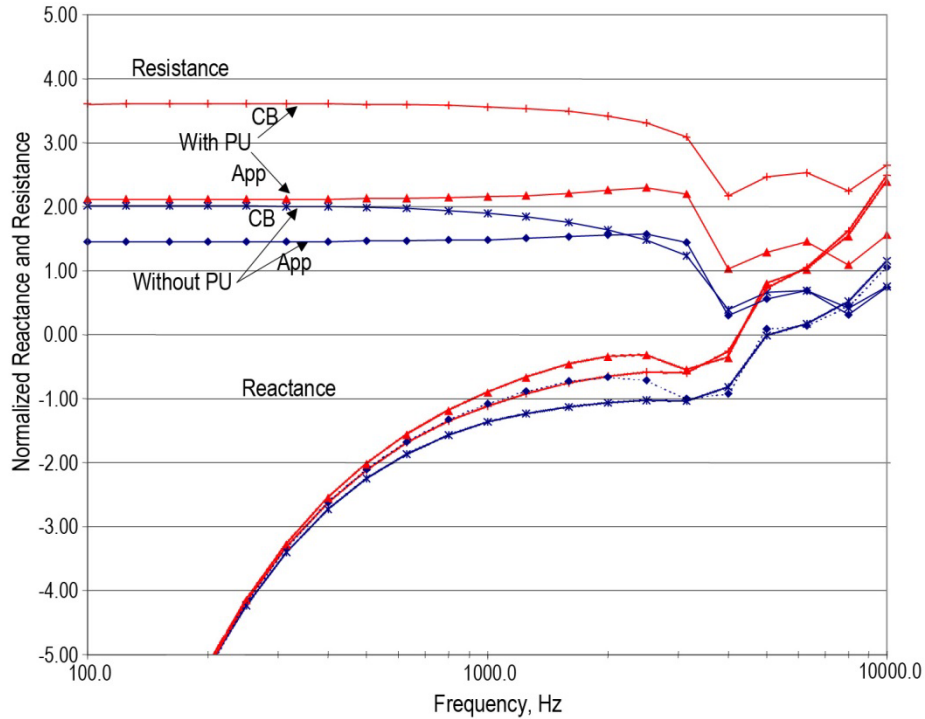
Figure 14.—Impedance of advanced fan case liners.

2.1.6 Impedance Confirmation

Impedance measurements were made on the completed scarf inlet to verify that the acoustic linings behaved as designed (Figure 15). Measurements were made at approximately 200 locations distributed over the inlet with about 100 measurements within the aft diffuser. The measurements were made with a 3 cm tube "portable impedance meter" similar to that conventionally used for lining samples in the laboratory. The primary difference between the portable device and the laboratory device is that the portable device uses a rubber seal to define the lining measurement face sheet area and the laboratory device cuts the lining test sample out of the panel and contains it within the impedance tube (Figure 16). As shown in Figure 16, the cavity volumes outside the edge defined by the seal influence the measurement by the portable device. The measured data therefore must be compared to a calculation of the impedance of the lining segment that accounts for this edge effect. Considered in this way the test data showed impedance variations of ±0.5 rhoc for a given lining design over the inlet and the average impedance differed from that of the specified lining by ±0.5 rhoc depending on frequency. It was estimated that the average impedance deviation from the specified lining would have no effect on the inlet component EPNL and the variation could only have a worst case variation of ±0.5 EPNdB.

Acoustics engineer at work
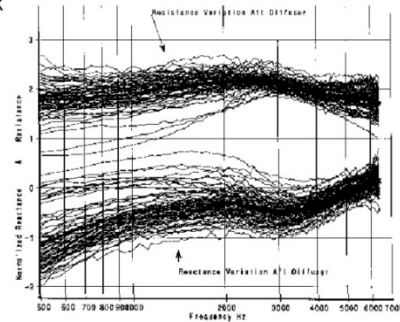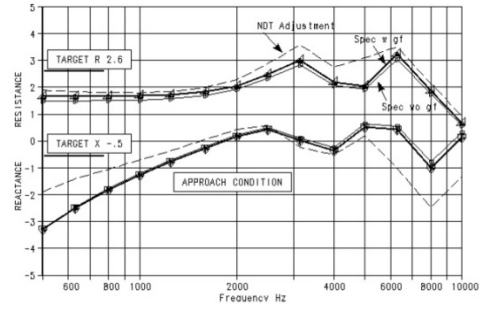
Indicated change to mean impedance ⟶
No change to EPNL
± 0.5 rhoc variation ⟶
± 0.5 EPNL

Impedance Measurements at 100 locations

Figure 15.—Acoustic impedance verification.
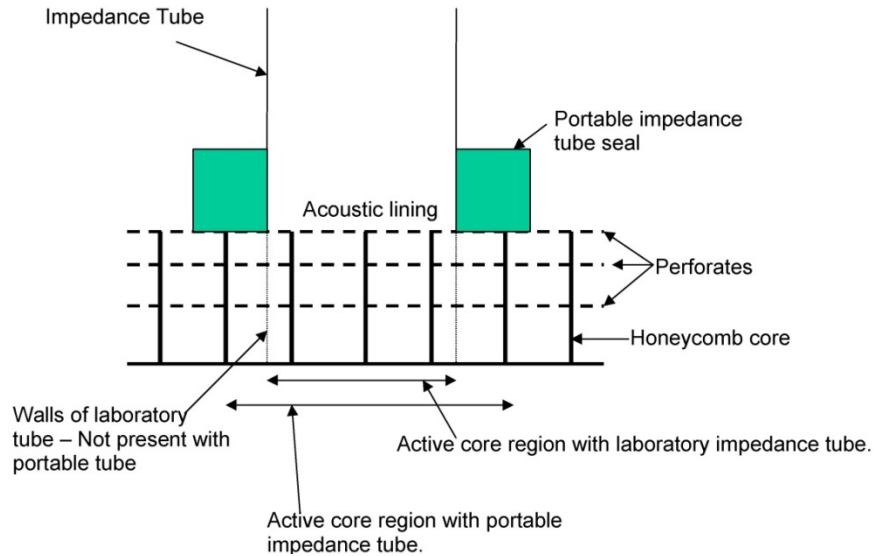
Figure 16.—Portable impedance meter.

2.1.7 Conclusions

The decision to use a flight lip resulted in high Mach number flow near the lip and thicker boundary layer at the fan face relative to flight.

The expected flow deviations from flight get smaller as engine power is reduced. It was therefore expected that they would not be acoustically significant at approach power. However, cutback power was a concern. The inlet lip contours were within specification. The inlet-fan case interface was out of specification but was probably not significant for fan tone generation or for broadband noise.

The measured variation of acoustic impedance was ±½ rhoc with a 0 to 1 rhoc shift in the mean depending on frequency. This was not expected to be significant.
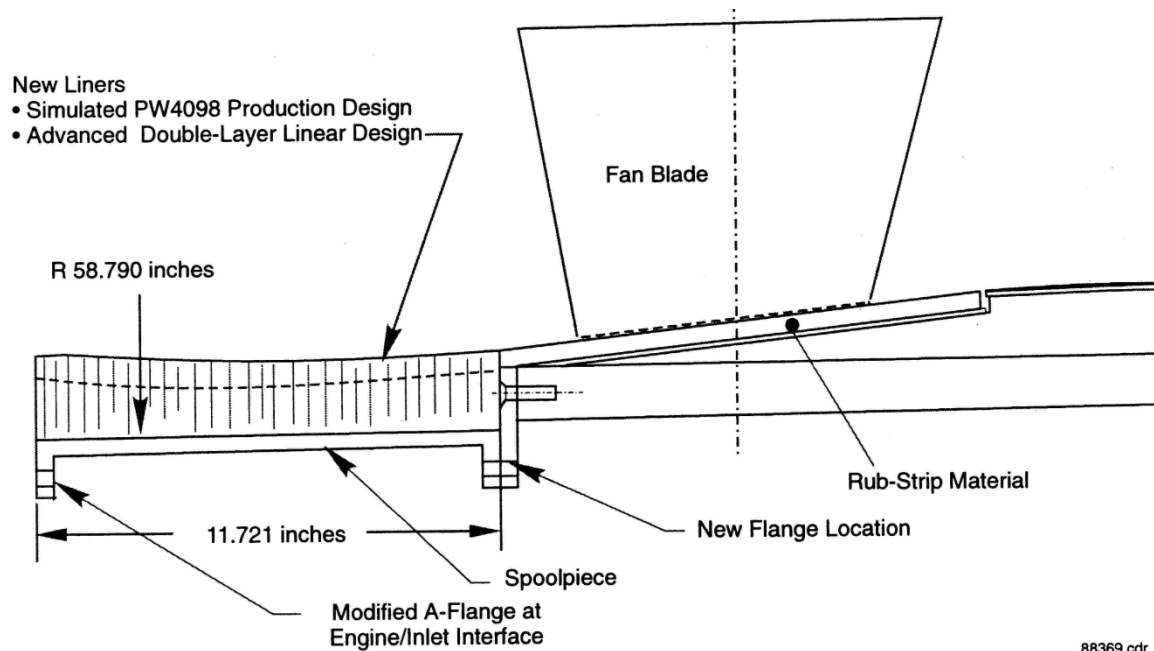
Figure 17.—PW4098 forward fan containment case—modified to incorporate new treatment.

2.2   P&W Forward Fan Case

The new forward fan case provided for this program has the capability to accept alternate liners forward of the fan. The case was modified to accept bolt-on spool pieces that featured the increased acoustic area and thickness associated with the advanced liners, as well as the production PW4098 acoustic treatment. In order to accommodate these spool pieces, the fan case forward flange was relocated aft by the width of the spool piece and the Kevlar fan blade containment material was removed. The spool pieces were designed with a larger diameter inlet bolt circle than the production design at the A-flange engine/inlet interface in order to house the increased thickness treatment. A schematic view of the lower half of the modified fan case is shown in Figure 17. Two spoolpieces were designed and built by P&W, one which incorporated the P&W supplied PW4098 production treatment and the other featuring the advanced Goodrich treatment.

2.3   Goodrich Case Liner

2.3.1   Design Criteria

Two acoustic liner design targets were specified for the PW4098 forward fan case (Figure 17). The first design target was to match Boeing's scarf inlet diffuser's optimum liner impedance criterion. In this criterion, the average optimum impedance at the approach condition is $Z/\rho c = (R + jX) = 2.6 - j0.5$ and for the cutback condition is $Z/\rho c = 3.3 - j0.8$ (See Table 1 for the definitions of symbols). The range of design frequencies is from 630 to 3150 Hz to cover both BPF (blade passage frequency) tone, BPF derivatives and broadband noise. Since optimum impedance is a function of in-duct Mach number (higher Mach number has higher resistance component), the diffuser's optimum liner impedance near the A1 flange is about $Z/\rho c = 2.0 - j0.5$ for approach and $Z/\rho c = 3.1 - j0.8$ for cutback. The Mach number in the fan case section is very close to the inlet diffuser section near A1 flange. Therefore, the optimum impedance with a lower resistance component was chosen as the first forward fan case liner design target.

The second design target is for cutback BPF and MPT noise suppression. The optimum impedance is $Z/\rho c = (2.0 - j1.0)$ at 1000 Hz. In addition, the acoustic liner must have uniform impedance properties and no more than two axial splices. The splice width was to be no more than 1/2 in.

TABLE 1.—DEFINITIONS OF SYMBOLS

$Z/\rho c$	a complex number representing normalized impedance
$R/\rho c$	the normalized acoustic resistance
j	is $\sqrt{-1}$ (imaginary number)
$X/\rho c$	the normalized acoustic reactance
ρ	the air density and c is the speed of sound
ρc	the characteristic impedance (unit: cgs - rayl)

2.3.1.1   Design Input Parameters

Boeing and Pratt & Whitney (PWA) provided design parameters, which include in-duct spectra, Mach number, and boundary layer thickness at approach and cutback conditions. Since the design parameters were based on estimated data, the spectra provided by Boeing and PWA were slightly different. Figure 18 and Figure 19 show the details of all input parameters.

2.3.2   Liner Configurations

Rohr, Inc., developed an innovative design concept to achieve both design targets with minimum additional cost for the fan case test panel fabrication. The design is a DDOF hybrid linear liner, which is composed of a removable laser drilled polyurethane (PU) film bonded on a perforate face sheet, a fine non-metallic mesh septum, solid back skin, and two 3/8 in. size aluminum core blankets bonded between perforate plate sheet, mesh septum, and solid back skin. This DDOF liner not only provides necessary structural strength but also ensures a near locally reactive acoustic behavior. The DDOF mesh septum liner with laser drilled PU film, which provides a higher acoustic resistance component, is designed to meet the first target. When the PU film is removed from the DDOF liner surface, the liner is designed to meet the second target, which has a lower acoustic resistance component. Table 2 lists the design configurations with and without PU-film. Figure 20 is a cross section drawing of the liner. It shows that the depth of upper core (between face sheet to septum) is a constant 0.45-in. However, the depth of lower core (between septum and back skin) varies slightly with the average value being 1.60 in. The minimum total core depth is 2 in.

TABLE 2.—ACOUSTIC LINER DESIGN CONFIGURATIONS FOR FORWARD FAN CASE

Liner Configuration with PU film	Liner Configuration without PU film
PU Surface: Pu-POA = 18; diam. = 0.0062 in.; thick = 0.015 in. Perforate sheet: Pf-POA = 32; diam. = 0.05 in.; thick = 0.032 in. Upper Core depth: 0.45 in. Mesh Septum: R(105) = 90 rayl and NLF = 1.3 Lower core depth = 1.60 in.	PU Surface: PU film removed. Perforate sheet: Pf-POA = 32; diam. = 0.05 in.; thick = 0.032 in. Upper Core depth: 0.45 in. Mesh Septum: R(105) = 90 rayl and NLF = 1.3 Lower core depth = 1.60 in.

2.3.3   Predicted Liner Impedance

Figure 21 to Figure 24 show the predicted acoustic impedance at approach and cutback conditions with and without PU film. Since PWA and Boeing have slightly different estimate spectra, the predicted acoustic impedance levels also show a small difference. The liner configuration with laser drilled PU film is designed for the first target.

At the approach condition, Figure 21 indicates that resistance components derived from either Boeing or PWA spectrum are near the design target of 2.0ρc at a frequency range up to 3150 Hz. The reactance components derived from either Boeing or PWA spectrum are also close to the –0.5ρc target value at frequencies between 1250 to 3150 Hz. At the cutback condition, Figure 22 shows that the resistance is slightly higher than target value by using PWA's spectrum, but it hit the design target if Boeing's spectrum is used. The reactance components are near the design target at the frequency range from 1000 to 3150 Hz.

The liner configuration without laser drilled PU film (film removed) is designed for the second target. Figure 24 indicates that both resistance and reactance components are near the design target $(2.0 - j1.0\rho c)$ at 1000 Hz frequency.

	Approach-0.3M	
FREQ.	PWA-SPL	BAC-SPL
50.0	121.1	115.5
63.0	121.8	123.5
80.0	122.3	122.5
100.0	119.2	120.0
125.0	119.4	120.0
160.0	121.4	121.0
200.0	122.4	123.0
250.0	121.8	122.5
315.0	122.8	122.5
400.0	123.6	123.0
500.0	124.2	123.5
630.0	**132.6**	**133.5**
800.0	128.8	126.5
1000.0	128.0	123.5
1250.0	**133.0**	**127.5**
1600.0	132.0	126.5
2000.0	134.6	128.5
2500.0	135.1	128.0
3150.0	135.0	130.0
4000.0	135.4	132.0
5000.0	136.0	133.0
6300.0	135.8	133.0
8000.0	136.1	133.0
10000.0	132.1	129.0

CM = 0.300 TMP = 527.0 R
SPR = 13.7 in., BL = 0.175 in.
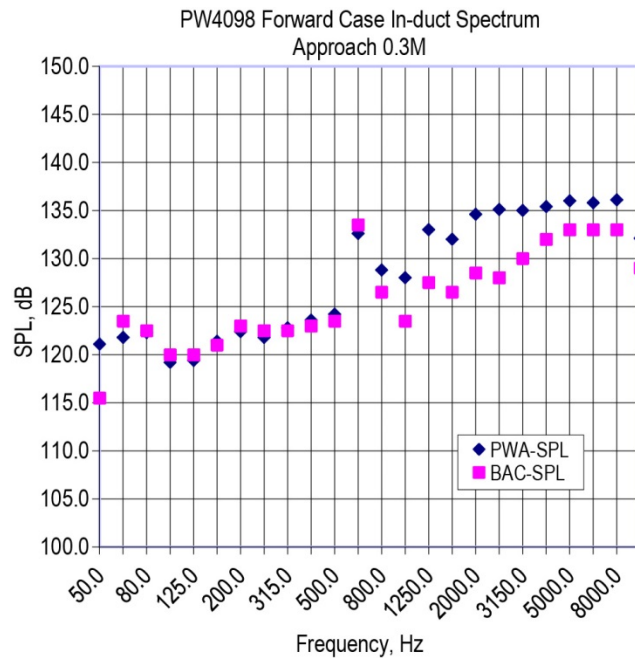
Figure 18.—Forward fan case design input parameters at approach condition.

Cutback-0.48M

FREQ.	PW-SPL	BAC-SPL
50.0	135.3	122.0
63.0	136.0	137.0
80.0	137.1	138.0
100.0	137.9	140.0
125.0	139.2	140.0
160.0	136.0	137.0
200.0	141.8	137.5
250.0	147.1	139.5
315.0	149.3	145.5
400.0	149.9	145.0
500.0	150.0	145.0
630.0	152.5	145.0
800.0	152.5	146.5
1000.0	**159.3**	**156.5**
1250.0	149.6	144.5
1600.0	150.3	143.5
2000.0	**148.3**	**144.0**
2500.0	144.9	138.5
3150.0	141.2	137.0
4000.0	136.3	133.0
5000.0	133.0	132.0
6300.0	131.1	131.5
8000.0	130.7	131.0
10000.0	126.9	126.6
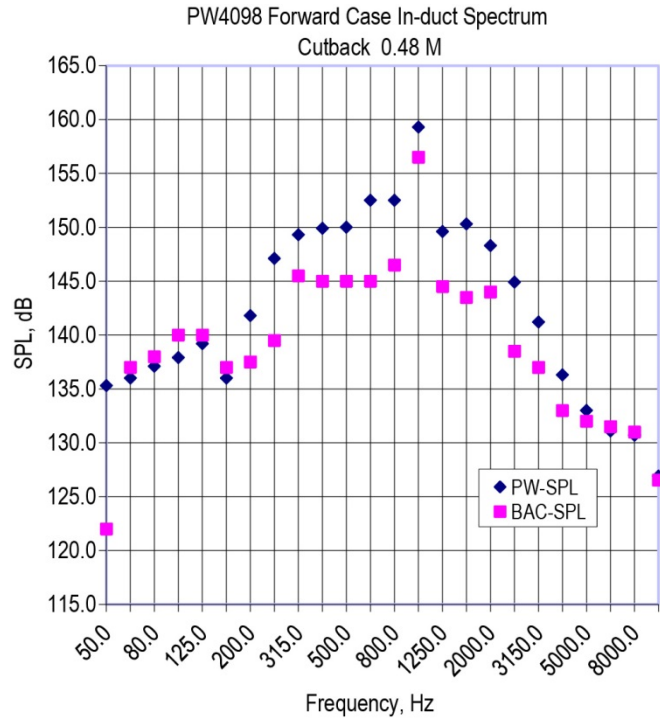
CM = 0.480 TMP = 513.0 R
SPR = 12.5 in., BL = 0.175 in.

Figure 19.—Forward fan case design input parameters at cutback condition.
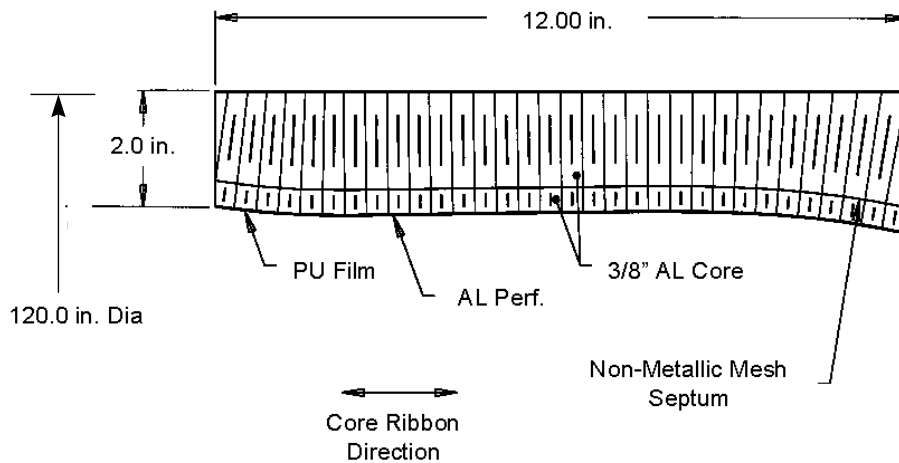
Figure 20.—Forward fan case liner configuration sketch.
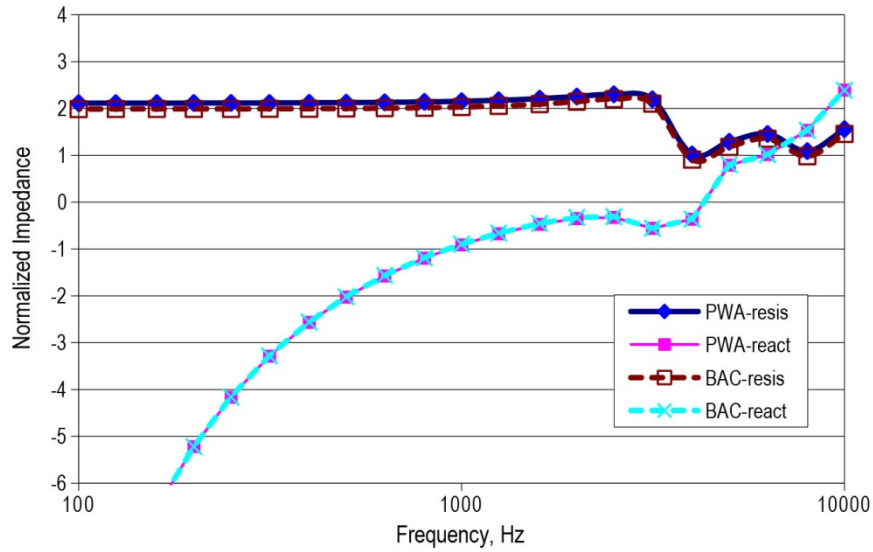
Approach-0.3M

FREQ.	PWA-SPL	RESIS	REAC		FREQ.	BAC-SPL	RESIS	REAC
50.0	121.1	2.12	-20.99		50.0	115.5	1.99	-20.99
63.0	121.8	2.12	-16.66		63.0	123.5	1.99	-16.66
80.0	122.3	2.12	-13.11		80.0	122.5	1.99	-13.11
100.0	119.2	2.12	-10.49		100.0	120.0	1.99	-10.48
125.0	119.4	2.12	-8.38		125.0	120.0	1.99	-8.38
160.0	121.4	2.12	-6.54		160.0	121.0	1.99	-6.54
200.0	122.4	2.12	-5.22		200.0	123.0	1.99	-5.22
250.0	121.8	2.12	-4.16		250.0	122.5	1.99	-4.16
315.0	122.8	2.12	-3.29		315.0	122.5	1.99	-3.28
400.0	123.6	2.12	-2.56		400.0	123.0	2.00	-2.56
500.0	124.2	2.13	-2.02		500.0	123.5	2.00	-2.02
630.0	**132.6**	**2.13**	**-1.57**	**BPF**	**630.0**	**133.5**	**2.01**	**-1.57**
800.0	128.8	2.14	-1.20		800.0	126.5	2.02	-1.19
1000.0	128.0	2.16	-0.91		1000.0	123.5	2.03	-0.90
1250.0	**133.0**	**2.18**	**-0.67**	**2BPF**	**1250.0**	**127.5**	**2.06**	**-0.66**
1600.0	132.0	2.21	-0.47		1600.0	126.5	2.09	-0.45
2000.0	**134.6**	**2.26**	**-0.35**	**3BPF**	**2000.0**	**128.5**	**2.15**	**-0.33**
2500.0	135.1	2.30	-0.33		2500.0	128.0	2.20	-0.31
3150.0	135.0	2.20	-0.56		3150.0	130.0	2.11	-0.56
4000.0	135.4	1.02	-0.36		4000.0	132.0	0.91	-0.36
5000.0	136.0	1.29	0.79		5000.0	133.0	1.18	0.80
6300.0	135.8	1.46	1.02		6300.0	133.0	1.36	1.02
8000.0	136.1	1.09	1.54		8000.0	133.0	0.98	1.54
10000.0	132.1	1.56	2.40		10000.0	129.0	1.46	2.39

Figure 21.—Liner impedance at approach condition with PU film.
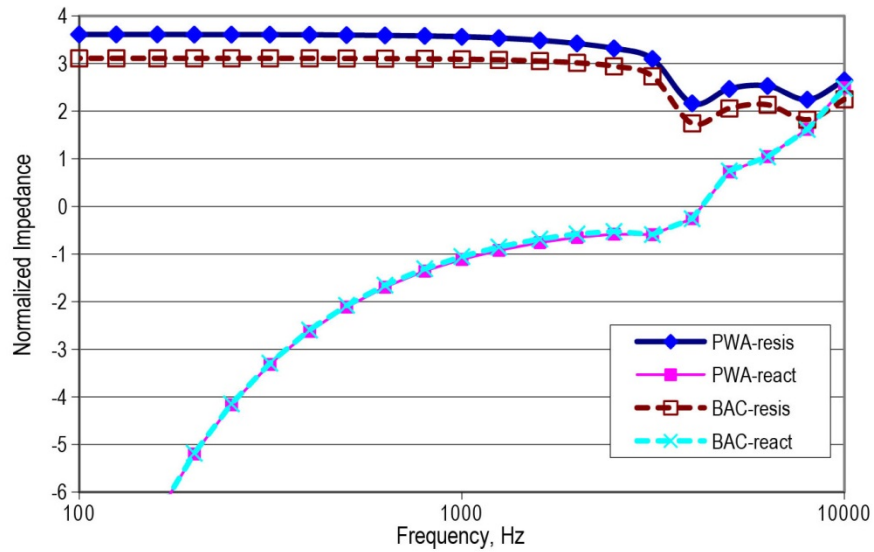
Ct-0.48M

FREQ.	PW-SPL	RESIS	REAC		FREQ.	**BAC-SPL**	RESIS	REAC
50.0	135.3	3.61	-20.73		50.0	122.0	3.11	-20.72
63.0	136.0	3.61	-16.45		63.0	137.0	3.11	-16.45
80.0	137.1	3.61	-12.96		80.0	138.0	3.11	-12.95
100.0	137.9	3.61	-10.37		100.0	140.0	3.11	-10.36
125.0	139.2	3.61	-8.30		125.0	140.0	3.11	-8.29
160.0	136.0	3.61	-6.49		160.0	137.0	3.11	-6.48
200.0	141.8	3.61	-5.20		200.0	137.5	3.11	-5.18
250.0	147.1	3.61	-4.17		250.0	139.5	3.11	-4.15
315.0	149.3	3.61	-3.32		315.0	145.5	3.11	-3.29
400.0	149.9	3.60	-2.62		400.0	145.0	3.11	-2.60
500.0	150.0	3.60	-2.11		500.0	145.0	3.11	-2.08
630.0	152.5	3.59	-1.69		630.0	145.0	3.10	-1.65
800.0	152.5	3.58	-1.36		800.0	146.5	3.10	-1.31
1000.0	**159.3**	**3.56**	**-1.11**	**BPF**	**1000.0**	**156.5**	**3.09**	**-1.05**
1250.0	149.6	3.54	-0.92		1250.0	144.5	3.08	-0.85
1600.0	150.3	3.49	-0.76		1600.0	143.5	3.05	-0.68
2000.0	**148.3**	**3.42**	**-0.65**	**2BPF**	**2000.0**	**144.0**	**3.02**	**-0.58**
2500.0	144.9	3.32	-0.58		2500.0	138.5	2.94	-0.53
3150.0	141.2	3.10	-0.59		3150.0	137.0	2.73	-0.59
4000.0	136.3	2.16	-0.26		4000.0	133.0	1.74	-0.26
5000.0	133.0	2.47	0.73		5000.0	132.0	2.06	0.75
6300.0	131.1	2.53	1.05		6300.0	131.5	2.13	1.04
8000.0	130.7	2.24	1.62		8000.0	131.0	1.82	1.62
10000.0	126.9	2.65	2.50		10000.0	126.6	2.25	2.48

Figure 22.—Liner impedance at cutback condition with PU film.
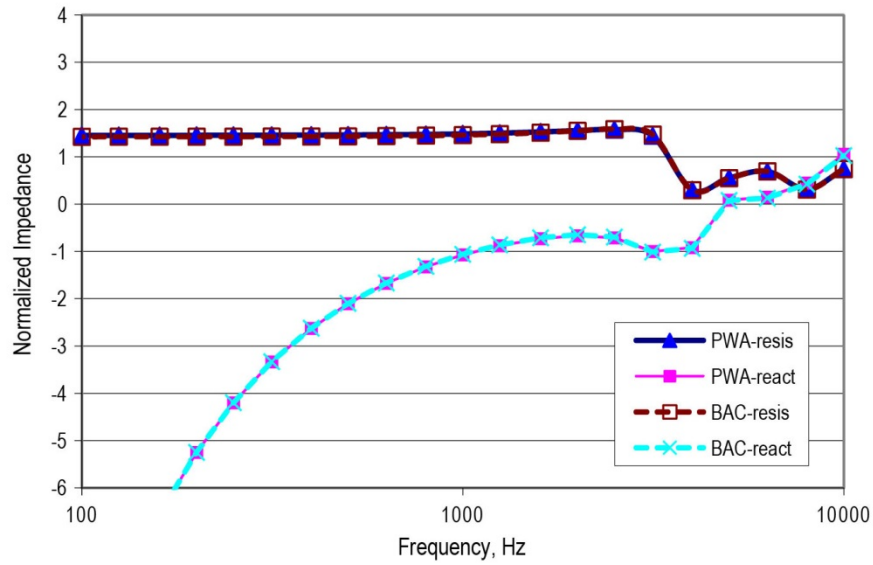
App-0.3M

FREQ.	PWA-SPL	RESIS	REAC		FREQ.	BAC-SPL	RESIS	REAC
50.0	121.1	1.45	-21.00		50.0	115.5	1.42	-21.00
63.0	121.8	1.45	-16.67		63.0	123.5	1.42	-16.67
80.0	122.3	1.45	-13.13		80.0	122.5	1.42	-13.13
100.0	119.2	1.45	-10.50		100.0	120.0	1.42	-10.50
125.0	119.4	1.45	-8.40		125.0	120.0	1.43	-8.40
160.0	121.4	1.45	-6.56		160.0	121.0	1.43	-6.56
200.0	122.4	1.46	-5.25		200.0	123.0	1.43	-5.25
250.0	121.8	1.46	-4.20		250.0	122.5	1.43	-4.20
315.0	122.8	1.46	-3.34		315.0	122.5	1.43	-3.33
400.0	123.6	1.46	-2.63		400.0	123.0	1.43	-2.62
500.0	124.2	1.46	-2.10		500.0	123.5	1.43	-2.10
630.0	**132.6**	**1.47**	**-1.67**	**BPF**	**630.0**	**133.5**	**1.44**	**-1.67**
800.0	128.8	1.48	-1.33		800.0	126.5	1.45	-1.32
1000.0	128.0	1.49	-1.07		1000.0	123.5	1.46	-1.06
1250.0	**133.0**	**1.50**	**-0.88**	**2BPF**	**1250.0**	**127.5**	**1.48**	**-0.86**
1600.0	132.0	1.53	-0.73		1600.0	126.5	1.51	-0.71
2000.0	134.6	1.56	-0.67		2000.0	128.5	1.55	-0.65
2500.0	135.1	1.58	-0.71		2500.0	128.0	1.59	-0.70
3150.0	135.0	1.45	-1.00		3150.0	130.0	1.47	-1.01
4000.0	135.4	0.30	-0.92		4000.0	132.0	0.30	-0.94
5000.0	136.0	0.55	0.09		5000.0	133.0	0.55	0.08
6300.0	135.8	0.69	0.15		6300.0	133.0	0.70	0.13
8000.0	136.1	0.32	0.45		8000.0	133.0	0.31	0.42
10000.0	132.1	0.74	1.06		10000.0	129.0	0.74	1.03

Figure 23.—Liner impedance at approach condition without PU film
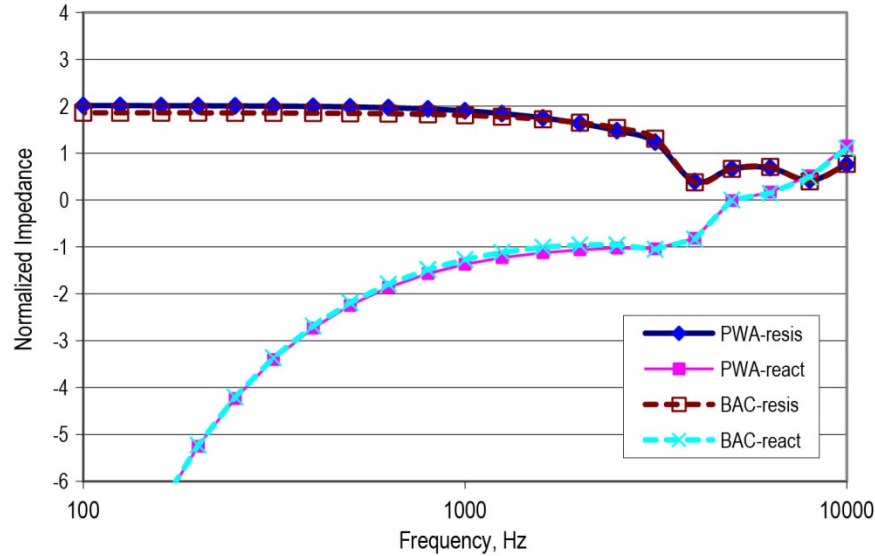
Cut-0.48M

FREQ.	PW-SPL	RESIS	REAC		FREQ.	**BAC-SPL**	RESIS	REAC
50.0	135.3	2.01	-20.74		50.0	122.0	1.86	-20.73
63.0	136.0	2.01	-16.47		63.0	137.0	1.86	-16.46
80.0	137.1	2.01	-12.98		80.0	138.0	1.86	-12.97
100.0	137.9	2.01	-10.40		100.0	140.0	1.86	-10.39
125.0	139.2	2.01	-8.33		125.0	140.0	1.86	-8.32
160.0	136.0	2.01	-6.53		160.0	137.0	1.86	-6.51
200.0	141.8	2.01	-5.25		200.0	137.5	1.86	-5.23
250.0	147.1	2.01	-4.23		250.0	139.5	1.86	-4.21
315.0	149.3	2.00	-3.40		315.0	145.5	1.86	-3.37
400.0	149.9	2.00	-2.73		400.0	145.0	1.85	-2.69
500.0	150.0	1.99	-2.25		500.0	145.0	1.85	-2.19
630.0	152.5	1.97	-1.86		630.0	145.0	1.84	-1.80
800.0	152.5	1.94	-1.57		800.0	146.5	1.83	-1.48
1000.0	**159.3**	**1.90**	**-1.37**	**BPF**	**1000.0**	**156.5**	**1.81**	**-1.27**
1250.0	149.6	1.84	-1.23		1250.0	144.5	1.77	-1.12
1600.0	150.3	1.75	-1.12		1600.0	143.5	1.72	-1.01
2000.0	**148.3**	**1.63**	**-1.06**	**2BPF**	**2000.0**	**144.0**	**1.65**	**-0.96**
2500.0	144.9	1.48	-1.03		2500.0	138.5	1.54	-0.96
3150.0	141.2	1.23	-1.04		3150.0	137.0	1.31	-1.05
4000.0	136.3	0.39	-0.82		4000.0	133.0	0.38	-0.84
5000.0	133.0	0.66	-0.01		5000.0	132.0	0.66	0.00
6300.0	131.1	0.69	0.17		6300.0	131.5	0.70	0.14
8000.0	130.7	0.42	0.52		8000.0	131.0	0.40	0.49
10000.0	126.9	0.75	1.15		10000.0	126.6	0.77	1.10

Figure 24.—Liner impedance at cutback condition without PU film.

2.3.3.1 DC Flow Resistance Data

The DC flow resistance measurements for the liner septum were conducted at airflow rates of 30, 60, 105, 150, and 200 cm/sec. All the data were normalized to reference ambient conditions (70 °F and 29.92 in. Hg). The first order least squares curve fit was used to generate required data R(105), and NLF. The R(105) is DC flow resistance data at 105 cm/sec and the NLF, which is referred as non-linear factor, is the ratio of resistance data at 200 cm/sec to data at 20 cm/sec (R(200)/R(20)). Table 3 shows the measured DC flow resistance of the actual test article. The data indicates that the acoustic test panel is within 90 ± 20 rayl specification.

TABLE 3.—MEASURED SEPTUM DC FLOW RESISTANCE

	Section 1	Section 2	Section 3	Section 4
1	109.7	118.5	88.5	97.2
2	117.6	121.2	90.9	92.1
3	106.1	100.4	88.3	95.6
4	111.2	104.6	81.0	91.2
5	101.6	96.4	91.2	87.5
6	107.3	103.5	84.1	82.0
7	106.0	99.2	89.1	82.3
8	106.0	98.2	88.8	83.2
9	99.6	97.9	93.0	81.4
10	103.5	98.4	94.5	83.0
11	104.8	99.0	94.3	88.0
12	113.7	105.0	85.5	87.8
13	102.6	105.0	90.5	80.7
14	110.2	99.4	84.3	84.7
15	98.0	101.0	98.3	87.3
16	97.8	101.3	82.8	81.9
17	95.6	97.4	94.1	87.5
18	104.7	109.1	87.8	81.9
19	101.0	97.1	93.2	84.0
20	100.8	100.4	82.6	87.2
21	96.0	98.2	96.2	82.3
22	98.0	102.9	82.9	87.8
23	113.4	106.3	95.6	94.6
24	110.9	123.1	94.0	92.2
Average				
R(105)	**104.8**	**103.5**	**89.63**	**86.8**
NLF	**1.32**	**1.32**	**1.37**	**1.28**

Specification:
Average Septum DC flow Resistance measured at 105 cm/sec. R(105) = 90 ± 20 RAYLS
Individual Septum DC flow Resistance measured at 105 cm/sec. R(105) = 90 ± 35 RAYLS
NLF = R(200)/R(20) < 1.5

2.3.3.2   PU Film and Perforate POA

The measurements of POA and hole diameter on the final test panels were not performed. However, the small coupon sample measurement indicates that the PU film met the 18 POA design-target with a hole diameter of 0.00624 in. The perforate sheet is 34 POA with a hole diameter of 0.05 in. before bonding. The installed POA is approximately 32 ± 2 with a hole diameter between 0.048 to 0.050 in.

3.0   Test Program

3.1   Test Site Characteristics

The test site has negligible influence on the engine's noise generating processes and, except for ground surface effects, negligible influence on the propagation of sound from the engine to the microphone. See Figure 25.

3.1.1   Overall Site

The C-11 test site is located in an open area having relatively flat terrain which is free of structures and other obstacles that affect far-field sound pressure measurements.

Figure 25.—Overall View of PW C11 Stand Far Field Acoustic Arena.

One-third octave band sound pressure levels of ambient noise are sufficiently low so that engine noise measurements are not significantly contaminated by noise from environmental or manmade sources.

3.1.2 Engine Support Structure and Test Engine

The engine support structure is designed for minimal sound interference characteristics. That is, the structure does not impede sound propagation nor does it have any acoustically reflective surfaces close to noise radiating regions. The engine centerline height above the acoustical arena surface is 15 ft (4.57 m), or no less than one and one half times the fan diameter.

The test engine was a PW4098. This is a modern high bypass turbofan engine with wide chord shroudless fan blades. The 112 in. diameter fan rotor has 22 blades and the Fan Exit Guide Vanes consists of 60 static airfoils. There are 10 Intermediate Case struts behinds the FEGV row including the lower duct bifurcation. The engine as configured for Phase 1B testing is shown on the test stand with a production bill of material inlet, but with a mini-bellmouth lip at the highlight in Figure 26.

Static noise tests in the Fall of 1998 and summer of 1999 evaluated 1) an innovative inlet design (Boeing Ideal Scarf inlet) with advanced acoustic treatment, 2) advanced acoustic treatment installed in the engine forward fan containment case (FFCC), 3) the impact of inlet probes on fan inlet noise and 4) the effect of hard walled sections representative of production type FFCC liner joints.

3.1.3 Acoustical Arena

The acoustical arena is the surface area that extends from beneath the engine to a distance that is at least 25 ft (7.6 m) beyond all microphones. The area has the following characteristics: Flat with no undulations that cause focusing or scattering of sound or collection of standing water. A slight slope or curvature subtending about 0.25° (4 cm/10 m) has been built in to aid in drainage. A thermally reflective surface of light concrete is used to minimize solar heating and thermal gradients near the ground. The surface is uniformly smooth and hard so as to approximate the acoustical impedance of a perfect sound reflector over the frequency range of interest.

3.1.4 Acoustic Barriers

Acoustic barriers were set up to block aft radiated noise from contaminating the inlet radiated noise measured by the far field microphones. The walls were about 30 ft (9 m) in height and for this test are arranged as shown in Figure 27.

Figure 26.—PW4098 Test Engine with production flight inlet.
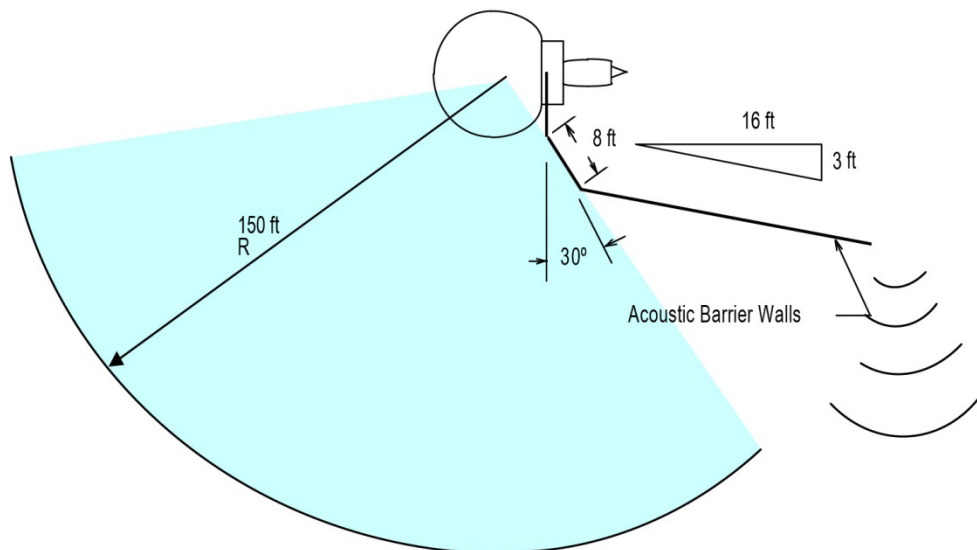
Figure 27.—Far field mic array and aft acoustic barriers.

3.2   Engine and Noise Measurement

3.2.1   Data Acquisition and Reduction System

3.2.1.1   Acoustical Data Acquisition and Real Time Analysis System

The acoustical far field data acquisition system consists of microphones, signal conditioning and transmission components (e.g., pre-amplifiers, power supplies, and cables) and includes data storage and retrieval equipment (e.g., magnetic tape recorders). The objective of this system is to acquire accurate measurements of engine sound pressure levels and do on-line digital signal analysis over the range of one-third octave bands having nominal center frequencies from 50 to 10,000 Hz. Deviations from a uniform frequency response are determined from instrument manufacturer's data, calibrations, or combinations of both. A Dell GXA computer is programmed to operate two Honeywell 28 track FM tape recorders, 12 B&K, model 2131, one-third octave band analyzers, six B&K, model 2032, Spectrum Analyzers, and a Computer Products Model 7431 Real Time Peripheral (RTP) input/output device. During data acquisition, tape recording and one-third octave analysis of up to 70 acoustic signals may be obtained. Additionally, measurements of engine speeds, temperatures, relative humidity, and wind conditions are measured at a rate of nearly two times per second.

Internal inlet noise in the Boeing Ideal Scarf Inlet was recorded on magnetic tape during Phase 1A by six Kulites mounted in two axial arrays of three each along the crown and keel. Thirteen static pressure taps were installed in the inlet in axial arrays along the crown and at ±90° from top dead center.

Location of Scarf Inlet Kulite Microphones
Approximate Distance From A Flange (in.) .
Along Keel   3.4, 40.6, 80.3 (K1,K2,K3)
Along Crown   3.4, 29.4, 61.4 (K4,K5,K6)

Location of Scarf Inlet Pressure Taps
Approximate Distance From A Flange (in.)
Along Crown (0°)   63.6, 58.8, 56.7, 53.2, 50.0, 44.9, 39.9, 34.9 (p11-p18)
                      70.9,65.7, 63.6, 60.6, 55.4 (p1-p6, p7-p10)

A special array of 198 dynamic pressure transducers were arrayed on the Inflow Control Device (ICD) in Phase 1A of the test. The ICD is a large spherical shaped inflow conditioner mounted in front of the engine during acoustic testing. The ICD can be seen in Figure 25. The array was connected to a special data acquisition and analysis system for phased array analysis, mode and source identification.

During Phase 1B testing, an internal array of transducers was mounted in the inlet adapter ring between the inlet and the engine front fan case. The array consisted of 26 Kulites arranged in a 180° circumferential pattern for rotating mode measurements. Four blade mounted transducers were installed on the blade pressure surface near the tip. Special transducer locations are shown in Figure 28. A customized P&W telemetry system with a 1 per rev trigger signal was used to transmit data from the rotating reference frame to an antenna mounted on the inlet and the signals were transmitted by cable into the control room for analysis with a data system supplied by Boeing.

The far field microphone and related components had the following characteristics: Microphones are located on a 150 ft (45.7 m) radius array. The microphones are 1/2 in. (1.27 cm) B&K 4134, & Larson Davis, 2559 (pressure type), condenser cartridges and installed 1/4 in. (7 mm) above the acoustic arena ground plane, with symmetrical protective angular grids on. A diagram of the far field microphone array is shown in Figure 27. The microphone angles measured from forward CL and centered on MARP for this test were:

Most Configurations: 24 angles, 10° to 120° at 5°, 130°
Configuration 17: 32 angles, 5° to 160° at 5°
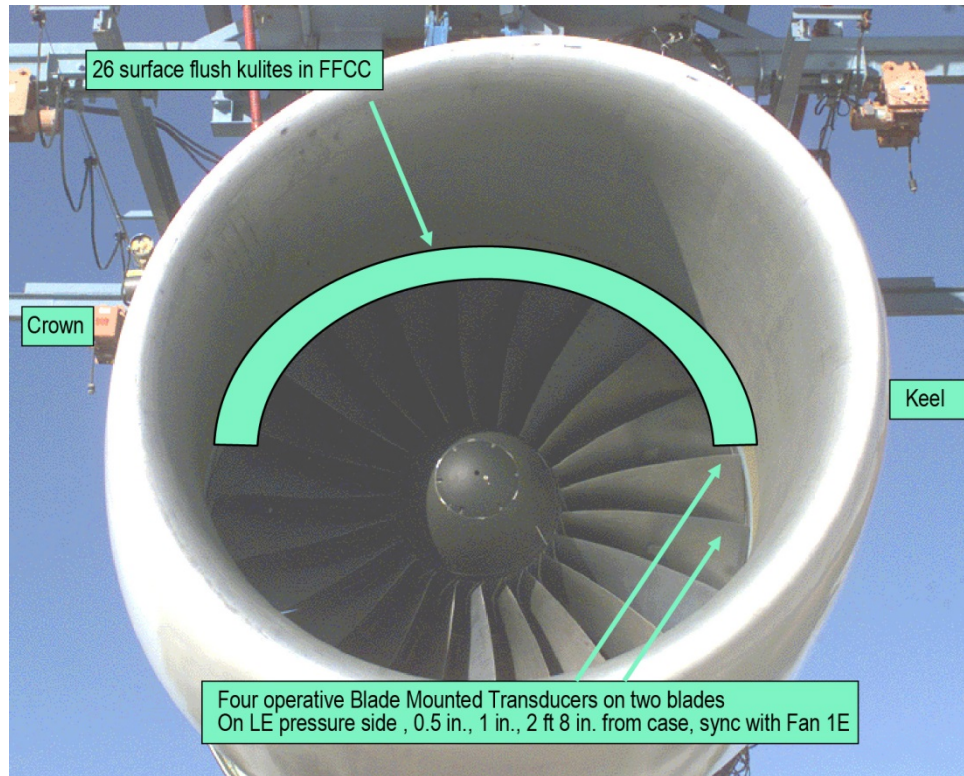
Figure 28.—Locations of special internal transducers

The frequency response and stability characteristics were within those specified by the SAE Aerospace Recommended Practice, ARP-1846, February 1990. No windscreens were installed. B&K preamplifiers Type 2619, or equivalent were used. Cables were routed from the microphone location over the surface to central points close by where they were attached to underground cables extending into the control room where they attach to the B&K, Type WB0690, Power Supply and Signal Conditioners.

3.2.1.2   Meteorological Measurement System

The meteorological measurement system consisted of instruments to measure wind speed, wind direction, ambient air temperature, relative humidity and atmospheric pressure. The objective was to monitor meteorological conditions to ensure that static noise tests were conducted within acceptable meteorological limits and to provide information needed for acoustical data normalization to reference meteorological conditions

Meteorological sensors for wind (speed and direction), air temperature and relative humidity were located in the vicinity of the microphone array over the same surface that extends from the engine to the far-field microphones. Wind speed and direction were measured at approximately engine centerline measure ground wind speed to provide guidance on wind shear effects on noise radiation. Ambient air temperature was measured at approximate engine centerline height, 15 ft (4.6 m) and about 1/2 in. (1.27 cm) above the ground surface.

Relative humidity is calculated from measurements of dry bulb air temperature and temperature of the dew point taken at approximately engine centerline height. Ambient atmospheric pressure is measured in the vicinity of the acoustical arena.

3.2.1.3 Engine Performance Measurements

Instruments are provided to define the prime engine power setting parameter (e.g., fan rotor speed). The objectives are to ensure that the engine is set at the desired operating condition and is stable when sound pressure signals are recorded. The instruments have the capability of determining the value of the power setting parameter within an accuracy consistent with a rotor speed measurement accuracy of ± 1 percent. A once per rev rotor speed signal was provided for the mode measurement analysis and the blade mounted transducers.

3.2.2 Acoustical Calibrations

3.2.2.1 Calibrations—General

All components of the test instrumentation were calibrated and certified to comply with the manufacturer's specifications and FAR 36 practices.

3.2.2.2 Calibrations—Frequency Response

Calibrations were performed to determine deviations of the entire far field recording and reproducing and real time data system from a uniform frequency response. The non-uniformity's were determined in terms of time averaged one-third octave band sound pressure levels measured at each preferred one-third octave band center frequency reference signal (250 Hz).

The one-third octave band and narrowband corrections required to adjust the recording and reproducing and real time data systems to a uniform frequency response were applied to the measured data for microphone frequency response, cable losses, analyzer center frequency response and filter shape response.

3.2.2.3 Calibrations—Amplitude

Before and after each test period the overall electro-acoustical response of the microphone system was determined by use of a signal from a calibrated acoustical calibrator (pistonphone) generating a known sound pressure level, 124.0 dB at 250 Hz. The level was corrected by the difference in output level of the pistonphone between the calibrated level at standard day barometric pressure and the output level at the barometric pressure when the pistonphone was applied to the microphones.

3.2.3 Test Procedures, Engine and Noise Data Acquisition

3.2.3.1 General Test and Meteorological Conditions

The acoustic surface was free of extraneous clutter, standing water, or other objects that could alter the nominal acoustical characteristics of the surface. Testing was conducted within certain atmospheric condition limits. Examples of limits for temperature, relative humidity and wind conditions that were used are:

Wind Speed:	$\pm$ 8 kn average	At engine C_L height
	$\pm$ 10 kn maximum	At engine C_L height
Cross Wind:	$\pm$ 6.5 kn average	At engine C_L height
Surface Wind:	$\pm$ 7 kn maximum	At 2 in. above ground plane
Temperature	36 to 95 °F (2.2 to 35 °C)	
Temperature Gradient	(Surface Temp.-Centerline Temp.) $\pm$ 7.0 °F (3.9 °C)	
Relative Humidity	20 to 95 percent	
Precipitation:	None permitted	

3.2.3.1.1 Typical Acoustic Test Data Acquisition Procedures

A single frequency acoustic calibration of the microphone systems was performed with Bruel & Kjaer Model 4220 or 4228 pistonphone. The pistonphone output had a current laboratory calibration certificate

traceable to the NIST. Immediately before each data recording session, the pistonphone calibrator was applied to each microphone system. The calibrated output level was normalized to a constant output voltage level at the input to the 1/3 octave and narrow band analyzers and the tape recorders and recorded on the pistonphone calibration record. Immediately after each recording session, the pistonphone calibration procedure was repeated (without normalization adjustments) and the system's performance was accepted if during the acquisition period the sensitivity variation of each microphone system did not exceed ± 0.5 dB

The electronic equivalent sound pressure reference level sinewave at 250 Hz was applied to all channels of the real time analyzer system and time averaged for a minimum of 30 sec to establish a sound pressure level reference for the analyzers. This was done at the start and end of every data recording session. The reference level in volts with respect to the pistonphone calibration level in dB was noted on the recorder log sheet. At the beginning and end of every data acquisition period, a pink noise signal, at optimum recording level, was applied to and analyzed by the real time analyzers for a minimum of 30 sec. The level of the pink noise was set at an optimum recording level. Data were considered reliable if the difference between the pink noise at the beginning and end of each acquisition period or each tape did not exceed ± 0.8 dB for any of the one-third octave bands.

An Inflow Control Device (ICD), designed to minimize inflow distortion and turbulence into the fan was used. It is intended to simulate the clean inflow conditions seen by the engine in flight. It consisted of a support structure which includes the frame, transport wheels, perforated plate and honeycomb panels. The ICD was positioned such that the engine inlet protruded into the ICD. Both the Boeing Production inlet and the Boeing Ideal Scarf inlet were set to similar penetrations into the ICD. A non-porous sail-cloth seal was attached to the ICD and the engine to eliminate flow leakage through the annulus between the inlet and the ICD opening. The ICD was inspected for damage and screen blockage prior to testing.

Just prior to engine start up for each data recording session, an ambient noise data record was acquired. The data were acquired on the real time and the tape recording system. The real time data were reviewed immediately prior to engine start up to ensure acceptable ambient noise conditions.

A test matrix of engine speed or power settings was defined prior to conduct of test. The test conditions included rotor speeds typical of the acoustic conditions of sideline, cutback and approach. Configuration descriptions are provided in Table 4, and pictorial representations are shown in Figure 29. A complete list of individual data points by Configuration and Run Number are provided in the Appendix. Selected points were repeated once or twice to establish repeatability or confidence limits based on data scatter. Prior to the first data acquisition of each data recording session, the engine was temperature stabilized for 5 min. For each test condition, before initiating data acquisition, the engine was stabilized such that the engine fan corrected rotational speed did not vary more than ± 15 rpm or ± 1 percent of the lowest engine speed recorded.

Real time acoustic data were acquired using an averaging time of 32 sec during which one-third octave and narrowband data were processed simultaneously from each microphone. Groups of two 12 microphone sequences were analyzed sequentially during a data point acquisition. Data from the 24 microphone array were acquired in about 2 min. Third-octave band data was reviewed on stand within minutes of data acquisition and displayed graphically on computer terminals set up in the test stand control room. Each data record was identified by a unique record number (see the Appendix). All backup acoustic data records on magnetic tape were 60 sec in length.

The low-pressure shaft rotational speed was sampled at a sufficiently high rate such that a continuous representation of this parameter was displayed. The once per rev signal used during Phase 1B testing was fed to the Boeing data analysis system for the blade mounted transducers. Temperature, relative humidity, wind speed and direction were measured during the period of time when sound pressure signals were being measured, recorded and displayed on-line. The speed signal was also recorded on magnetic tape with the acoustic signals. The rotational speed during data acquisition was averaged and displayed after the data point acquisition. It also displayed the maximum and minimum deviations of engine speed during the data acquisition and analysis time.

TABLE 4.—ACOUSTIC CONFIGURATION SUMMARY

Config. and run no	Inlet	Wall	Front Fan Containment Case (FFCC)	Inlet treatment	Front FCC treatment	Inlet position	Objective of Test
1 16078	PW4098 Flight Lip	Aft	BOM	HW	HW	Keel to mics	HW Inlet Production Baseline
2 16079	PW4098 Flight Lip	Aft	BOM	Treated	BOM Treated	Keel to mics	Prod Inlet Treatment versus HW
3 16082	Boeing Ideal Scarf	Aft	Modified FCC	HW	HW	Keel to mics	Effect of HW Scarf versus HW Base
12 16083	Boeing Ideal Scarf	Aft	Modified FCC	Treated diffuser, HW Lip	HW	Keel to mics	Effect of inlet treatment forward of the throat with HW FFCC
14 16084	Boeing Ideal Scarf	Aft	Modified FCC	Treated diffuser and lip	HW	Keel to mics	Effect of inlet treatment forward of the throat with HW FCC
4 16085	Boeing Ideal Scarf	Aft	Modified FCC	Treated diffuser and lip	Simulated BOM	Keel to mics	Effect of Scarf Trt versus HW and Trt Scarf Versus Trt BOM
5 16086	Boeing Ideal Scarf	Aft	Modified FCC	Treated diffuser and lip	Adv 2 in. Deep Dbl Layer (R1)	Keel to mics	Advanced FFCC Treatment R1 Compare to BOM base FFCC
6 16087	Boeing Ideal Scarf	Aft	Modified FCC	Treated diffuser and lip	Adv 2 in. Deep Dbl Layer (R2) (Tear off Perf. Poly)	Keel to mics	Advanced FFCC Treatment R2 Compare to BOM base FFCC And Adv R1
7 16088	Boeing Ideal Scarf	Aft	Modified FCC	Treated diffuser and lip	Adv 2 in. Deep Dbl Layer (R2)	Keel to mics	Effect of HW FFCC Splices 8 Eq Sp 3-in. wide axial splices
8 16089	Boeing Ideal Scarf	Aft	Modified FCC	Treated diffuser and lip	Adv 2 in. Deep Dbl Layer (R2)	Keel to mics	Effect of HW FFCC Splices 3 Eq Sp 3-in. wide axial splices
9 16090	Boeing Ideal Scarf	Aft	Modified FCC	Treated diffuser and lip	Adv 2 in. Deep Dbl Layer (R2)	Keel to mics	Effect of HW FFCC Splices 3 Eq Sp 1.25-in. wide axial splices
11 16091	Boeing Ideal Scarf	Aft	Modified FCC	Boeing Ideal	Adv 2 in. Deep Dbl Layer (R2)	Keel to mics	Effect of HW FFCC Splices 3 Eq Sp 0.625-in. wide splices
10 16092	Boeing Ideal Scarf	Aft	Modified FCC	Treated diffuser and lip	Adv 2 in. Deep Dbl Layer (R2)	Keel to mics	Effect of HW FFCC Splices 3 Eq Sp 1.25-in. axial wide splices + 6 in. circumferential HW area in front of fan
End of Phase 1A Testing							
Start of Phase 1B Testing							
P3 16101	PW4098. BM Lip	Aft	BOM	BOM Treated	BOM treated	Keel to mics	Diagnostics: Prod inlet baseline with BOM Trt FFCC with ICD ground plane
P3 16102	PW4098. BM Lip	Aft	BOM	BOM Treated	BOM treated	Keel to mics	Diagnostics: Prod inlet baseline with BOM Trt FFCC with NO ICD ground plane
S1 16103	Boeing Ideal Scarf	Aft	BOM	Treated diffuser and lip	BOM treated	Keel to Mics	Diagnostics: BMTs, FFCC Modal array NO ICD ground plane
S3 16104	Boeing Ideal Scarf	Aft	BOM	Treated diffuser and lip	BOM treated	Keel to Mics	Diagnostics: BMTs, FFCC Modal array, Flow viz tufts near inlet crown, NO ICD ground plane
S13A 16105	Boeing Ideal Scarf	Aft	BOM	HW bottom diffuser and lip	BOM treated	Keel to mics	Effect of inlet treatment at keel; HW ±45° about keel from "A" flange to inlet highlight
S15A-1 16106	Boeing Ideal Scarf	Aft	BOM	HW circumfer. strip	BOM treated	Keel to mics	Effect of Inlet HW 3-in. wide circumferential strip just fwd of "A" flange
S15A-3 16107	Boeing Ideal Scarf	Aft	BOM	Treated diffuser and lip	BOM treated	Keel to mics	Effect of HW Inlet Splices 3 Eq Sp 3- by 6-in. axial splices just fwd of "A" flange
S15-A4 16108	Boeing Ideal Scarf	Aft	BOM	HW throat and lip at keel	BOM treated	Keel to mics	Effect of inlet throat and lip treatment at keel; HW ±45° about keel
S16 16109	Boeing Ideal Scarf	Aft	BOM	Treated diffuser and lip	BOM treated	Keel rotated with keel to ground	Effect of scarf geometry on directivity
S13-A1 16112	Boeing Ideal Scarf	Aft	BOM	HW at keel diffuser only	BOM treated	Keel rotated with keel to ground	Effect of inlet diffuser treatment at keel; HW ±45° about keel from "A" flange to inlet throat
S17 16113	Boeing Ideal Scarf	None	BOM	Treated diffuser and lip	BOM treated	Keel To Mics	Contribution of aft radiated noise with Boeing Ideal Scarf inlet; Compare with Run 16065, Production BOM treated inlet
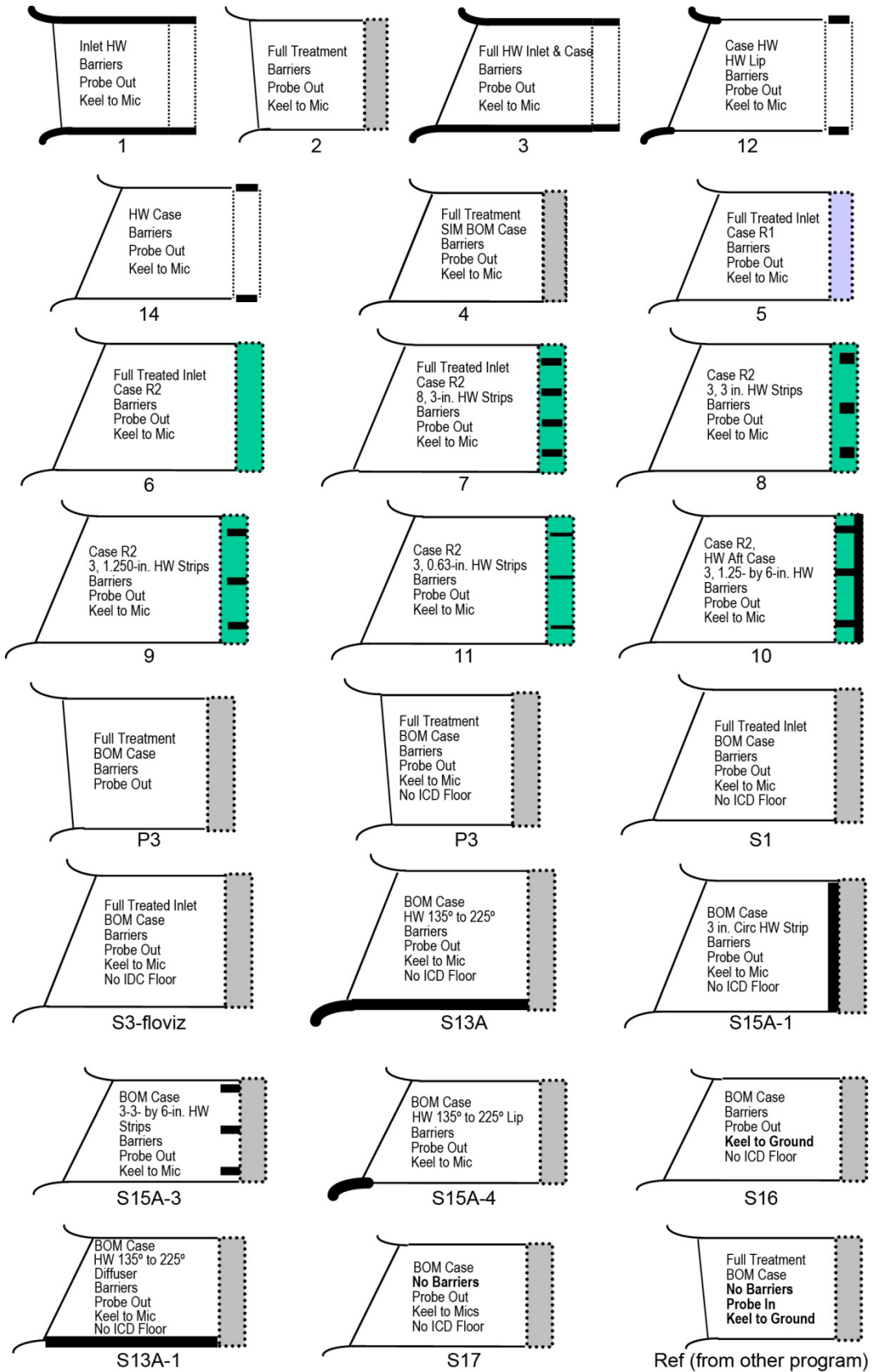
Figure 29.—Phase 1A and 1B Configurations.

A data point information summary and recorder log were maintained for each data acquisition period. The log contains pertinent information about the test; especially the engine model, engine number, test date, configuration definition, low rotor speed, meteorological conditions, time and date. The same information was also part of each data record as stored on the PW Acoustic Data Base and was included when the data is transmitted to the customer. See the Appendix. A chronological record of the record number, engine low rotor speed, time of data point, outside temperature, relative humidity, and a channel by channel record of the amplifier gain or attenuator settings were also maintained.

At the conclusion of the acoustic data acquisition for each engine condition, the data point was accepted based on meeting all the following criteria: 1) Data acquisition successfully completed and all required acoustical signals appeared good. 2) All weather parameters remained within prescribed limits throughout the acquisition time period. 3) The engine performance was within the prescribed target condition limits. 4) There was no suspected contamination of the signals from aircraft flyovers or other test stand.

3.2.4 Test Data Processing Procedures for Far Field Real Time Data

3.2.4.1 Data Corrections

Appropriate corrections to the time averaged one-third octave band and narrowband sound pressure levels were applied to account for:

- Microphone pressure response
- Pressure-to-free-field response for 90° incidence, microphone protective grids on
- Pistonphone reference amplitude response
- Microphone system electrical frequency response
- Real time data reduction system response
  - Analyzer effective bandwidth response

3.2.4.2 Adjustment to Reference Day Atmospheric Conditions

Differences between test and reference day atmospheric absorption coefficients obtained from ARP 866A were applied to each appropriate one-third octave band sound pressure level over the measurement distance. The reference day conditions are 77 °F (25 °C) and 70 percent relative humidity.

4.0 Test Results

4.1 Far Field Data

This section presents the far field noise results for all the configurations tested. All data is inlet radiated noise and has been "flown" at typical 777 approach (Mtip ~ 0.8) and cutback (Mtip ~ 1.1) conditions and altitudes. The data has been adjusted to remove the "leakage" of low frequency jet noise around the aft barrier at high powers. Results and comparisons are presented for the following configurations:

- Production inlet and hardwalled production inlet – baseline
- Hardwalled production inlet and hardwalled scarf inlet
- Benefits of treated scarf inlet plus front fan containment case (FFCC) configurations
- FFCC benefits
- Scarf inlet diffuser treatment benefits
- Inlet Lip Treatment Benefits
- FFCC splice penalties
- Inlet splice penalties
- Scarf inlet orientation effects
- Scarf inlet effect on aft noise

For each of these comparisons a schematic is presented that describes the configurations being compared which is followed by a bar graph that shows the comparison benefit or debit. Following these results graphs are presented that show noise measurements for approach and cutback versus far field mic angle and SPL versus frequency at the mic angle position of interest.

4.1.1 Production Inlet Versus Hardwall Production Inlet—Baseline

The first result shown in Figure 30 presents a baseline comparison of the fully treated production inlet compared to a hardwalled production inlet to establish the benefit for production inlet treatment. As indicated in the bar graph the treated inlet provides a 7.2 dB benefit at cutback and a 2.8 dB benefit at approach. These attenuations represent noise energy reductions of about 80 and 45 percent, respectively. As shown in Figure 31, significant liner attenuations are evident over a wide range of angles and frequencies due to the current production liner.
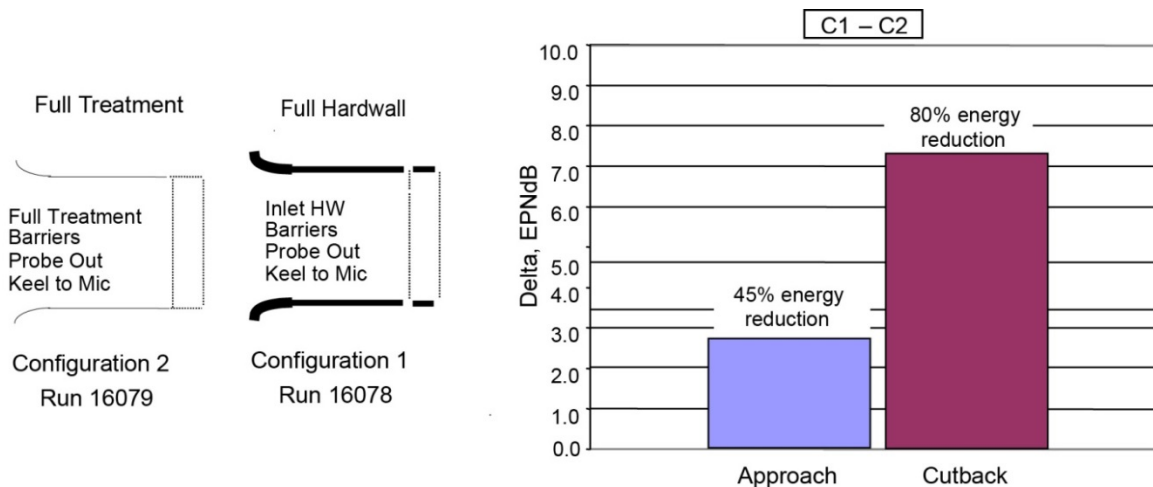
Figure 30.—Treated production inlet versus hardwall production inlet.
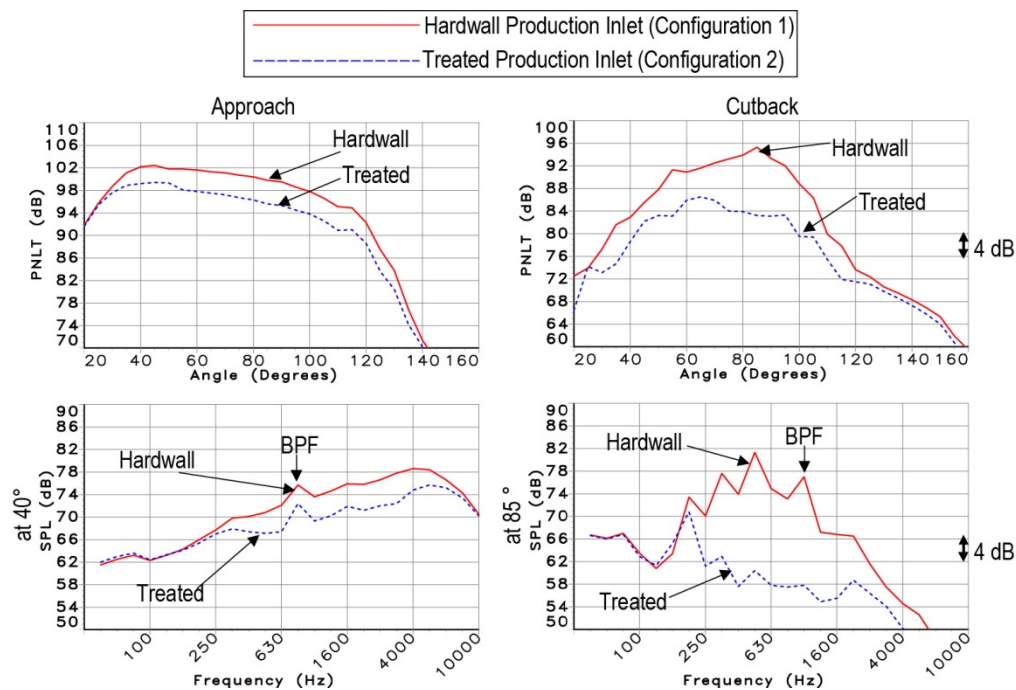
Figure 31.—Production inlet and case noise measurements.
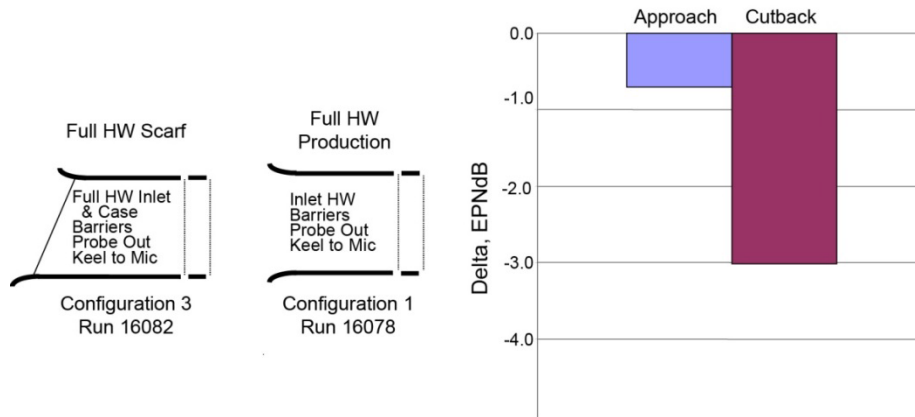
Figure 32.—Hardwall scarf versus hardwall production inlet.
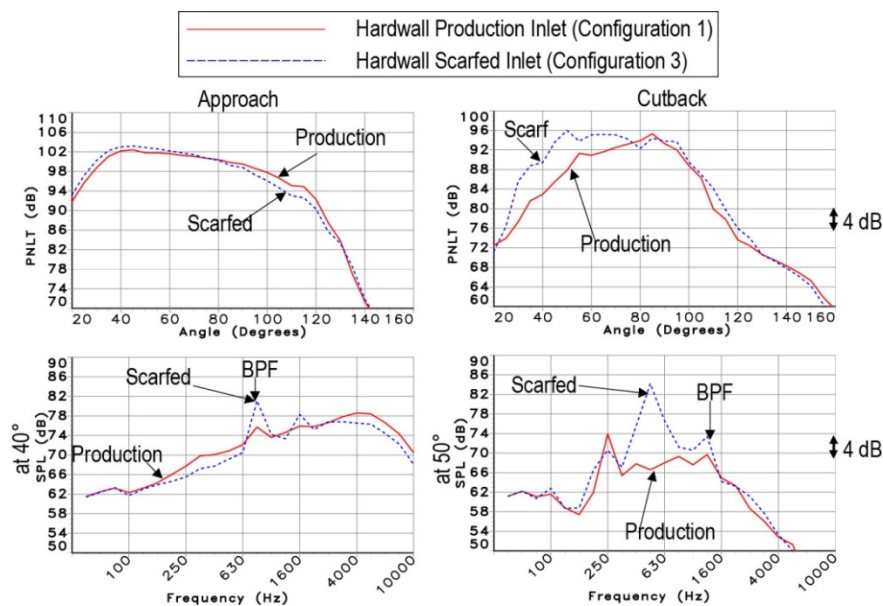
Figure 33.—Hardwall scarf inlet versus hardwall production inlet noise measurements.

4.1.2 Hardwalled Scarf Inlet Versus Hardwalled Production Inlet

In comparing the hardwalled scarf inlet and the hardwalled production inlet, Figure 32 shows that the scarf inlet is noisier by 3.0 dB at cutback and 0.7 dB at approach than the production inlet. As shown in Figure 33, at approach power the scarf inlet was actually quieter at most angles and frequencies, but an inspection of the spectra shows that there is a source of BPF and 2 BPF noise for the scarf inlet that has been attributed to flow distortion from the crown region of this inlet. Similarly at cutback power, there is an increase in BPF noise and buzzsaw noise for the scarf inlet, particularly at angles near 50°. These effects will be discussed in more detail later in this report.

4.1.3 Benefits of Treated Scarf Inlet Plus FFCC

In Figure 34 the package of principle features of this noise reduction program are compared to a fully hardwalled version of the scarf inlet. Configuration 5, which comprises the fully treated scarf inlet and the R1 BFG FFCC (two in. deep double layer treatment with perforated polyurethane face sheet) and Configuration 6 featuring the fully treated scarf inlet with R2 FFCC (R1 case with the perforated polyurethane removed) are compared to a fully hardwalled scarf inlet and FFCC (Configuration 3). The fully treated scarf inlet with a simulated production FFCC (Configuration 4) is also compared to the fully hardwalled scarf inlet and FFCC.

As indicated in Figure 34, the fully treated scarf inlet with the R1 FFCC produced the greatest noise reduction compared to the fully hardwalled inlet and FFCC, indicating that the higher resistance liner associated with the perf poly face sheet is better, particularly at cutback power where the combined inlet and fan case treatment provided almost 13 EPNdB inlet noise reduction. This corresponds to noise energy suppression of about 95 percent. As shown in Figure 35, the extraneous source of BPF and buzzsaw noise from the scarf inlet has been attenuated by as much as 25 dB at cutback power.

The bar chart of Figure 36 shows how the best scarf inlet configuration (C5) compares to the fully treated production inlet (C1) when both are referenced to the hardwalled production inlet and FFCC. The chart shows the C5 scarf inlet configuration provides an 80 percent dB suppression improvement at approach and a 50 percent dB improvement at cutback compared to the production inlet (C1).
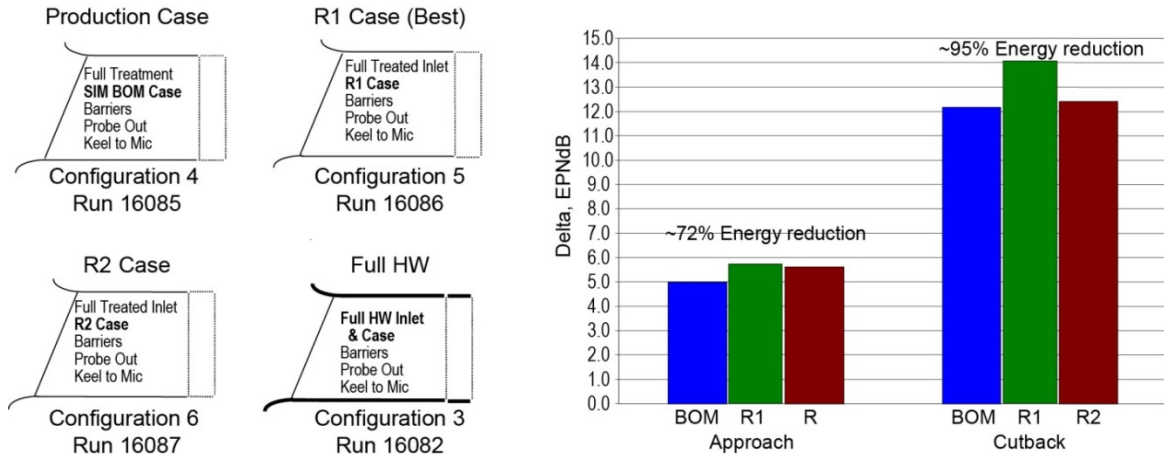
Figure 34.—Total scarf inlet and FFCC case effectiveness.
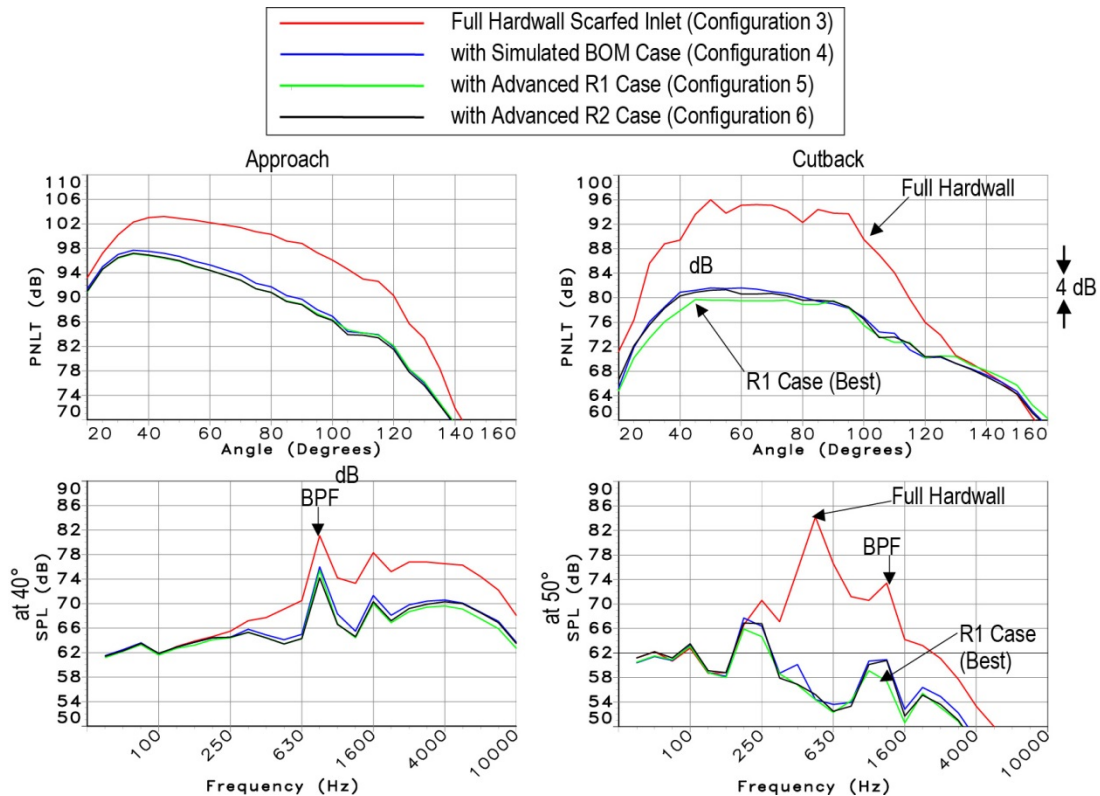
Figure 35.—Total scarf inlet and FFCC case noise measurements.
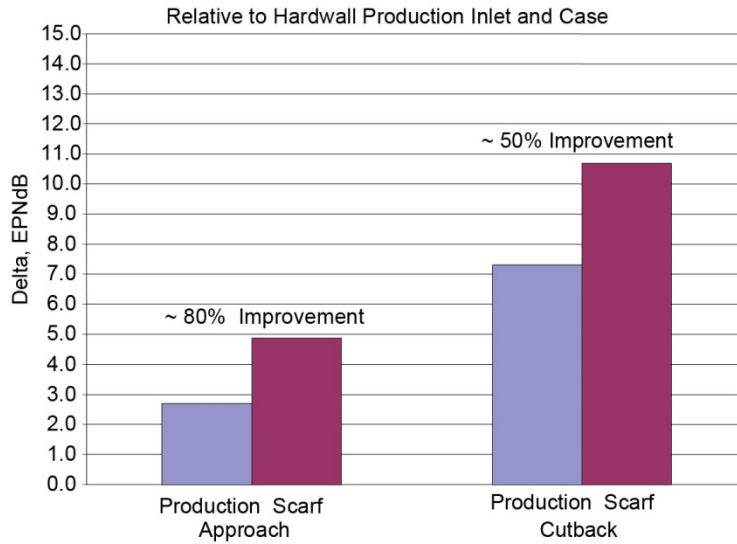
Figure 36.—Best scarf inlet benefit relative to production inlet.
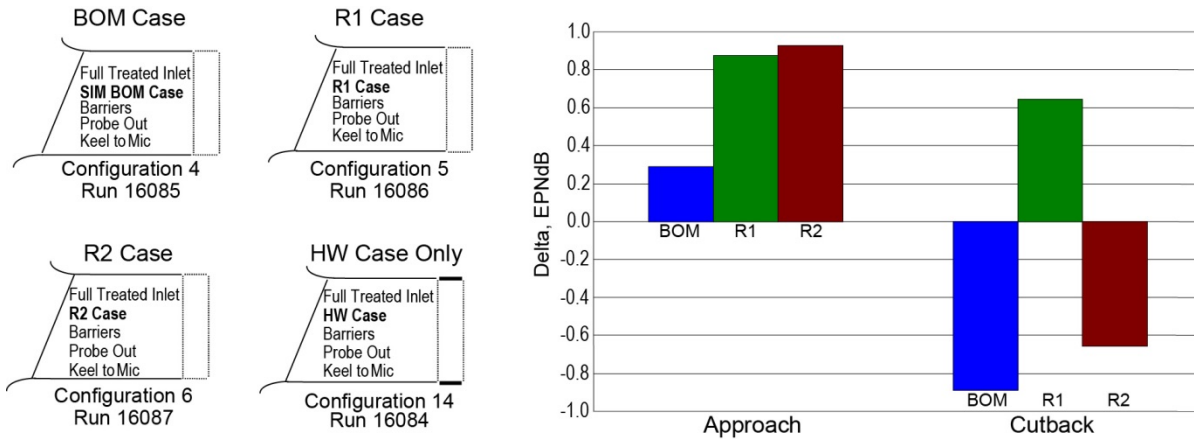
Figure 37.—Forward fan containment case benefits.

4.1.4   Forward Fan Case Treatment Benefits

Figure 37 shows the results of comparisons of the R1, R2, and simulated BOM cases to a hardwalled case, all when installed with a fully treated scarf inlet. The current BOM liner in the PW4098 was only moderately effective at approach power because of area and backing depth constraints imposed by fan containment concerns. At cutback power this BOM treatment actually increases noise relative to the hardwalled case. This is attributed, as discussed in more detail later, to noise scattering by the number and width of hardwall splices in the BOM case, which separate the three circumferential segments in this design. At approach power it can be seen that both the advanced liner impedances provided almost 1 EPNdB noise suppression (Figure 38). However, at cutback power the R1 resistance associated with the perforated poly film provided the best attenuation. Evidently the removal of this film, providing the R2 impedance, uncovered some impedance non-uniformities that actually increased the noise at cutback power through noise scattering.
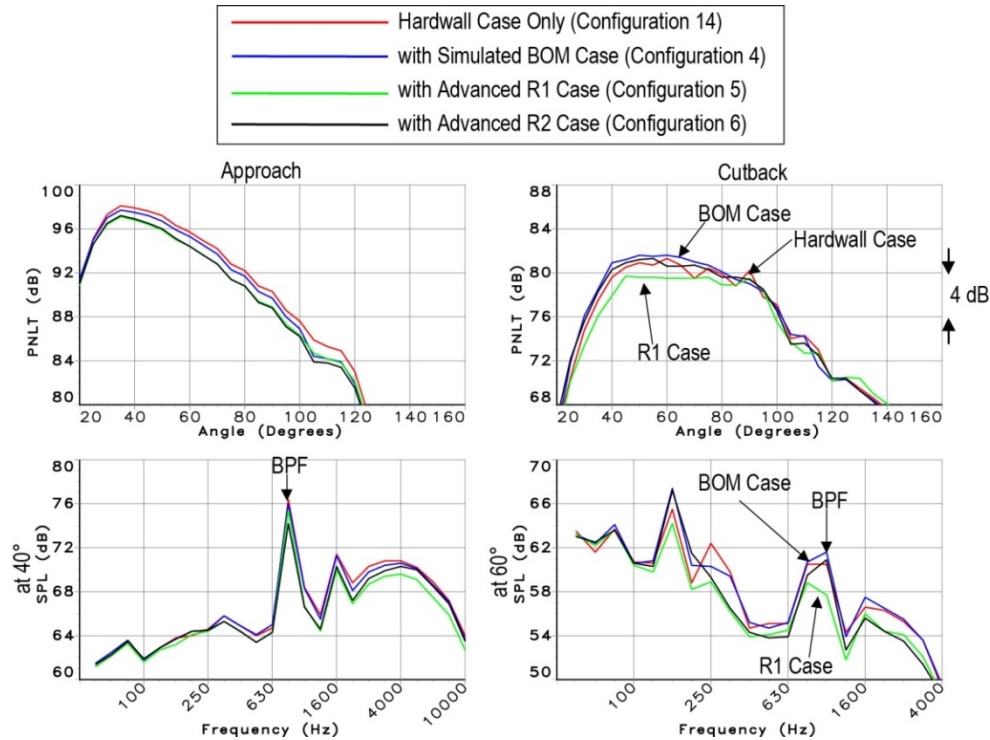
Figure 38.—Forward fan containment case treatment noise measurements.

4.1.5 Scarf Inlet Diffuser Treatment Benefits

In order to evaluate the effectiveness of the diffuser section of the scarf inlet, comparisons were made between a fully treated diffuser (C12) and a hardwalled diffuser (C3) with the inlet lip and FFCC hardwalled. A comparison was also made between a diffuser with its bottom 90° hardwalled (C13A-1) and fully treated (C S1) since Boeing analytical studies indicated that bottom diffuser treatment may be ineffective. Figure 39 presents these configurations and the corresponding noise differences. The bar chart shows that full diffuser treatment relative to hardwall provides a 4.5 dB benefit at approach and a 11.7 dB benefit at cutback. It also shows that 90° of hardwall on the diffuser bottom produces very little noise difference relative to a fully treated diffuser, thereby validating the Boeing analysis. Figure 40 and Figure 41 show the noise directivity and spectral features of these benefits.
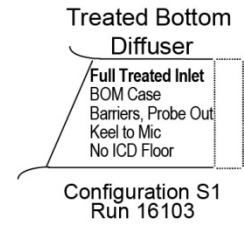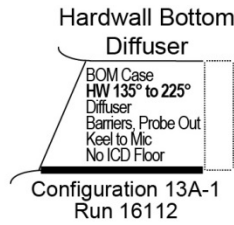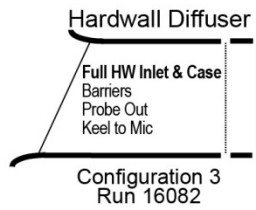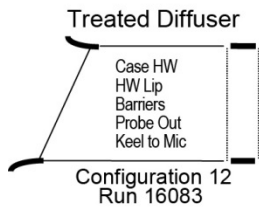
Configuration 12 versus 3

Configuration 13A-1 versus S1
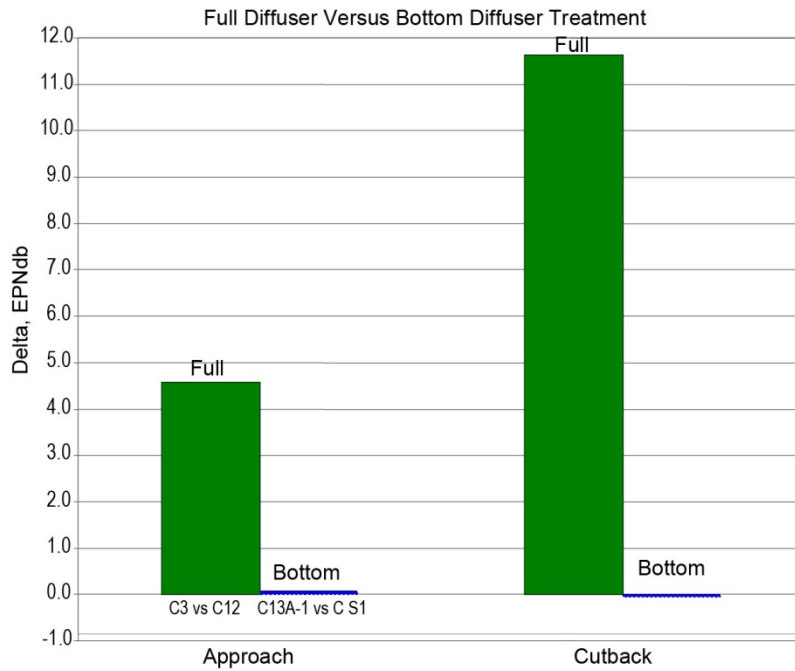
Figure 39.—Diffuser treatment benefits.
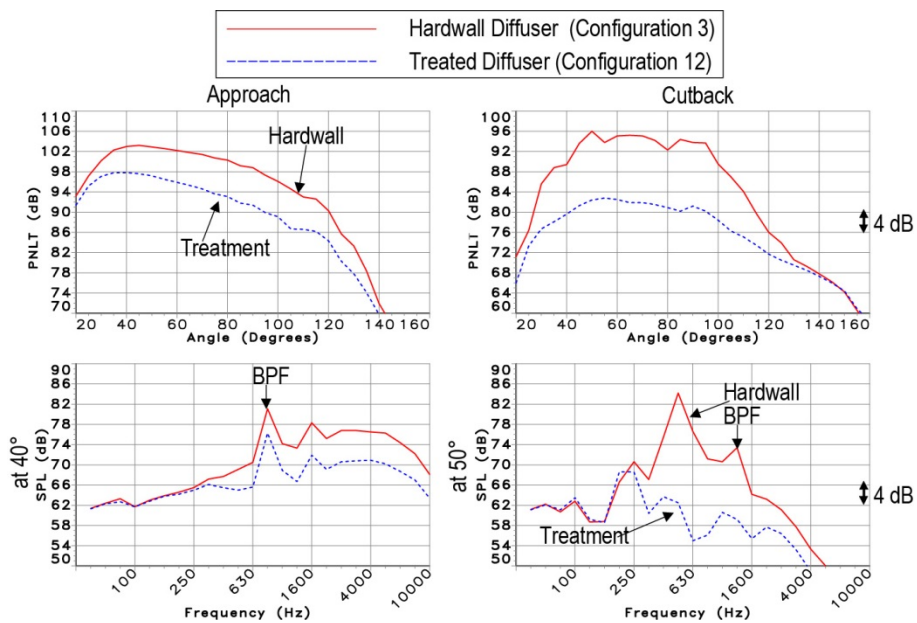
Figure 40.—Full diffuser treatment noise measurements.
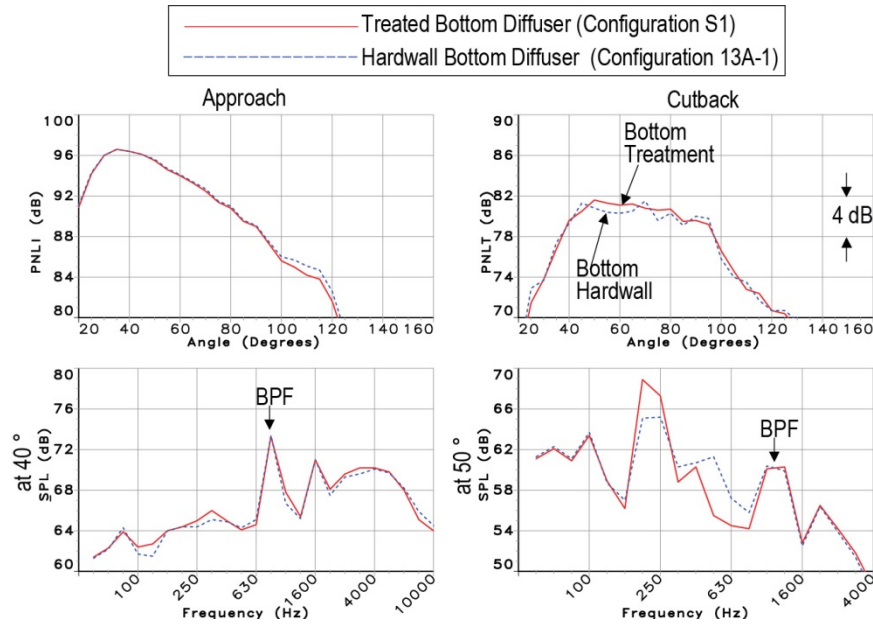
Figure 41.—Bottom diffuser treatment noise measurements.

Configuration 14 versus 12

Configuration 15A-4 versus S1
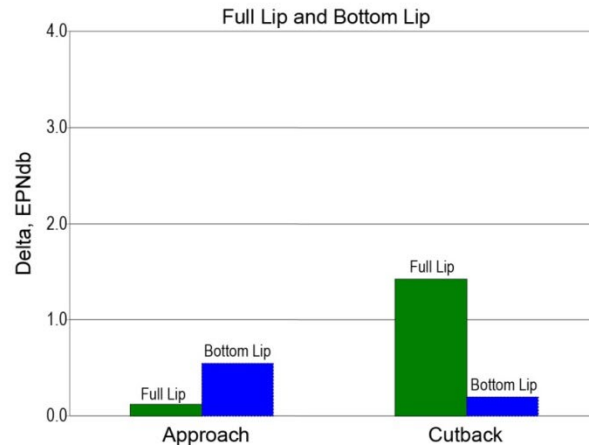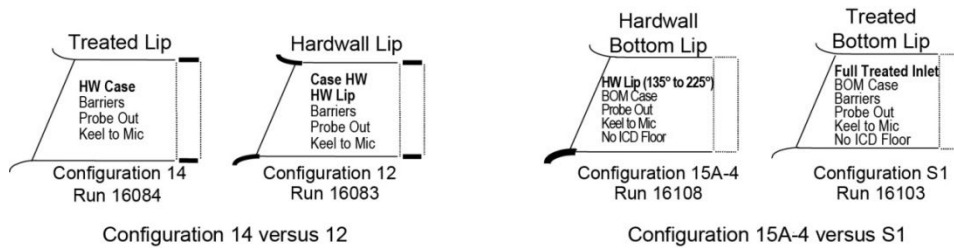
Figure 42.—scarf lip treatment benefits.

4.1.6 Inlet Lip Treatment Benefits

The effectiveness of treatment on the lip section of the inlet was studied by comparing a fully treated lip (C14) to a hardwalled lip (C12), both with a hardwalled FFCC and by comparing a fully treated lip (C S1) to a lip with the bottom 90° hardwalled (C15A-4), both with the BOM FFCC. The results show that full lip treatment is better than a full hardwall lip by 1.5 dB at cutback and ~0.1 dB at approach. A lip with the bottom 90° hardwalled is noisier than a fully treated lip by ~0.2 dB at cutback and 0.5 dB at approach. Figure 42 and Figure 43 show the results.
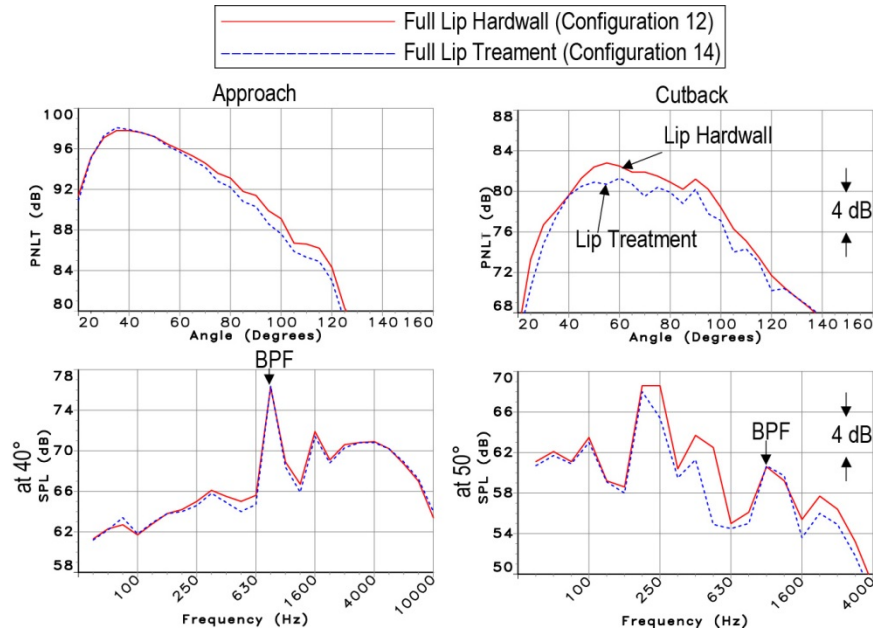
Figure 43.—Full lip treatment with hardwall case noise measurements.

4.1.7 Fan Case Liner Splice Penalties

Configurations were tested to determine what effect treatment splices in the FFCC have on inlet noise. A number of previous studies at PW and by other engine and nacelle manufacturers have indicated that these splices can have a large impact on perceived noise levels, primarily due to increases in the blade passing frequency (BPF) tone levels. This is particularly the case at high subsonic and low supersonic fan tip speeds. PW has developed an analytical model for this phenomenon that involves scattering of BPF noise by the impedance discontinuities that these splices represent. This scattering involves a transfer of energy from the very high levels of axially decaying BPF tone energy very near the fan into propagating modes at the BPF frequency. The degree of energy scattering is predicted to increase with both the splice width and the splice number. If the treatment can be made very uniform near the fan, this high amplitude decaying sound field will decay uninterrupted and will not scatter high sound energy into propagating modes. In many cases this is not possible and significant scattering has been observed. In some cases, it has even been found desirable to completely hardwall the treated segments just forward of the fan in order to avoid this BPF noise increase.

In the current test program the number and the width of various simulated splices (simulated by applying strips of tape for testing) were investigated as shown in Figure 44 to Figure 47. The results show that uniformity of treatment near the fan is very important. Figure 44 shows the effects of splice number, for a constant splice width of 3 in. As expected eight splices results in more scattering (higher noise) than three splices at both approach and cutback conditions. At cutback power, where the blade tip speeds are slightly supersonic, the BPF noise energy is carried by a series of oblique shock waves from the tip regions of each blade. The strength of these shockwaves decays rapidly forward of the fan blades in a hardwall duct. But if impedance discontinuities (e.g., splices) are placed in this region, the shockwave energy is scattered into propagating modes, whose levels can be quite high, particularly if the number or width of these discontinuities is large. Figure 44 shows that at this condition (i.e., cutback power), a large penalty of 4 EPNdB was measured for C7, featuring eight splices, 3 in. wide. Figure 45 shows that this is due primarily to the fact that BPF levels were increased by almost 10 dB for this configuration, relative to a uniform hardwalled FFCC.
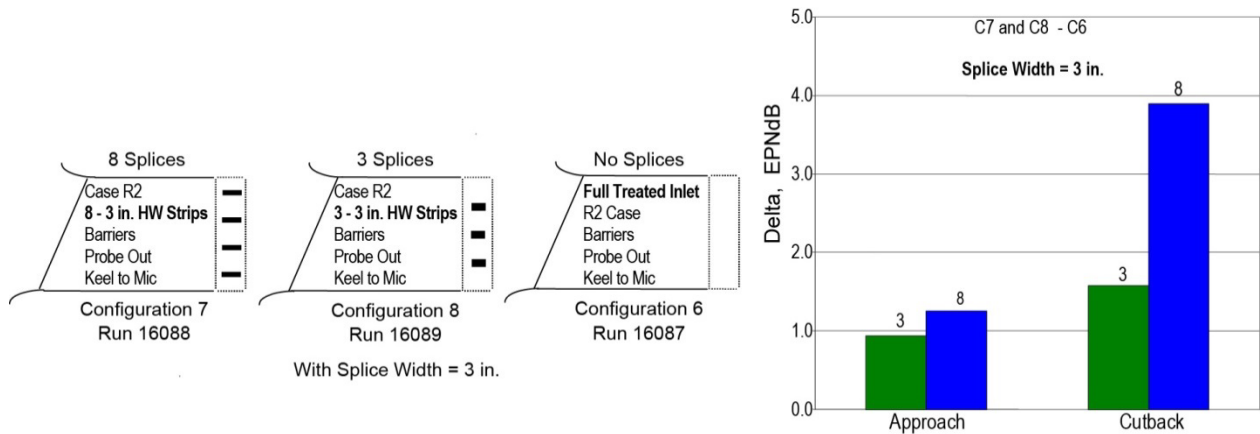
Figure 44.—Effect of splice number.
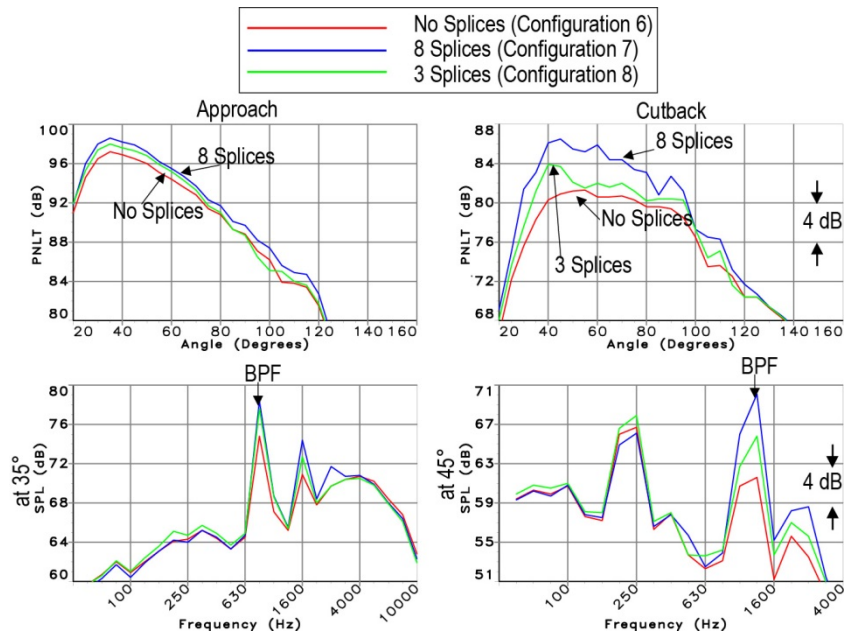
Figure 45.—Splice number noise measurements.

The effect of splice widths ranging from 0.62-in. wide to 3.0 in. wide for a constant splice number (i.e., three) is shown in Figure 46 and Figure 47. Here it can be seen that there is very little penalty if the splices can be made thin enough (e.g., about 0.62-in. wide). However, when the three splices were made to be 3 in. wide, a penalty of up to 1.6 EPNdB resulted at cutback power. Again, this resulted from a BPF tone level increase of about 6 dB, as shown in Figure 47.

With 3 Splices

3 in. Splices
Case R2
3 - 3 in. HW Strips
Barriers
Probe Out
Keel to Mic
Configuration 8
Run 16089

1.25 in. Splices
Case R2
3 - 1.25 in. HW Strips
Barriers
Probe Out
Keel to Mic
Configuration 9
Run 16090

0.62 in. Splices
Case R2
3 - 0.62 in. HW Strips
Barriers
Probe Out
Keel to Mic
Configuration 11
Run 16091

No Splices
Full Treated Inlet
R2 Case
Barriers
Probe Out
Keel to Mic
Configuration 6
Run 16087

Splice Width Penalty
C8, C9, C11 versus C6

Splice Number = 3
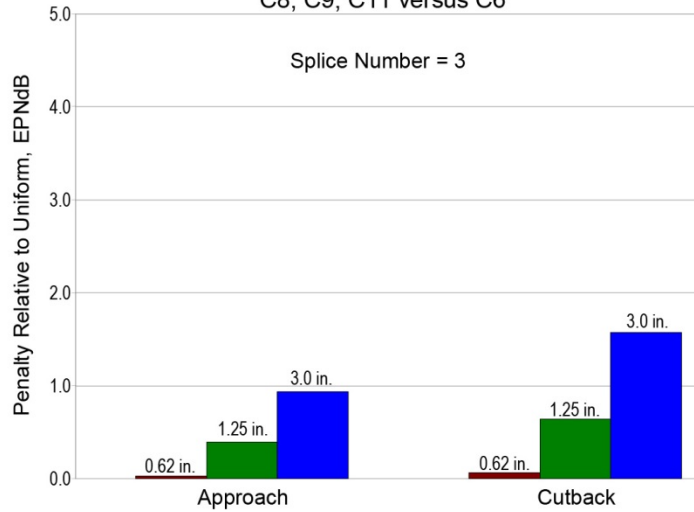
Figure 46.—Fan case splice penalties.

Full Treatment, No Splices (Configuration 6)
3 in. Splices (Configuration 8)
1.25 in. Splices (Configuration 9)
0.62 in. Splices (Configuration 11)
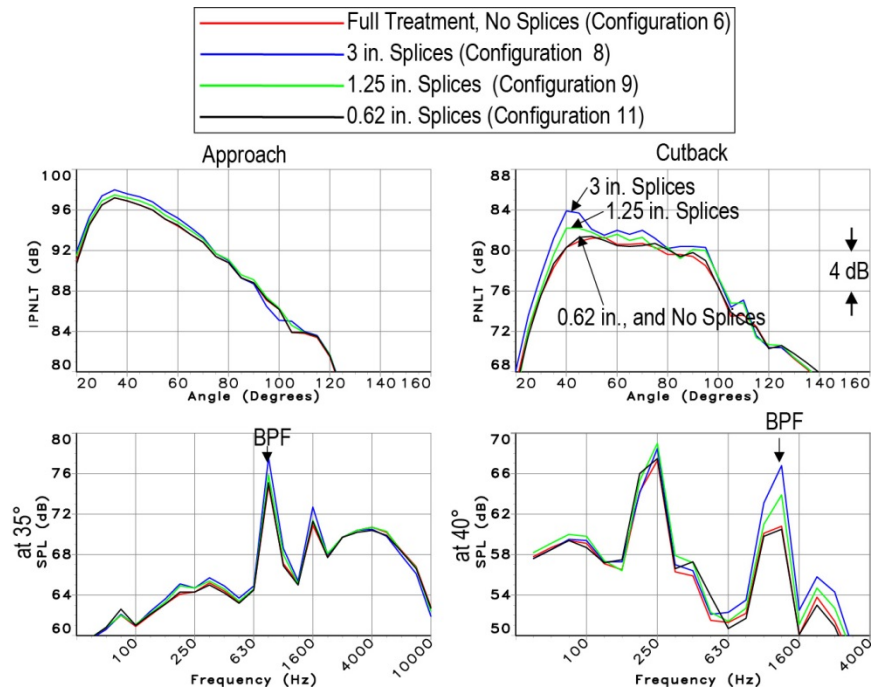
Figure 47.—Fan splice width noise measurements.

4.1.8 Inlet Liner Splice Penalties

The effects of placing splices in the inlet liner forward of the FFCC was also measured. A circumferential splice forward of "A" flange (C15A-1) and three 3-in. wide axial splices (C15A-3) were investigated. Comparisons were made to C S1and are shown in Figure 48 to Figure 52. The effect of the uniform circumferential splice is seen to be about 0.2 to 0.4 EPNdB. This increase is entirely consistent with the loss of treated area associated with configuration 15A-1.

The effect of three, 3 in. splices in the inlet are shown in Figure 50. The noise penalty associated with these splices is seen to be minimal. For reference, the much larger penalties for this same splice simulation in the FFCC is also shown. The reason for the difference is that the inlet splices are spaced axially at a much larger distance from the fan blades, thus allowing the high levels of decaying BPF tone levels to decay naturally before getting scattered by the inlet splices. The message here is that it is extremely important to have treatment uniformity near the fan, but it is less important that uniformity exists for treatment further upstream.
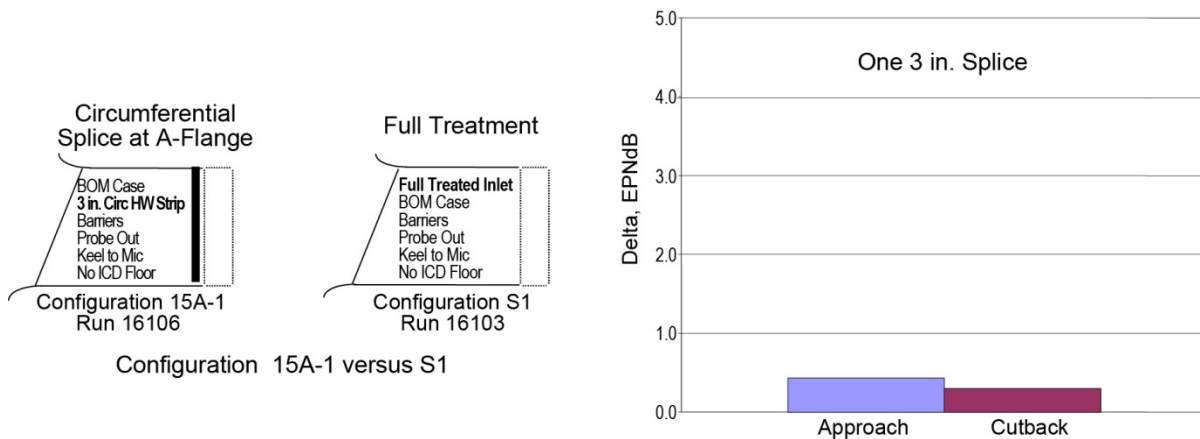
Figure 48.—Inlet circumferential splice penalty.
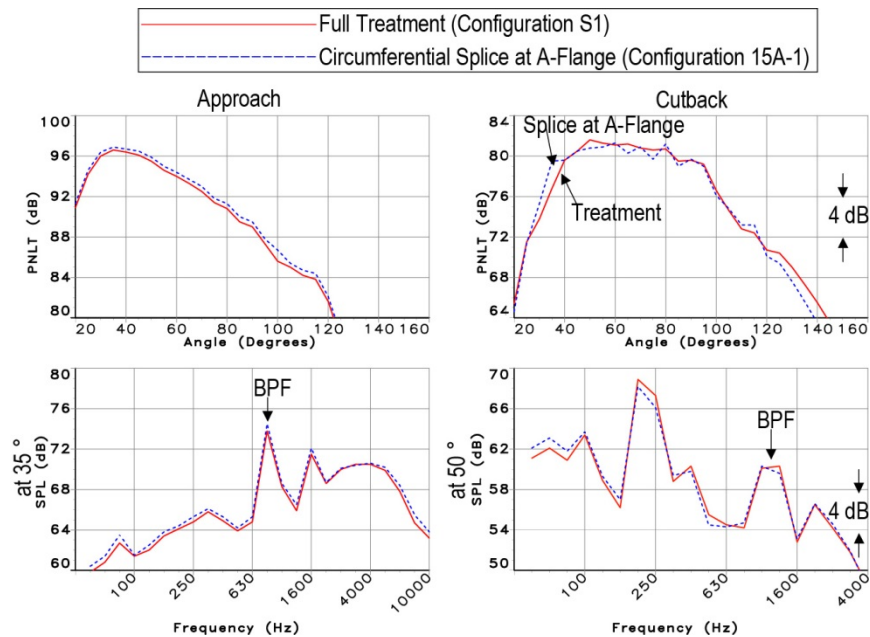
Figure 49.—Inlet circumferential splice noise measurements.
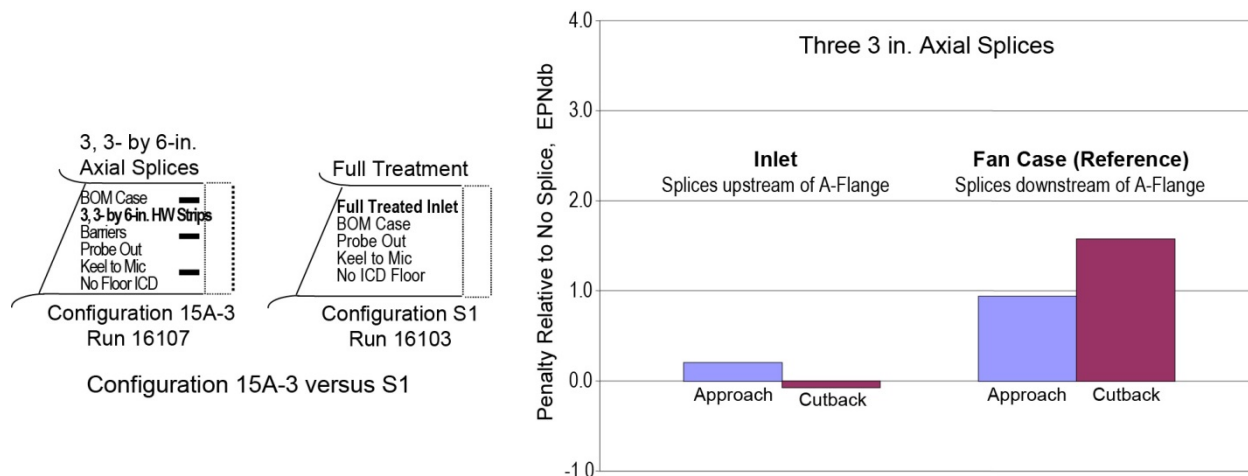
Figure 50.—Inlet versus fan case axial splice penalties.
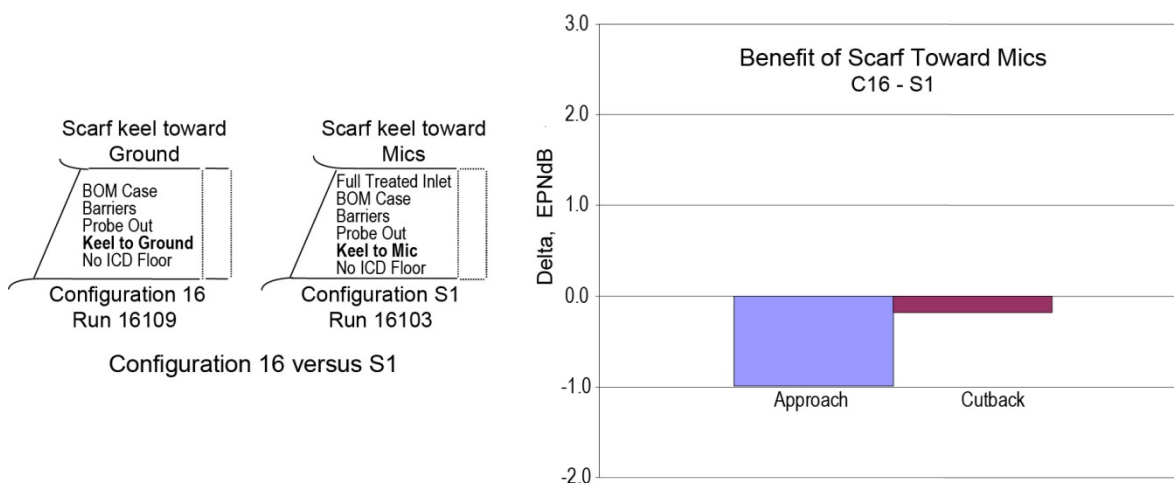
Figure 51.—Inlet orientation effects.

4.1.9   Inlet Orientation Effects

The effects of inlet orientation—scarf keel pointed toward the ground (C16) versus scarf keel pointed towards the mics (C S1)—were measured. The results showed no apparent benefit for the scarf keel being oriented towards the mics. As shown in Figure 50, noise measurements with the keel pointed to the mics were actually higher by 1.0 EPNdB at approach and ~0.1 EPNdB at cutback.

4.1.10   Scarf Effect on Aft Noise

The effect of the scarf inlet on aft fan noise was measured by removing the wall barriers and comparing a production inlet configuration with the scarf inlet and a BOM FFCC, (C17). The results in Figure 53 show that aft fan noise is not appreciably influenced by the scarf inlet.
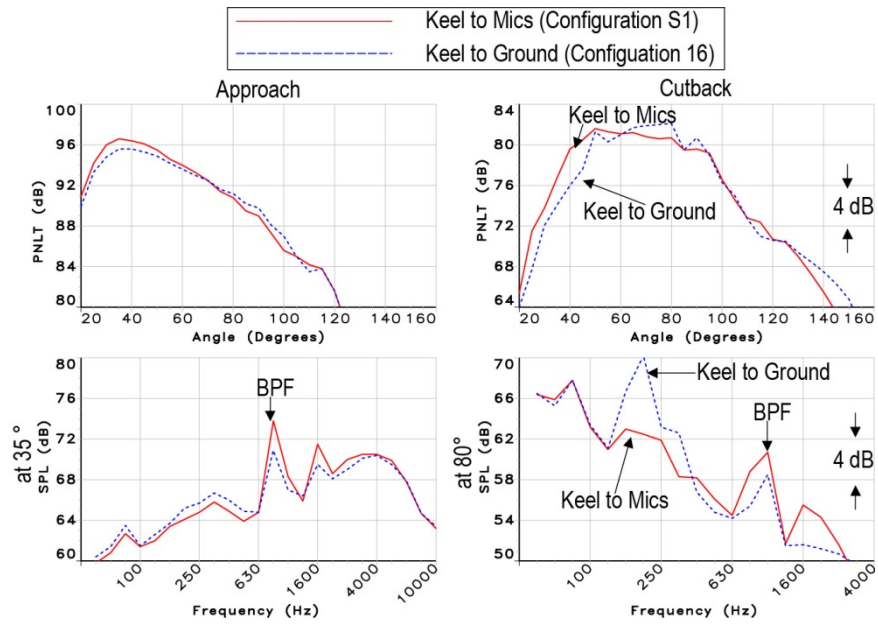
Figure 52.—Inlet orientation effects: benefits of scarf toward mics.
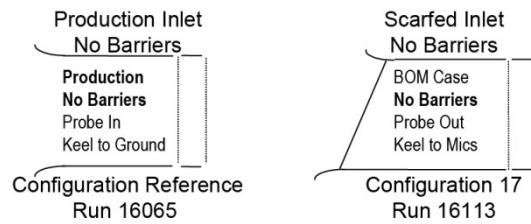
Figure 53.—Scarf effect on aft noise.
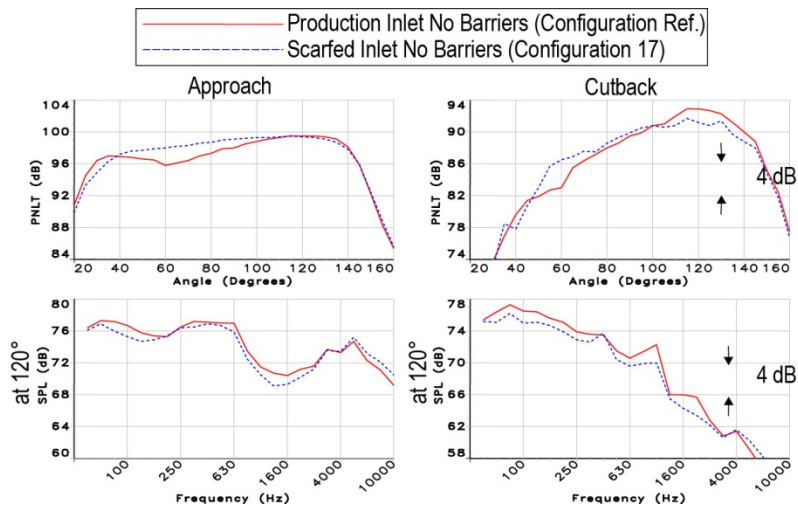
Figure 54.—Scarf effects on aft noise—noise measurements.

4.1.11 Summary of Various Treatment Benefits

Figure 55(a) and (b) summarize the benefits at cutback and approach powers, respectively, associated with various segments of treatment that were tested in the production inlet, the scarf inlet and the forward fan containment case (FFCC). These benefits are plotted against treatment length divided by duct radius. At cutback power, the complete production package (inlet and FFCC) are seen to result in about 7 EPNdB noise reduction. The complete scarf inlet (diffuser plus lip), combined with the advanced R1 fan case, resulted in a benefit of almost 11 EPNdB, or about 4 EPNdB more than the production design. The treatment non-uniformities contained in the R2 and production fan cases actually had a negative benefit on noise for reasons discussed earlier.

At approach power (see Figure 55(b)) the total noise benefit of the scarf inlet and advanced R2 FFCC treatment is seen to be about 5 EPNdB, compared to less than 3 EPNdB provided by the production inlet and FFCC treatment. The slopes of the attenuation versus L/R curve segments shown in Figure 55(a) and (b) are an indication of how effective (e.g., attenuation/treatment area) the various sections of liner are in the inlet and FFCC. These slopes are plotted in Figure 56. Here it can be seen that the scarf inlet treatment is more effective than the production inlet at both approach and cutback conditions. In addition, the R1 and R2 FFCC liners both provided about 4 EPNdB per L/R at approach power, similar to the scarf inlet.
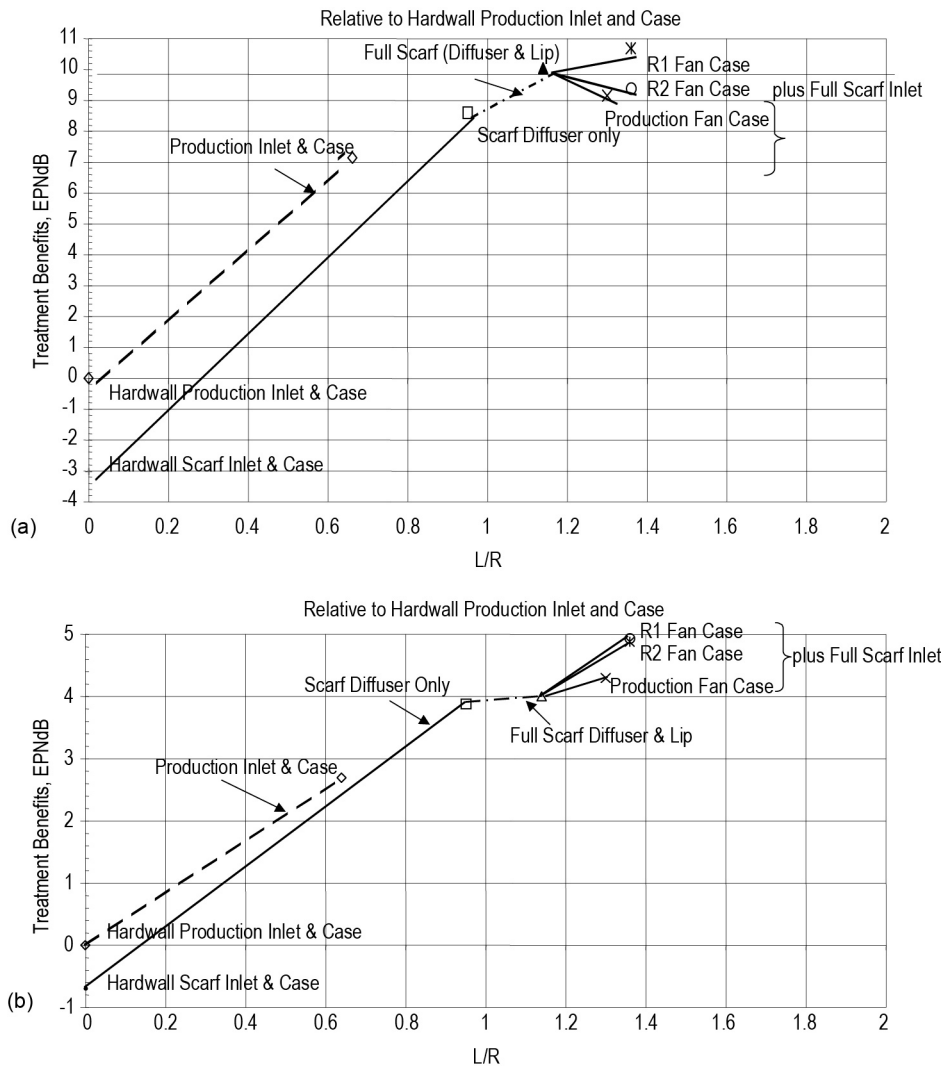
Figure 55.—(a) Summary of inlet and fan case treatment benefits at cutback power.
(b) Summary of inlet and fan case treatment benefits at approach power.
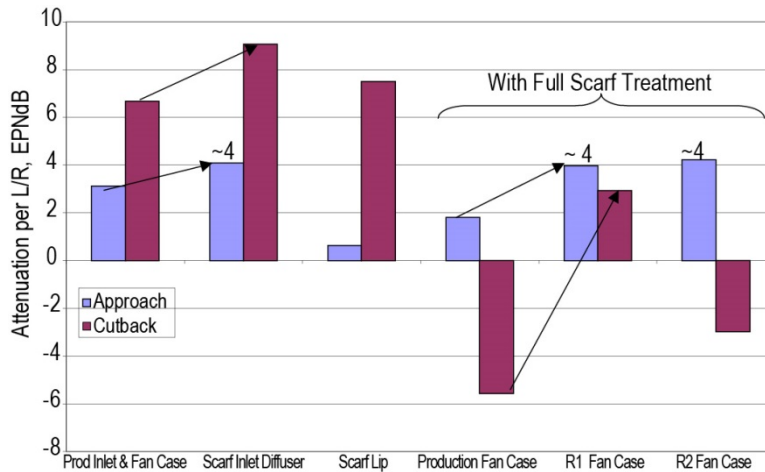
Figure 56.—Relative effectiveness of various liners—normalized by L/R

4.1.12 Conclusions—Far Field Data

- The treated scarf inlet with the advanced (R1) FFCC is 2 to 4 EPNdB quieter in inlet fan noise than the production inlet and fan case at approach and cutback powers. Approximately 80 percent dB nacelle suppression improvement was observed at approach power and 50 percent dB suppression improvement at cutback power.
- The Scarf inlet with advanced FFCC has a significant BPF distortion tone, preventing larger benefits. Without the extra BPF noise an additional 1 EPNdB in noise reduction was expected.
- The hardwalled scarf inlet has higher buzzsaw noise levels than the production inlet but treatment suppressed it very well.
- The bottom 90° of diffuser liner is ineffective at all conditions.
- The scarf lip liner effectiveness at cutback power is about the same per unit length as the diffuser treatment.
- The scarf lip liner at approach power is effective over a wide frequency range, but not for the BPF distortion tone thus preventing a significant EPNdB benefit.
- At approach power both advanced FFCC liners (R1 and R2) have the same effectiveness per unit length as the scarf inlet liner.
- At cutback power the higher resistance fan case liner (R1) showed a significant benefit while the lower resistance liner (R2) was detrimental, primarily due to impedance non-uniformities.
- Treatment uniformity near the fan is very important. Simulated production type hardwall splices in the FFCC liner show large penalties of up to 4 EPNdB at cutback power for eight 3 in. splices. Penalties increase with both splice number and width. The mechanism is scattering, by impedance discontinuities, of high level but fast decaying blade pressure fields at BPF ($m = B$) into high level propagating modes.
- The treatment uniformity further forward in the inlet is not critical. Penalties associated with axial or circumferential splices are associated only with lost treated area.
- There is no apparent benefit of the scarf keel being oriented toward the microphones, relative to being oriented 90° away. This may be due to the effect of the scarf geometry on distortion tone generation or on azimuthal buzzsaw noise variations.
- Aft fan noise is not influenced appreciably by the scarf inlet.

4.2   RDIFF Prediction Comparisons

4.2.1   RDIFF Prediction Code

The RDIFF computer code (Ref. 1) used for the acoustic design of the scarf inlet is a ray tracing code in which it was assumed that the noise source consisted of uncorrelated monopoles distributed over the outer 1/3 radius of the fan. The full 3D shape of the inlet was modeled with the lining distribution accounted for by specifying the lining's locally reacting impedance in lining segments. Twenty-nine lining segments were used to model the inlet and forward fan case. The effect of flow is considered for calculation of the liner impedance and for calculation of the ray incidence angle to the lining. The (plane wave) reflection coefficient is then calculated for each source ray. No nonlinear propagation effects (buzzsaw) are evaluated and ray diffraction is applied at inlet lip to account for sound propagation to the rear of the inlet.

4.2.2   Approach Power

4.2.2.1   Production Inlet—Approach Power

Figure 57 compares the RDIFF predictions for the fully treated production inlet (PTr) with test results. The predictions and data have been extrapolated to a nominal 777 approach condition. The prediction curves were generated by subtracting the production inlet RDIFF predicted 1/3 octave spectral and directional 1/3 octave SPL differences, (hardwall – full treatment), from the measured production inlet hardwall data. Comparisons are shown for the PNLT time history and spectra at angles from the inlet axis of 30° to 80°. The agreement of the prediction curves with the measured data is quite good until about 70°.
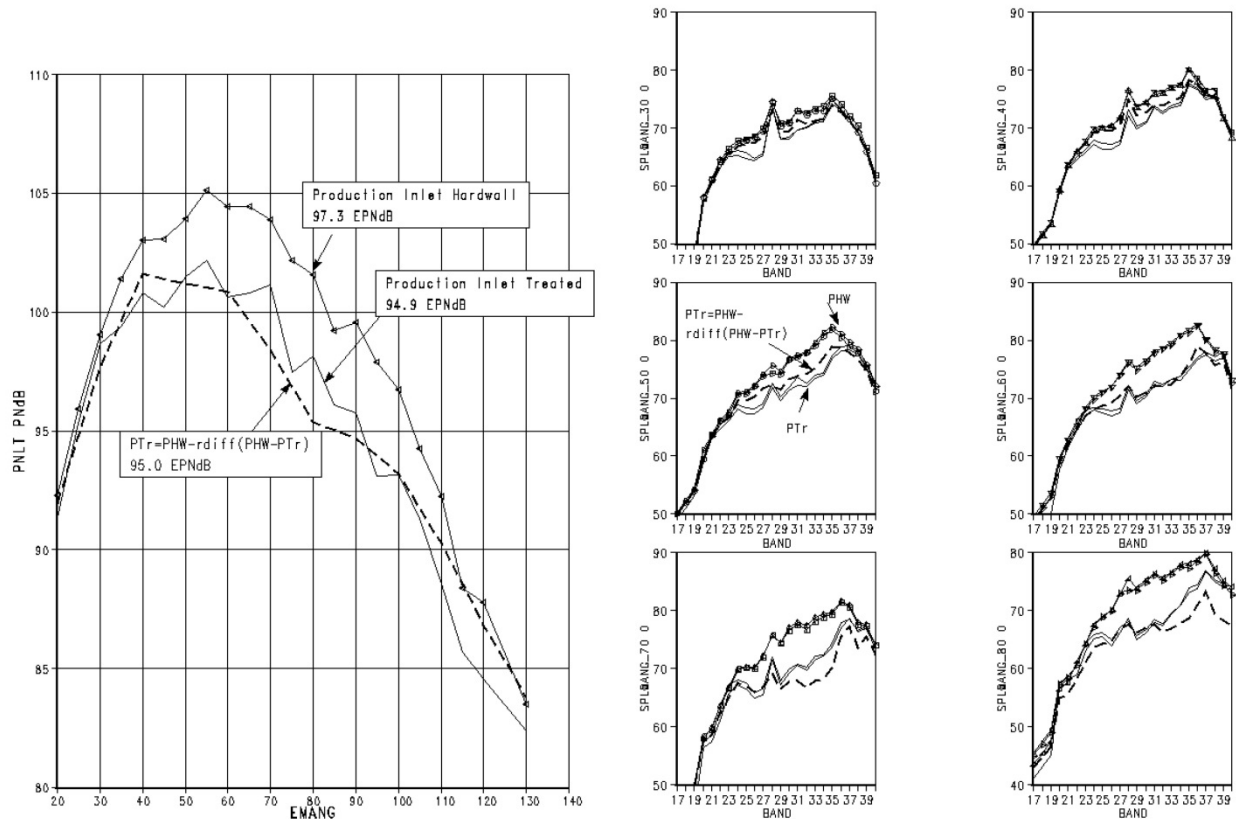
Figure 57.—Fully treated production inlet noise prediction—approach.

4.2.2.2   Scarf Inlet—Approach Power

Figure 58 shows the same comparison for the hardwall scarf inlet (SHW) at approach power. Again the RDIFF predicted difference between the hardwall production inlet (PHW) and the inlet configuration of interest was subtracted from the hardwall production inlet test data to obtain the prediction curves. For this comparison, only the effect of the inlet shape difference is calculated, no lining effects were included. It is seen that the prediction is quite good forward of 70°, except for the BPF and 2BPF tone increase observed with the scarf inlet relative to the production inlet.

The prediction/data comparison for the fully treated scarf inlet (STr) is shown in Figure 59. Again the prediction reference is the fully hardwall production inlet. As for the hardwall scarf inlet, the BPF/2BPF tone levels are not predicted by this RDIFF process. Forward of 70°, the predicted and measured spectra compare well except for the BPF/2BPF tones. But there are still problems with the aft angles.
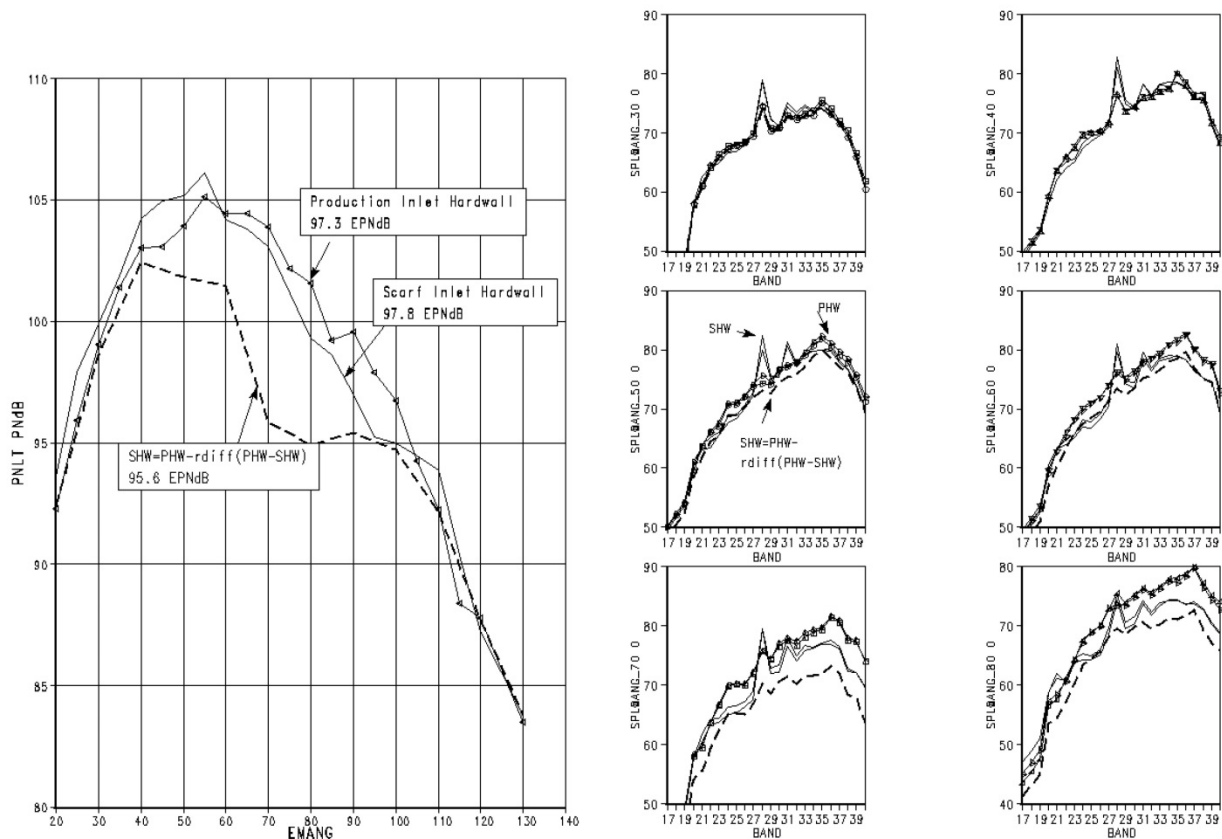
Figure 58.—Hardwall scarf inlet noise prediction—approach.
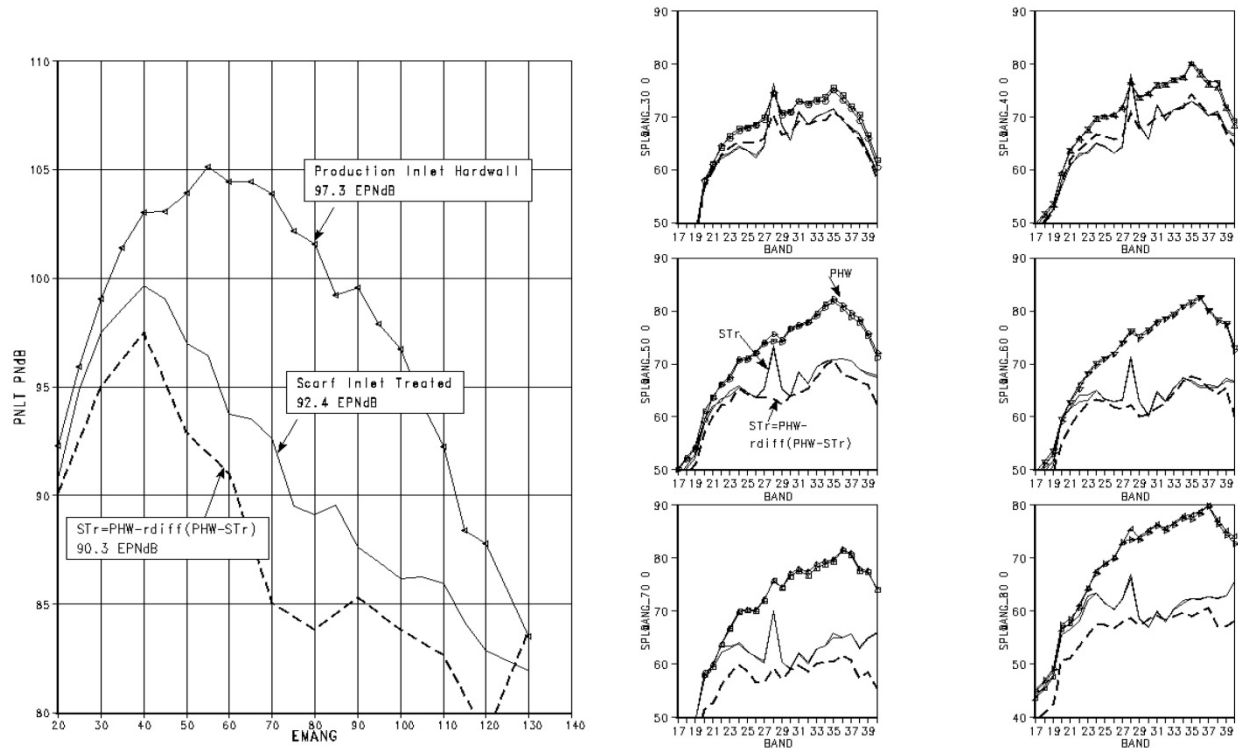
Figure 59.—Fully treated scarf inlet noise prediction—approach.

Figure 60 shows attenuation directivity examples for three one third octaves centered at 800 Hz, 2 and 4 kHz. The 800 Hz band contains the BPF, so the comparisons with the measured scarf inlet attenuations relative to the production inlet are poor because of the anomalous BPF source that occurred with the scarf inlet. Forward of 70°, with the above exception, the RDIFF predicted deltas compare well with the measured data. The 2 and 4 kHz comparisons are repeated in Figure 61 with the test results on the same plot as the RDIFF predictions for easier comparison. Aft of 70° the scarf inlet lining attenuation (SHW-STr) is somewhat under predicted. The production inlet lining attenuation (PHW-PTr) and the scarf shape effect (PHW-SHW) deltas are over predicted around 70° and 80° and mostly under predicted further aft. In this region the ray diffraction calculation controls the prediction for the scarf inlet but may not control the 70° and 80° region for the production inlet (This needs further investigation). The scarf inlet lining attenuation includes the effect of a treated lip. It appears that the attenuation of the diffracted rays with lip treatment is under predicted and the hardwall lip diffraction is inconsistently predicted.

Predicted attenuation spectra for angles 40°, 60° and 80° are compared to test data in Figure 62. The 40° and 60° comparisons are repeated in Figure 63 with the test results directly compared to the RDIFF predictions for easier comparison. The attenuations relative to the production inlet for the 1/3 octaves in the range of the BPF and 2BPF are generally poorly predicted. The measured scarf lining attenuation (SHW-STr) is seen to be lower at BPF than the adjacent frequencies as well. This is not predicted by the RDIFF code, but this may be related to the mode structure of the anomalous BPF source that occurred with the scarf inlet. The BPF tone attenuation for the production inlet lining is reasonably well predicted at 60° but is underpredicted at 40°.

RDIFF Predictions   Test Data

Predicted vs. Test Data
800 Hz, 2 kHz & 4 kHz

Scarf Shape = PHW-SHW
Prod Lining = PHW-PTr
Scarf Lining = SHW-STr
Scarf Shape+Lining = PHW-STr
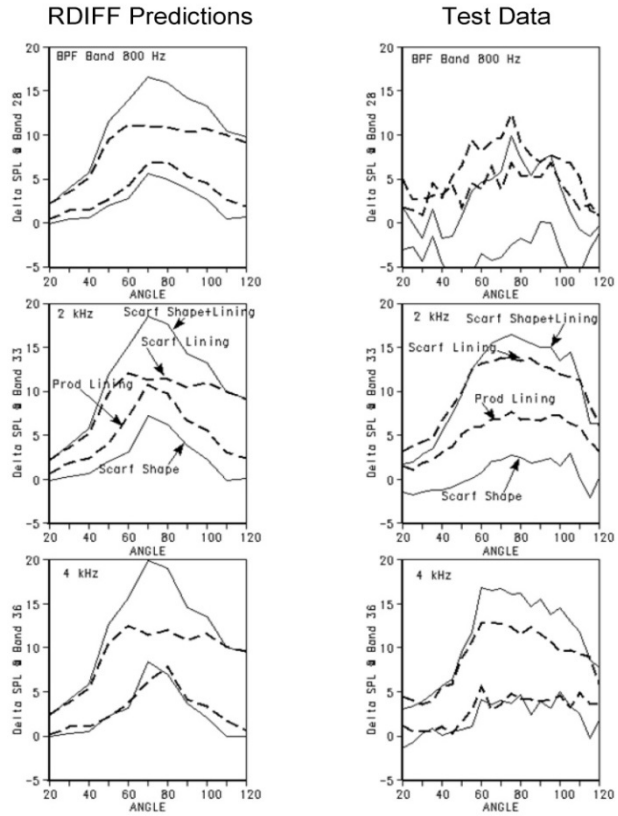
Figure 60.—Attenuation directivity—approach power.

Predicted vs. Test Data
2 and 4 kHz

Scarf Shape = PHW-SHW
Prod Lining = PHW-PTr
Scarf Lining = SHW-STr
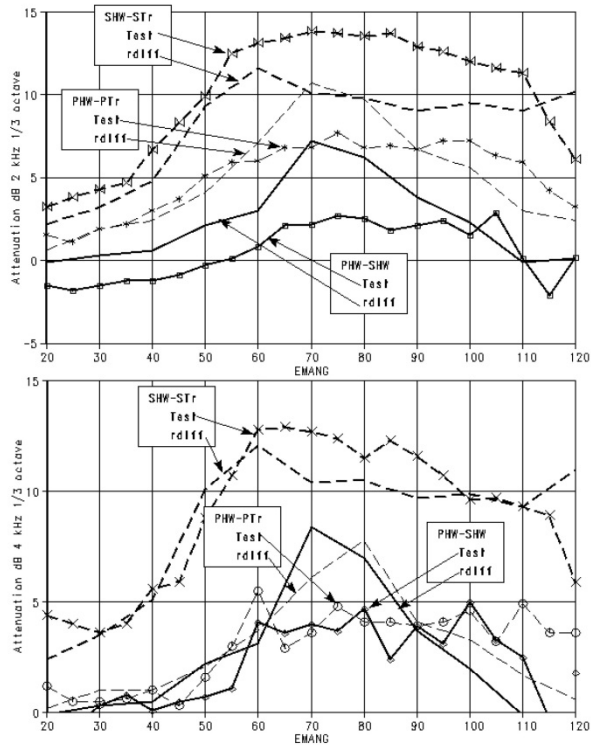
Figure 61.—Attenuation directivity—approach power.

RDIFF Predictions   Test Data

Predicted versus Test Data
40°, 60° & 80°

Scarf Shape = PHW-SHW
Prod Lining = PHW-PTr
Scarf Lining = SHW-STr
Scarf Shape+Lining = PHW-STr
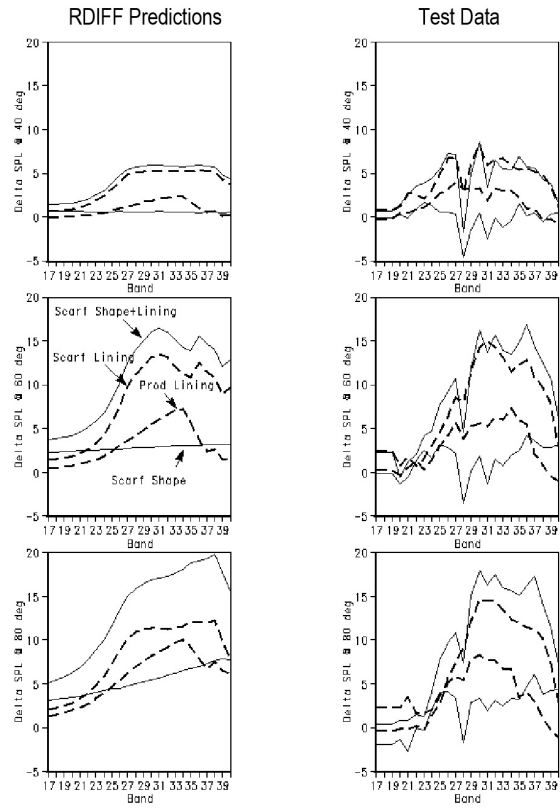
Figure 62.—Attenuation spectra—approach power.

Predicted versus Test Data
40° & 60 °

Scarf Shape = PHW-SHW
Prod Lining = PHW-PTr
Scarf Lining = SHWSTr
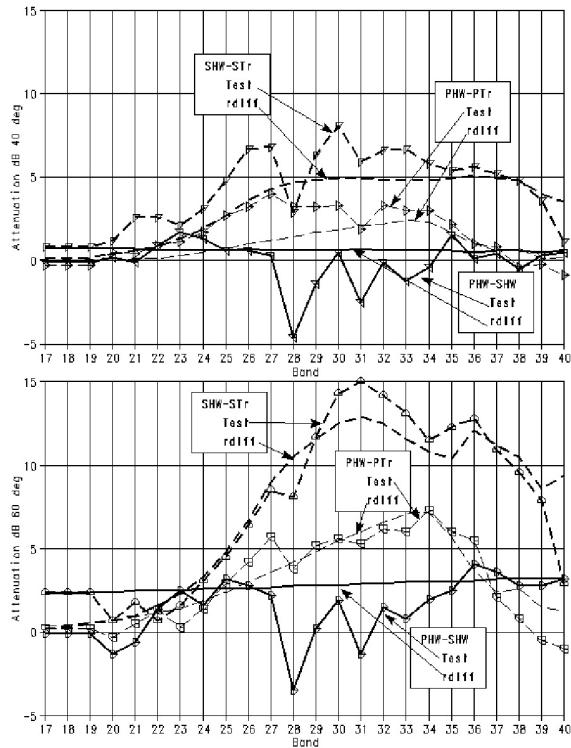
Figure 63.—Attenuation spectra—approach power.

4.2.2.2.1 Attenuation Versus Lining Area—Approach Power

Figure 64 compares measured and RDIFF predicted approach inlet noise EPLN attenuations relative to the hardwall production inlet EPNL. As shown above, the RDIFF calculation for the scarf inlet excludes the effect of the anomalous BPF and 2 BPF tone increases. This plot clearly brings out the nearly factor of two lining area increase in the fully treated scarf inlet relative to the fully treated production inlet. The RDIFF prediction curve for the production inlet was extended beyond the production inlet lining area by first assuming the inlet lip was treated similarly to the fully treated scarf inlet by adding lip lining and then "stretching" the inlet so that the lining area equals the lining area of the scarf inlet. At the fully treated scarf inlet lining area it is seen that the measured scarf data is about 1 EPNdB lower than the calculated production inlet level and the "no anomalous tone" scarf prediction is about 3 EPNdB quieter. A prediction for the fully treated scarf inlet is also shown assuming the production double layer lining in the scarf inlet, rather than the tested triple layer lining. With equal linings the "no anomalous tone" scarf prediction is about 2 EPNdB quieter than the "stretched" production inlet, essentially maintaining the hardwall scarf inlet shape benefit predicted.

4.2.3 Cutback Power

4.2.3.1 Hardwall Scarf Inlet—Cutback Power

The RDIFF prediction for the hardwall scarf inlet at cutback power is compared with the cutback extrapolation of the test data in Figure 65. As for the approach power comparisons, the RDIFF scarf inlet hardwall (SHW) prediction curves were calculated by subtracting the RDIFF delta (PHW-SHW) from the production hardwall (PHW) test data. Figure 65 shows that the measured cutback power noise level of the SHW was significantly higher than the PHW. Examination of narrow band data shows that this increased noise is primarily due to buzz saw noise. The increased buzz saw noise cannot be predicted by the RDIFF code since it does not predict fan noise source changes or non-linear propagation effects. The RDIFF code will predict a directivity change due to the inlet shape but it is clear that in this case the radiated sound power is increased. Using the PHW data as a base for the resulting RDIFF prediction, SHW = PHW-RDIFF(PHW-SHW) is therefore seen to significantly under predict the measured SHW data.
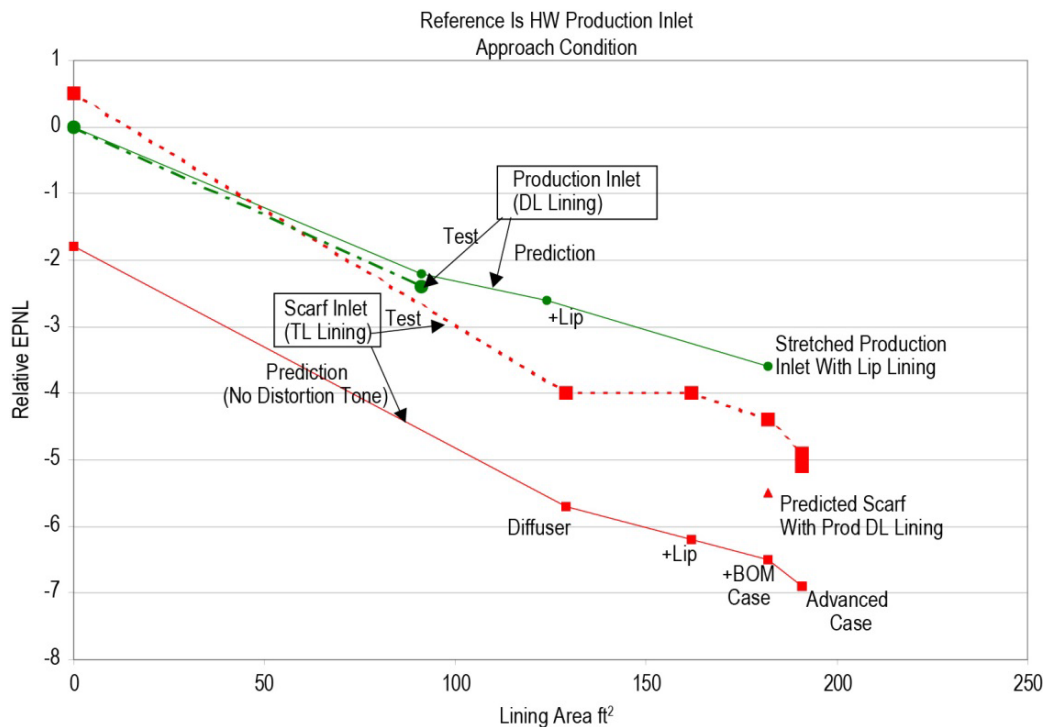
Figure 64.—Relative attenuation versus lining area—approach power.
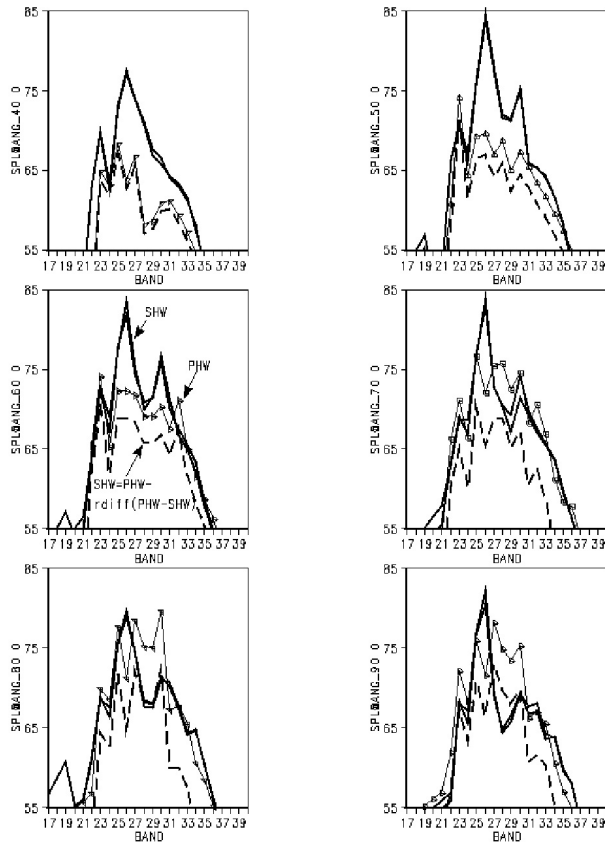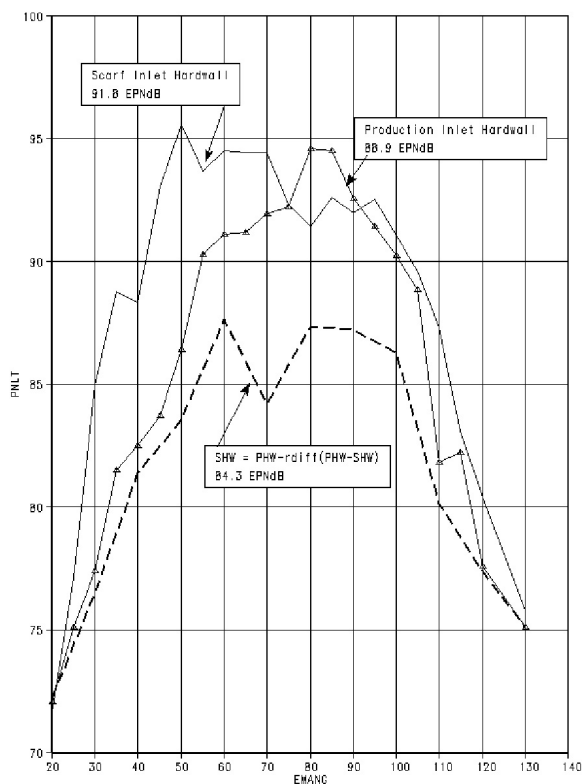
Figure 65.—Hardwall Scarf Inlet Noise Prediction—Cutback

4.2.3.2 Fully Treated Scarf Inlet—Cutback Power

Since RDIFF does not predict buzzsaw noise attenuation, it was not possible to use the PHW data as a base for the STr predictions at cutback. As an experiment it was decided to try a prediction using the PTr data as a base. The results of this calculation are shown in Figure 66. Surprisingly the resulting spectral predictions compare fairly well with the measured STr data below frequency 1/3 octave band 31(1250 Hz). This was especially surprising in light of the large buzz saw noise increase measured for the SWH relative to the PHW. For the treated scarf inlet the acoustic lining appears to suppress most of this increased buzz saw noise and the difference between the production and scarf acoustically treated inlets can be accounted for by linear acoustics. For frequency bands above band 31 the RDIFF treated scarf inlet prediction shows much larger suppression relative to the PTr levels than the measured data. This is primarily responsible for the large under prediction of the PNLT's, since this part of the noise spectrum has the largest NOY weighting.

Figure 67 shows that the attenuation spectra predicted by RDIFF are fairly similar for approach and cutback power conditions. The measured attenuation spectra however are seen to be quite different. For frequencies greater than 1200 Hz the measured data attenuations drop off monotonically as engine power is increased, contrary to the predictions. The reason for this discrepancy is not known. It is speculated that the increasing lip wall Mach numbers with increased engine power may be related. Examination of the hardwall lip data showed the same behavior so it was concluded that the attenuation fall off was not due to noise generation by the flow over the lip lining. Another possibility is a propagation effect through the high Mach number flow, which reduces the hardwall and treated inlet noise levels increasingly as engine power is increased while reducing the effect of the lining since the high Mach number flow is adjacent to the lining. The other feature of the measured data attenuation spectra seen in Figure 67 worth noting is the large low frequency attenuation seen at the cutback condition. This is buzz saw noise attenuation. This is clearly not seen in the RDIFF predicted cutback power attenuation spectrum.
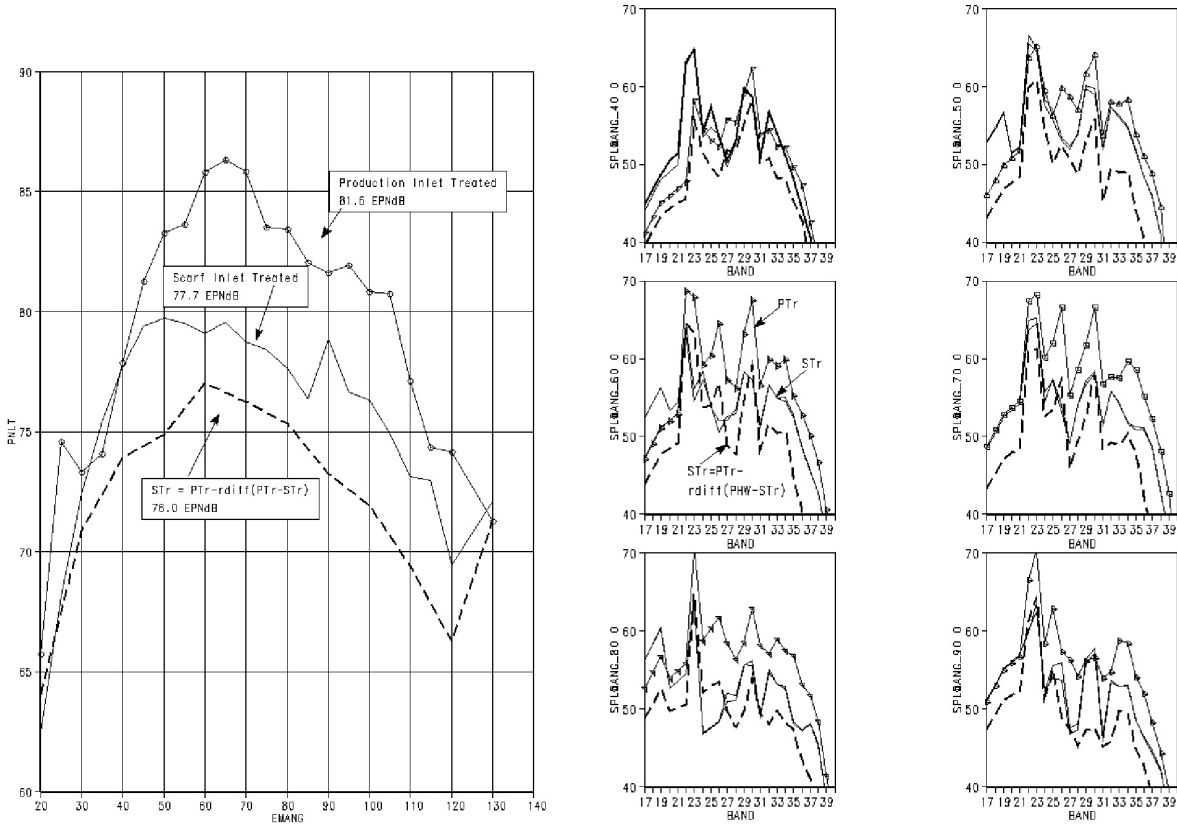
Figure 66.—Fully treated scarf inlet noise prediction—cutback.

Predicted attenuation similar for approach and cutback power.

Measured attenuation at approach power similar to prediction.

Measured high frequency attenuation falls off rapidly as engine power increases.

Low frequency buzzsaw noise attenuation much larger than predicted attenuation
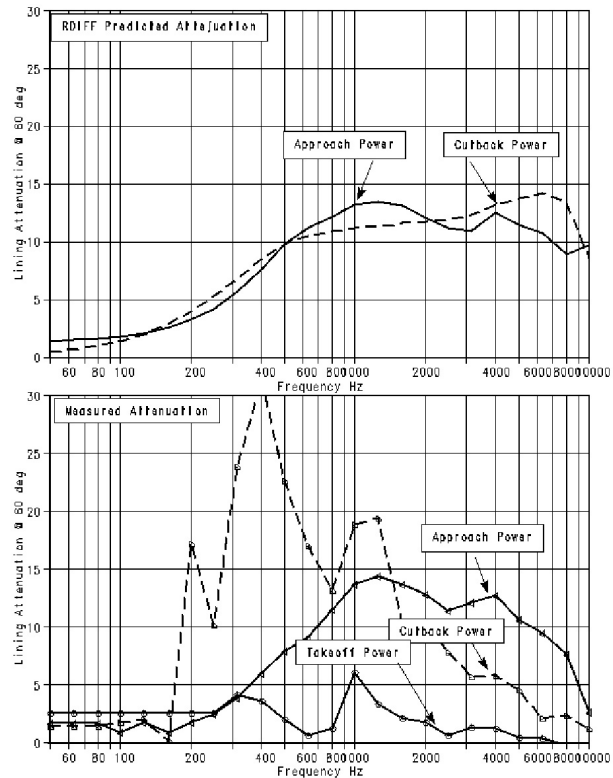
Figure 67.—Predicted versus measured attenuation spectra.
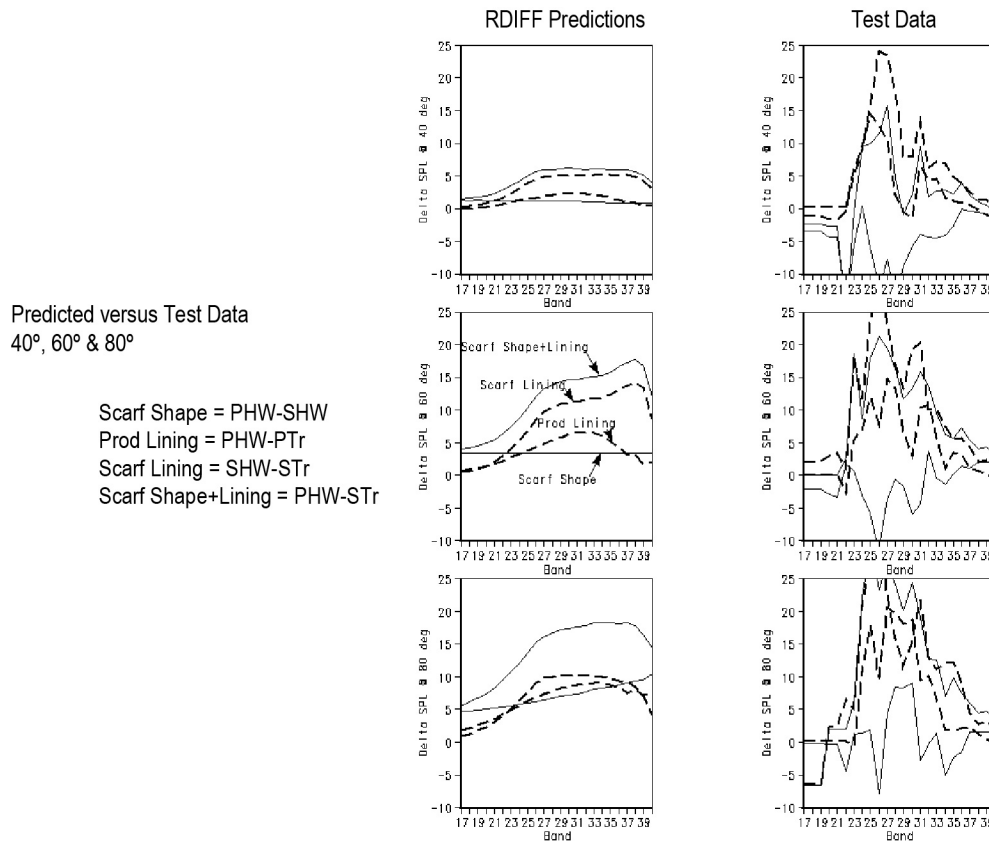
Figure 68.—Attenuation spectra—cutback power.

Additional cutback power measured and treated attenuation spectra are shown in Figure 68. The effects of the measured increased buzz saw noise for the hardwall inlets and the large buzz saw noise attenuation for the treated inlets are again contrasted with the RDIFF predictions.

4.2.3.3   Attenuation Versus Lining Area—Cutback Power

Figure 69 is a plot of the scarf inlet EPNL attenuation relative to the production inlet versus lining area for cutback power, similar to Figure 64 for approach power. A major difference is that the measured treated production inlet data is used as the reference for the treated scarf inlet predictions and the increased lining area production inlet predictions because of the inability of RDIFF to predict buzz saw noise attenuation. The RDIFF predictions therefore assume no buzz saw noise source increase and no fall off of high frequency attenuation as observed in the test data. This is considered a prediction of the noise changes relative to the production inlet that would be observed in flight assuming that the high frequency attenuation loss and the increased hardwall buzz saw noise are due to static test flow anomalies. As was the case for approach power, the prediction for the scarf inlet shows a benefit even if the production inlet were "stretched" and lining added to the lip so that they have equal lining area. The benefit of the triple layer lining is predicted to be significantly less than was the case for approach power.
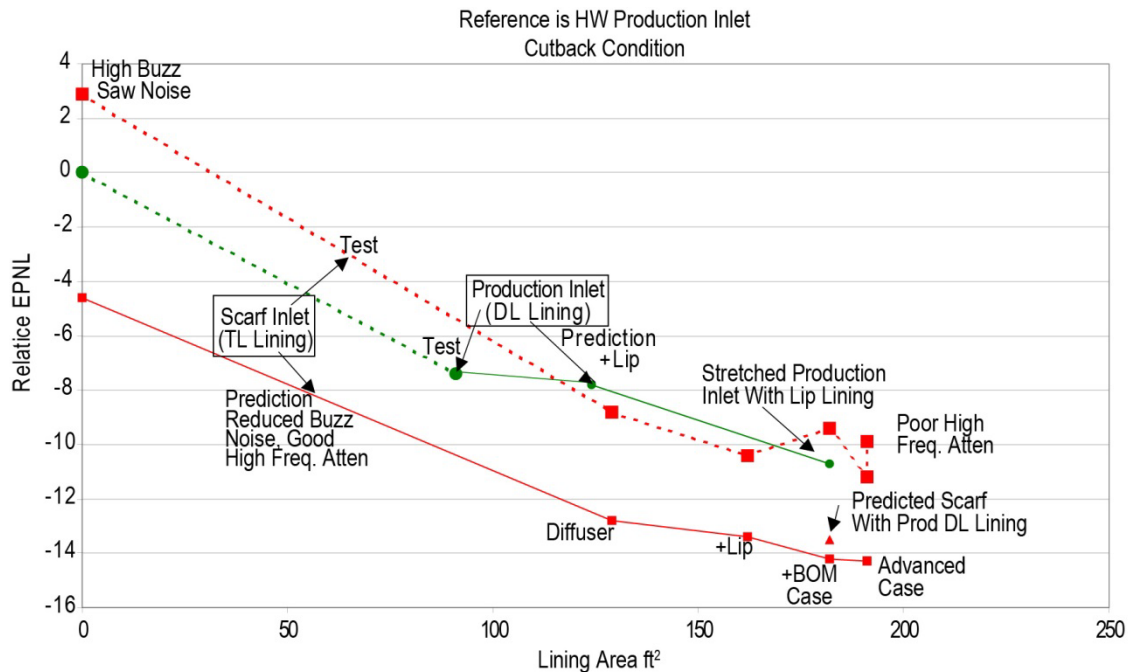
Figure 69.—Relative attenuation versus lining area—cutback power.

4.2.4 Scarf Lining Variations

The scarf inlet was tested with a number of lining variations. Figure 70 shows comparisons of the measured and RDIFF predicted inlet noise component EPNL attenuations for these variations as follows:

Full Inlet + R1 Case (Scarf full hardwall—Scarf full treatment with the advanced fan case with PU overlay (R1)).

Full Diff (Scarf full hardwall—Scarf with hardwall forward fan case and lip, full diffuser treatment.

Bott Diff (Scarf with hardwall bottom diffuser, full treatment otherwise—Scarf with full treatment)

BOM Case (Scarf with hardwall fan case, full treatment otherwise—Scarf with full treatment and simulated BOM fan case)

R1 Case (Scarf with hardwall fan case, full treatment otherwise—Scarf with full treatment and R1 fan case)

R2 Case (Scarf with hardwall fan case, full treatment otherwise—Scarf with full treatment and simulated R2 fan case)

Full Lip (Scarf with hardwall fan case and lip, treated diffuser—Scarf with hardwall fan case, treated lip and treated diffuser)

Bot Lip (Scarf with hardwall lower lip, full treatment otherwise—Scarf with full treatment)

"A" Flange (Scarf with 360° hardwall region at "A" flange extending 3 in. upstream into inlet—Scarf with full treatment)

As discussed above, the RDIFF code does not predict the buzz saw noise attenuation well. This accounts for the poor agreement between the prediction and measurement for the cutback condition for the full inlet and full diffuser treatment configurations. The BOM and R2 fan case treatments are seen to have increased noise at the cutback condition (because of the hardwall circumferential discontinuities). The effect of scattering of the rotor bound field by lining discontinuities is not included in the RDIFF prediction and therefore results in poor agreement for these cases. The full lip treatment was more.
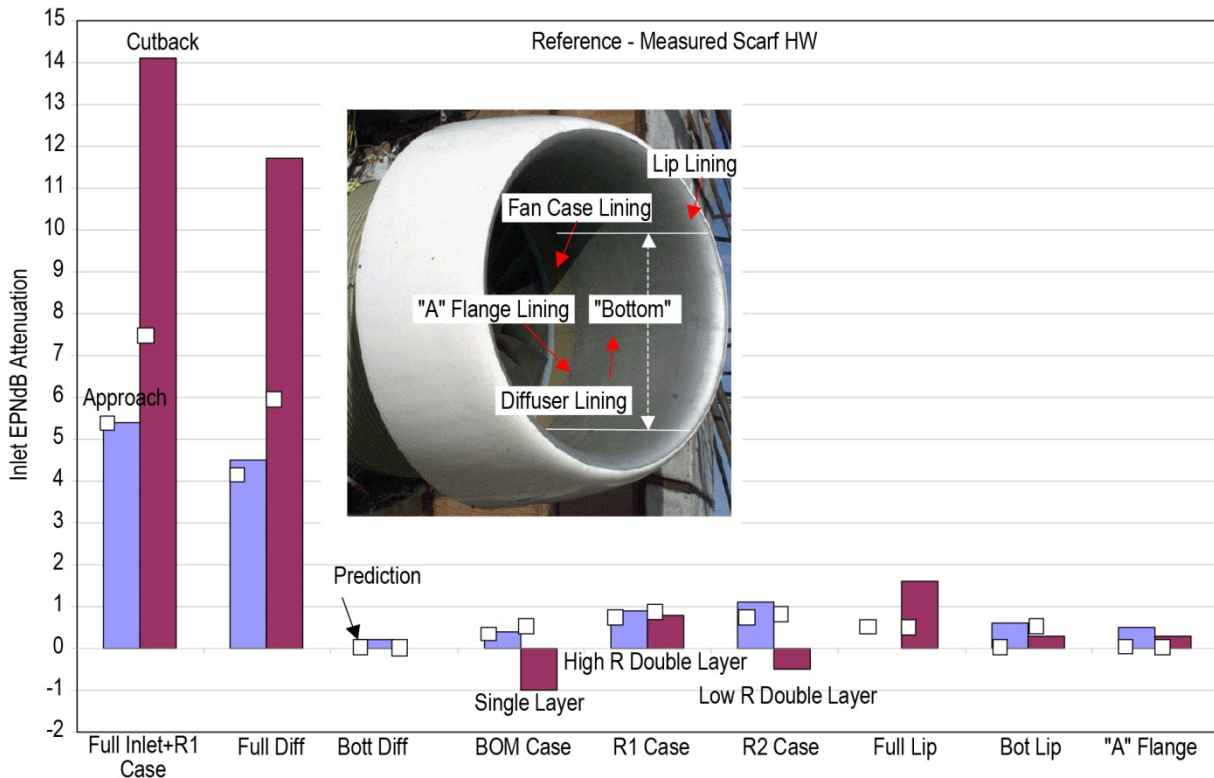
Figure 70.—Inlet lining elements attenuation.

effective at the cutback condition than predicted. This also appears to be the result of more buzz saw attenuation than predicted by RDIFF. At approach power the lip treatment was effective at frequencies other than the BPF but the lack of BPF attenuation resulted in no EPNL attenuation. It is unclear why the bottom lip liner shows more effectiveness than the entire lip liner at approach power. It is possible that hardwalling the upper lip reduced the distortion into the fan which was causing the increased BPF with the scarf inlet. Hardwalling approximately 7 ft^2 of acoustic lining at the "A" flange was not predicted to have any effect on the inlet EPNL. The test results showed a small effect of about 0.5 EPNdB at approach and less at cutback.

4.2.5   Conclusions

At the approach power condition it is concluded that the RDIFF predictions for tone and broadband lining attenuation generally were within about 15 percent of the measured data in the direct radiation field but only within about 50 percent in diffraction dominated field (aft of 70°). However, the very high frequency lining attenuation (8 to 10 kHz) was not accurately predicted. The scarf shape shielding effects were predicted well except for in the diffraction-dominated field also. The RDIFF prediction process of applying the RDIFF predicted noise change (PHW-configuration) to the measured production inlet test data was used to estimate the scarf inlet noise if the BPF and 2BPF tone increase did not occur. This is believed to be a valid flight condition prediction since it is believed that the flow distortion causing the tone increases will not be present with forward motion. It was concluded that without the BPF and 2BPF aggravation the 13° biplanar scarf shape is worth about 2 EPNdB and the triple layer lining is worth about 1 EPNdB relative to a production inlet with lip lining and "stretched" to have the same total lining area as in the scarf inlet.

At cutback power it was concluded that the scarf shape significantly increases buzzsaw noise, but, except for the high frequencies (2 kHz and higher), the lining attenuated it to levels expected based on the measured treated production inlet levels. The RDIFF code however does not predict the attenuation of the

buzz saw noise. The RDIFF calculated acoustic wave attenuation for the treated scarf inlet relative to the treated production inlet at the dominant buzz saw noise frequencies (<1 kHz) appeared to be reasonably close to the measured data. Besides buzz saw noise attenuation prediction, the other major miss by the RDIFF code was the prediction of the high frequency (2 kHz and higher) noise attenuation at the higher power conditions. Contrary to the RDIFF predictions, the measured high frequency attenuations were observed to fall off rapidly with increased power setting. It is speculated that this is due to a propagation effect through the high Mach number flow, which reduces the hardwall and treated inlet noise levels increasingly as engine power is increased while reducing the effect of the lining which is adjacent to the high Mach number flow. If this is true the RDIFF high frequency predictions may be valid for flight where the lip Mach numbers are much lower.

If the predicted high frequency attenuation is realized, the 13° biplanar scarf shape is worth about 3 EPNdB and the triple layer lining is worth about 0.75 EPNdB relative to a production inlet with a treated lip and "stretched" to have lining area equal to the tested scarf inlet.

4.3   ICD Microphone Array Test Results

4.3.1   Background

As part of the NASA Engine Validation of Noise Reduction Concepts test program, a scarf inlet was tested on a PW4098 engine at the Pratt & Whitney static engine test stand at West Palm Beach, Florida in November 1998. In an effort to characterize the noise radiation properties of the inlet/engine combination, the inflow control device was fitted with 198 Kulite microphones. The Boeing Phased Array Data system was used to measure acoustic data from the ICD array. The system was installed at the C-11 stand in August 1998 and checked out on a PW4098 certification test prior to the NASA test in November. Phased array data was processed to form cross-spectral matrices. These were used in beamforming to make images of the fan and low pressure compressor sources. A spinning mode decomposition process was applied to create mode plots. Results from the NASA test are presented here for eleven configurations: a production inlet with production acoustic lining, the production inlet with the acoustic lining covered with tape, and ten configurations of the scarf inlet with various acoustic lining arrangement.

4.3.2   Instrumentation

Kulite model MIC-093 transducers with B-screens were installed nylon sleeves and attached to the perforated plate surface of the ICD with screws (Figure 71 to Figure 73). The layout of the transducers (Figure 74) was designed for two purposes: beamforming to make images of the noise source distribution and spinning mode decomposition.

From U.S. Patent Mar. 31, 1981 4,258,823
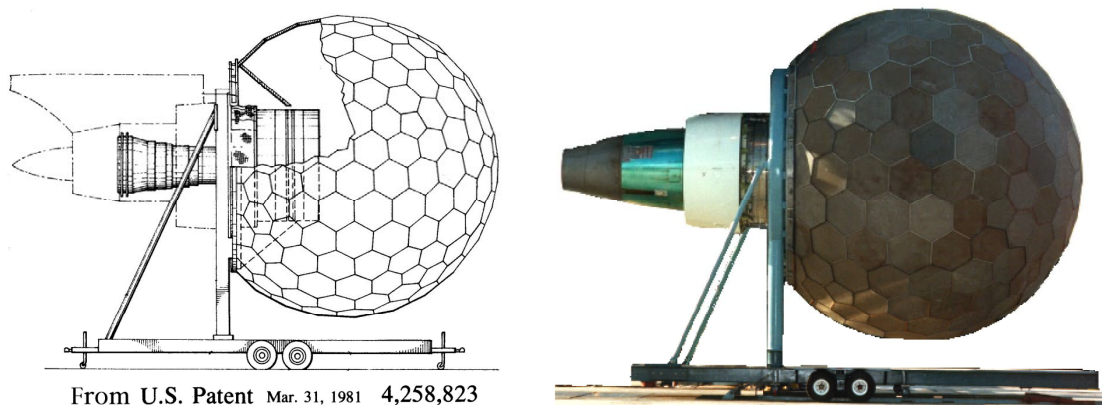
Figure 71.—Inflow control device. (Engine depicted is not the PW4098 engine used in the present test.)
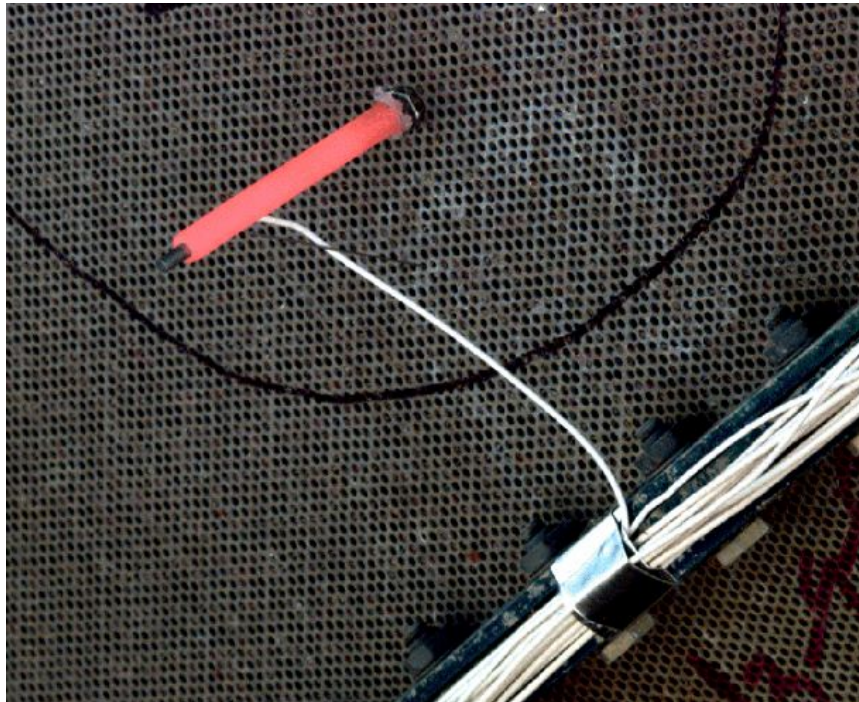
Figure 72.—MIC-093 Kulite and the nylon sleeve for mounting it the IDC. The signal lead and the vent tube can be seen. A small hook is used to clamp the fixture the perforated plate.
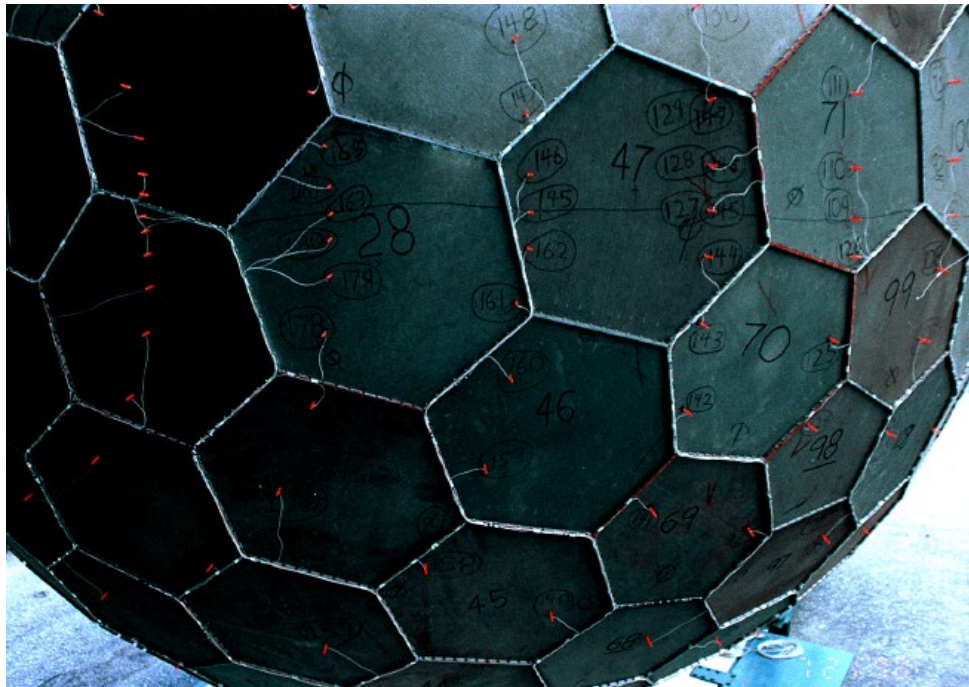
Figure 73.—Photograph of the installed microphones.
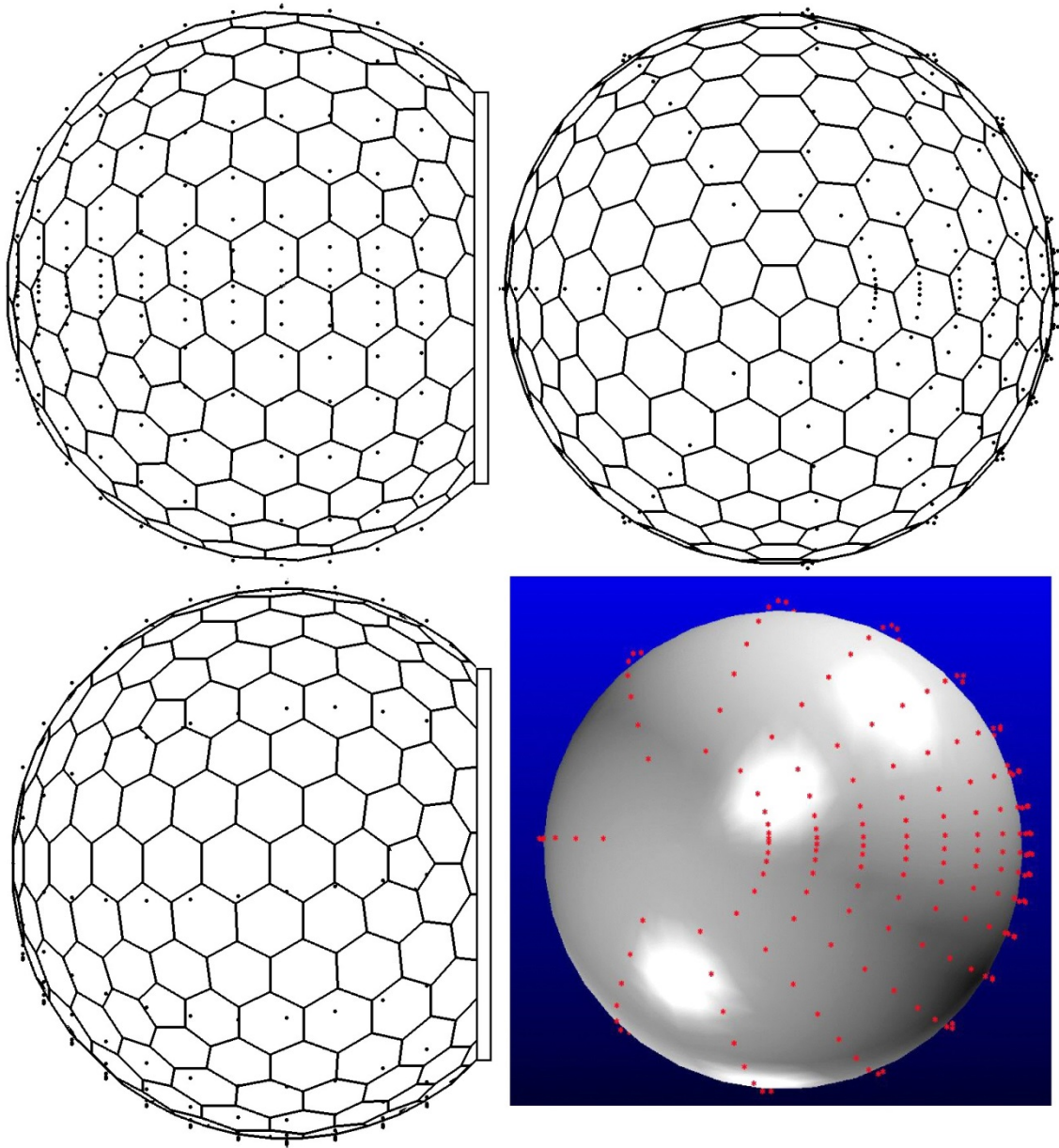
Figure 74.—Layout of the Kulites on the ICD.

The theoretical performance of the array for separating spinning modes is indicated in Figure 75. Paper templates were used to place the microphones near their intended locations (Figure 76).

700 Hz
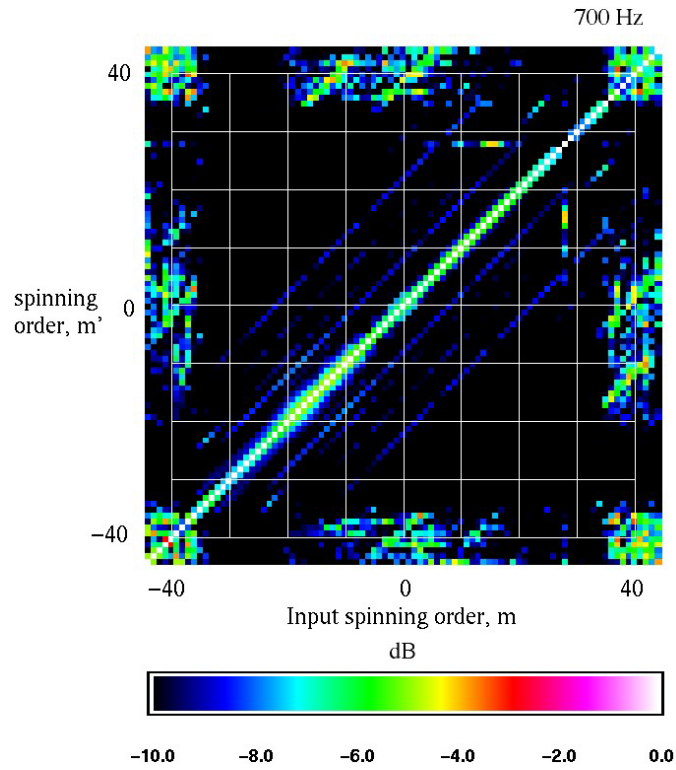
Figure 75.—Theoretical performance of the array design for spinning mode measurements.

Figure 76.—Paper templates used to locate microphones on the ICD.

Photogrammetry was used to measure the positions of the Kulites (Table 5).

TABLE 5.—POSITIONS OF THE KULITE MICROPHONES AS DETERMINED BY PHOTOGRAMMETRY

Kulite	X	Y	Z	Kulite	X	Y	Z	Kulite	X	Y	Z
1	-15.22	0.00	-124.32	67	-89.05	128.99	-63.41	133	-179.27	-90.75	-62.11
2	-15.56	-11.36	-125.90	68	-86.95	99.45	-103.52	134	-179.27	-109.19	-13.08
3	-15.25	-30.27	-122.67	69	-86.27	69.88	-124.64	135	-179.27	-92.38	59.66
4	-15.41	-48.30	-116.59	70	-87.00	45.04	-136.30	136	-179.93	-0.20	110.40
5	-14.55	-71.95	-102.45	71	-86.14	25.77	-140.92	137	-179.27	92.38	59.66
6	-14.63	-96.82	-79.16	72	-86.75	11.36	-142.47	138	-179.27	109.19	-13.08
7	-16.13	-118.30	-41.72	73	-112.47	0.25	-140.94	139	-178.49	90.55	-61.46
8	-15.22	-122.84	19.14	74	-114.12	-9.35	-140.57	140	-178.79	65.09	-87.64
9	-15.20	-88.92	86.62	75	-111.93	-22.45	-139.56	141	-175.85	44.57	-102.10
10	-14.89	0.08	124.78	76	-111.88	-41.44	-134.74	142	-178.47	28.16	-108.47
11	-15.22	89.22	86.57	77	-111.93	-65.42	-125.32	143	-180.93	14.53	-111.95
12	-15.22	122.84	19.14	78	-111.45	-94.46	-104.46	144	-179.86	6.04	-110.17
13	-15.22	118.04	-39.00	79	-111.93	-124.81	-66.39	145	-196.76	-0.39	-92.27
14	-15.22	96.40	-78.50	80	-111.70	-141.12	-1.22	146	-196.69	-5.19	-91.95
15	-15.19	69.27	-104.58	81	-111.93	-112.09	86.15	147	-197.06	-13.06	-91.33
16	-14.83	47.07	-116.57	82	-111.50	-0.14	141.78	148	-196.64	-22.43	-89.85
17	-14.67	28.31	-122.55	83	-111.99	111.46	86.13	149	-196.44	-35.48	-85.58
18	-15.65	11.56	-124.52	84	-111.93	141.37	-1.15	150	-196.66	-52.72	-76.82
19	-39.60	2.17	-134.09	85	-113.60	124.42	-67.83	151	-197.03	-73.58	-55.42
20	-37.90	-12.13	-134.35	86	-110.51	94.91	-104.67	152	-196.97	-91.18	-14.17
21	-37.21	-27.59	-132.43	87	-111.45	65.58	-124.72	153	-196.97	-78.81	47.99
22	-37.79	-48.26	-126.21	88	-112.76	41.73	-134.63	154	-196.97	0.00	92.27
23	-36.80	-73.16	-113.69	89	-111.93	23.31	-139.44	155	-196.97	78.81	47.99
24	-38.31	-101.35	-90.47	90	-112.21	10.32	-140.02	156	-196.66	92.17	-12.64
25	-38.58	-125.50	-49.02	91	-136.96	-0.01	-134.96	157	-196.46	74.18	-54.12
26	-37.90	-134.04	15.12	92	-137.07	-8.47	-134.29	158	-196.59	52.96	-75.41
27	-37.80	-99.94	91.37	93	-137.23	-20.13	-133.00	159	-196.55	35.20	-85.82
28	-37.86	0.15	134.64	94	-136.08	-37.23	-129.48	160	-197.67	21.82	-90.38
29	-37.66	99.52	91.28	95	-136.35	-58.96	-121.13	161	-198.83	10.80	-91.65
30	-37.90	134.04	15.12	96	-135.58	-86.84	-103.58	162	-196.76	4.37	-92.29
31	-37.90	126.06	-48.01	97	-136.10	-116.56	-67.90	163	-211.16	0.01	-71.82
32	-36.87	100.32	-91.81	98	-135.59	-134.64	-6.62	164	-211.15	-3.44	-71.83
33	-37.33	72.94	-113.97	99	-136.10	-109.19	79.20	165	-211.46	-8.74	-71.36
34	-36.96	47.89	-126.35	100	-136.10	0.50	135.10	166	-211.79	-15.46	-69.73
35	-37.13	27.53	-132.78	101	-136.64	109.45	79.17	167	-212.24	-25.75	-67.03
36	-37.43	12.42	-134.30	102	-136.10	134.75	-6.23	168	-211.32	-39.31	-60.05
37	-62.95	0.19	-140.65	103	-135.81	115.67	-69.11	169	-211.67	-56.38	-45.70
38	-61.68	-12.09	-140.16	104	-135.99	85.86	-103.55	170	-211.71	-70.41	-13.86
39	-61.74	-27.41	-138.43	105	-136.24	58.78	-121.28	171	-211.32	-62.25	35.73
40	-63.28	-47.84	-132.82	106	-136.17	37.31	-129.97	172	-211.32	0.00	71.78
41	-61.77	-72.60	-120.50	107	-136.10	20.61	-133.31	173	-213.41	61.01	37.86
42	-60.31	-103.17	-96.99	108	-137.52	8.78	-134.38	174	-211.20	70.50	-12.67
43	-64.07	-130.41	-55.59	109	-159.25	0.26	-124.64	175	-211.89	55.83	-44.08
44	-62.07	-141.01	10.05	110	-159.48	-6.69	-124.13	176	-210.71	39.89	-59.39
45	-61.53	-107.55	93.53	111	-159.86	-17.26	-123.30	177	-211.33	25.78	-67.76
46	-61.81	-0.06	140.93	112	-158.44	-32.16	-120.63	178	-211.62	15.62	-70.70
47	-61.66	107.15	92.51	113	-159.37	-51.89	-113.59	179	-211.33	7.78	-71.69
48	-62.07	141.01	10.05	114	-158.81	-76.67	-98.18	180	-211.52	3.02	-72.21

TABLE 5.—POSITIONS OF THE KULITE MICROPHONES AS DETERMINED BY PHOTOGRAMMETRY

Kulite	X	Y	Z	Kulite	X	Y	Z	Kulite	X	Y	Z
49	-62.07	129.82	-55.98	115	-158.78	-105.03	-66.52	181	-223.15	0.89	-50.58
50	-62.07	102.08	-97.81	116	-158.86	-123.74	-8.95	182	-223.01	-2.20	-50.85
51	-61.19	72.81	-121.62	117	-158.78	-102.59	70.22	183	-222.68	-4.81	-50.62
52	-62.07	47.36	-133.20	118	-158.33	0.33	124.09	184	-222.30	-9.47	-49.77
53	-61.16	27.61	-138.76	119	-158.78	102.59	70.22	185	-221.15	-16.95	-46.05
54	-60.07	11.09	-140.97	120	-158.78	123.89	-10.34	186	-221.89	-25.80	-41.77
55	-88.03	-0.89	-143.11	121	-158.12	105.25	-65.14	187	-222.08	-36.62	-33.20
56	-87.16	-10.50	-142.36	122	-158.29	76.90	-97.06	188	-222.23	-48.10	-10.01
57	-89.62	-24.13	-139.73	123	-158.52	51.66	-112.64	189	-221.47	-42.63	22.69
58	-87.44	-44.88	-135.45	124	-157.94	32.11	-120.05	190	-219.84	0.37	48.86
59	-87.01	-69.91	-124.69	125	-161.76	18.06	-122.58	191	-223.67	43.73	24.44
60	-86.23	-99.72	-102.96	126	-158.95	5.85	-125.15	192	-222.49	48.72	-9.77
61	-87.00	-129.34	-62.28	127	-179.83	-0.06	-110.11	193	-221.95	37.98	-31.41
62	-87.15	-144.26	5.52	128	-179.66	-6.10	-109.50	194	-221.81	26.33	-41.99
63	-83.67	-110.93	91.65	129	-179.24	-15.14	-108.55	195	-221.71	16.77	-46.99
64	-87.88	-0.87	143.46	130	-178.66	-27.45	-106.25	196	-222.13	10.37	-49.14
65	-86.71	111.33	90.17	131	-179.02	-44.26	-100.76	197	-222.37	5.89	-49.80
66	-87.00	143.48	4.45	132	-179.23	-66.05	-88.71	198	-222.85	2.85	-50.42
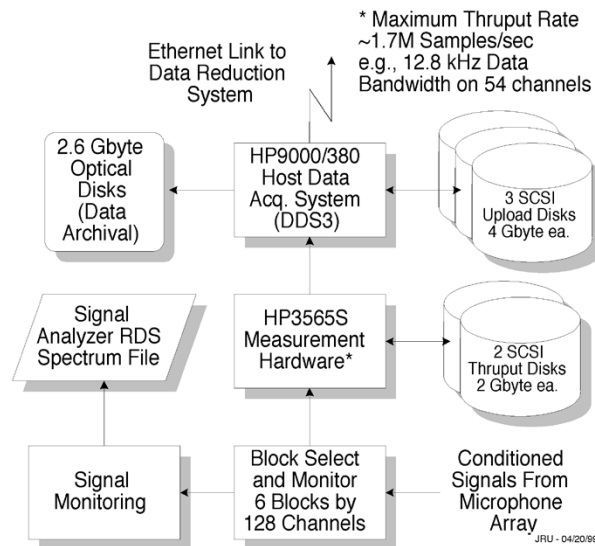
Figure 77.—Block diagram of the Boeing Phased
Array Data Acquisition System.

A block diagram of the Boeing Phased Array Data Acquisition System in given in Figure 77.
The Kulites were connected to Boeing Dual Purpose Power Supplies located in weatherproof
enclosures near the test stand (Figure 78). Coaxial cables led from the test stand to the host data
acquisition system, DDS3, which was installed in the control room in the blockhouse at the C-11 test
stand.
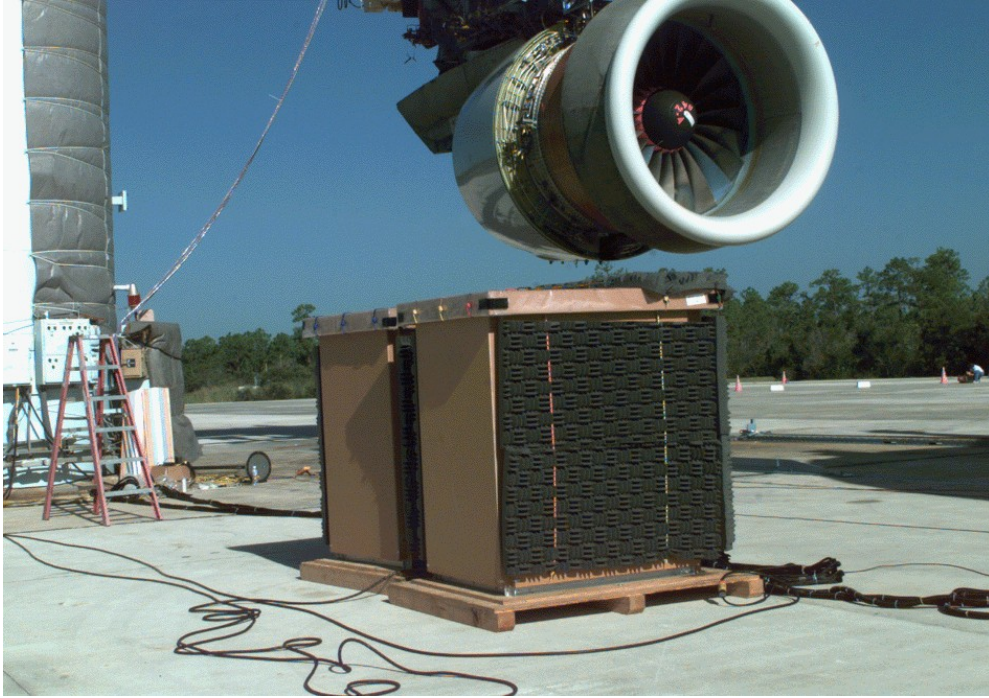
Figure 78.—Weatherproof enclosures for the Boeing dual purpose power supplies.
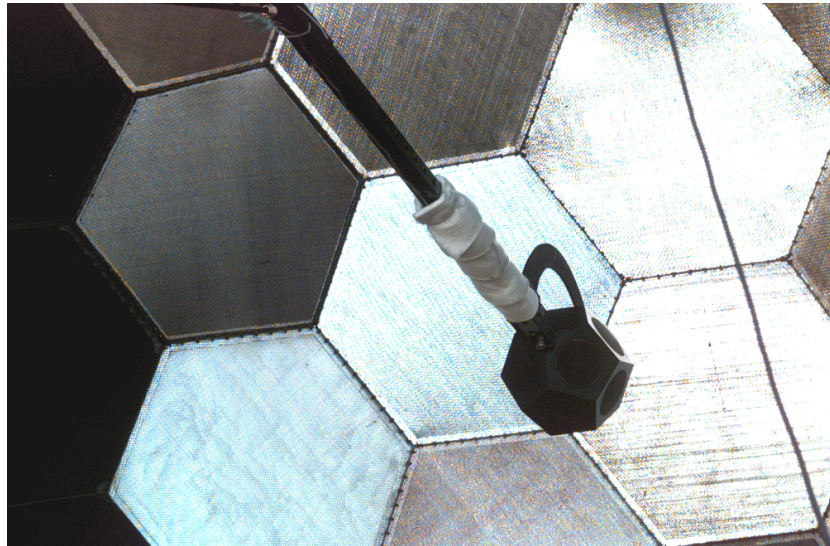
Figure 79.—Omnidirectional speaker used for array calibration.

4.3.3 Phase Calibration

Speaker calibration was performed with an omnidirectional speaker (Figure 79 and Figure 80) and a pipe speaker. As shown in Figure 80 the pipe speaker that was used for high frequency calibration was positioned at the opening of the ICD, rather than the center, to optimize the uniformity of its radiation pattern over the array.

The omnidirectional speaker was applied for frequencies below 2000 Hz and the pipe speaker was used for the frequency range of 2 to 6 kHz. The cross-spectral matrices were calibrated using factors determined by ratio of the expected and the measured speaker data.
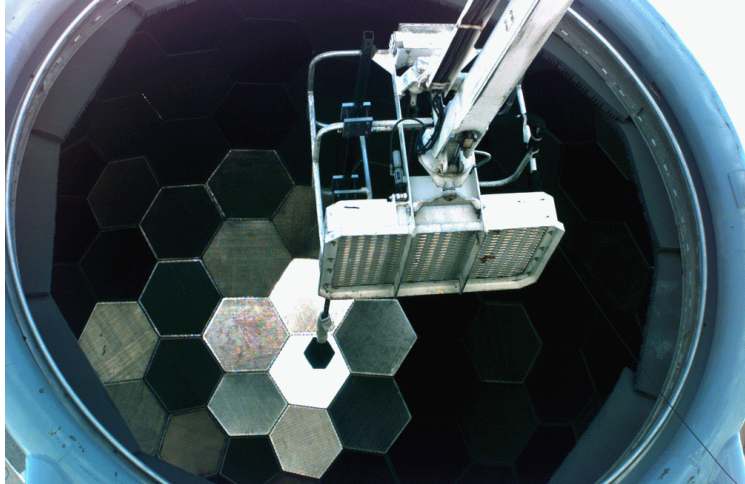
Figure 80.—Method for positioning the omnidirectional calibration speaker
in the center of the ICD.

4.3.4   Processing Methods

Two cross spectral matrices were computed for each condition: an "A" matrix with a 10 Hz
processing bandwidth and 200 center frequencies from 10 to 2010 Hz, and a "B" matrix with a 30 Hz
processing bandwidth and 200 center frequencies from 30 to 6030 Hz.

4.3.4.1   Travel Times For Conventional Beamforming

Conventional phased array beamforming (Ref. 1) was used to make images of the noise source
distributions for selected frequencies and conditions. Flow effects were taken into account by starting
with computed flowfields for the production and scarf inlets. A beamforming grid in the fan plane was
defined, and a straight ray between each beamforming grid point and each microphone was computed.
The acoustic travel time for each microphone-grid point pair was approximated by assuming that the
sound travels along the ray with speed $v_{ray} = c + \hat{n} \bullet \vec{v}$, where c is the speed of sound in quiescent air, $\vec{v}$ is
the local flow velocity, and $\vec{n}$ is the direction of the ray. This approximation was adopted after the more
rigorous approach of computing the actual, curved, rays proved unworkable in this case. It is believed that
the curved rays failed to converge because the extreme flow gradients near the inlet lip scattered the rays
in all directions. The travel times, computed by the straight-ray method (using a code called ray_grid.f),
were used the compute the phase for beamforming.

4.3.4.2   Spinning Mode Decomposition

To estimate the spinning mode levels, an annular grid was defined in the inlet (Figure 81 and Figure
82) and used as a source surface. For each spinning order, m, eight radial orders were considered. Source
modes of the form

$$S(n,m;r,\phi) = e^{im\phi}\cos\left(n\frac{r - r_0}{r_1 - r_0} \right)$$

Were postulated for $n = 0, 1, …, 8$. The cosine factor is intended to account for the radial mode
variability. The fact that the cosine function differs from the actual mode shape (expressed in terms of
Bessel functions for some ideal cases) is not believed to be important because the results are ultimately
summed over the radial modes. For each spinning order, m, the power of the spinning mode was
estimated by considering each radial order, n, in turn. Given a pair (n,m), the source function S was
computed at each point in the annular grid. A Rayleigh integral for each microphone location was
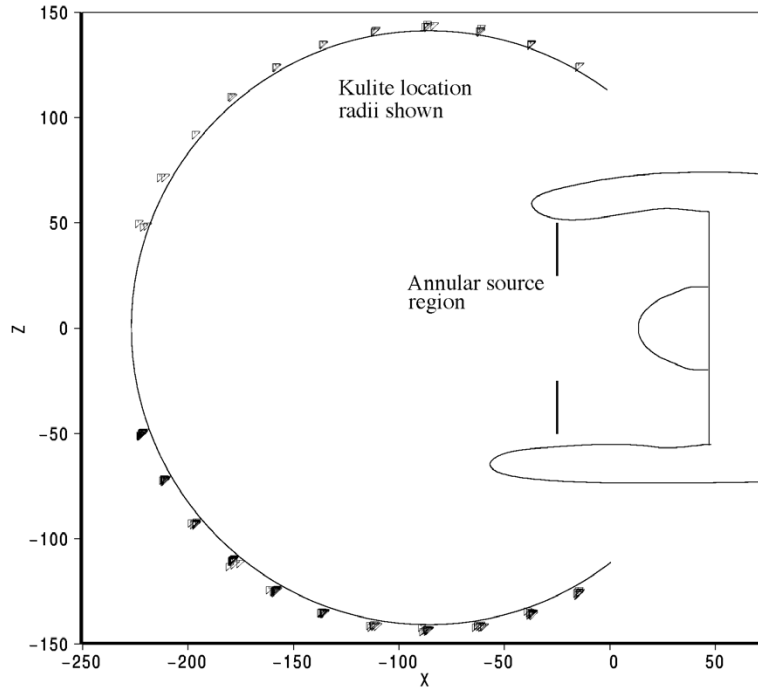
Figure 81.—Position of the annular grid used for spinning mode breakdown.
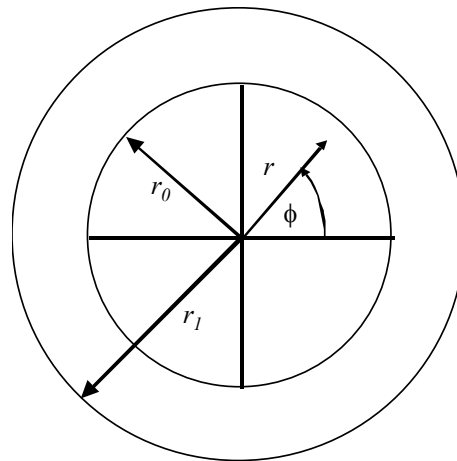
Figure 82.—Coordinates used for the annular grid source region.

approximated by summing over the grid points and using a free-space, no-flow model for the travel times. These integrals became elements of array steering vectors, which were used with the cross-spectral data matrices in a beamforming expression. The (spinning mode) beamforming results were summed over n to give the required estimates of the radiated spinning mode power.

4.3.5 Test Configurations

Compressor foil counts of the test engine are given in Table 6. These values are used to compute the expected spinning mode orders.

The eleven configurations for phased array data are listed in Table 7. The non-scarf inlet is a production intake configuration with a flight lip. The scarf inlet is a 13° biplanar design that also has a flight lip. Three forward fan cases and several inlet and fan case tape configurations were tested. All phased array data set were taken with the inlet keel rotated toward the polar arc of far filed microphones.

TABLE 6.—COMPRESSOR BLADE AND VANE COUNTS OF THE TEST ENGINE

	Fan		Low Pressure Compressor		High Pressure Compressor	
	Blades	Vanes	Blades	Vanes	Blades	Vanes
Inlet vanes		0		92		38/36
Stage 1	22	60	53	84	40	30/31
Stage 2			91	100	51	26/27
Stage 3			93	104	56	32/33
Stage 4			100	120	53	114
Stage 5			108	110	72	108
Stage 6			94	104	74	120
Stage 7			81	88	78	128
Stage 8					84	112
Stage 9					92	116
Stage 10					90	124
Stage 11					80	110

TABLE 7.—CONFIGURATIONS FOR PHASED ARRAY DATA REPORTED HERE.

Cfg.	Run	Corr. rpm N1C	Obs. rpm N1	Inlet	Forward Fan Case	Acoustic lining and HW tape
1	A07809 A07826 A07830	1802 2450 2900	1828 2494 2967	Prod.	Prod.	Harwall inlet and F/C
2	A07908 A07918 A07923	1806 2454 2904	1835 2489 2946	Prod.	Prod.	Production lining
3	A08107 A08217 A08222	1804 2454 2904	1843 2506 2964	Scarf	Sim. BOM	Hardwall inlet and F/C
4	A08508 A08518	1805 2451	1847 2505	Scarf	Sim. BOM	Full lining
5	A08608 A08618 A08623	1803 2455 2900	1834 2497 2949	Scarf	2 in. R1	Full lining
6	A08708 A08718 A08741	1802 2450 2907	184 2502 2969	Scarf	2 in. R2	Full lining
7	A08809 A08819	1803 2452	1834 2493	Scarf	2 in. R2	8 3 in. tape strips on the F/C
8	A08909 A08919	1804 2453	1840 2504	Scarf	2 in. R2	3 3 in. tape strips on the F/C
9	A09009 A09019	1804 2453	1849 2513	Scarf	2 in. R2	3 1.25 in. tape strips on the F/C
12	A08309 A08319 A08324	1804 2451 2904	1847 2508 2973	Scarf	2 in. R2	Hardwall lip
14	A08409 A08419 A08419	1802 2452 2907	1849 2503 2969	Scarf	Taped HW	Hardwall F/C

4.3.5.1 Expected Spinning Modes

Figure 83 and Figure 84 give the inlet spinning modes expected from the engine at approach and cutback power according to Tyler-Sofrin theory (Ref. 3). Cutoff effects are not considered in the figure. For fan modes, it was assumed that three splices are present in the fan case acoustic lining.

The green diagonal line at the bottom of Figure 83 represents difference tones for various stages of the LPC. The blue diagonal line near the bottom is the corresponding feature for the high pressure compressor. The group of green diagonal lines cutting across the center of the figure is composed of first-order LPC tones. The horizontal red lines are fan tones.

Figure 84 shows the general form of buzzsaw noise. The diagonal red line passing through (0,0) is the rotor-locked field for various numbers of blades. The parallel diagonal lines are interactions with the hypothesized splices in the lining.

4.3.6 Results

4.3.6.1 Spinning Modes: Approach Power

Figure 85 gives the measured spinning modes for the 11 inlet configurations at approach power. The non-scarf inlet in the hardwall configuration (Figure 85(a)) shows the expected co-rotating broadband noise near the cutoff line. This exists in the same area of the plot as the LPC difference tones. The first two fan harmonics are quite evident. The first order LPC tones are also very clear. There is a suggestion of the HPC difference tones.

The treated non-scarf inlet (Figure 85(b)) shows a substantial reduction of the fan noise, but little change in the LPC noise relative to the hardwall case.

The hardwall scarf inlet (Figure 85(c)) appears to have more fan tone noise and less fan broadband noise than the hardwall baseline. The reduction in broadband fan noise can be interpreted as the scarf shielding effect, since the ICD array microphones were clustered on the keel side of the inlet. The LPC noise is similar to the previous cases.

The treated scarf inlet (Figure 85(c) to (k)) have dramatically less high frequency LPC noise than the non-scarf and the hardwall scarf inlets. The exception is the low-order modes around 2500 to 3000 Hz, which are not significantly attenuated.

The fan case changes (Figure 85(c) to (i) and (k)) alter the fan noise slightly. The hardwall lip (Figure 85(j)) has increased fan broadband noise relative to the treated lip configurations.
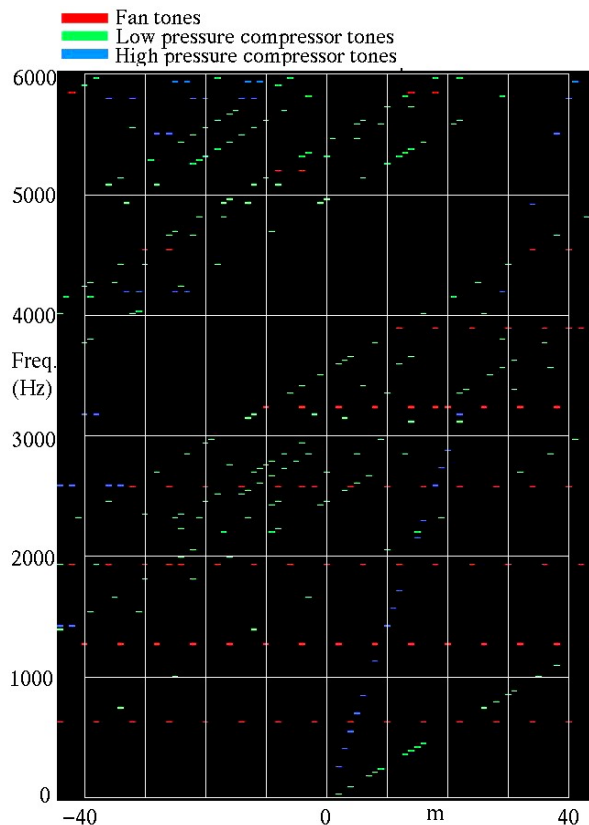
Figure 83.—Expected spinning modes at approach power. (Assumes three splices in the fan case lining.)
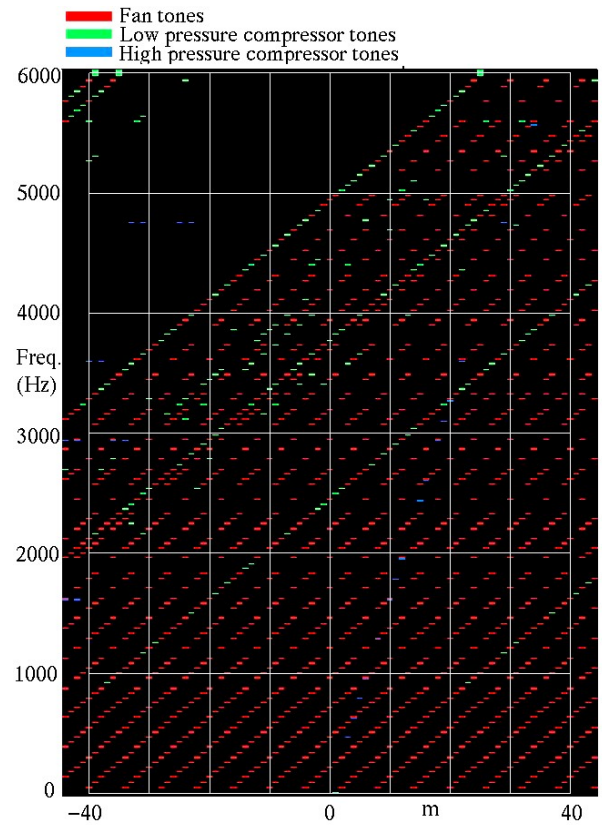
Figure 84.—expected spinning modes at cutback power. (Assumes three splices in the fan case lining.)
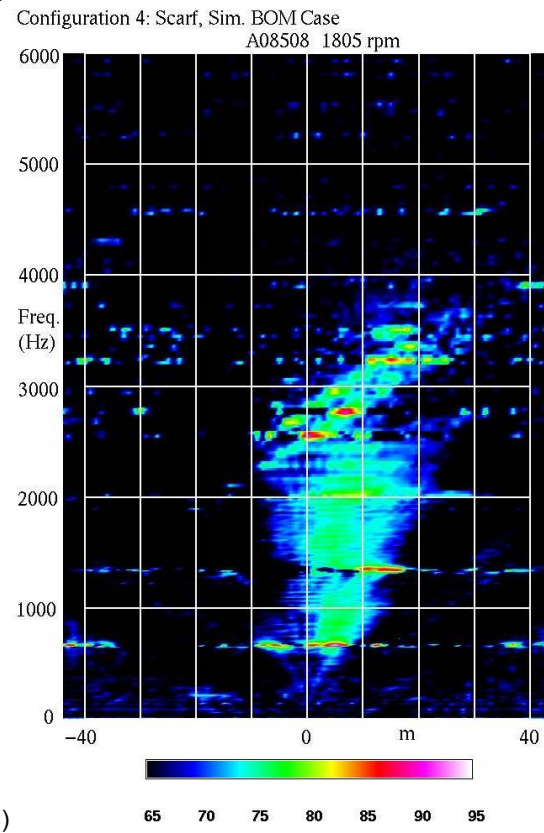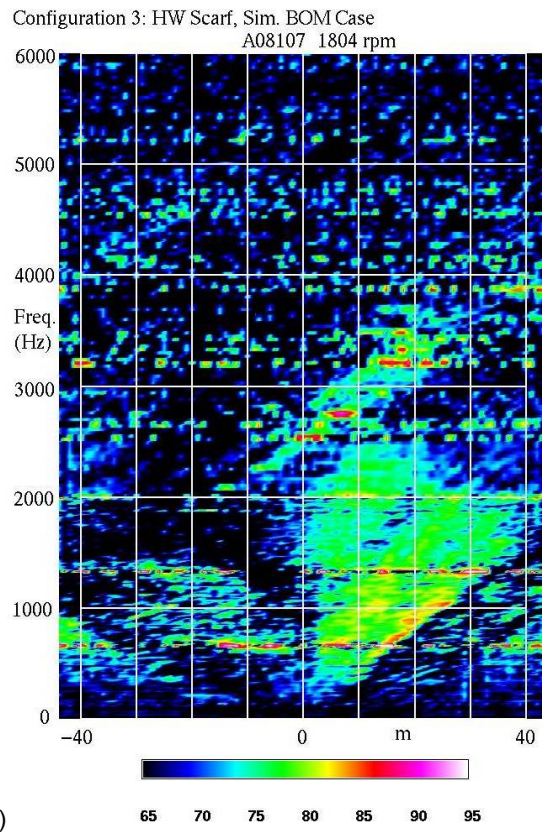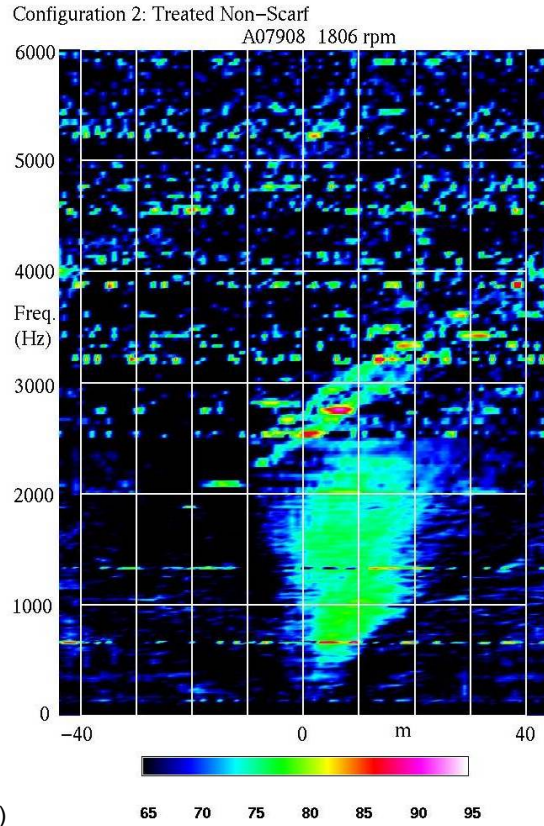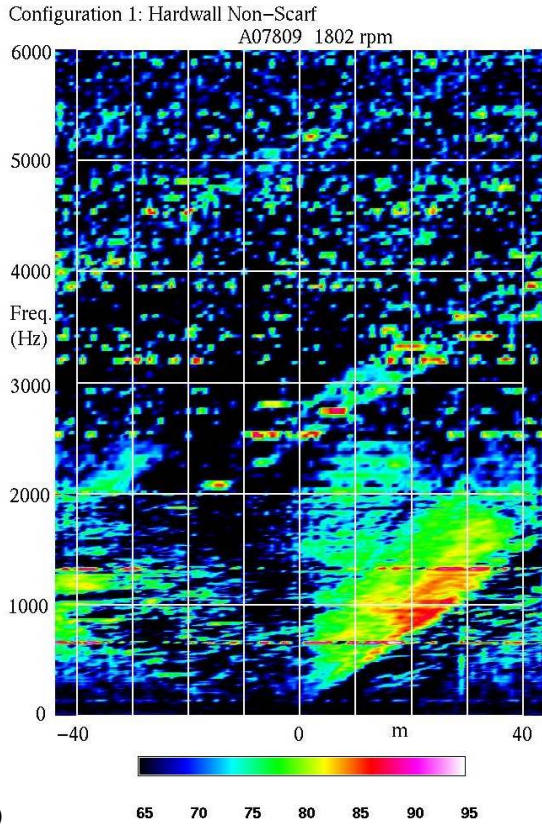
Figure 85.—Measured spinning modes for the 11 inlet configurations at approach power.

Configuration 5: Scarf, 2 in. Case R1
A08608 1803 rpm

(e)

Configuration 6: Scarf, 2 in. Case R1
A08708 1802 rpm

(f)

Config. 7: Scarf, 2 in. Case R2, 8 strips 3 in. wide
A08809 1803 rpm

(g)

Config. 8: Scarf, 2 in. Case R2, 3 strips 3 in. wide
A08909 1804 rpm
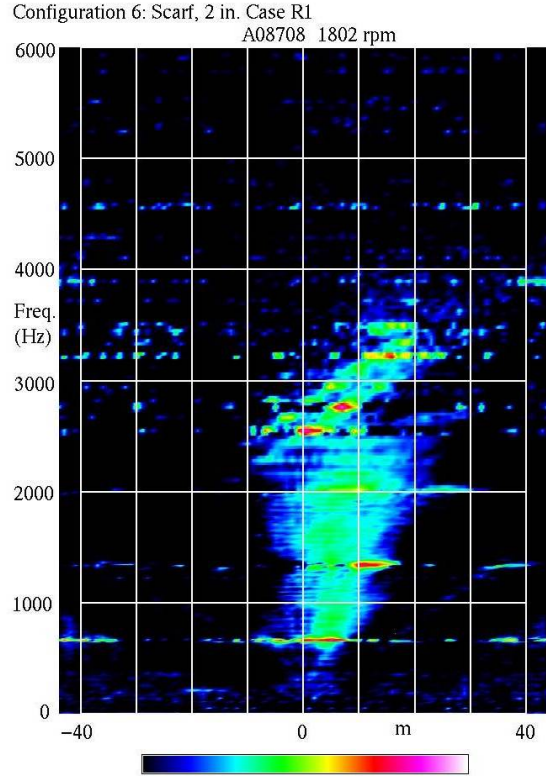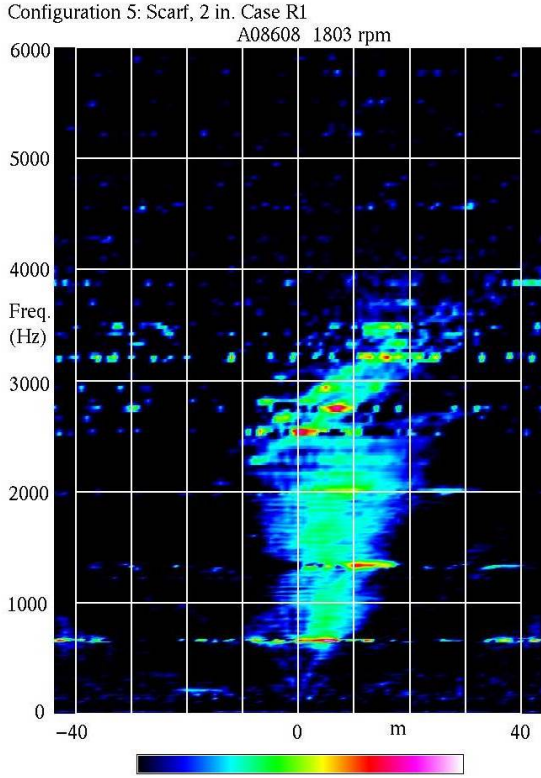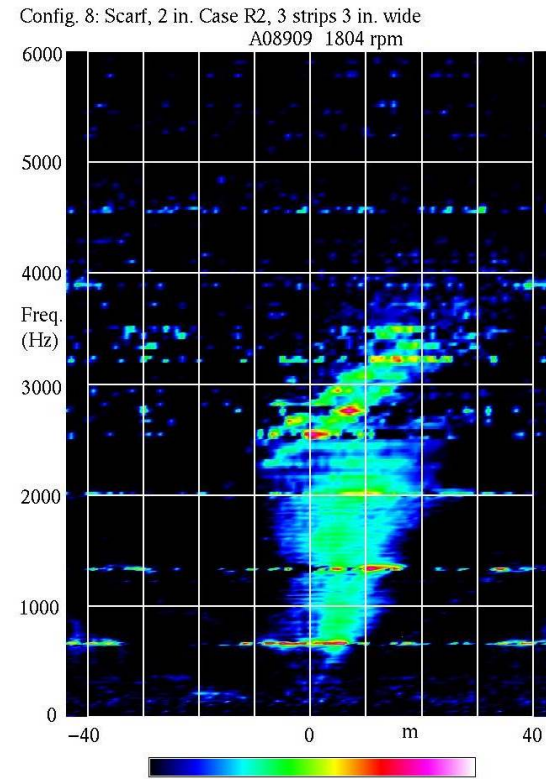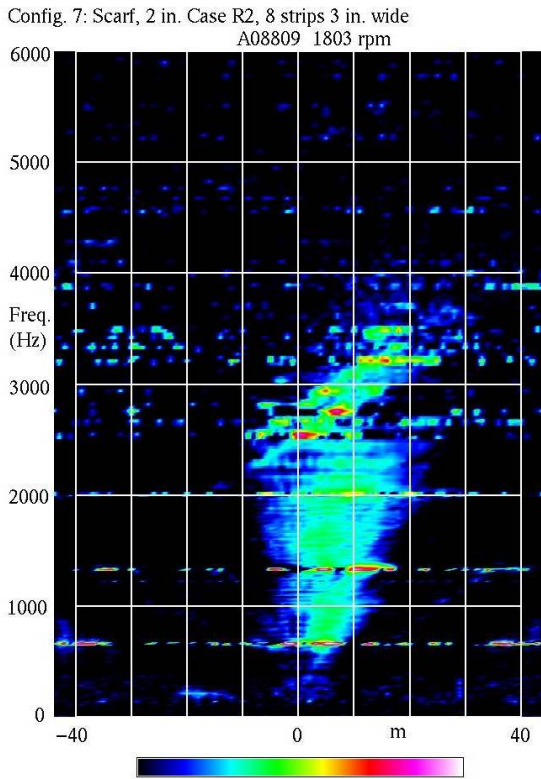
(h)

Figure 85.—Continued.

Cfg. 9: Scarf, 2 in. Case R2, 3 strips 1.25 in. wide
A09009   1804 rpm
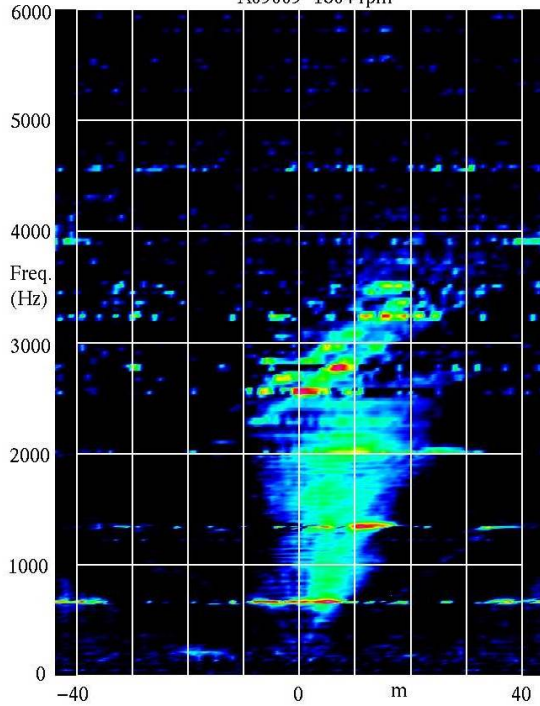
Configuration 12: Scarf, Hardwall lip, 2 in. Case R2
A08309   1804 rpm

(i)
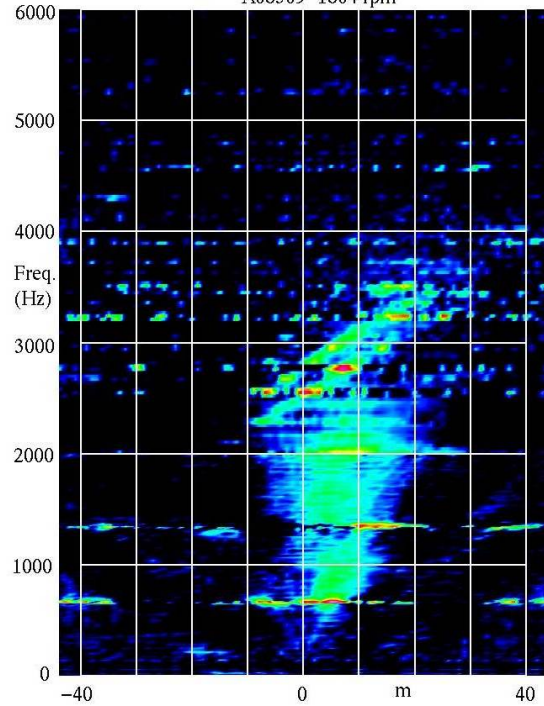
(j)

Configuration 14: Scarf, Case taped hardwall
A08409   1804 rpm
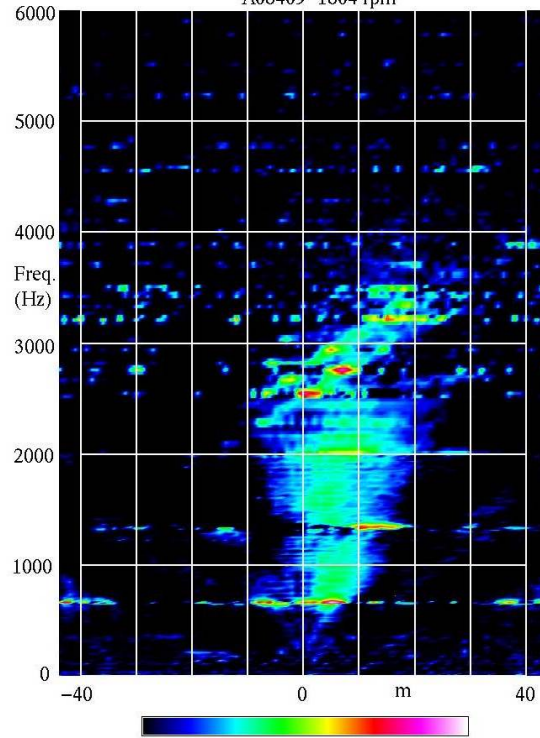
(k)

Figure 85.—Concluded.

4.3.6.2 Spinning Modes: Cutback Power

The spinning mode plots for cutback power are given in Figure 86. The hardwall non-scarf plot (Figure 86(a)) has the expected buzzsaw modes. The production lining gives a substantial, but not complete reduction in buzzsaw noise (Figure 86(b)). The hardwall scarf inlet (Figure 86(c)) has a little more buzzsaw noise than the hardwall baseline. The treated scarf inlets generally do not radiate buzzsaw noise. The exceptions are the configurations with fan case scattering strips (Figure 86(g) to (i)) and especially the hardwall lip (Figure 86(j)). Surprisingly, the buzzsaw noise with the hardwall lip appears in low order modes. The hardwall fan case (Figure 86(k)) produces a small increase in buzzsaw noise. Figure 86(j) has increase fan broadband noise relative to the treated lip configurations.
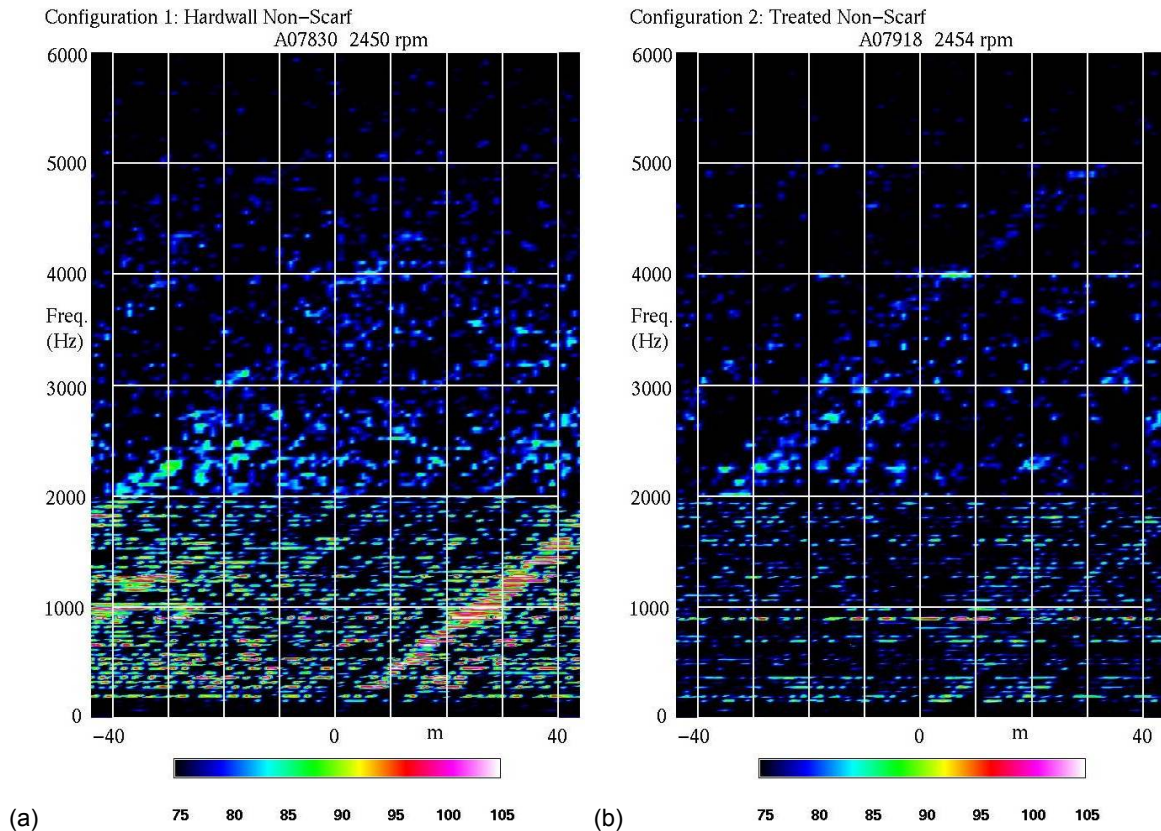
Figure 86.—Measured spinning modes for the 11 inlet configurations at cutback power.
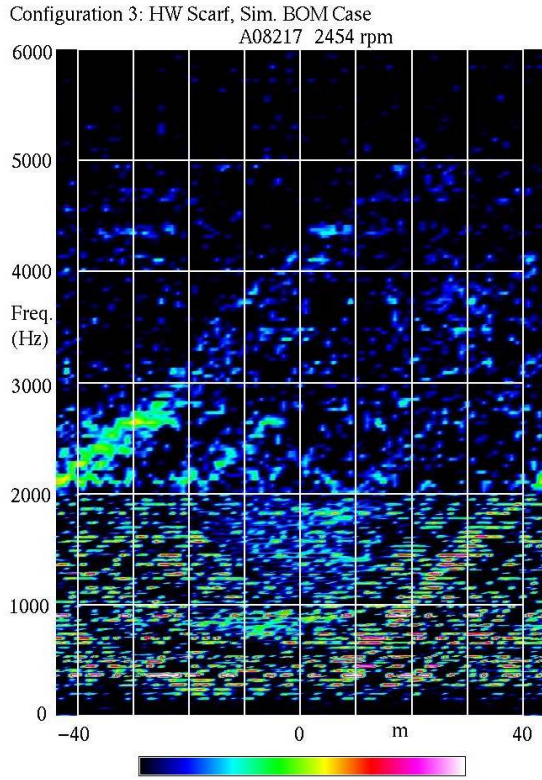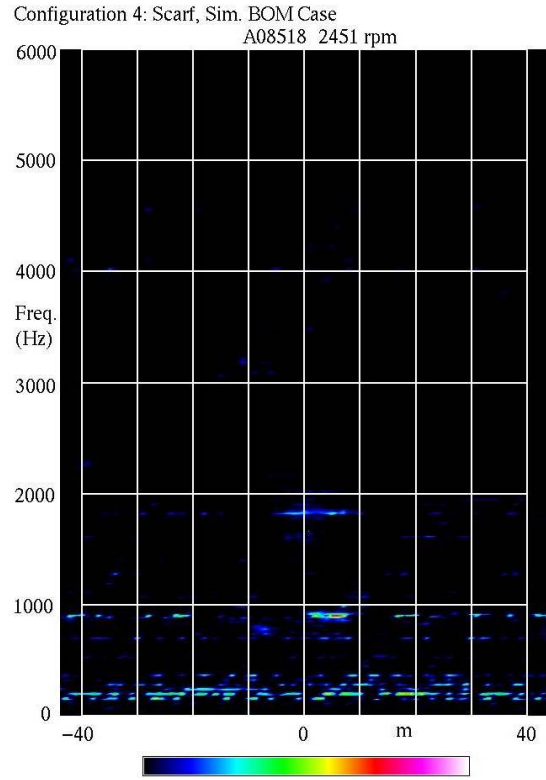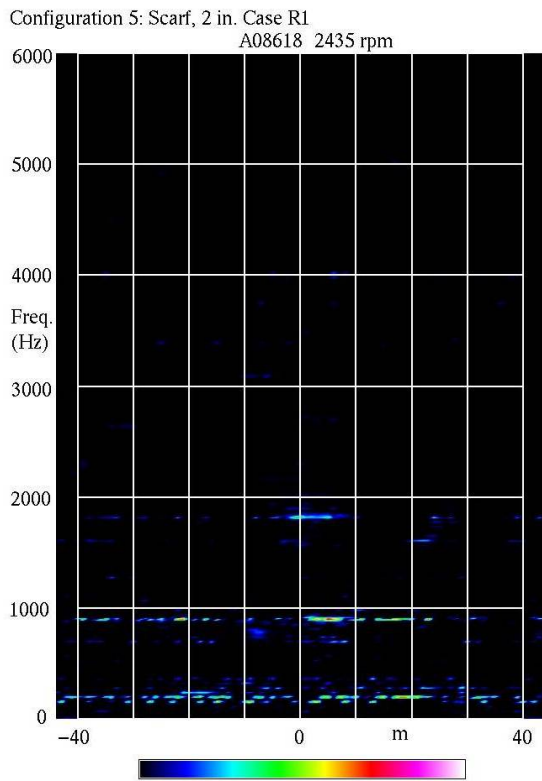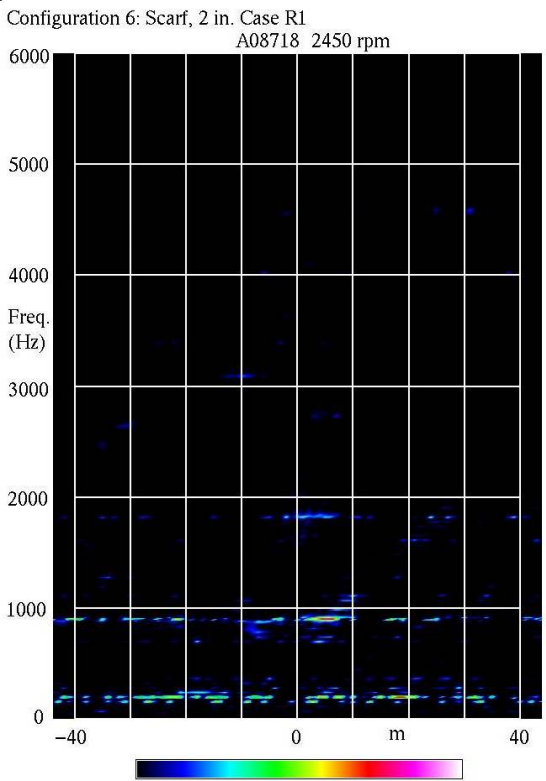
Figure 86.—Continued.

Config. 7: Scarf, 2 in. Case R2, 8 strips 3 in. wide
A08819 2454 rpm

Config. 8: Scarf, 2 in. Case R2, 3 strips 3 in. wide
A08919 2453 rpm

(g)

(h)
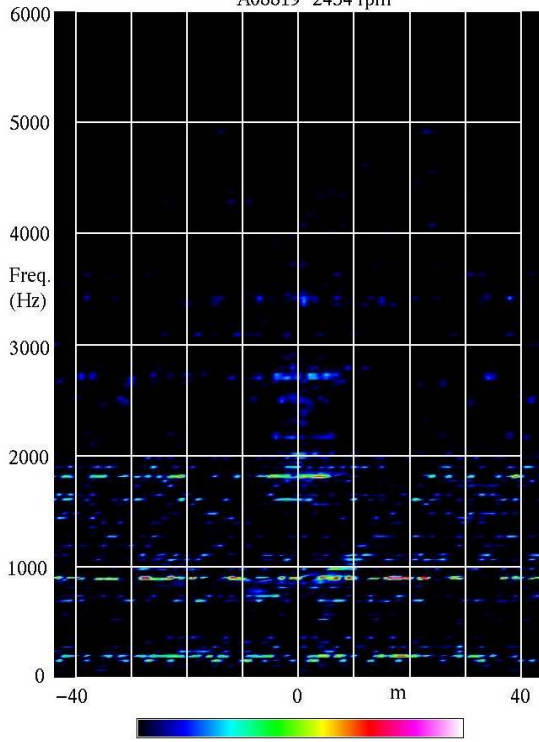
Cfg. 9: Scarf, 2 in. Case R2, 3 strips 1.25 in. wide
A09019 2453 rpm
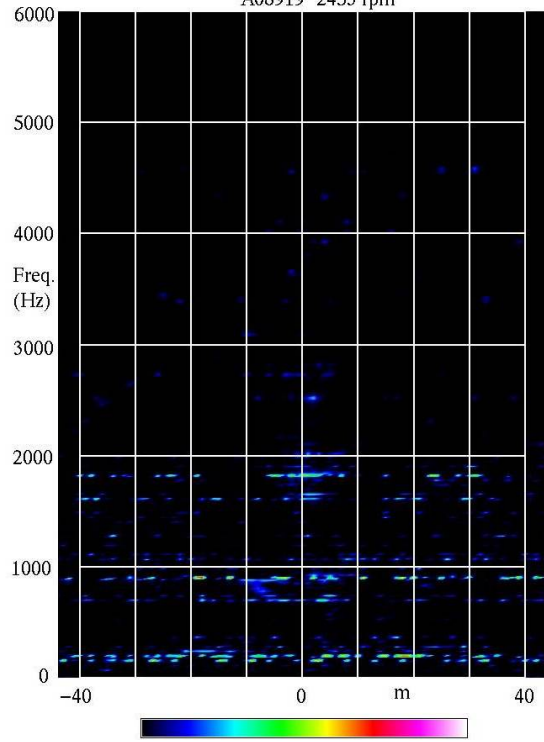
Configuration 12: Scarf, Hardwall lip, 2 in. Case R2
A08319 2451 rpm

(i)

(j)

Figure 86.—Continued.

Configuration 14: Scarf, Case Taped Hardwall
A08419 2452 rpm

(k)
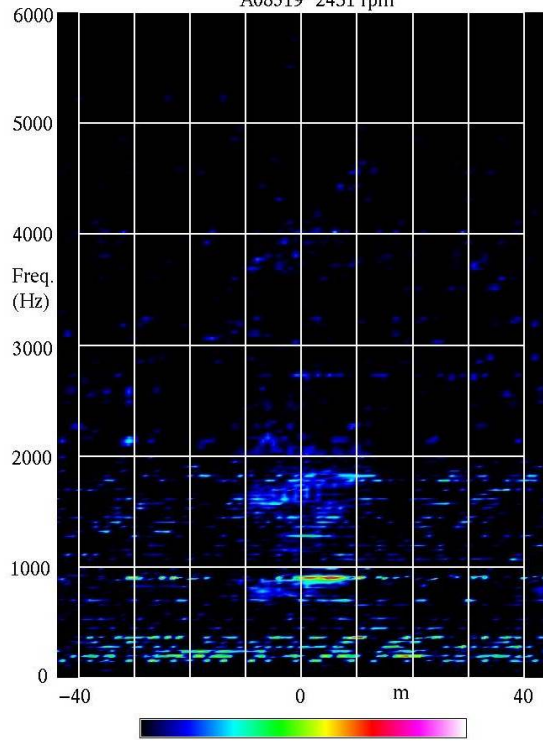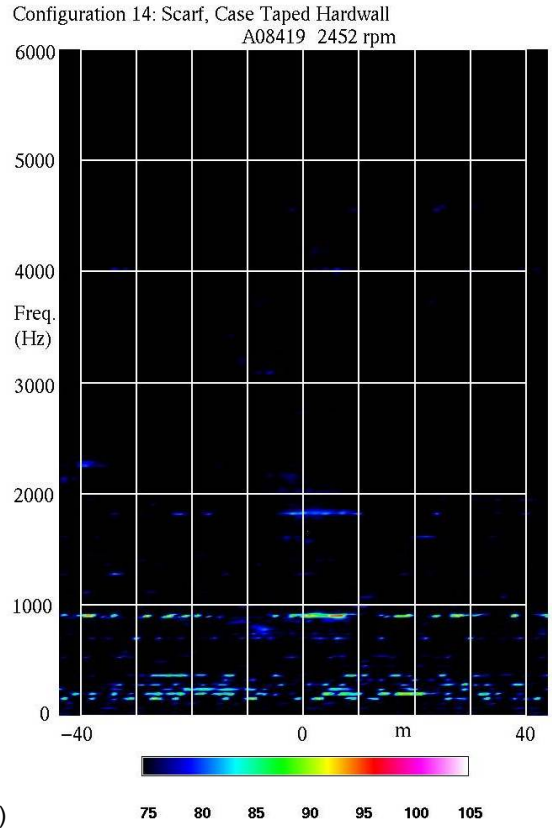
Figure 86.—Concluded.

4.3.6.2.2   Spinning Modes: Takeoff Power

The spinning mode plots for takeoff power are given in Figure 87. The treated and hardwall plots are in the non-scarf case (Figure 87(a) and (b)) are very similar. This indicates that the production lining is ineffective at takeoff power. The hardwall scarf inlet has significantly more buzzsaw noise at takeoff power that the non-scarf inlet (Figure 87(c)). The treated scarf inlets, except for the one with the hardwall lip (Figure 87(d) to (f)) have similar noise characteristics as the non-scarf cases. Figure 87(f) suggests that the lip lining is the most important section of lining at takeoff power.
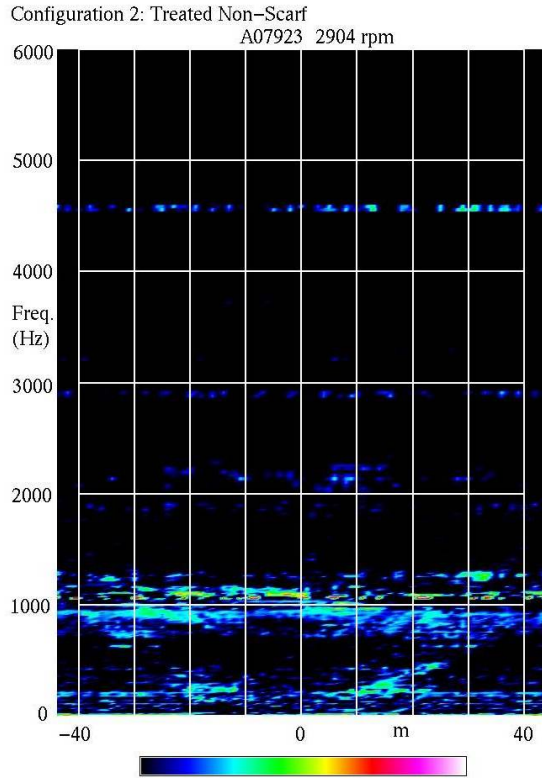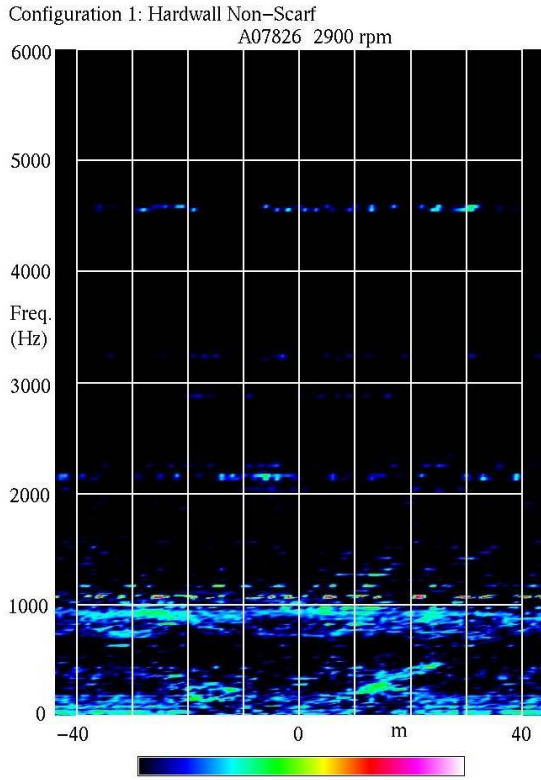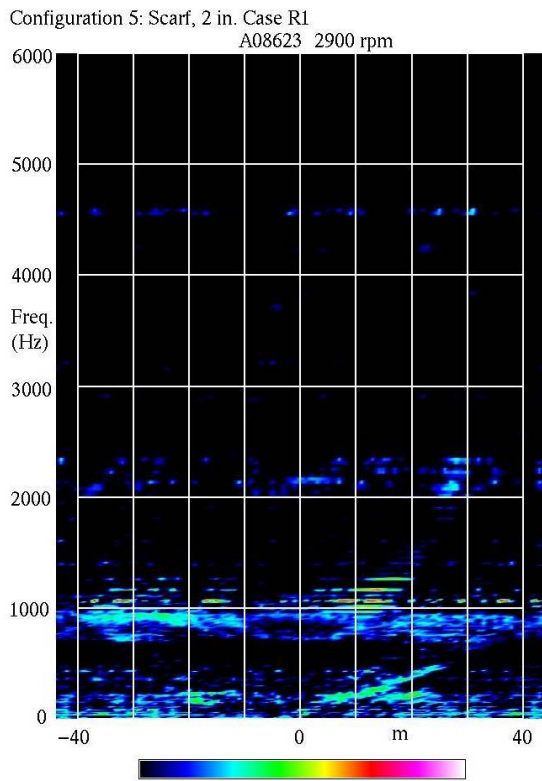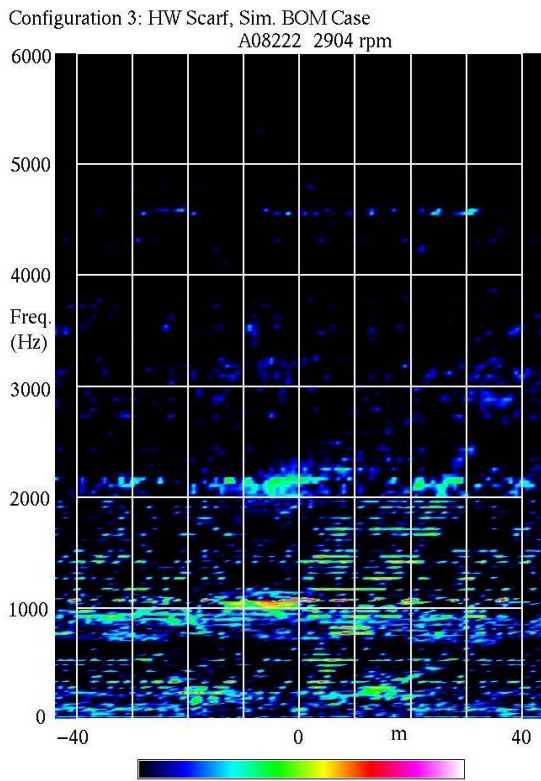
Figure 87.—Measured spinning modes at takeoff power.
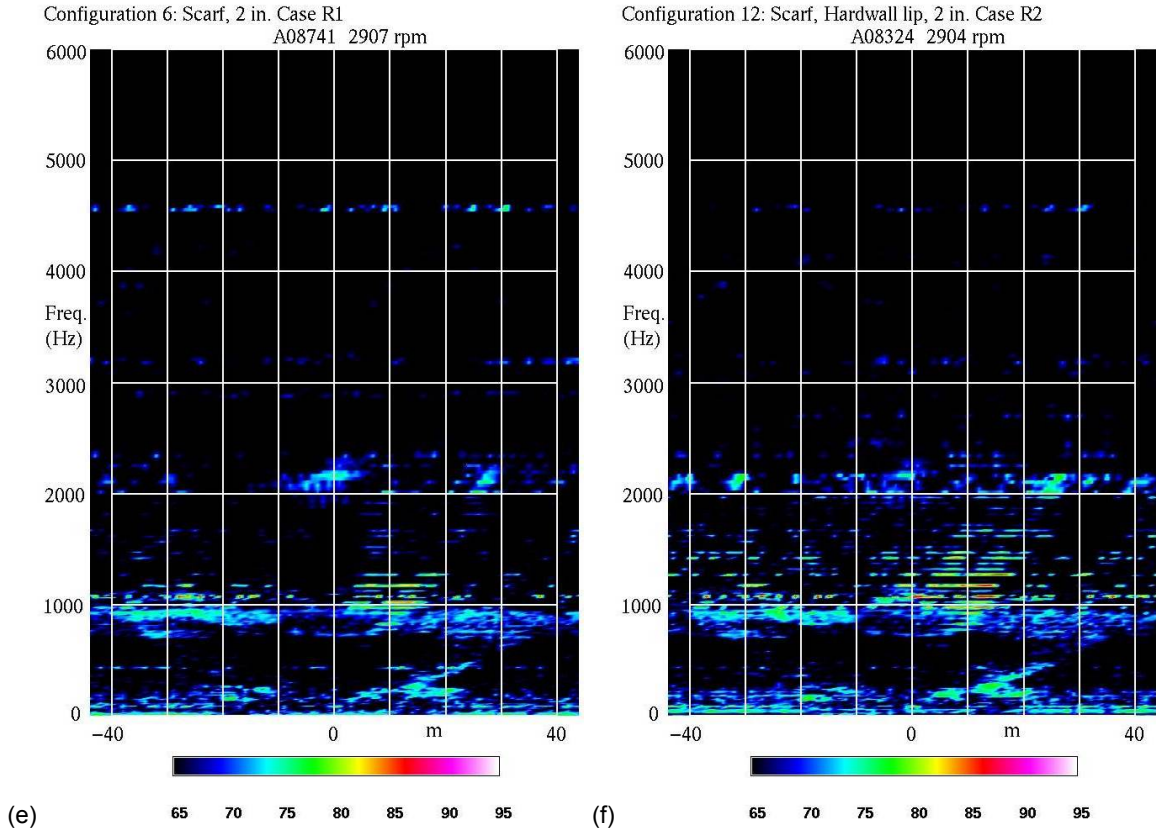
Figure 87.—Concluded

4.3.6.3   LPC and Fan Harmonic Noise

Figure 88 to Figure 91 demonstrate that the ICD array finds the LPC spinning modes and higher frequency fan harmonics at the expected spinning orders.

Figure 88 shows identifiable spinning modes from as far into the LPC as the fourth stage.

Figure 89 gives conventional beamforming plots at the fan face for modes that were identified as co-rotating and counter-rotation. The co-rotating modes appear to come from the lower portion of the LPC due to the direction of fan and mode rotation (counterclockwise looking into the inlet), and the apparent perspective point of the array at the main cluster of microphones on the left side of the inlet. The counter-rotating modes come from the top of the LPC.

Figure 90 and Figure 91 show interactions between the fan and the LPC inlet guide vanes, and the fan and the first stage LPC rotor.
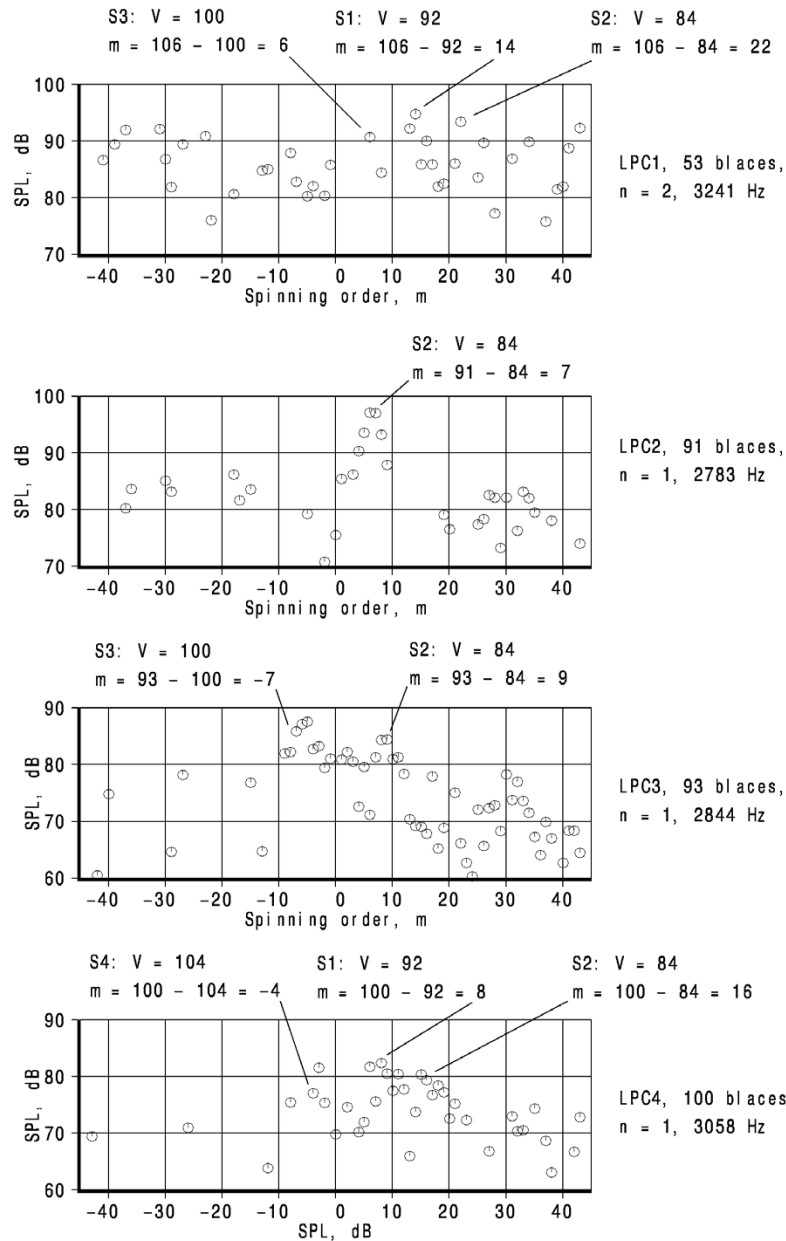
Figure 88.—Single-frequency spinning mode plots for selected low pressure compressor tones (with the hardwall non-scarf inlet) at 1802 rpm. The mechanical rpm (see Table 7) is 1828 rev./min. Interaction modes are shown for LPC stages 1 to 4.

Run A08508, Configuration 4

2800 Hz

2862 Hz

BF SPL, dB

BF SPL, dB

75   76   77   78   79

67   68   69   70   71
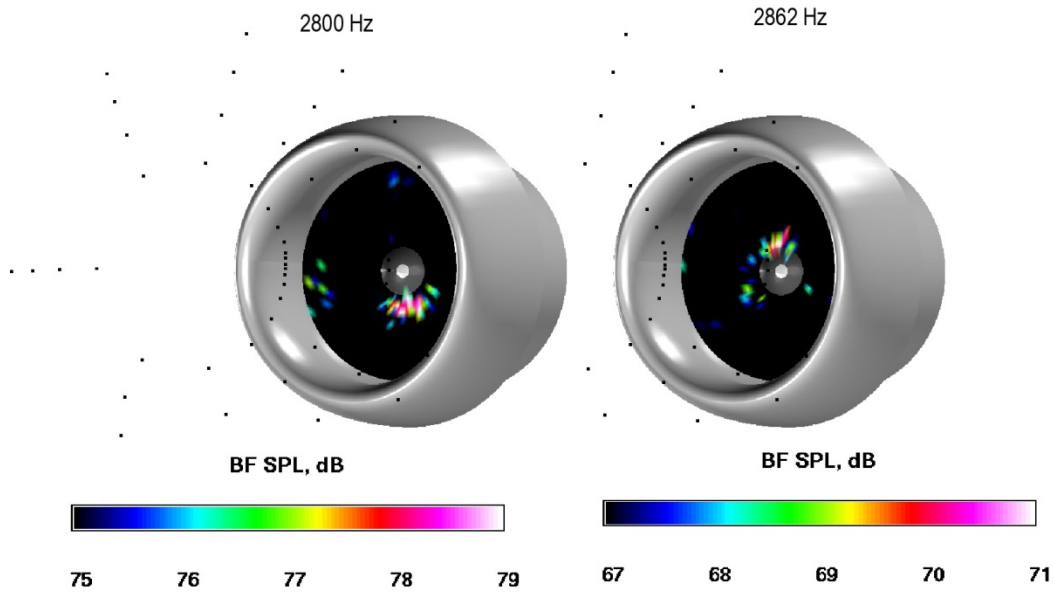
Figure 89.—Fan-face beamforming plots for a co-rotating LPC mode (m = 7 from the first harmonic of the second stage of the LPC interacting with the vanes ahead of it), and a counter-rotating LPC mode (m = –7 from the third stage of the LPC). Run A08508 (the scarf with the simulated BOM fan case) at 1805 rpm corrected, and 1847 rpm mechanical.

S1: V = 92
m = 88 – 92 = –4

4 BPF, 22 blades,
n = 4, 2691 Hz

S1: V = 92
m = 128 – 92 = 36

Fan-LPC interaction
tone. Fan + 2 LPC1
22 + 2*53 = 128
3914 Hz
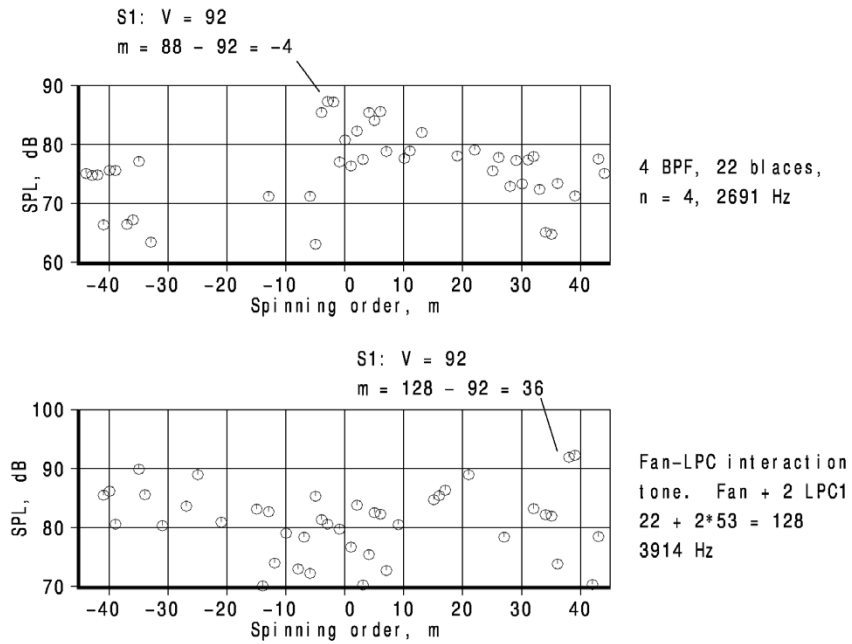
Figure 90.—Single-frequency spinning mode plots for interactions between the fan and the LPC. In the upper plot, the fan interacts with the inlet guide vanes of the LPC. The lower plot shows an interaction between the fan, the first stage LPC rotor, and the LPC inlet guide vanes. The same run as Figure 88 is represented.

Run A08508, Configuration 4
2708 Hz
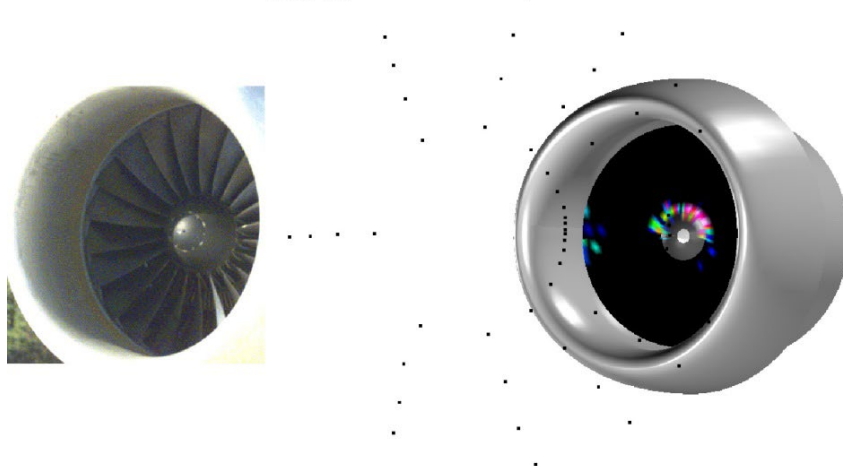
Figure 91.—A fan-face beamforming plot for the fan-LPC IGV interaction show
in Figure 90. The mechanical rpm is 1847 (it is the same run as Figure 89).
This is higher than the 1828 rpm of Figure 90, so the frequency is shifted from
2691 to 2708 Hz. A counter-rotating mode ($m = -4$) is shown.
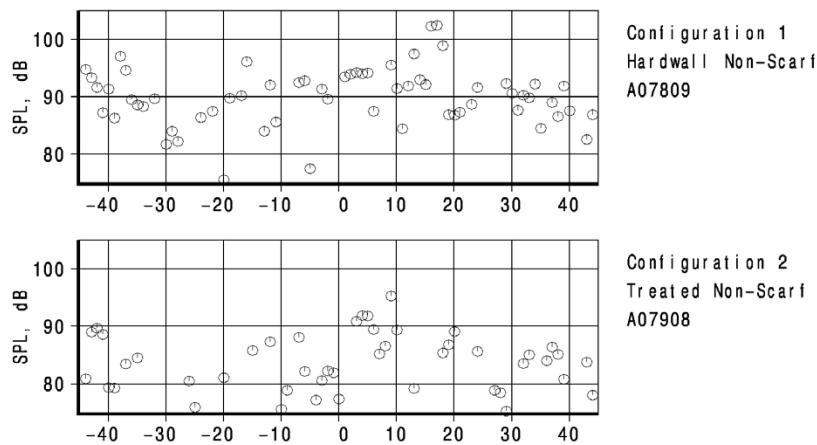
Figure 92.—Spinning modes at blade passage frequency for the hardwall
and treated non-scarf inlet at approach power.

4.3.6.4   Blade Passage Frequency Noise

Figure 92 to Figure 98 give results for the blade passage frequency noise of the various configurations at approach power. The hardwall non-scarf inlet has a strong blade passage mode in $m = 17$-18. (Figure 92). In the treated case, the primary mode appears to be $m = 9$.

The hardwall scarf inlet has elevated BPF energy in a number of modes, including $m = 17$ (Figure 93). The treated case is dominated by $m = 5$.

Beamforming images of the hardwall inlets (Figure 94) show most of the noise coming from the general area of the crown in the case of scarf inlet. The noise source distribution appears to have periodic structure. The repetitive structure is also evident in the case of the treated scarf inlet and perhaps also the treated non-scarf inlet (Figure 95).

Figure 96 to Figure 98 explore the effect of fan case changes on blade passage frequency tones. The 3 and 1.25 in. tape strips increase the noise appreciable (Figure 98 and Figure 99); the other changes do not. It is unclear if the modes introduced by the tape strips are in the expected orders (22-3k and 22-8k for three and eight strips, respectively, and integer k).
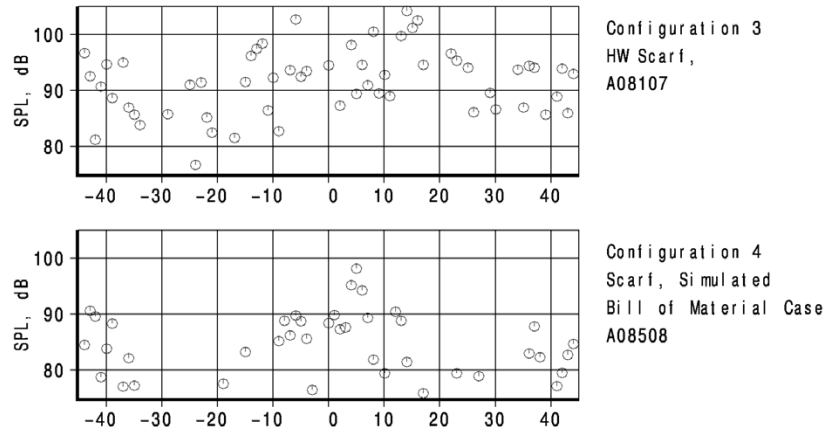
Figure 93.—Spinning modes at blade passage frequency for the hardwall and treated scarf inlet at approach.
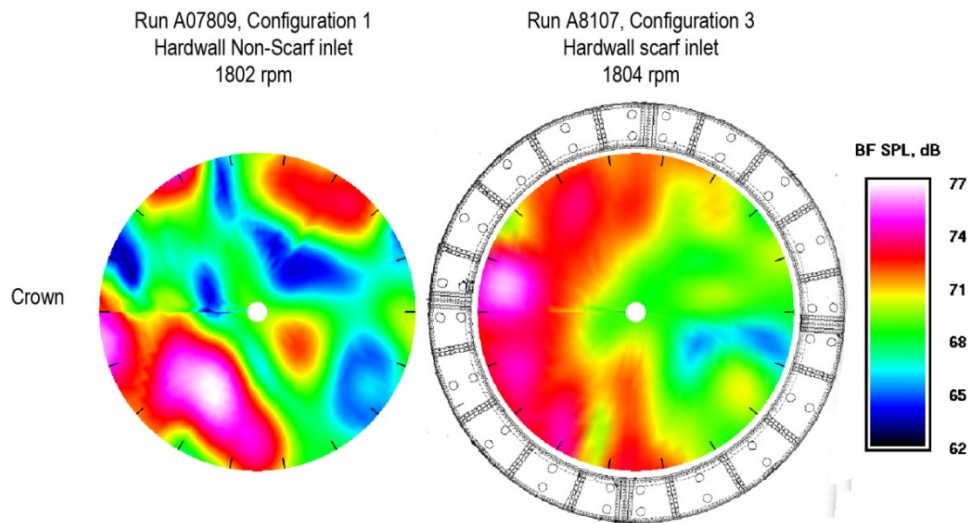
Figure 94.—Beamforming plots for the hardwall non-scarf and scarf inlets at blade passage frequency at approach power.
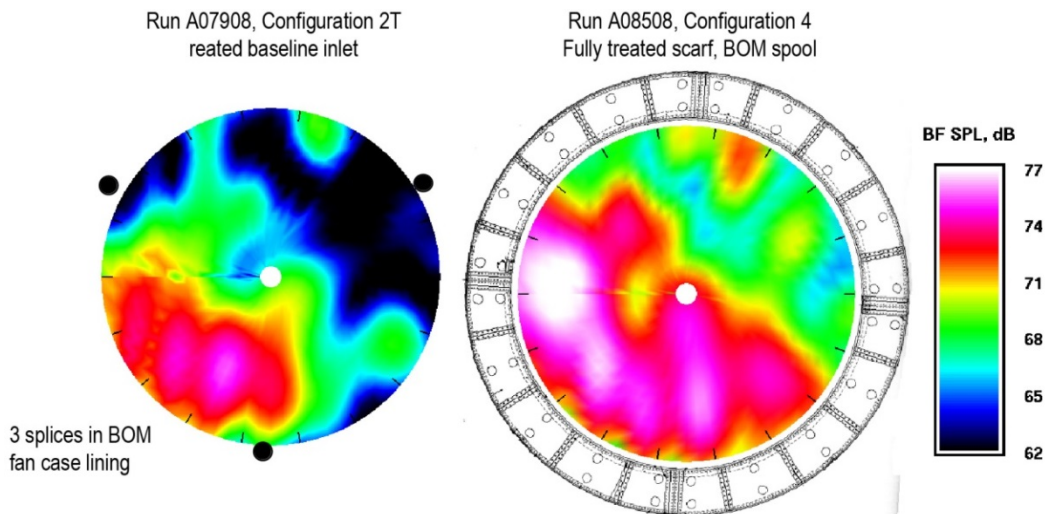
Figure 95.—Beamforming plots for the treated non-scarf and scarf inlets at blade passage frequency at approach power.
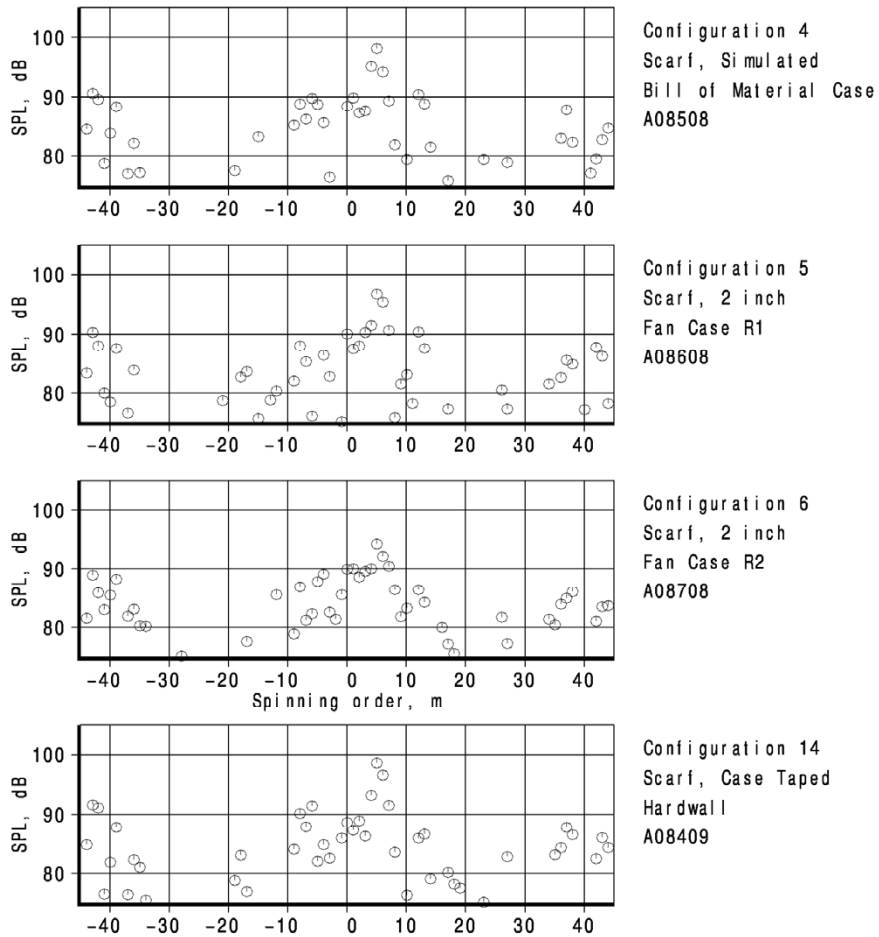
Figure 96.—Spinning modes at blade passage frequency for four fan cases at approach power.
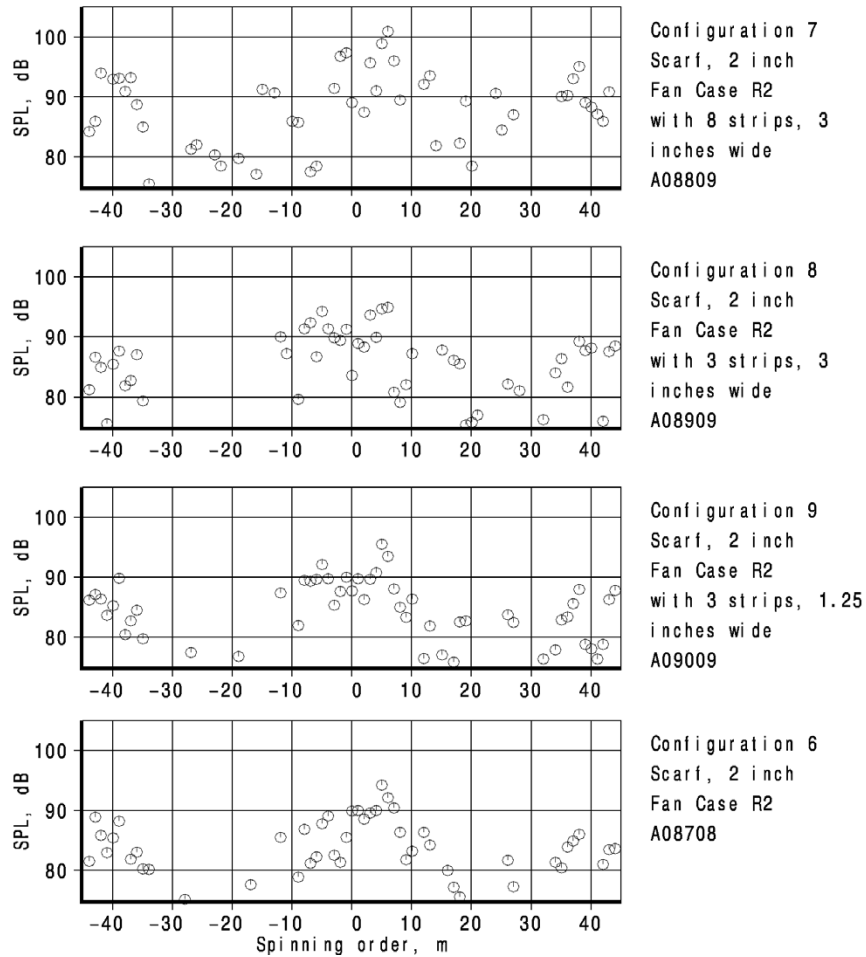
Figure 97.—Spinning modes at blade passage frequency for three arrangement of scattering strips on the fan case. The R2 case with now strips is shown again for comparison.

BF SPL, dB
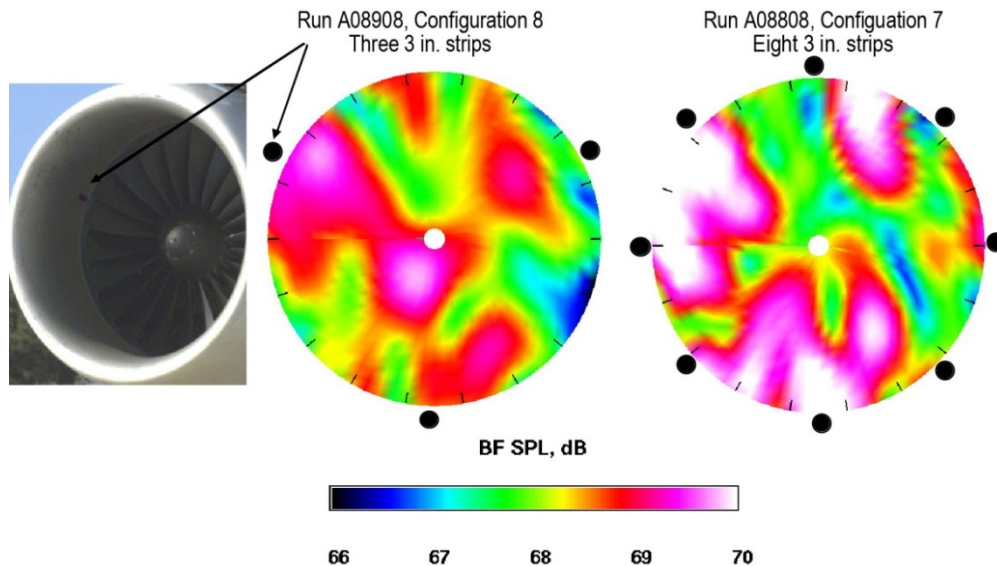
Figure 98.—Fan face beamforming plots at blade passage frequency for two configurations of mode scattering strips.

4.3.7 Conclusions

The ICD phased array can measure low-pressure compressor noise in the expected spinning modes. The results for blade passage frequency are promising, but not completely satisfactory. This is probably due to the scattering of the modes by the nonuniform inlet and flow geometry. At approach power, the inlet noise of the PW4098 has a strong contribution from the low pressure compressor. Blade passage tones and broadband fan noise are also important. High pressure compressor noise may play a role. Blade passage frequency noise for the hardwall baseline inlet is dominated by the mode $m = 17\text{-}18$. There is no obvious mode in the treated case. The blade passage frequency noise of the treated scarf inlet is strongly concentrated around $m = 5$. Beamforming images show a periodic source structure that may be consistent with generation of this mode. Inlet lip lining is very effective in attenuating buzzsaw noise at low spinning orders. The production lining is ineffective at takeoff power. The production lining is largely ineffective for low-pressure compressor noise at approach power.

4.4 PW4098 Blade-Mounted Transducer and Mode Array Tone Diagnostic Test Results

4.4.1 Data Acquisition and Instrumentation

4.4.1.1 Data Acquisition System

Figure 99 shows a schematic of the data acquisition system. This system was comprised of a network of two laptop computers (233 MHz) and one desktop computer (133 MHz) with an external Iomega Jaz drive. Connection to the Boeing network was accomplished by modem.
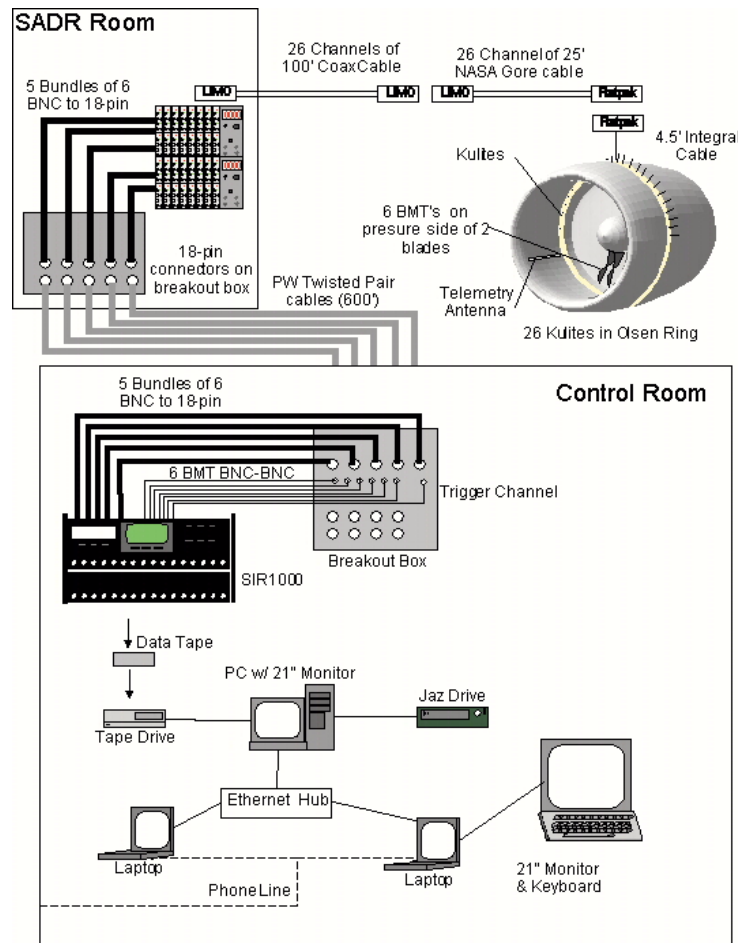
Figure 99.—Schematic of Instrumentation setup.

A Sony SIR-1000 system with a 32-channel capacity was used for data acquisition. The system was capable of measuring 32 channels simultaneously at a sampling rate of 48 kHz. Data was digitally recorded onto a Sony 8 mm tape, which was played back through an AIT (Advanced Intelligent Tape) drive unit, (model number SDX-S300C) and converted to an ASCII file on the PC.

4.4.1.2 Blade-Mounted Transducers (BMT)

Eight Kulite pressure sensors (Model LQ-47-50A) were mounted to the pressure side of two fan blades at the locations shown in Table 8. A nominal distance of 0.1 in. was assumed to be the gap between the blade tip and the wall. The distance from the blade tip to the transducers was therefore the value shown in Table 8 are -0.1 in. Four transducers were mounted on the number-1 and number-22 blades as shown in Figure 100. The telemetry system only allowed six signals to be transmitted at any time, but due to some complications, a maximum of five BMT's were used. The increased boundary layer thickness in the scarf inlet required a distribution of Kulites extending to greater distance from the wall than the Production inlet.

Before the transducers were bonded to the blades, the blades were heated in an autoclave to remove any dirt and oil that may have contaminated the blade surface. The leads from the sensors were routed as shown in Figure 100 along the blade mid-chord, and into the hub.

The Pratt & Whitney telemetry system was mounted in the spinner in order to transmit the pressure signals to an antenna in the inlet. The antenna was secured to the inlet with Rhino tape in the keel region as shown in Figure 101.

TABLE 8.—BMT LOCATIONS ON FAN BLADES

Blade 1		Blade 22	
Transducer	Distance from wall, in.	Transducer	Distance from wall, in.
1A	0.5	2A	1.0
1B	1.5	2B	2.0
1C	2.5	2C	4.0
1D	3.25	2D	8.0
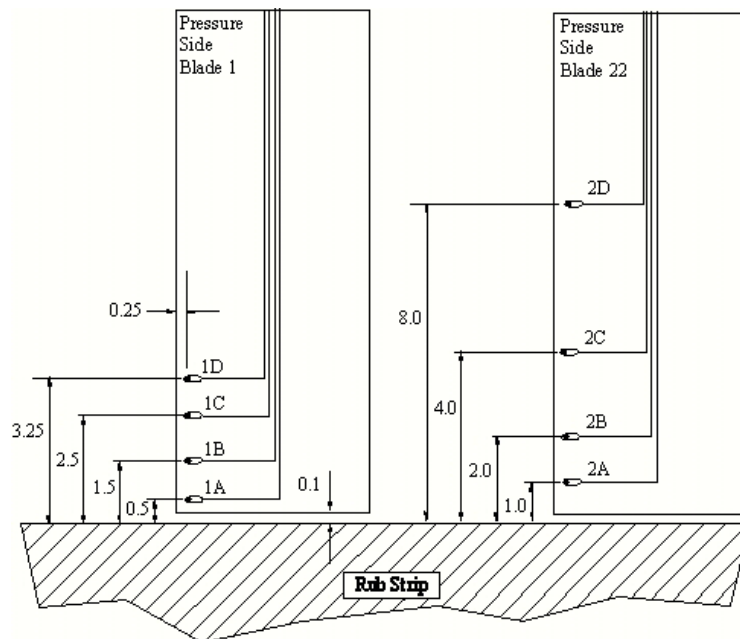
Figure 100.—Locations of BMT's on Blades 1 and 22 (not to scale).
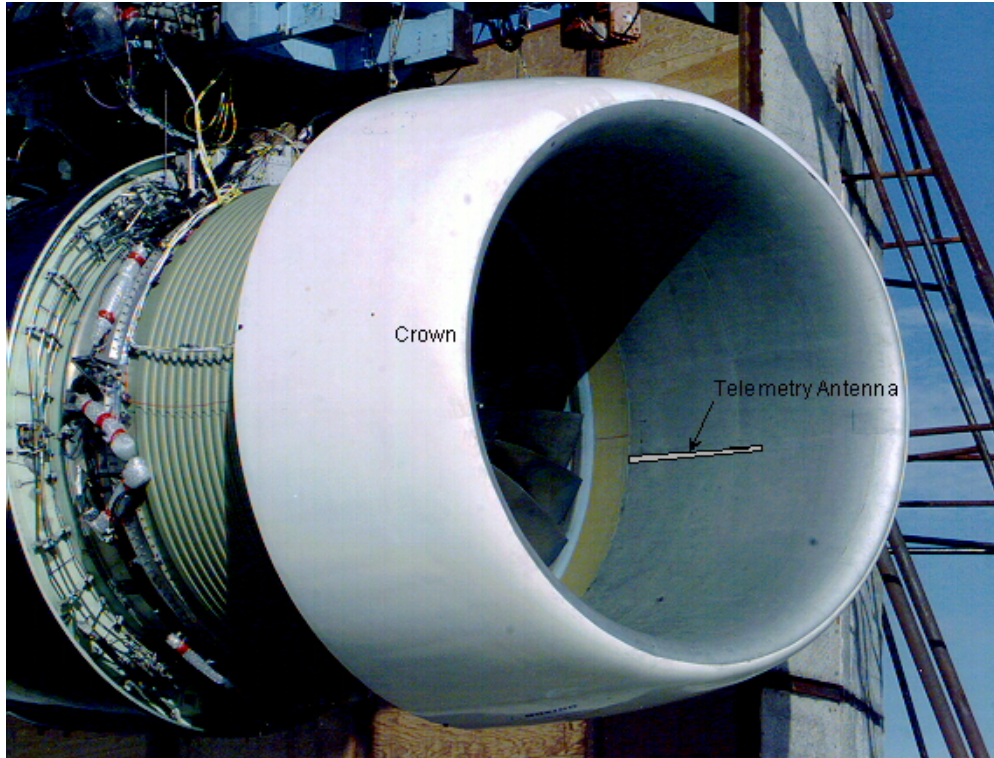
Figure 101.—Photograph of scarf inlet indicating the location of the telemetry antenna.

4.4.1.3   Inlet Mode Array

In the second half of testing, May to June 1999, an adapter ring was made to allow the production case to be used with the scarf inlet. This provided an opportunity to add a circumferential microphone array in the inlet for measuring the acoustic modes. A 26-transducer, half-circular array spanning the top half of the engine was designed into the adapter ring, which can be seen in Figure 102.

The transducers were located at the attach flange (STA 121) which is approximately 13 in. from the fan face. The transducers are evenly spaced 6.92° apart spanning half the circumference of the inlet. Special pressure transducers were used, which had very little phase variations between them. These transducers were developed to support other NASA sponsored work to measure broadband modes for the Source Diagnostic Test currently scheduled for February of 2000. The transducers were a slight variation of Kulite Model XCQ-125B-093-15A having an RTV layer over the diaphragm instead of a protective screen. The piezo-resistive transducers are capable measuring the pressure without the need for a phase calibration between the sensors.
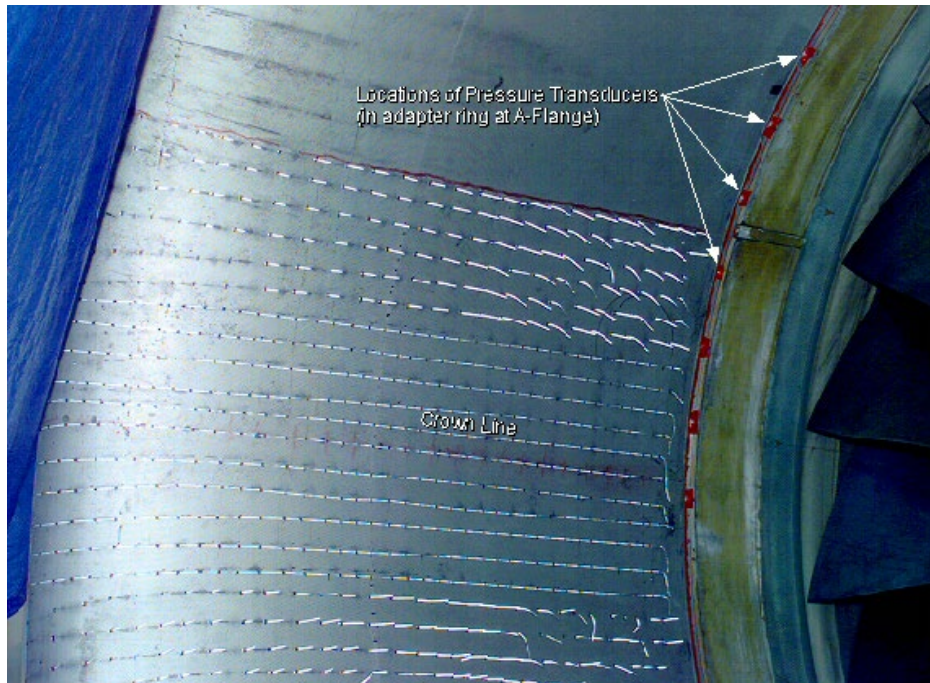
Figure 102.—Location of the mode transducers.
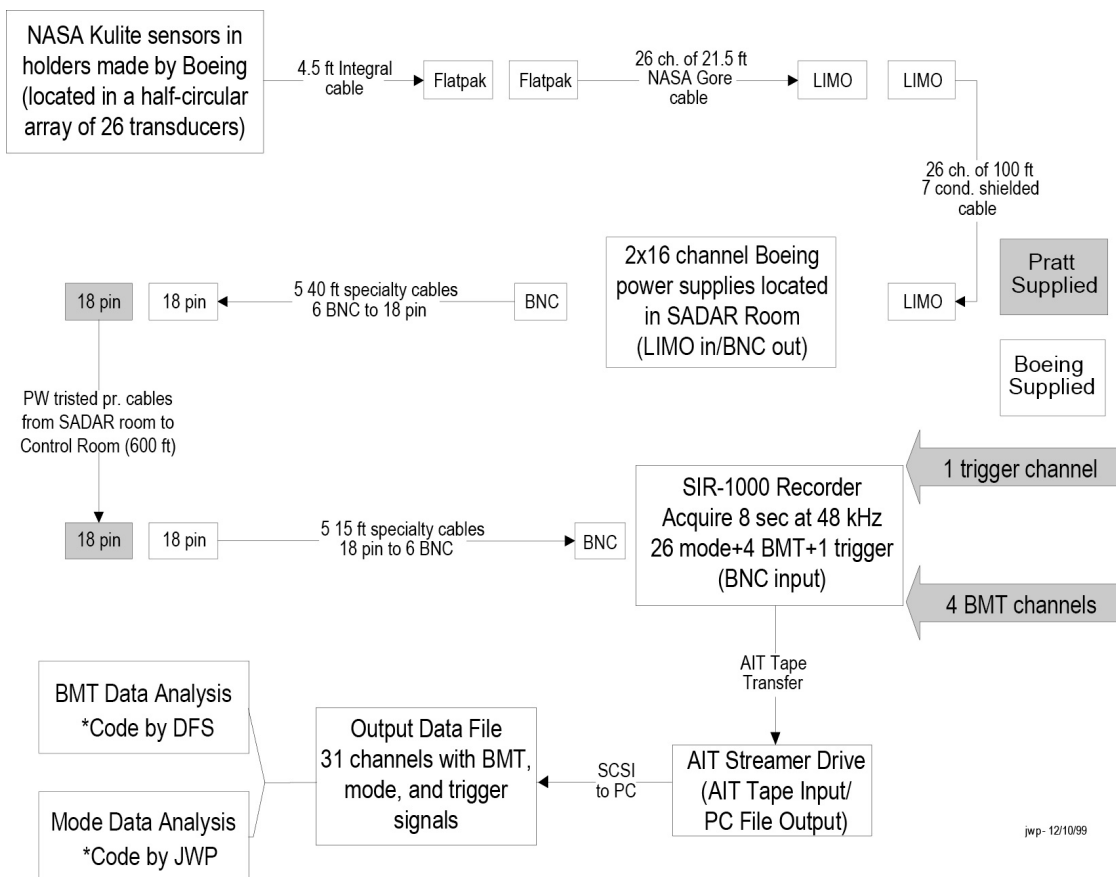
Figure 103.—Ideal Inlet Mode Data System block diagram.

A disadvantage of these sensors is that they are very easily damaged because the diaphragm is exposed. Approximately 15 transducers were lost during testing. Most were lost due to a design flaw in the adapter ring that didn't allow for trouble-free sensor installation.

The sensors were wired to the bridge/balance power supplies located in a room near the test stand (see Figure 102) using 126 ft of wire. The voltage signals from the power supplies were then connected to the Control Room over the P&W existing ground lines by using specialty cables. A Sony SIR-1000 recorder was used to simultaneously record 8-sec samples at 48 kHz for the 31 input channels onto an 8 mm Advanced Intelligent Tape (AIT).

A Sony AIT Streamer Drive was used to transfer the data from tape onto a network of personal computers for processing. Analysis codes were written at Boeing to process the data to produce pulse- and non-pulse synchronous data.

4.4.1.4   Data System Trigger

A "short tooth" gear was used as the trigger signal for data acquisition and pulse-synchronized averaging. Figure 104 is a typical trace of the trigger signal as measured by the data acquisition system. Table 9 provides the details of the pulse signal.

(a) 587 RPM   (b) 1833 RPM   (c) 587 RPM   (d) 1833 RPM
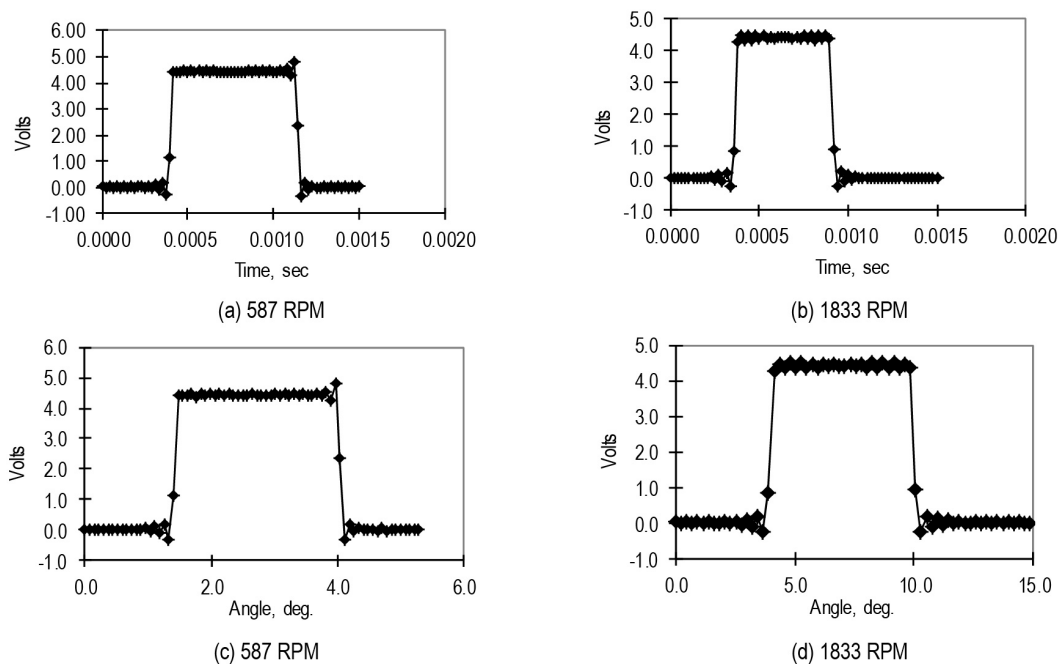
Figure 104.—Typical trace of trigger signal. (a) 587 rpm, Volts versus time, (b) 1833 rpm, Volts versus time, (c) 587 rpm, Volts versus angle, and (d) 1833 rpm, Volts versus Angle.

TABLE 9.—DETAILS OF TRIGGER SIGNAL

	587 rpm		1833 rpm	
	Rise	Fall	Rise	Fall
Edge Slope, V/ms	113.6	-122.8	108.5	-111.0
Edge Width, ms	0.0417 ms	0.0417 ms	0.0417 ms	0.0417 ms
Edge Width, deg.	0.147°	0.147°	0.46°	0.46°
Pulse Width, sec	0.792 ms		0.604 ms	
Pulse Width, deg.	2.79°		6.64°	

4.4.2   BMT Data Analysis

Voltage signals from the pressure transducers and trigger channel were recorded simultaneously. Once the data were recorded, they were then re-sampled at the desired angular resolution, which allowed pulse-synchronized mean and rms pressures to be calculated. By knowing the location of the instrumented blade, these values could then be converted from their respective time traces to their physical position relative to the inlet. A complete data set covered 8 sec of run-time for a single engine operating-point, which amounted to approximately 213 revolutions at 1600 rpm, and 386 revolutions at 2800 rpm.

A trigger level of 2 V on the falling edge was used as the starting point for each block of data, which typically consisted of one revolution. Since the operating speed of the fan is not perfect, small variations in fan rpm occur for each revolution. In order to ensure that each revolution in the averaging process had data points at exactly the same angular location, the time between the closest acquisition sample and the 2V location was calculated for each rotation. From this the entire time series for that revolution was shifted and re-sampled with the desired angular resolution. Since the original data set was sampled at 48 kHz, the worst angular resolution possible was at the highest rpm; e.g., at 2800 rpm, this corresponded to 1028 pt/rev, or an angular resolution of 0.35°. The majority of the re-sampling was performed with a resolution of 0.5° or 1°.

Four fundamental analyses were performed on the data as shown in Figure 105, Pulse-synchronized mean pressures, pulse-synchronized rms pressures, power spectrum of the pulse-synchronized mean pressure, and the mean power spectrum of the individual spectra from each rotation.

The pulse-synchronized mean pressure was calculated by averaging the pressure at a given blade location over the entire number of revolutions in the data set. Since the transducers measured the unsteady pressure (AC coupled), the time average around the circumference is theoretically zero. This analysis provides a measure of the deviation of the pressure at a specific angular location relative to this zero-mean pressure for one revolution of the fan. The absolute pressure sensed by the blade is therefore equal to the mean pressure in the inlet plus this calculated mean pressure.

The RMS pressure at a specific angular location was then calculated by using the previously calculated mean pressure at a specific location and the pressures from each revolution for that location. The RMS pressure provides an indication of the unsteady pressure at each angular location relative to the local mean pressure at that angular location.

The power spectrum of the mean pressure was calculated by applying a temporal Fourier transform to the mean pressure signal. The frequency domain was then converted to distortion orders around the inlet. A distortion order of 1 implies that the BMT senses a one-cycle distortion as the fan makes one revolution. Since the time series was averaged prior to the Fourier transform, randomness of the time series was removed and hence lower "broadband" levels occur for this analysis.

By applying the Fourier transform to a block of data, which corresponds to one fan revolution, the different distortion modes from each revolution are retained. When these spectra are averaged, a higher broadband spectrum will result in significant differences exist between the individual fan rotations.
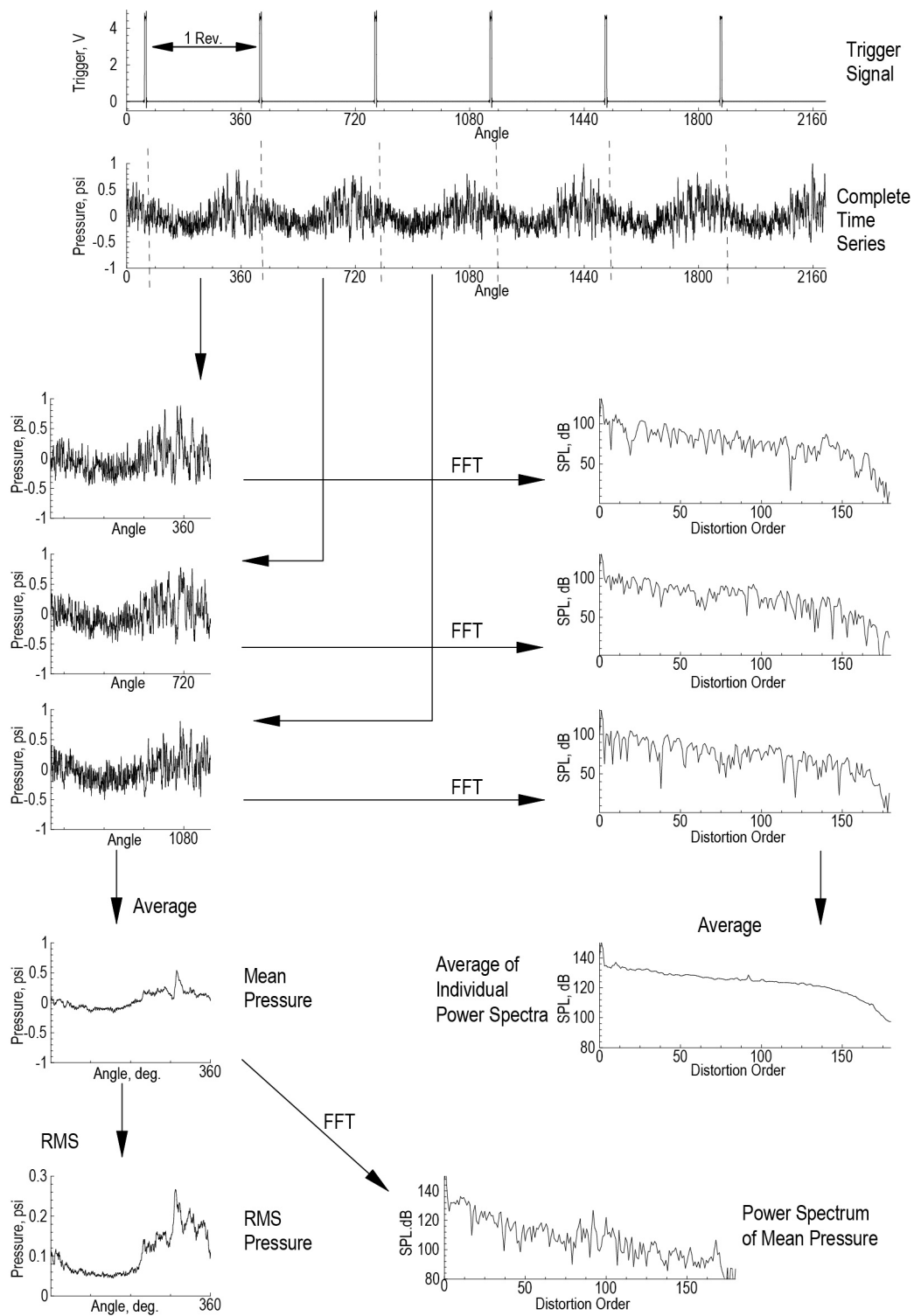
Figure 105.—Schematic of BMT data analysis.

4.4.2.1 BMT Results

The mean pressure profiles for the range of BMT locations is shown in Figure 106 for the 1620 N1C condition for the production inlet with and without the ICD, and the scarf inlet with the ICD. (The scarf was never operated without the ICD.) These plots show the mean pressure around the circumference of the inlet for a particular radial location. The value of the pressure indicates the variation of pressure from a mean value of zero around the circumference of the inlet. Each trace shows the characteristic once-per-revolution variation in the static pressure, which has been associated with the inlet droop. The amplitude of this variation increases with fan speed.

The production inlet without the ICD shows the lowest variations in mean pressure around the circumference of the inlet for the BMT's within 1 in. of the inlet wall. When the ICD is installed on the production inlet, large stationary disturbances occur in the boundary layer. The scarf inlet shows some regions of stationary disturbances that are on the order of those seen in the production inlet when the ICD is installed, with the dominant feature being the large distortion in the crown region. This distortion exists for all BMT locations out to 8 in. from the inlet wall.

The unsteady RMS pressure traces are shown in Figure 107 for the 1620 N1C condition. These values indicate the amount of variation in the static pressure at a given radial and angular position around the inlet. When the ICD is installed, the unsteady pressures decrease at all circumferential and radial locations for the production inlet. The scarf inlet shows the highest unsteady pressures in the crown region, which will later be shown to be due to the lateral motion of the boundary layer flow. Once out of the boundary layer, both inlets show similar levels of unsteady pressure, although the scarf still has some evidence of increased unsteadiness near the crown.
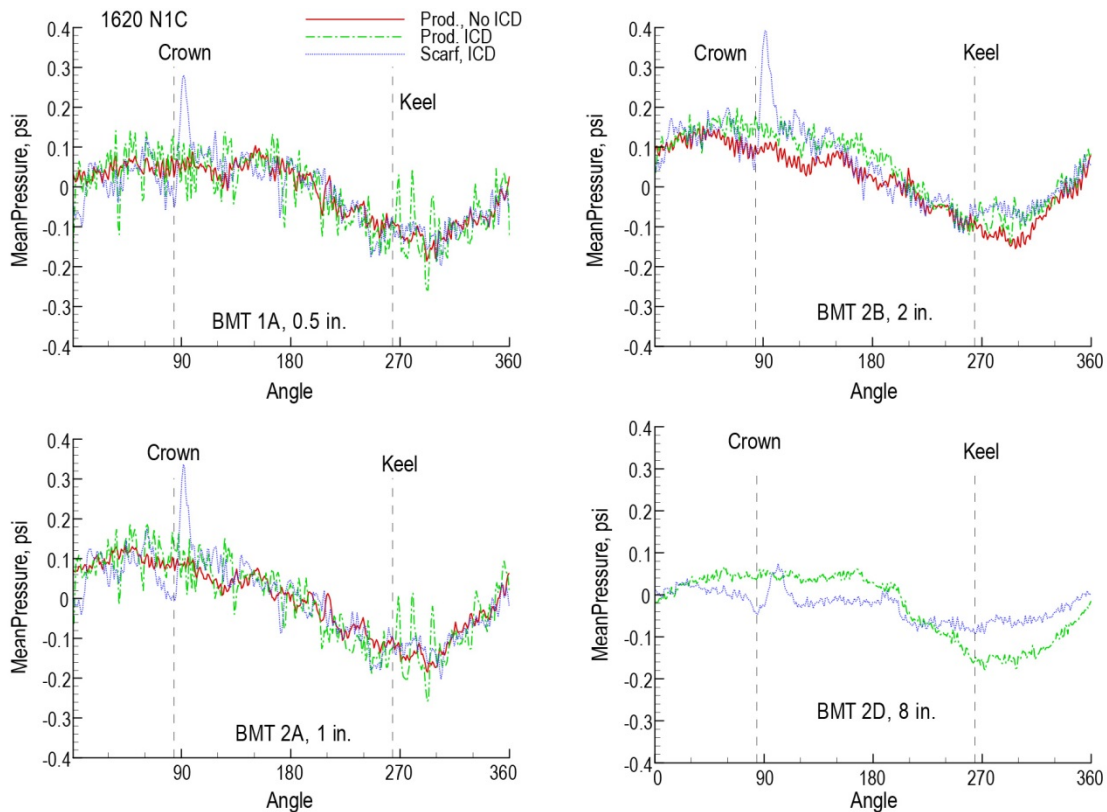
Figure 106.—Mean pressure traces for BMT's at 0.5, 1.0, 2.0, and 8.0 in. for the 1620 N1C condition.
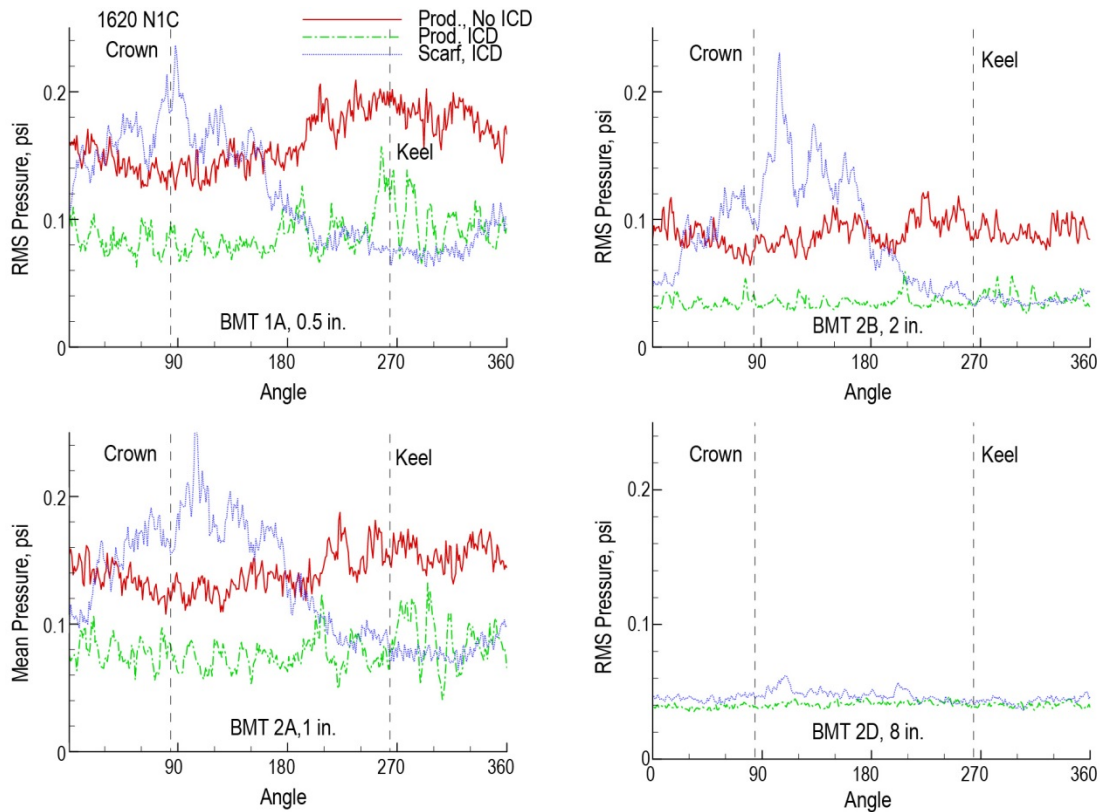
Figure 107.—RMS pressure traces for BMT's at 0.5, 1.0, 2.0, and 8.0 in. for the 1620 N1C condition.

The once-pre-rev variation in the mean pressure around the inlet was removed by performing a Fourier transform of the mean pressure, setting the fundamental mode to zero, and then taking the inverse Fourier transform. These data are shown in Figure 108 in the form of contour plots of the mean pressure and the associated unsteady pressure for the 1620 N1C condition. The plots have been stretched radially to accentuate the contours, and thus are not to scale. The no-ICD case only had BMT's out to 2 in. from the wall, while the other cases had BMT's out to 8 in. from the wall. Without the ICD, the unsteady flow is the dominant feature in the keel region of the inlet. When the ICD is installed on the production inlet, some steady distortions are seen in the inlet boundary layer, while the unsteadiness is greatly reduced. For the scarf inlet the large distortion near the crown dominates the steady pressure, and shows a region of unsteadiness at ±90° around the crown. The steady distortions in the keel region that were seen in the production inlet with the ICD are not apparent with the scarf. Since the scarf inlet has a flight lip, the boundary layer develops over a region with a much larger pressure gradient than the bellmouth on the production inlet. Because of this, the scarf boundary layer is more susceptible to disturbances that would amplify the boundary layer instabilities, and hence cause a more rapid growth of the boundary layer, possibly smearing out the steady distortions seen in the production inlet.
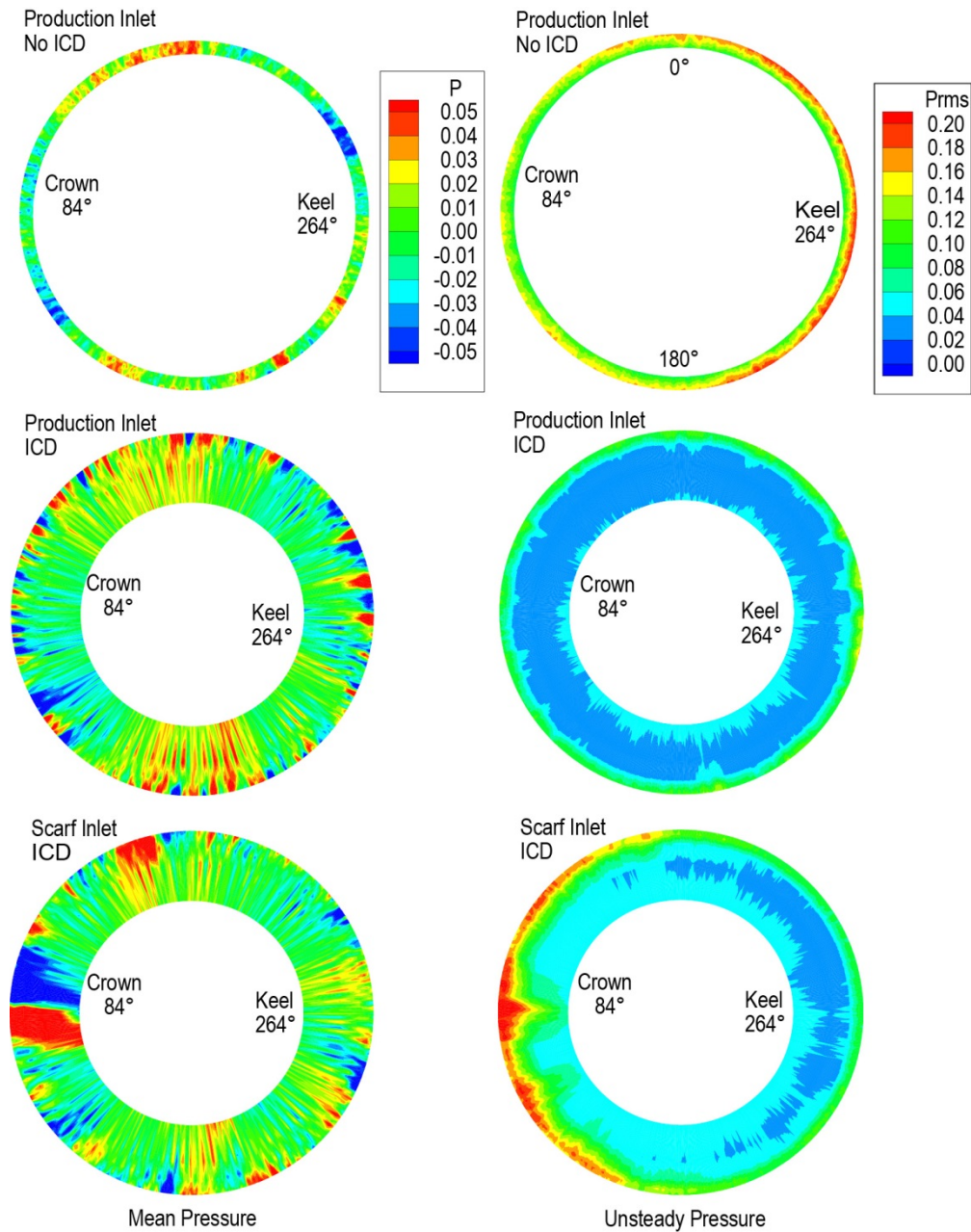
Figure 108.—Mean and unsteady pressure contours for the 1620 N1C condition.

Waterfall plots of the measured pressure are shown in Figure 109 for the first 50 revolutions of the fan for BMT 1A, which was 0.5 in. from the inlet wall. The No-ICD case shows structures that exist over many revolutions of the fan, yet shift in the azimuthal direction during operation. From 0° to 30° for the first 20 revolutions a structure is seen which moves in a counterclockwise direction. Near the 26th to 36th revolutions in this same angular region, another structure moves in the opposite direction. Similar structures are seen over the full circumference of the inlet when the ICD is not installed. The movement of these structures is what creates the high unsteady pressures that were measured at a given angle by the BMT's. Since these structures exist over several rotations of the fan, their interaction with the fan blades will result in BPF noise. The movement of these disturbances will modulate the tone spreading the BPF energy to the neighboring sidebands.
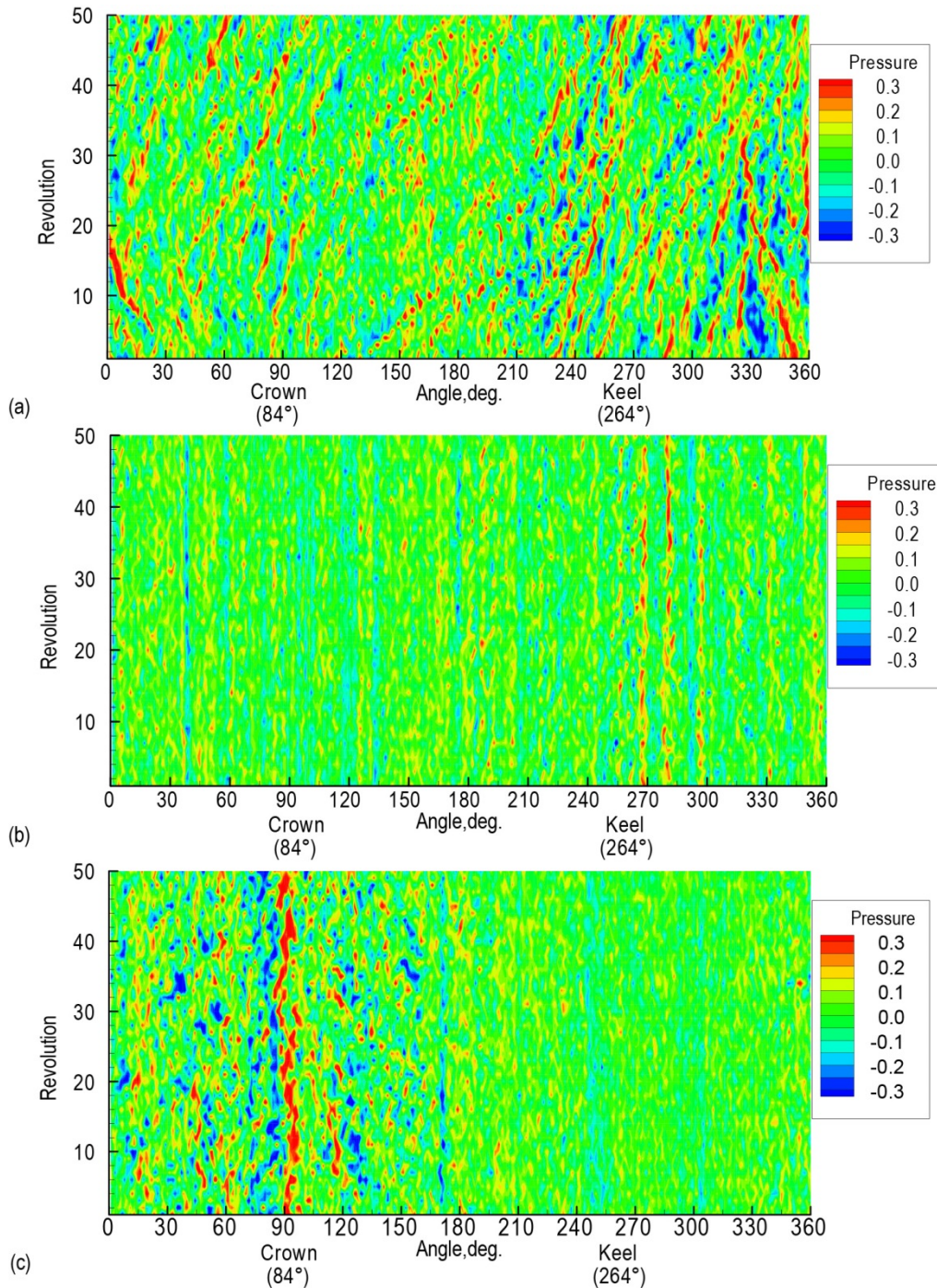
Figure 109.—Waterfall plots of raw pressure signal for BMT 1A (0.5 in. from wall) at 1620 N1C;
(a) production inlet, no ICD, (b) production inlet with ICD, and (c) scarf inlet with ICD.

When the ICD is installed on the production inlet (Figure 109(b)), the amplitude and unsteadiness of these coherent structures at a given angle diminishes. The only remaining disturbances are quite steady in space and exist most strongly in the keel region. These structures are coherent over numerous revolutions and will generate BPF tones as in the non-ICD case, but since they are stationary, the resulting tone will be narrower.

When the scarf is installed with the ICD as seen in Figure 109(c) high-amplitude steady distortions are seen in the crown region. On either side of the crown coherent structures exist which are drawn to the crown region because of the circumferential pressure gradient. The lateral velocity of these distortions was calculated to be around 8 ft/s, or 4 in. of lateral movement for each fan revolution. These structures and the dominant disturbance at the crown interact with the fan blades to generate the BPF tone. The modulations in space and amplitude of these disturbances will also broaden the BPF tone spreading energy into the sidebands.

By taking the Fourier transform of the pulse-synchronized mean pressure signal, the inlet steady distortion modes may be calculated. These are shown in Figure 110 for the 1620 N1C case and describe the amplitude of the steady distortion modes that are encountered by the fan blades. These interactions will generate spinning modes based on the Tyler-Sofrin interaction: $m = \sigma B \pm k$, where m is the spinning mode, σ is the harmonic of the blade passage frequency, B is the number of blades, and k is the inlet distortion mode order. At 1620 N1C, spinning modes less than about 14 will propagate, indicating distortion orders from 8 to 36 will contribute to the BPF.

For the data shown in Figure 110, the production inlet without the ICD shows the lowest amplitude steady distortion modes because most of the disturbances seen by the fan blades are unsteady. When the ICD is installed on both the production and scarf inlets, the unsteady atmospheric distortions are broken up and dissipated by the turbulence. An attempt was made to relate the spacing of the ICD panels around the nacelle to these distortion orders, but no clear connection was found. The steady distortions from the scarf inlet show up in the low orders because of the impulse-like structure of the crown distortion whose energy is spread among all of the modes.

As the distance from the wall increases, the amplitudes of the higher-order modes decrease. Peaks are seen in the modal spectrum around 90 to 110, which are due to the interaction of the fan with the acoustic field of the low-pressure compressor blades. These acoustic fields not only interact with the sensors farthest from the wall, but also with those that are well within the boundary layer.
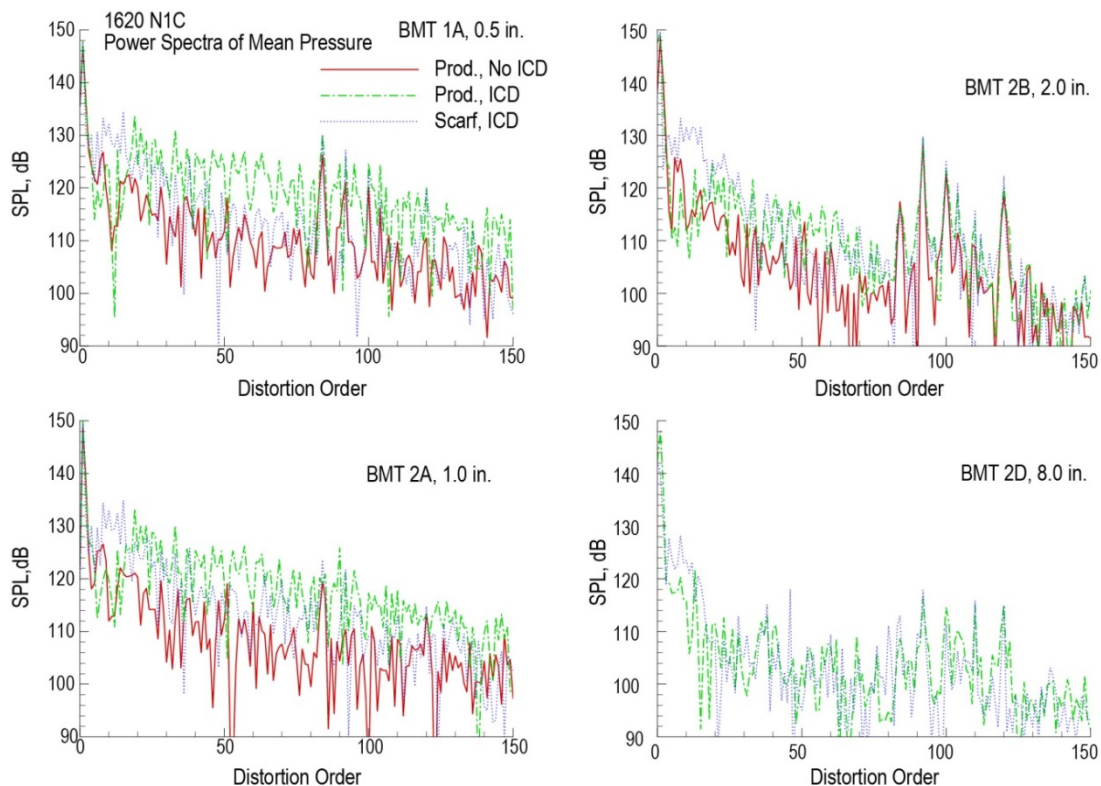
Figure 110.—Power spectra of mean spectra for BMT's at 0.5, 1.0, 2.0, and 8.0 in. for the 1620 N1C condition.
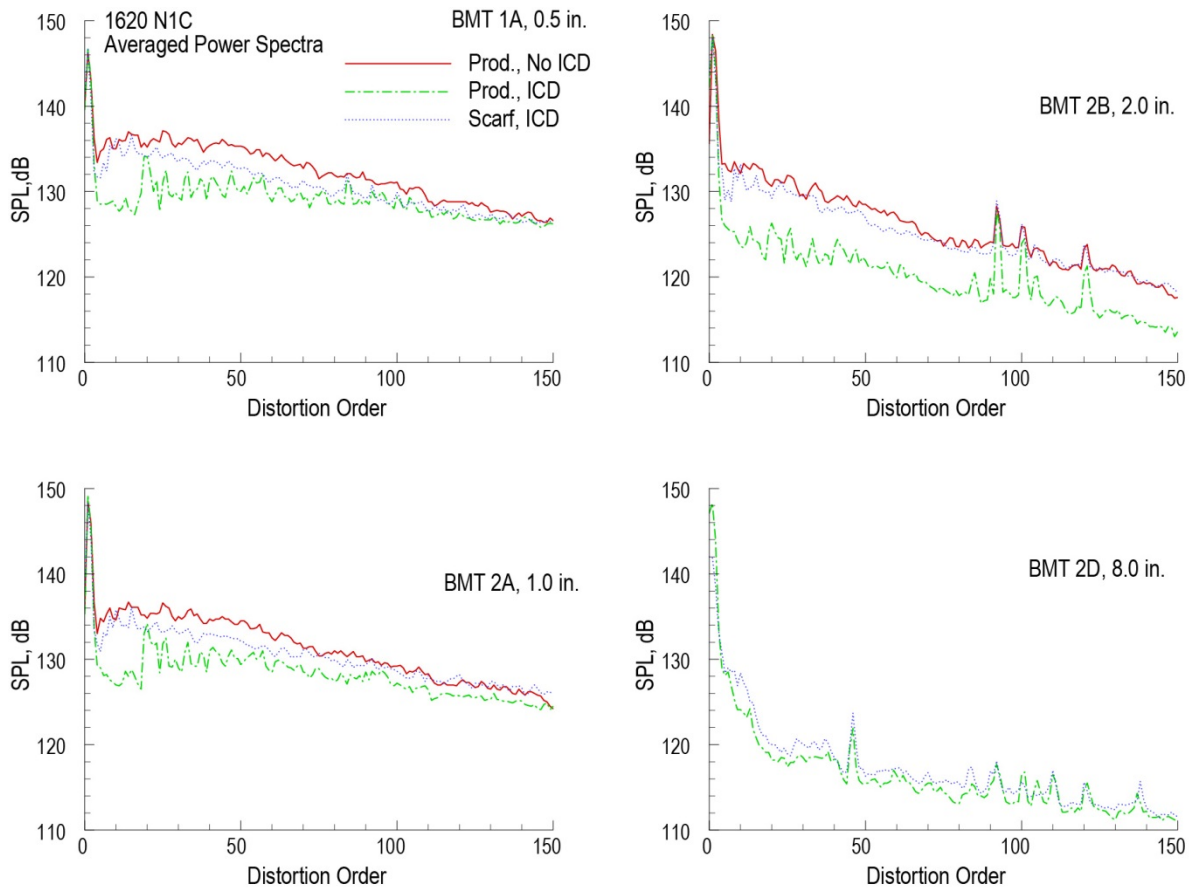
Figure 111.—Averaged power spectra of phase-locked pressures for BMT's at 0.5, 1.0, 2.0, and 8.0 in. for the 1620 N1C condition.

If the power spectrum is calculated for each revolution and then averaged, the slowly moving disturbances that contribute to the unsteady pressures will remain in the distortion mode amplitudes. Figure 111 shows the amplitudes of the distortion orders for a range of radial locations. For this analysis the production inlet without the ICD shows the highest amplitudes since each revolution of the fan experiences more abundant and higher-amplitude distortions than when the ICD is installed. This is true for all radial locations and fan speeds. The scarf inlet shows moderately high distortion mode amplitudes since unsteady distortions exist in the crown region. In addition to this, energy from the impulse-like distortion in the crown region of the scarf will also be spread out over all other distortion modes.

4.4.2.2   Rotated Scarf Inlet Results

For the previous data, the inlet crown was at approximately the 10:00 position relative to the engine. The scarf inlet was also tested in a rotated configuration on the engine such that the crown was at the 12:00 position and the keel was closest to the ground. The distortion in the crown region however, did not rotate the same amount as the inlet. This is illustrated in Figure 112 for the mean pressure contours with the first distortion order removed for the 2450 N1C condition. These plots also indicate a 2nd order distortion that does not rotate with inlet and exists for both the production and the scarf inlet. The high-pressure regions are near 50° and 230°, while the low-pressure regions are near 140° and 320°.
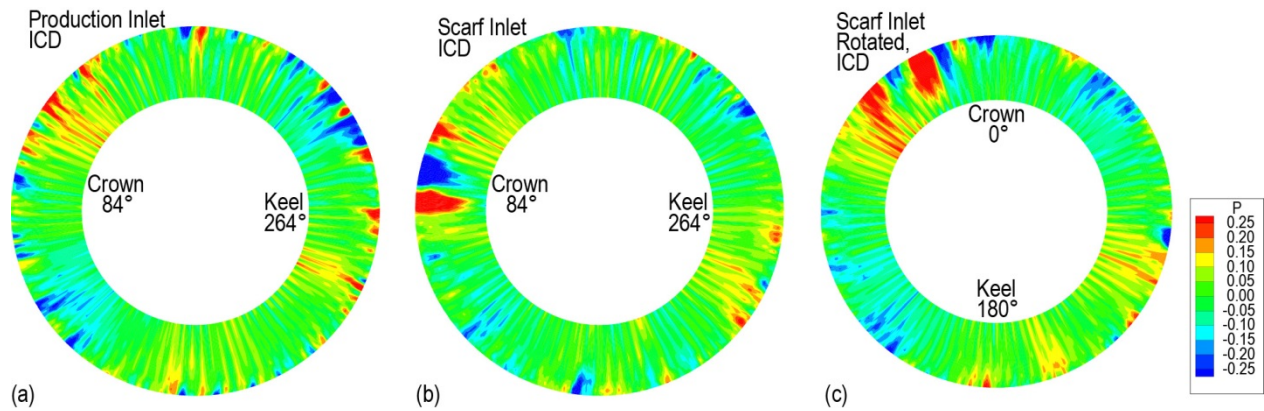
Figure 112.—Mean pressure contour plots at 2450 N1C, *k* = 1 distortion mode removed; (a) production inlet with ICD, (b) scarf inlet with ICD, and (c) rotated scarf inlet with ICD (crown at 0°).
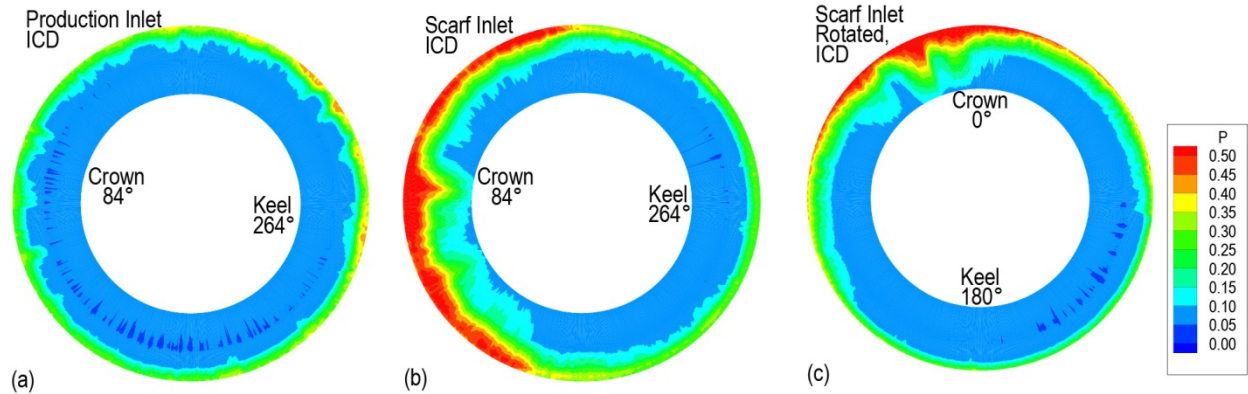
Figure 113.—RMS pressure contour plots at 2450 N1C; (a) production inlet with ICD, (b) scarf inlet with ICD, and (c) rotated scarf inlet with ICD (crown at 0°).

The mean and rms pressure profiles for each configuration are shown in Figure 114 and Figure 115 where the data from the rotated scarf has been shifted 84° to coincide with the inlet orientation of the other configurations. The mean pressures show that not only is the scarf crown-distortion shifted, but the droop induced once-per-rev variation has been altered as well. The unsteady pressures also show a different character for the rotated condition.

The second order distortion and the displacement of the crown distortion in the scarf could be an effect of the pressures imposed by the secondary flow path in the engine due to the pylon and support struts. Other factors contributing to these differences may be the external support structure, ground effects, or the aft-fan acoustic barrier.
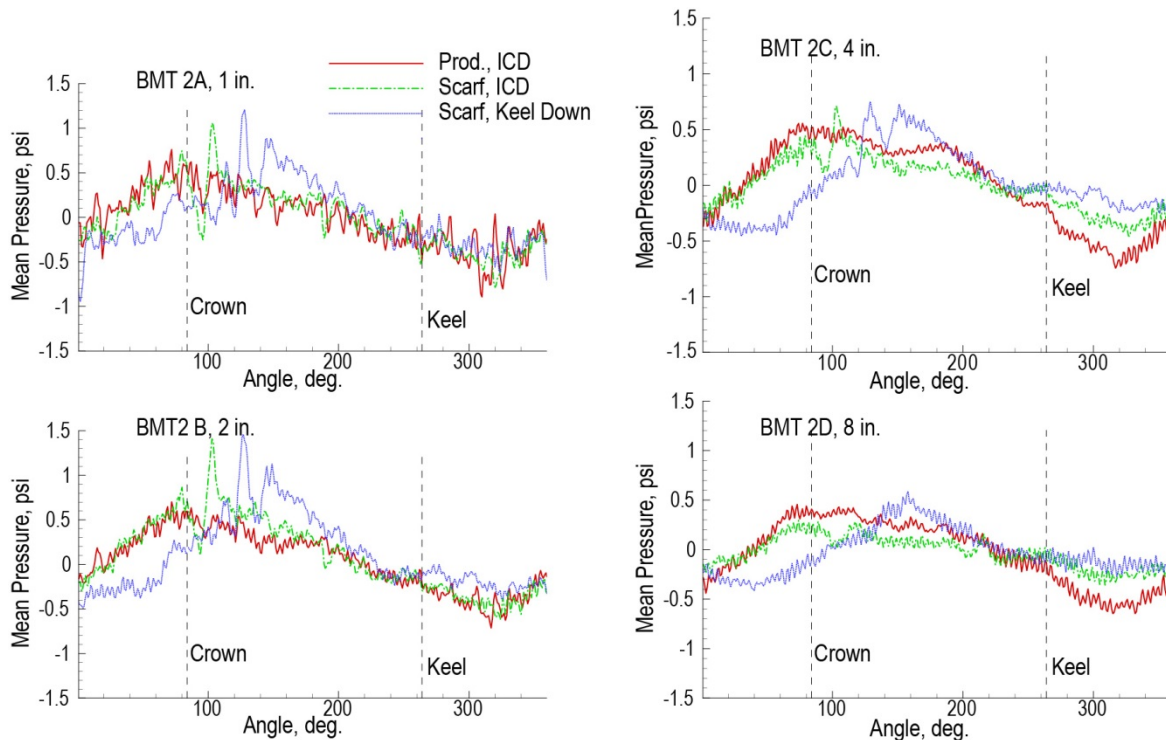
Figure 114.—Mean pressure comparisons for the rotated scarf inlet at four BMT locations.
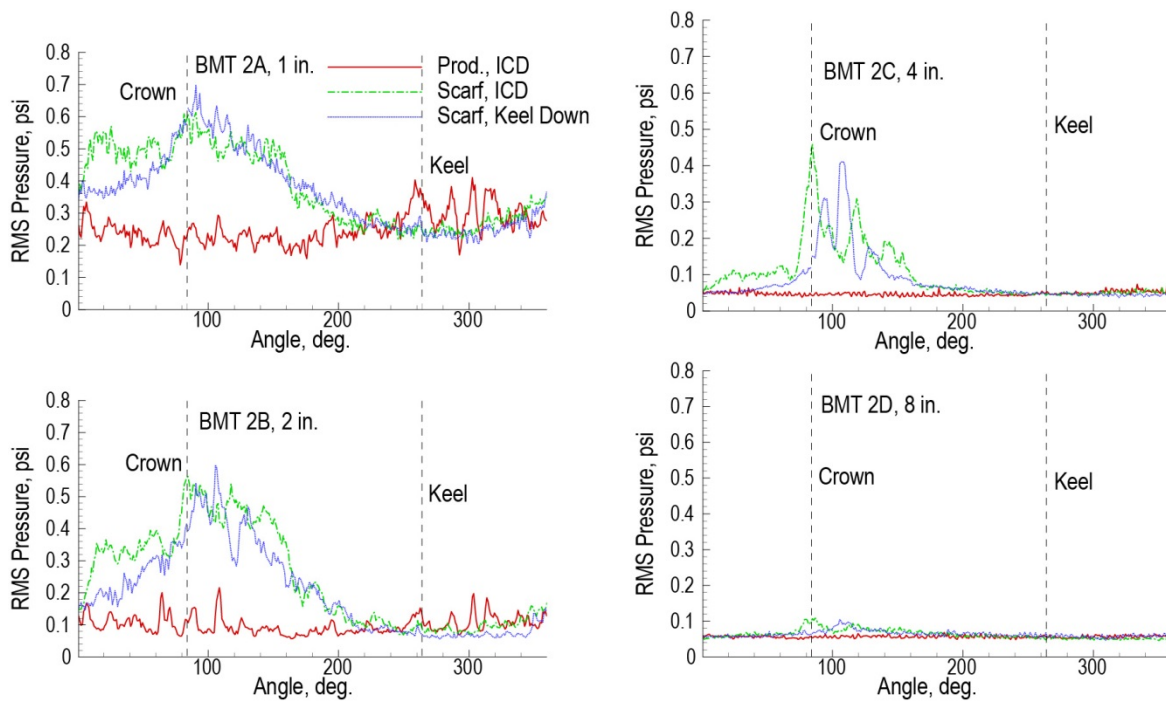
Figure 115.—RMS pressure comparisons for the rotated scarf inlet at four BMT locations.

4.4.2.3 Conclusions

The ICD has been shown effective in eliminating the large-scale atmospheric disturbances, and the accompanying unsteady pressures they create. The presence of the ICD however, did introduce some

steady distortions in the boundary layer of the production inlet that may contribute to the BPF tone. These steady distortions were not present with the scarf inlet, although a large distortion in the crown region existed due to separated flow aft of the throat. The lateral pressure gradient in the boundary layer of the scarf inlet caused axially coherent structures to migrate towards the crown which could cause a modulated BPF tone and subsequent harmonics which would be broader in frequency than the production inlet tone.

4.4.3   Flow Visualization

Flow visualization was used to indicate flow patterns and regions of separation in the scarf inlet. Retroreflective string was glued to the inlet with a hypodermic needle in a 2- by 2-in. grid in the crown region from the highlight to the A-flange The tufts were visualized by mounting a miniature camera and light source on the ICD and recording the tuft motion on videotape. Figure 116 shows a wide-angle view of the inside of the ICD. When the ambient air had sufficient humidity the moisture in the air would condense due to the acceleration of the flow. An example of the streaklines of the condensed air can also be seen at this fan speed. The video indicates motion of these of these structures, but it is not clear whether it is a similar motion of the structures that are seen in the waterfall plots, or merely a manifestation of the variation in air density combined with the shutter speed of the camera.

Figure 117 shows a close up of the tuft motion for the 2452 N1C condition. Downstream of the throat, tuft motion was seen for all fan speeds indicating separated flow. At the inlet lip the tuft motion was sufficient to scrub off the paint and cause breakage of the tufts indicating more separation and unsteady flow in lip region as well. No indication of flow direction other than axial was observed. From the waterfall plots, the transverse flow speeds of the convected disturbances were considerably less than the freestream, which would produce flow angles much less than 1°.

Figure 116.—Digitized image of retroreflective tufts and condensation flow visualization in the scarf inlet at 2800 rpm.
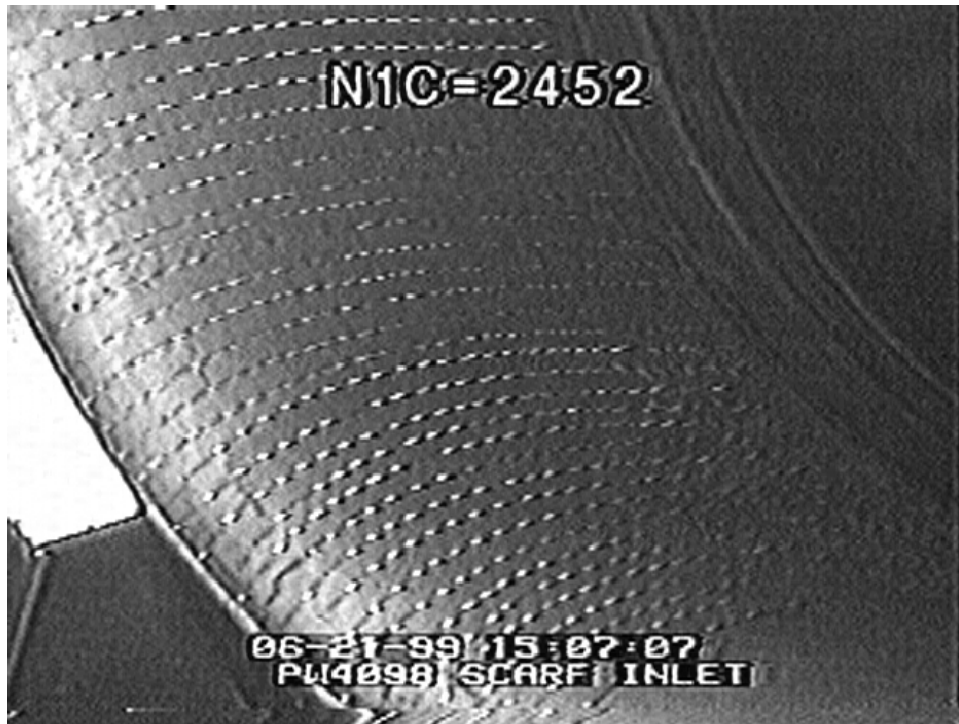
Figure 117.—Digitized image of retroreflective tufts in the scarf inlet at 2452 rpm.

4.4.4 Inlet Mode Array Analysis

The data was processed and plotted in several ways to help understand the source of the tone noise. Each method showed different aspects of the data, and thus all were useful in the analysis. Additionally, combining the results of the mode array with the results from the blade mounted transducers (BMT) allowed even greater understanding of the BPF tone generation mechanisms.

Much of the data shown in this document is from the lowest power setting (N1C = 1620 rpm). This was a particularly useful power setting because the BPF was cut-off and theoretically, there should not have been any BPF noise. The primary purpose of the mode array and BMT transducers was to determine the source of the BPF noise at subsonic tip speeds for the production inlet and determine the cause of the increase in BPF noise at subsonic tip speeds of the scarf over the production inlet.

4.4.4.1 Mode Array Pressure Traces

Analysis of data started with using the once-per-revolution pulse to re-sample the data at specific angular locations of the rotor. This required using a digital linear-phase finite impulse response (FIR) filter to first remove frequencies above the new Nyquist frequency in the data. A polynomial spline-interpolation routine was used to re-sample the data. The data was over-sampled by a factor of approximately 10 so that interpolation did not lead to significant errors.

Average pressure traces representing one rotation of the rotor were produced by averaging each re-sampled pressure trace over a period of eight seconds for each condition. For the low powers there were approximately 210 revolutions at the lowest power of N1C = 1620 rpm and approximately 380 revolutions at the highest power of N1C = 2800 rpm. By performing this pulse-synchronized averaging the random part of the signal, (unsteady between fan rotations), was reduced by $10*LOG_{10}(N)$ dB, where N is the number of blocks in the average.

The pulse-synchronized averaging process can dramatically reduce the non-synchronous noise and improve the ability to view "pure" tones. In this context, pure tones are tones that are completely deterministic and therefore have infinitesimally small bandwidth.

Figure 118 shows a comparison of the average pressures measured over one rotation for the scarf and production inlets as a function of power upstream of the keel. Note the pressure increase as each blade passes the transducer, which provides a very clear blade-to-blade pressure variation associated with each blade. At

the subsonic tip speeds, below N1C = 2200 rpm, the rotor locked field is cut-off and an *m* = 22 pattern should not propagate. However, the mode array is sufficiently close to the fan that the cut-off rotor-locked field dominates the pressure traces. In hindsight, it would have been beneficial to have the measurement array farther away from the fan to minimize the effect of the decaying, rotor-locked pressure field.
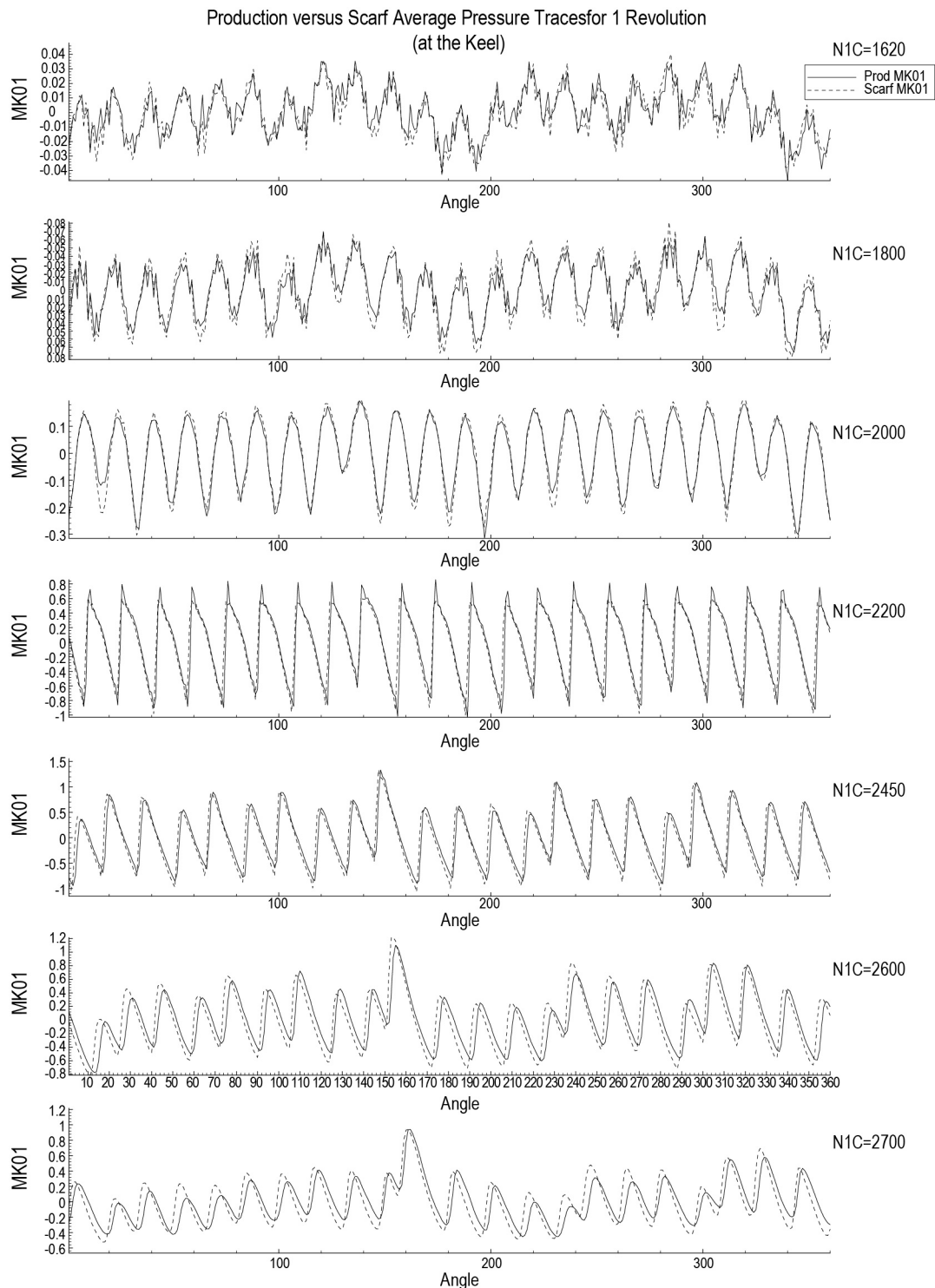
Figure 118.—Production versus scarf pressure profile at the keel.

Figure 119 shows the same comparison at the crown. Notice that the production and scarf pressure traces differ significantly in this region at the higher powers. Evidence from the flow visualization and BMT data indicate separated flow in the scarf inlet in this region.
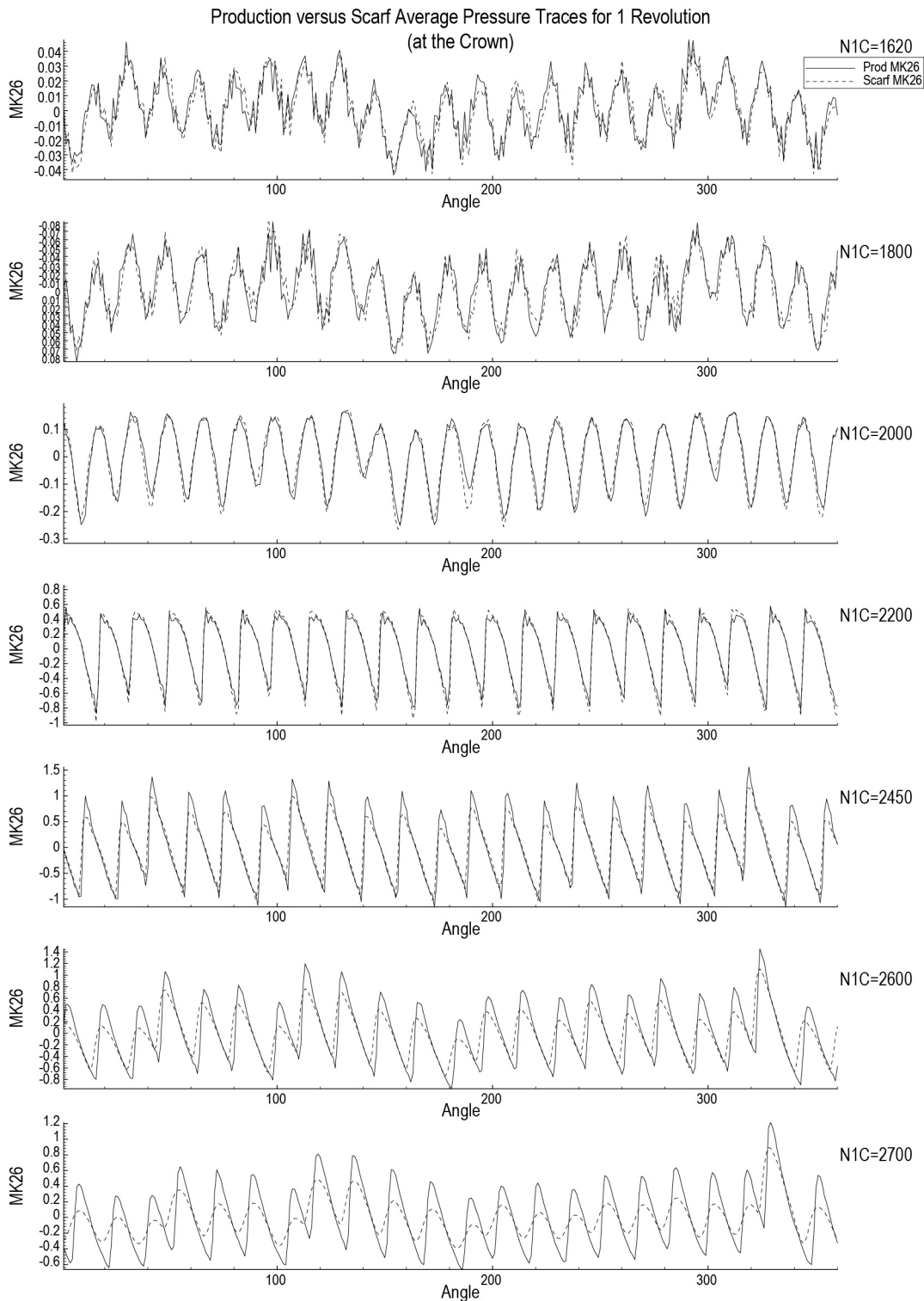
Figure 119.—Production versus scarf pressure profiles at the crown.
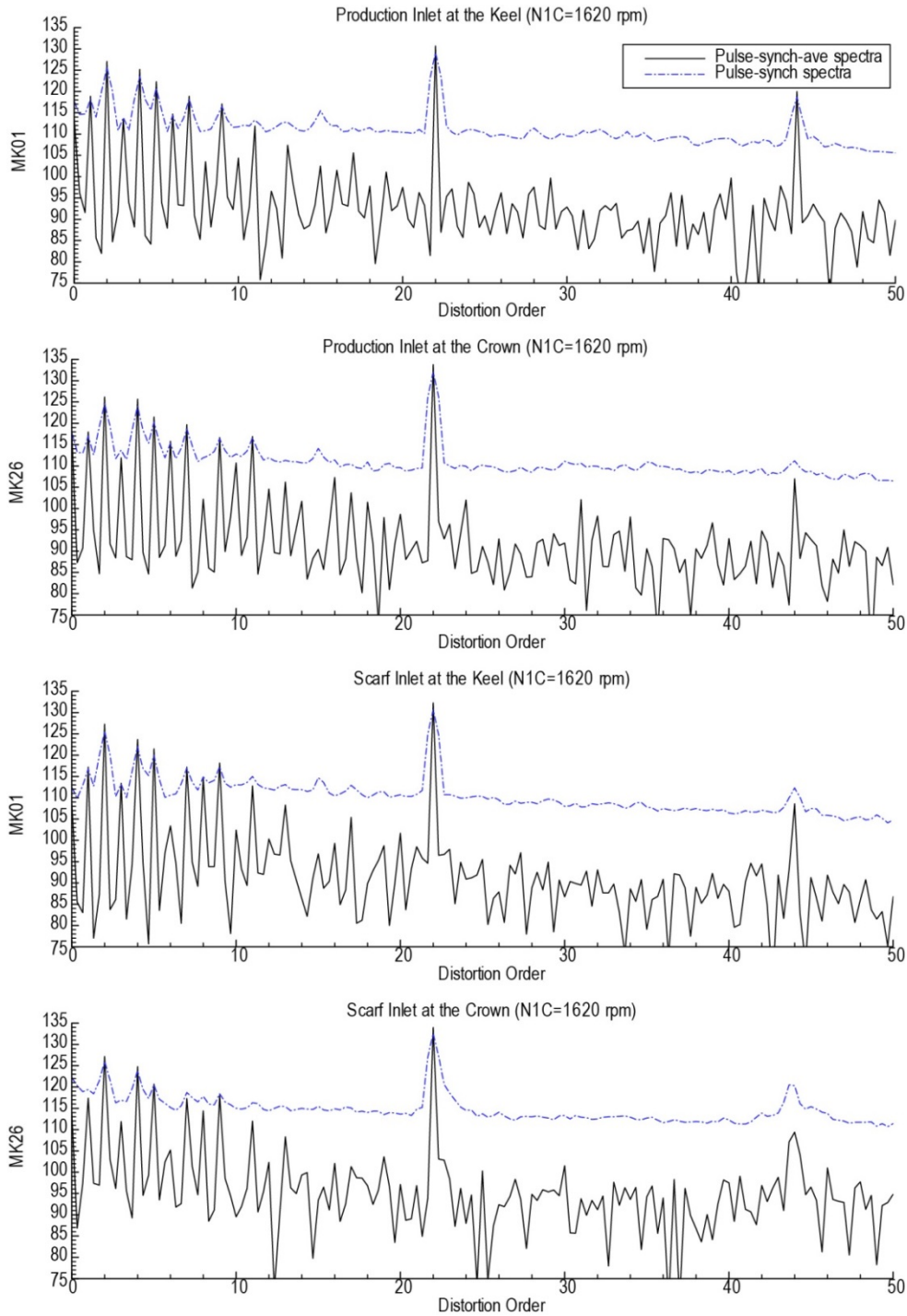
Figure 120.—Pulse synchronized average spectra, and pulse synchronized spectra.

4.4.4.2   Mode Array Power Spectra

The power spectra of the pulse-synchronized average pressures produces spectra which have reduced amplitudes between the BPF harmonics since the randomness is eliminated in the time-series averaging. This type of averaging is defined as, "pulse-synchronized average spectra". By averaging the spectra from each individual rotation, (pulse-synchronized spectra) the randomness from non-rotor-locked sources is maintained in the spectra as well as the deterministic sources, and hence higher levels appear between the BPF harmonics. The difference between these two processing techniques is evident in Figure 120. The

BPF (m = 22) tones generate similar levels in both processing techniques, with the difference being a 1.76 dB decrease in the peak level accompanied by a widening of the tone in the pulse-synchronized spectra due to the use of a Hanning window.

The difference between the two processing methods is particularly apparent in the broadband levels where one would expect the spectra to be dominated by non-synchronous sources. There is approximately a 17 dB difference between the two processing methods for this condition which corresponds to $10*LOG_{10}$(number of averages). At the lower frequencies, multiple pure tones exist, although these should not propagate at this low power condition.

The production inlet has relatively little change in levels from the crown to the keel as shown in Figure 121(a), while the scarf inlet has higher levels at the crown than at the keel as seen in Figure 121(b). The scarf inlet BPF tone is wider than the production inlet and the disparity increases as the crown is approached. This suggests there might be some tone modulation, causing spreading of energy in frequency, for the scarf compared to the production inlet.
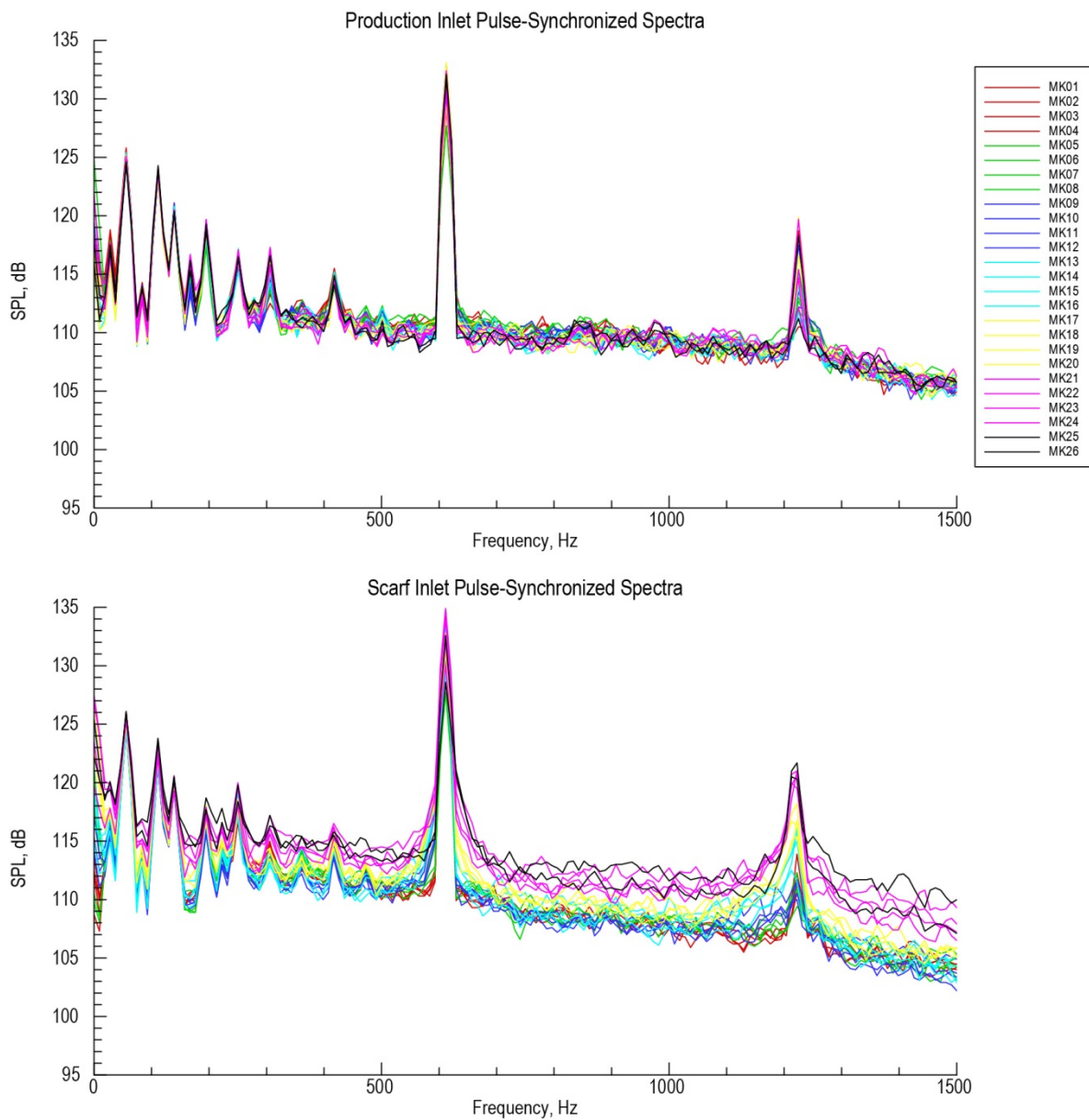
Figure 121.—Pulse-synchronized spectra at all microphone locations (a) production and (b) scarf.

4.4.4.3 Phase and Amplitude Modulation

Phase and amplitude modulation charts of the BPF tone were created from the FFT of the time-traces for each revolution. At a N1C of 2200 rpm the rotor locked pressure field propagated which increased the signal to noise ratio for the BPF tone. Figure 122 shows the amplitude and phase modulations of the BPF with respect to time for all of the transducers. These values were normalized by their average phase and the amplitudes, respectfully.
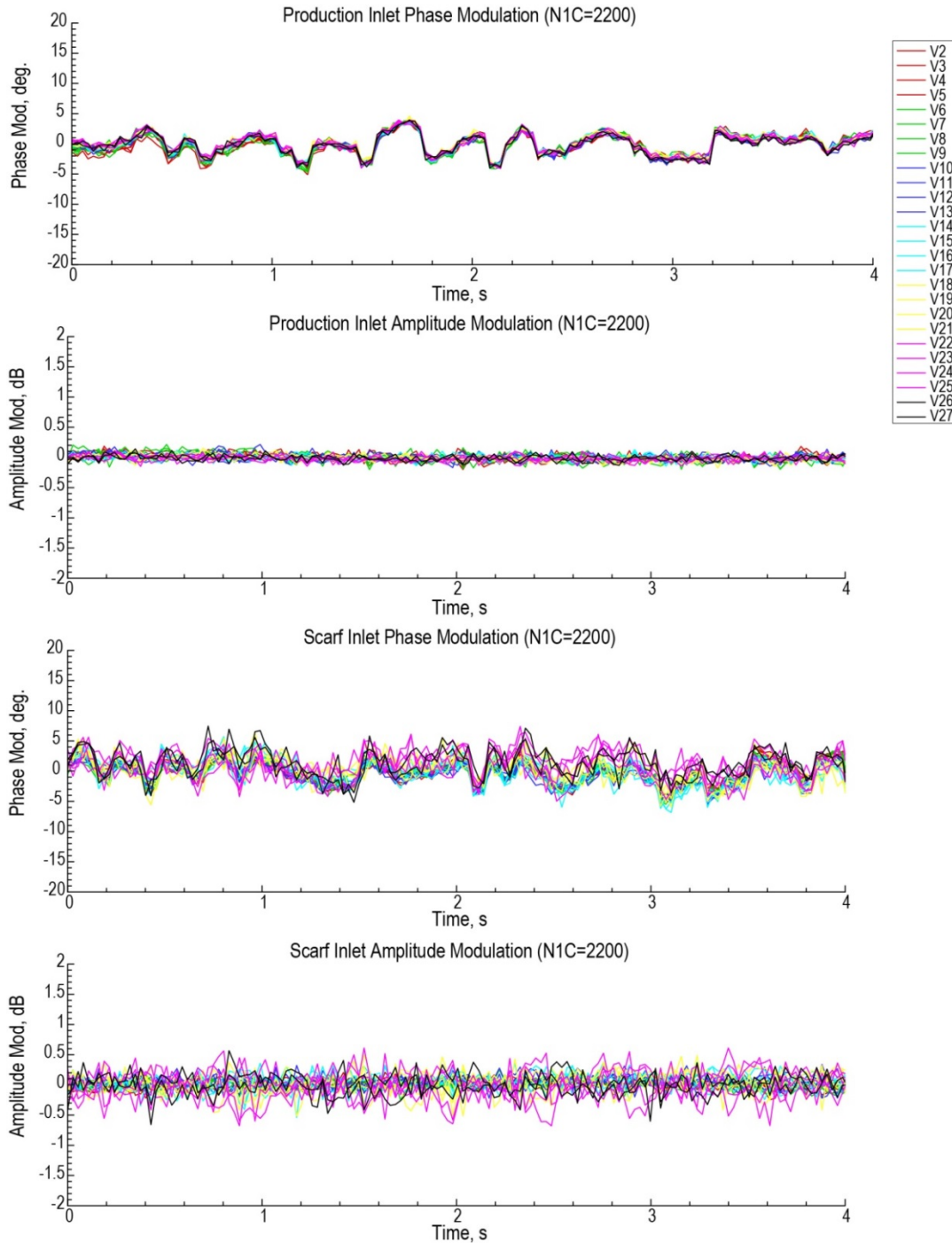
Figure 122.—Production and scarf modulation data.

The phase modulation of the production inlet shows similar modulation across all the sensors, which results from a source that effects all sensors simultaneously. Two possibilities exist. The first would be a problem with the trigger, although this is unlikely. The second possibility is that there is a large distortion across the inlet, which affects the phase at all transducers, possibly resulting from atmospheric variations. A similar phase modulation is observed with the scarf inlet, although it is somewhat masked by the differences that exist between the transducers. The production inlet also shows small differences in phase and amplitude modulation between transducers, while the scarf inlet shows considerable modulation. The largest variations for the scarf inlet occur in the crown region where it has been postulated that this variation of the BPF modulation is related to the cause of the increase in BPF noise of the scarf inlet.

4.4.4.4 Spinning Mode Charts

The pressure signals can be used to generate mode charts by applying a discrete Fourier transform (DFT) in both frequency and space (or angular position). The resulting spectra separate the pressure signals into frequencies and acoustic spinning modes. Figure 123 shows an example of a typical mode plot for the production inlet at 1620 N1C. The ordinate shows the frequency, and the abscissa contains the spinning orders, (m-orders). Since the array only covered half of the inlet circumference, only the even m-orders are can be calculated. Higher resolution methods were attempted to give some definition of the odd harmonics. These methods, however, generally failed for two reasons: 1) there was a very strong BPF, which leaked into the odd harmonics, 2) any spinning mode could exist so there were 2xN variables and 1xN pieces of data. Higher resolution methods likely would have worked had the sensors been further away from the source (to remove cut-off BPF noise), thus limiting the number of existing modes. Several horizontal lines are noticeable in Figure 123 representing different BPF and compressor tones and harmonics. There is a measured BPF tone at approximately 620 Hz, although it is theoretically cut-off at this low operating condition.

Modes near cut-off propagate down the duct very slowly and give increased pressure amplitudes at the wall transducers. This phenomenon generates a "V" in the plot which is originates at the $m = 0$ mode at zero frequency. Cutoff for this particular figure at the BPF is at $m = 16$. Another artifact of the data is the preponderance of co-rotating modes for the broadband noise. This is consistent with earlier work of Joppa (Ref. 1).
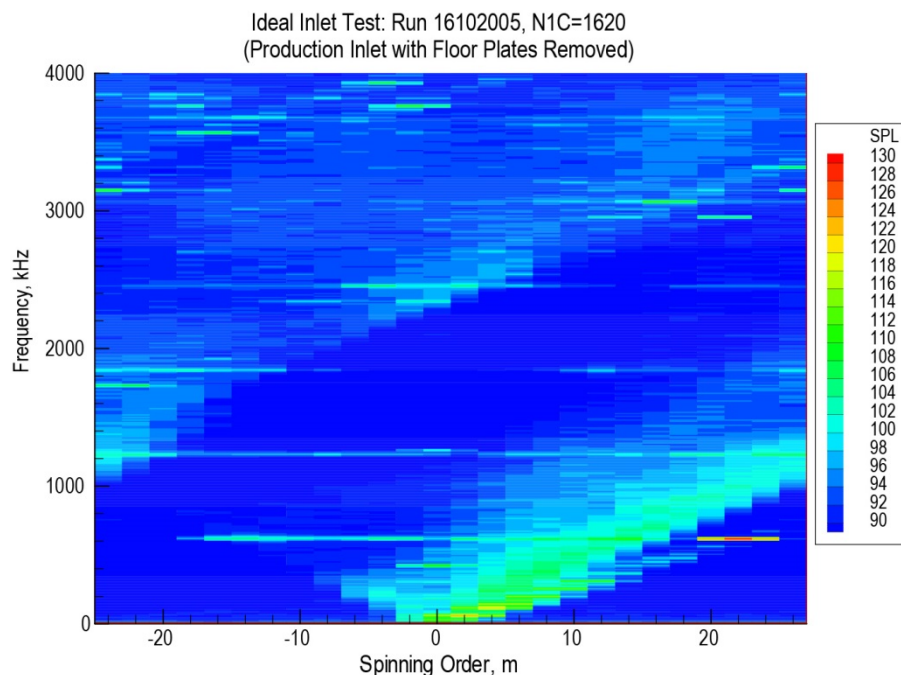
Figure 123.—Mode plot for the production inlet at N1C = 1620 rpm.

BPF for the Run 16102005, N1C=1620
(Production Inlet with Floor Plates Removed)
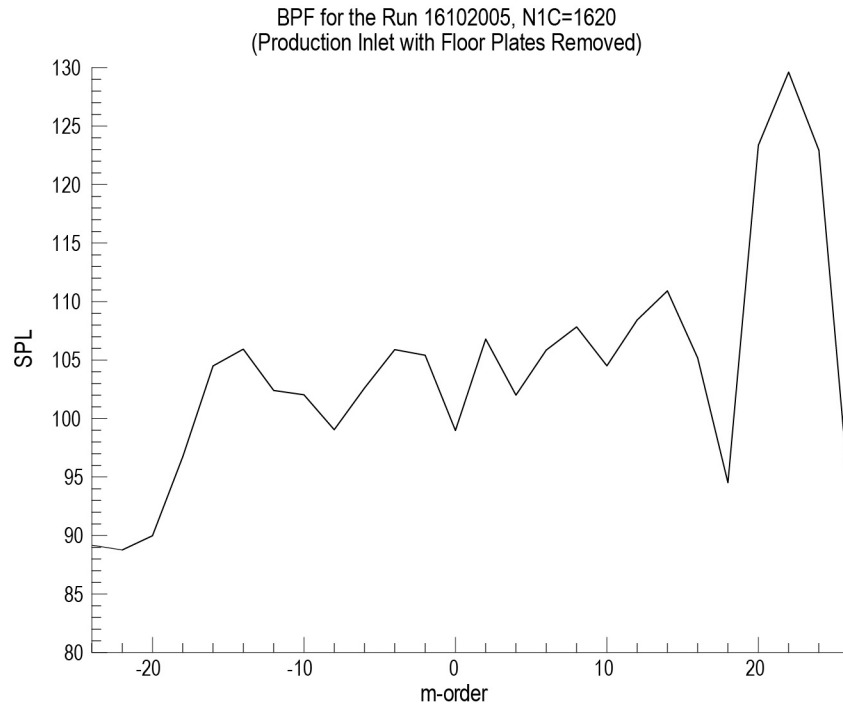
Figure 124.—BPF mode plot for the production inlet at N1C = 1620 rpm.

Figure 124 represents the mode amplitudes from the horizontal line at the BPF of Figure 123. Notice that the levels are very high for the cut-off $m = 22$ spinning order. Due to the close proximity of the array to the fan (about 13 in.), there is still significant energy present in this cut-off mode. Clearly, future mode measurements should be made upstream of the A-flange so that cut-off mode energy has sufficiently attenuated before the measurement transducers.

Figure 125(a) and (b) show the mode charts for the production and scarf inlets at 1620 N1C, respectively. Note that the levels are the same except near the negative spinning orders at the 620 Hz BPF, where the scarf inlet shows additional noise. Careful examination of this source shows that it seems to spread out in frequency as the spinning orders move away from the $m = 22$ spinning order. This is an indication that the additional noise source of the scarf inlet may be due to an interaction of the rotor with an unsteady disturbance with a long axial length scale. Figure 126 shows the same comparison at 2450 N1C with a BPF near 920 Hz. Note that the extra source is still visible although the far-field data showed little or no increase in BPF noise at this frequency. Since the rotor-locked pressure field cuts-on at this speed, the dominant $m = 22$ can propagate, and hence dominates the far-field levels. Therefore, this source is only important at subsonic tip speeds (below N1C of 2200 rpm).

Pulse-synchronized averaging can also be used for mode data to produce spectra that remove the random part of the signal as was done with the spectra from the individual sensors. Figure 127 shows a comparison of the BPF for the scarf and production inlets using the two spectral averaging methods at 1620 N1C. The production inlet shows the pulse-synchronized average spectra to be similar to the pulse-synchronized spectra. This suggests that the source of BPF noise for the production inlet is due to a deterministic mechanism.

A comparison of the production and scarf pulse-synchronized average spectra show similar levels at the cut-on spinning orders. This suggests the steady-state deterministic sources for these two inlets are not greatly different. This is contrary to expectations looking at the averaged pressure profiles for the BMT data. It suggests that the steady modulations in the boundary layer do not appreciably affect the acoustic pressures measured at the mode transducers.
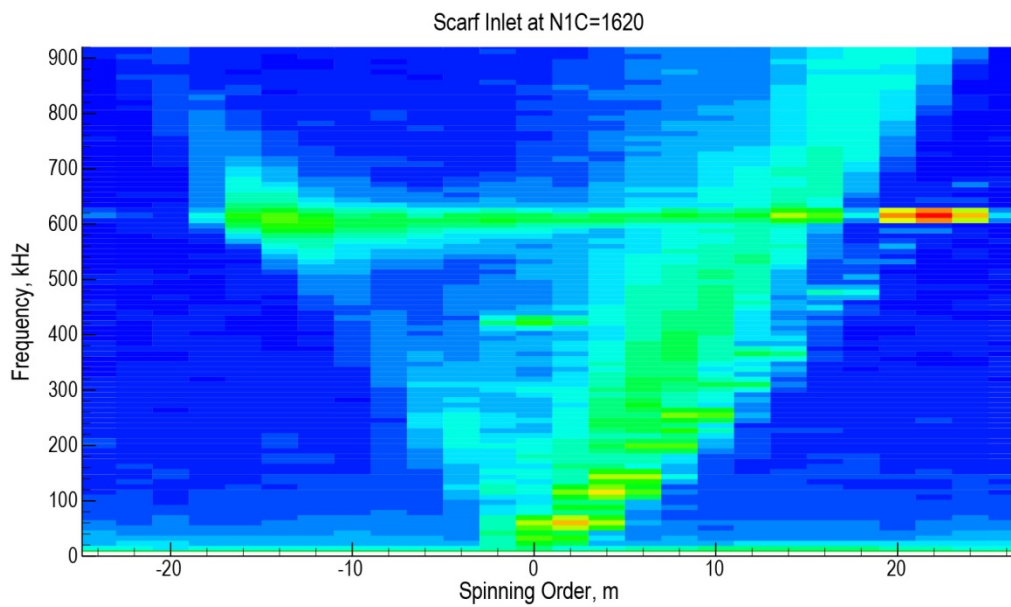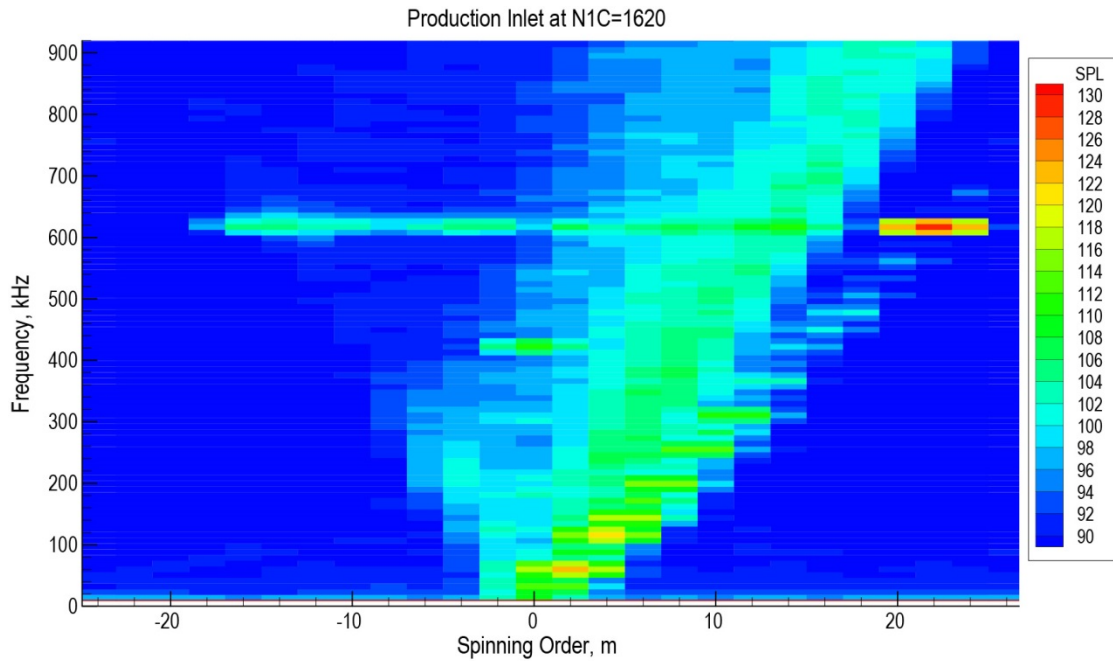
Figure 125.—Mode plots at N1C 1620, (a) production and (b) scarf.
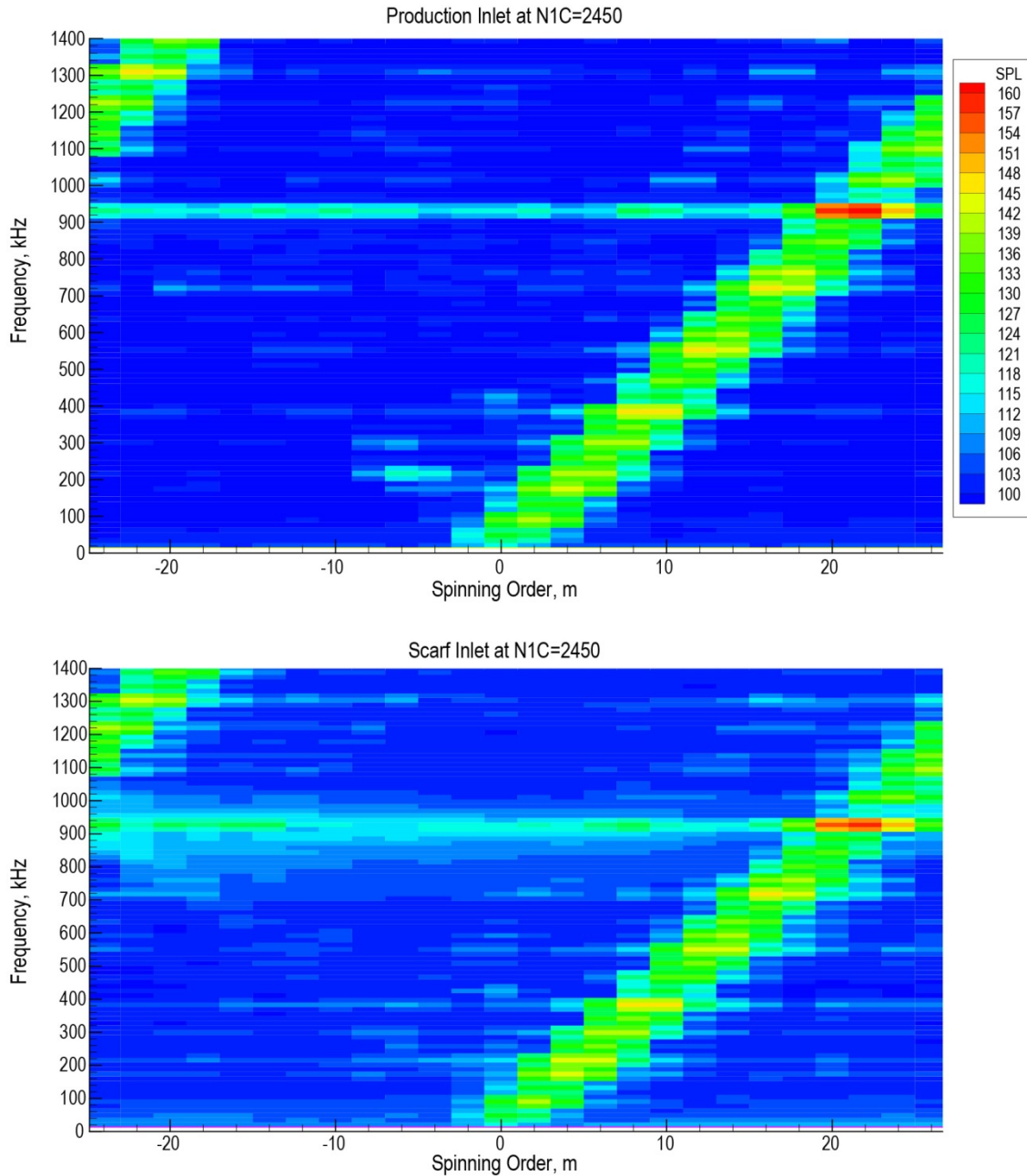
Figure 126.—Mode plots at N1C 2450, (a) production and (b) scarf.

A comparison of the two averaging methods for the scarf inlet spinning mode amplitudes show that there is an additional source, which is non-deterministic in nature that is particularly apparent at the negative spinning orders. This suggests that the additional scarf inlet noise mechanism does not exist in the production inlet.

The BMT data shown in Figure 109(c) clearly confirms the existence of flow disturbances with long axial length scales. This explains the source of the additional BPF noise of the scarf at subsonic tip speeds. Note that this type of source is only significant at subsonic tip speeds. When the tip speeds are sonic and the rotor locked field propagates, the rotor locked field, $m = 22$, is much stronger than the other spinning orders and controls the far-field levels. The far-field data clearly show an increase in noise of the scarf over the production until the rotor-locked field is cut-on. After which, the levels are similar.
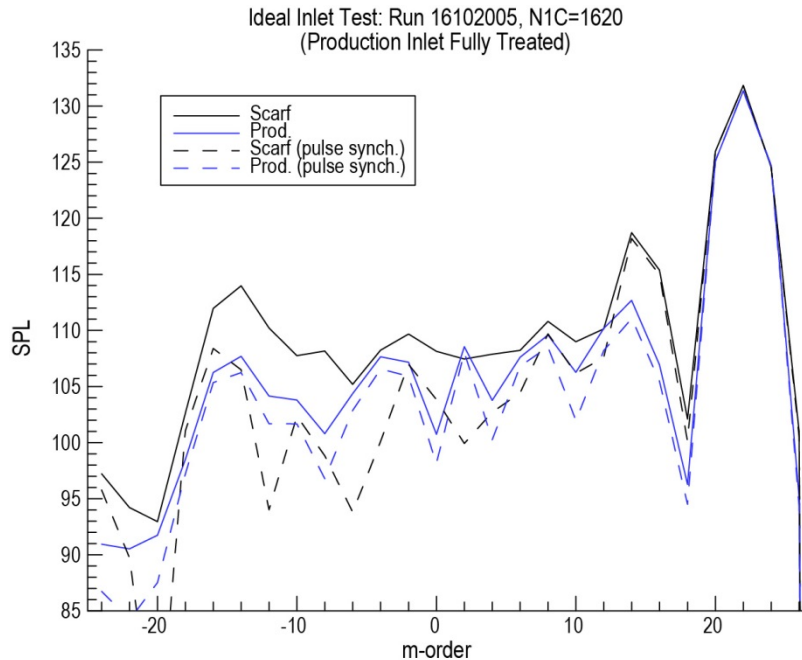
Figure 127.—Comparison of pulse and non-pulse synchronized data.

4.4.5   Conclusions and Recommendations

The mode array, in combination with the BMT's and the flow visualization techniques, provided insight into some of the BPF noise-generation mechanisms for the scarf and production inlets. These data show the additional BPF noise for the scarf over the production inlet at subsonic speeds is due to a flow problem at the crown. The current scarf inlet, without a bellmouth, separates at the crown, which causes vortices to be shed into the fan. These vortices have long axial length scales, which are not stationary and hence, generate a non-deterministic BPF noise source in spinning orders that propagate out the nacelle. High peak Mach numbers around the inlet lip of the scarf inlet can be reduced with the use of a bellmouth, thus reducing the possibility of separated flow. Recent CFD calculations indicate that the separated flow in the scarf inlet will be eliminated with forward flight. Additional work is underway to determine the possibility of testing the scarf inlet with a bellmouth inlet.

The production inlet with the ICD did not show evidence of a non-deterministic BPF noise source in the mode array or BMT data. Since the production inlet uses a bellmouth inlet which reduces the Mach number near the lip, the probability of flow separation is minimized thereby eliminating the existence of these unsteady flow distortions. In addition, CFD results have shown the scarf inlet to have higher peak Mach numbers than the production inlet due its flow lines. Recent CFD runs have shown some evidence that the scarf inlet would not have the separation BPF noise source if it was in forward flight or had a bellmouth inlet.

The cause of the BPF noise for the production inlet at subsonic speeds was never fully determined. The data was able to show that the production inlet BPF noise is due to a deterministic noise mechanism, but the source of the mechanism is not conclusive. The BMT data show steady distortions which exist in the boundary layer, yet it is not clear whether the noise generated from the interaction of the fan with these disturbances is sufficient to generate the observed BPF tones. The mode array data, however, shows that the noise source is spread out across all the propagating spinning orders. This implies that the source is not comprised of one interaction that can be determined and fixed. The source seems to be comprised of many propagating spinning orders. Mode measurements and/or BMT data during acceleration/deceleration and with the inlet rotated may provide the additional data to needed to help understand this noise source. These types of data were not taken during this test.

The mode array data did not provide any evidence of large differences between the production and scarf deterministic noise sources. However, the BMT data clearly showed large steady distortions in the pressures measured on the blades for both inlets. There is not currently enough data to determine the amount of additional noise due to the steady distortion as measured with the BMT's. The data clearly show that the unsteady part of the noise dominates the differences. Possibly, some of the fan-noise prediction codes could be used to predict the relative levels of the steady and unsteady noise sources from the BMT data to compare these sources. The data suggests that the steady source increase is insignificant in comparison.

Clearly the mode array, BMT's, and the visualization techniques are useful in helping understand complex BPF noise mechanisms. It is unlikely that the source of the BPF noise for the scarf inlet would have been discovered and so fully understood without these techniques. Likewise, there now exists a greater understanding of the type of source that needs to be eliminated in order to reduce subsonic BPF noise of current engines.

5.0 Conclusions

For convenience the test conclusions listed in various portions Section 4 are summarized here:

5.1 Far Field Data

- The treated scarf inlet with the advanced (R1) FFCC is 2 to 4 EPNdB quieter in inlet fan noise than the production inlet and fan case at approach and cutback powers. Approximately 80 percent dB nacelle suppression improvement was observed at approach power and 50 percent dB suppression improvement at cutback power.
- The Scarf inlet with advanced FFCC has a significant BPF distortion tone, preventing larger benefits. Without the extra BPF noise an additional 1 EPNdB in noise reduction was expected.
- The hardwalled scarf inlet has higher buzzsaw noise levels than the production inlet but treatment suppressed it very well.
- The bottom 90° of diffuser liner is ineffective at all conditions.
- The scarf lip liner effectiveness at cutback power is about the same per unit length as the diffuser treatment.
- The scarf lip liner at approach power is effective over a wide frequency range, but not for the BPF distortion tone thus preventing a significant EPNdB benefit.
- At approach power both advanced FFCC liners (R1 and R2) have the same effectiveness per unit length as the scarf inlet liner.
- At cutback power the higher resistance fan case liner (R1) showed a significant benefit while the lower resistance liner (R2) was detrimental, primarily due to impedance non-uniformities.
- Treatment uniformity near the fan is very important. Simulated production type hardwall splices in the FFCC liner show large penalties of up to 4 EPNdB at cutback power for eight 3 in. splices. Penalties increase with both splice number and width. The mechanism is scattering, by impedance discontinuities, of high level but fast decaying blade pressure fields at BPF (m = B) into high level propagating modes.
- The treatment uniformity further forward in the inlet is not critical. Penalties associated with axial or circumferential splices are associated only with lost treated area.
- There is no apparent benefit of the scarf keel being oriented toward the microphones, relative to being oriented 90° away. This may be due to the effect of the scarf geometry on distortion tone generation or on azimuthal buzzsaw noise variations.
- Aft fan noise is not influenced appreciably by the scarf inlet.

5.2   RDIFF Prediction Comparisons

At the approach power condition it is concluded that the RDIFF predictions for tone and broadband lining attenuation generally were within about 15 percent of the measured data in the direct radiation field but only within about 50 percent in diffraction dominated field (aft of 70°). However, the very high frequency lining attenuation (8 to 10 kHz) was not accurately predicted. The scarf shape shielding effects were predicted well except for in the diffraction-dominated field also. The RDIFF prediction process of applying the RDIFF predicted noise change (PHW-configuration) to the measured production inlet test data was used to estimate the scarf inlet noise if the BPF and 2BPF tone increase did not occur. This is believed to be a valid flight condition prediction since it is believed that the flow distortion causing the tone increases will not be present with forward motion. It was concluded that without the BPF and 2BPF aggravation the 13° biplanar scarf shape is worth about 2 EPNdB and the triple layer lining is worth about 1 EPNdB relative to a production inlet with lip lining and "stretched" to have the same total lining area as in the scarf inlet.

At cutback power it was concluded that the scarf shape significantly increases buzzsaw noise, but, except for the high frequencies (2 kHz and higher), the lining attenuated it to levels expected based on the measured treated production inlet levels. The RDIFF code however does not predict the attenuation of the buzz saw noise. The RDIFF calculated acoustic wave attenuation for the treated scarf inlet relative to the treated production inlet at the dominant buzz saw noise frequencies (<1 kHz) appeared to be reasonably close to the measured data. Besides buzz saw noise attenuation prediction, the other major miss by the RDIFF code was the prediction of the high frequency (2 kHz and higher) noise attenuation at the higher power conditions. Contrary to the RDIFF predictions, the measured high frequency attenuations were observed to fall off rapidly with increased power setting. It is speculated that this is due to a propagation effect through the high Mach number flow, which reduces the hardwall and treated inlet noise levels increasingly as engine power is increased while reducing the effect of the lining which is adjacent to the high Mach number flow. If this is true the RDIFF high frequency predictions may be valid for flight where the lip Mach numbers are much lower.

If the predicted high frequency attenuation is realized, the 13° biplanar scarf shape is worth about 3 EPNdB and the triple layer lining is worth about 0.75 EPNdB relative to a production inlet with a treated lip and "stretched" to have lining area equal to the tested scarf inlet.

5.3   ICD Microphone Array

The ICD phased array can measure low-pressure compressor noise in the expected spinning modes. The results for blade passage frequency are promising, but not completely satisfactory. This is probably due to the scattering of the modes by the nonuniform inlet and flow geometry.

At approach power, the inlet noise of the PW4098 has a strong contribution from the low pressure compressor. Blade passage tones and broadband fan noise are also important. High pressure compressor noise may play a role.

Blade passage frequency noise for the hardwall baseline inlet is dominated by the mode $m = 17\text{-}18$. There is no obvious mode in the treated case.

The blade passage frequency noise of the treated scarf inlet is strongly concentrated around $m = 5$. Beamforming images show a periodic source structure that may be consistent with generation of this mode.

Inlet lip lining is very effective in attenuating buzzsaw noise at low spinning orders.

The production lining is ineffective at takeoff power.

The production lining is largely ineffective for low-pressure compressor noise at approach power.

5.4   BMT and Mode Array Tone Diagnostics

The mode array, in combination with the BMT's and the flow visualization techniques, provided insight into some of the BPF noise-generation mechanisms for the scarf and production inlets. These data show the additional BPF noise for the scarf over the production inlet at subsonic speeds is due to a flow problem at the crown. The current scarf inlet, without a bellmouth, separates at the crown, which causes vortices to be shed into the fan. These vortices have long axial length scales, which are not stationary and hence, generate a non-deterministic BPF noise source in spinning orders that propagate out the nacelle. High peak Mach numbers around the inlet lip of the scarf inlet can be reduced with the use of a bellmouth, thus reducing the possibility of separated flow. Recent CFD calculations indicate that the separated flow in the scarf inlet will be eliminated with forward flight. Additional work is underway to determine the possibility of testing the scarf inlet with a bellmouth inlet.

The production inlet with the ICD did not show evidence of a non-deterministic BPF noise source in the mode array or BMT data. Since the production inlet uses a bellmouth inlet which reduces the Mach number near the lip, the probability of flow separation is minimized thereby eliminating the existence of these unsteady flow distortions. In addition, CFD results have shown the scarf inlet to have higher peak Mach numbers than the production inlet due its flow lines. Recent CFD runs have shown some evidence that the scarf inlet would not have the separation BPF noise source if it was in forward flight or had a bellmouth inlet.

The cause of the BPF noise for the production inlet at subsonic speeds was never fully determined. The data was able to show that the production inlet BPF noise is due to a deterministic noise mechanism, but the source of the mechanism is not conclusive. The BMT data show steady distortions which exist in the boundary layer, yet it is not clear whether the noise generated from the interaction of the fan with these disturbances is sufficient to generate the observed BPF tones. The mode array data, however, shows that the noise source is spread out across all the propagating spinning orders. This implies that the source is not comprised of one interaction that can be determined and fixed. The source seems to be comprised of many propagating spinning orders. Mode measurements and/or BMT data during acceleration/deceleration and with the inlet rotated may provide the additional data to needed to help understand this noise source. These types of data were not taken during this test.

The mode array data did not provide any evidence of large differences between the production and scarf deterministic noise sources. However, the BMT data clearly showed large steady distortions in the pressures measured on the blades for both inlets. There is not currently enough data to determine the amount of additional noise due to the steady distortion as measured with the BMT's. The data clearly show that the unsteady part of the noise dominates the differences. Possibly, some of the fan-noise prediction codes could be used to predict the relative levels of the steady and unsteady noise sources from the BMT data to compare these sources. The data suggests that the steady source increase is insignificant in comparison.

Clearly the mode array, BMT's, and the visualization techniques are useful in helping understand complex BPF noise mechanisms. It is unlikely that the source of the BPF noise for the scarf inlet would have been discovered and so fully understood without these techniques. Likewise, there now exists a greater understanding of the type of source that needs to be eliminated in order to reduce subsonic BPF noise of current engines.

Appendix

This appendix presents a complete listing of data records by Configuration and Run Number. The convention (or key) to data record ID (database ID) is as follows:

RRRRRGRXXX

RRRRR = 5 digit run number. A unique run number is assigned for every configuration. A configuration represents a hardware or test set up change.

GR = Microphone type code where GR means a ground plane microphone as part of a radial array.

XXX = An index counter, a new index is given to each data point acquired within a run number.

SOURCE: Run 16078 CONFIG 1
PW4098 X841-10A,BOM HW INLET+FFCC,KEEL TO MICS,ICD,AFT WALLS,NO PT2 PRB
*** SORTED BY N1C ***

RECORD ID	No. of ANGLES	N1CORR	N1OBS	DATE	TIME
16078GR017	24	0.	0.	111098	1257
16078GR024	24	0.	0.	111198	0740
16078GR003	24	571.	580.	110998	1321
16078GR001	24	571.	580.	110998	1310
16078GR002	24	571.	580.	110998	1314
16078GR004	24	1499.	1521.	110998	1634
16078GR033	24	1500.	1534.	111198	1221
16078GR005	24	1503.	1526.	110998	1658
16078GR006	24	1603.	1627.	110998	1702
16078GR034	24	1605.	1641.	111198	1224
16078GR035	24	1703.	1742.	111198	1227
16078GR007	24	1704.	1729.	110998	1706
16078GR008	24	1750.	1775.	110998	1710
16078GR036	24	1754.	1794.	111198	1231
16078GR009	24	1802.	1828.	110998	1713
16078GR028	24	1804.	1844.	111198	1153
16078GR010	24	1850.	1876.	110998	1721
16078GR037	24	1854.	1895.	111198	1235
16078GR011	24	1900.	1926.	110998	1725
16078GR038	24	1902.	1944.	111198	1239
16078GR012	24	2002.	2030.	110998	1728
16078GR013	24	2102.	2130.	110998	1733
16078GR014	24	2201.	2230.	110998	1738
16078GR029	24	2204.	2252.	111198	1158
16078GR046	24	2206.	2256.	111198	1311
16078GR039	24	2250.	2301.	111198	1243
16078GR015	24	2252.	2281.	110998	1743
16078GR016	24	2300.	2329.	110998	1747
16078GR040	24	2303.	2355.	111198	1246
16078GR018	24	2351.	2392.	111098	1729
16078GR041	24	2353.	2407.	111198	1249
16078GR042	24	2403.	2457.	111198	1254
16078GR019	24	2403.	2445.	111098	1735
16078GR030	24	2451.	2506.	111198	1204
16078GR020	24	2451.	2494.	111098	1738
16078GR021	24	2452.	2493.	111098	1741
16078GR043	24	2503.	2560.	111198	1257
16078GR022	24	2503.	2545.	111098	1746
16078GR023	24	2599.	2642.	111098	1751
16078GR044	24	2602.	2662.	111198	1301
16078GR027	24	2703.	2760.	111198	1119
16078GR031	24	2711.	2771.	111198	1209
16078GR045	24	2799.	2864.	111198	1305
16078GR025	24	2803.	2864.	111198	1104
16078GR032	24	2897.	2962.	111198	1214
16078GR026	24	2906.	2967.	111198	1108

SOURCE: 16079 CONFIG 2
PW4098 X841-10A,BOM TRT INL +FFCC,KEEL TO MICS,ICD,AFT WALLS,NO PT2 PR
*** SORTED BY N1C ***

RECORD ID	No. of ANGLES	N1CORR	N1OBS	DATE	TIME
16079GR001	24	0.	0.	111198	1732
16079GR002	24	0.	0.	111198	1735
16079GR003	24	566.	576.	111198	1748
16079GR004	24	1479.	1504.	111198	1753
16079GR042	24	1505.	1524.	111198	2044
16079GR024	24	1506.	1527.	111198	1934
16079GR025	24	1607.	1629.	111198	1937
16079GR005	24	1607.	1634.	111198	1758
16079GR006	24	1702.	1730.	111198	1801
16079GR026	24	1705.	1728.	111198	1940
16079GR007	24	1755.	1783.	111198	1804
16079GR027	24	1759.	1781.	111198	1944
16079GR028	24	1804.	1827.	111198	1946
16079GR008	24	1806.	1835.	111198	1808
16079GR029	24	1854.	1878.	111198	1950
16079GR009	24	1862.	1891.	111198	1813
16079GR030	24	1906.	1931.	111198	1952
16079GR010	24	1907.	1938.	111198	1816
16079GR011	24	2005.	2037.	111198	1819
16079GR012	24	2106.	2137.	111198	1844
16079GR031	24	2205.	2234.	111198	1955
16079GR013	24	2207.	2240.	111198	1848
16079GR032	24	2254.	2283.	111198	1958
16079GR014	24	2262.	2295.	111198	1852
16079GR015	24	2303.	2337.	111198	1854
16079GR033	24	2307.	2338.	111198	2001
16079GR034	24	2355.	2386.	111198	2004
16079GR016	24	2358.	2392.	111198	1857
16079GR035	24	2405.	2436.	111198	2007
16079GR017	24	2408.	2443.	111198	1900
16079GR036	24	2452.	2485.	111198	2010
16079GR018	24	2454.	2489.	111198	1903
16079GR037	24	2504.	2537.	111198	2013
16079GR019	24	2506.	2542.	111198	1907
16079GR038	24	2603.	2637.	111198	2016
16079GR020	24	2605.	2642.	111198	1910
16079GR039	24	2703.	2739.	111198	2019
16079GR021	24	2704.	2743.	111198	1913
16079GR022	24	2803.	2843.	111198	1916
16079GR040	24	2804.	2840.	111198	2022
16079GR041	24	2897.	2935.	111198	2026
16079GR023	24	2904.	2946.	111198	1919

SOURCE: 16082 CONFIG 3
C3:SCARF HW INL,SIM HW BOM FFCC ,KEEL TO MICS,ICD,AFT WALLS,NO PT2 PR
*** SORTED BY N1C ***

RECORD ID	No. of ANGLES	N1CORR	N1OBS	DATE	TIME
16082GR041	24	0.	0.	111798	0957
16082GR042	24	0.	0.	111798	1000
16082GR001	24	15.	15.	111698	0923
16082GR002	24	568.	581.	111698	1020
16082GR003	24	1503.	1534.	111698	1024
16082GR023	24	1505.	1536.	111698	1138
16082GR004	24	1596.	1629.	111698	1028
16082GR024	24	1604.	1637.	111698	1142
16082GR025	24	1705.	1740.	111698	1145
16082GR005	24	1706.	1742.	111698	1031
16082GR026	24	1753.	1789.	111698	1148
16082GR006	24	1754.	1792.	111698	1035
16082GR007	24	1804.	1843.	111698	1039
16082GR027	24	1806.	1845.	111698	1151
16082GR028	24	1854.	1893.	111698	1155
16082GR008	24	1858.	1898.	111698	1042
16082GR029	24	1900.	1940.	111698	1158
16082GR009	24	1902.	1943.	111698	1046
16082GR010	24	2003.	2046.	111698	1049
16082GR011	24	2102.	2147.	111698	1053
16082GR012	24	2202.	2249.	111698	1057
16082GR030	24	2204.	2251.	111698	1202
16082GR013	24	2252.	2299.	111698	1100
16082GR031	24	2252.	2299.	111698	1205
16082GR014	24	2302.	2351.	111698	1104
16082GR032	24	2304.	2352.	111698	1208
16082GR015	24	2351.	2401.	111698	1107
16082GR033	24	2352.	2401.	111698	1211
16082GR016	24	2403.	2455.	111698	1111
16082GR034	24	2403.	2453.	111698	1214
16082GR017	24	2454.	2506.	111698	1114
16082GR035	24	2454.	2505.	111698	1217
16082GR018	24	2500.	2553.	111698	1117
16082GR036	24	2501.	2554.	111698	1222
16082GR019	24	2600.	2656.	111698	1120
16082GR037	24	2606.	2663.	111698	1225
16082GR038	24	2701.	2758.	111698	1229
16082GR020	24	2703.	2762.	111698	1124
16082GR039	24	2803.	2862.	111698	1234
16082GR021	24	2805.	2864.	111698	1128
16082GR040	24	2901.	2964.	111698	1238
16082GR022	24	2904.	2964.	111698	1132

SOURCE: 16083 CONFIG 12
C12:SCARF TRT INL W/HW LIP,HW FFCC,KEEL-MICS,ICD,AFT WALLS;NO PT PRB
*** SORTED BY N1C ***

RECORD ID	No. of ANGLES	N1CORR	N1OBS	DATE	TIME
16083GR001	24	0.	0.	111798	1211
16083GR002	24	0.	0.	111798	1213
16083GR003	24	0.	0.	111798	1222
16083GR004	24	552.	566.	111798	1237
16083GR025	24	1499.	1534.	111798	1349
16083GR005	24	1503.	1538.	111798	1240
16083GR006	24	1598.	1636.	111798	1245
16083GR026	24	1602.	1639.	111798	1353
16083GR027	24	1704.	1743.	111798	1356
16083GR007	24	1707.	1748.	111798	1248
16083GR028	24	1755.	1796.	111798	1359
16083GR008	24	1757.	1799.	111798	1251
16083GR009	24	1804.	1847.	111798	1254
16083GR029	24	1804.	1846.	111798	1402
16083GR030	24	1852.	1895.	111798	1405
16083GR010	24	1858.	1902.	111798	1257
16083GR031	24	1902.	1947.	111798	1408
16083GR011	24	1908.	1953.	111798	1301
16083GR012	24	2006.	2053.	111798	1304
16083GR013	24	2102.	2153.	111798	1307
16083GR032	24	2200.	2253.	111798	1412
16083GR014	24	2207.	2261.	111798	1310
16083GR033	24	2253.	2307.	111798	1415
16083GR015	24	2255.	2310.	111798	1314
16083GR016	24	2301.	2360.	111798	1317
16083GR034	24	2305.	2361.	111798	1418
16083GR035	24	2351.	2410.	111798	1421
16083GR017	24	2355.	2412.	111798	1321
16083GR036	24	2401.	2460.	111798	1424
16083GR018	24	2402.	2459.	111798	1324
16083GR037	24	2450.	2510.	111798	1427
16083GR019	24	2451.	2508.	111798	1327
16083GR038	24	2501.	2564.	111798	1430
16083GR020	24	2503.	2562.	111798	1331
16083GR039	24	2602.	2667.	111798	1434
16083GR021	24	2605.	2666.	111798	1334
16083GR022	24	2701.	2764.	111798	1338
16083GR040	24	2703.	2768.	111798	1437
16083GR023	24	2803.	2869.	111798	1341
16083GR041	24	2804.	2870.	111798	1440
16083GR042	24	2903.	2973.	111798	1443
16083GR024	24	2904.	2973.	111798	1344

SOURCE: 16084 CONFIG 14
C14:SCARF TRT INL W/TRT LIP,HW FFCC,KEEL-MICS,ICD,AFT WALLS;NO PT PRB
*** SORTED BY N1C ***

RECORD ID	No. of ANGLES	N1CORR	N1OBS	DATE	TIME
16084GR001	24	0.	0.	111898	0733
16084GR003	24	0.	0.	111898	0853
16084GR043	24	0.	0.	111898	1247
16084GR044	24	0.	0.	111898	1251
16084GR002	24	1.	1.	111898	0735
16084GR004	24	589.	601.	111898	0902
16084GR005	24	1502.	1531.	111898	0907
16084GR025	24	1514.	1547.	111898	1009
16084GR006	24	1605.	1637.	111898	0910
16084GR026	24	1607.	1643.	111898	1011
16084GR027	24	1701.	1739.	111898	1014
16084GR007	24	1705.	1739.	111898	0913
16084GR008	24	1753.	1788.	111898	0916
16084GR028	24	1757.	1795.	111898	1017
16084GR009	24	1802.	1839.	111898	0920
16084GR029	24	1805.	1843.	111898	1020
16084GR034	24	1850.	1888.	111898	1038
16084GR010	24	1851.	1889.	111898	0923
16084GR011	24	1901.	1940.	111898	0926
16084GR035	24	1904.	1943.	111898	1041
16084GR012	24	2005.	2047.	111898	0929
16084GR013	24	2103.	2146.	111898	0932
16084GR030	24	2204.	2249.	111898	1025
16084GR014	24	2208.	2254.	111898	0935
16084GR015	24	2252.	2299.	111898	0938
16084GR036	24	2254.	2300.	111898	1044
16084GR037	24	2300.	2348.	111898	1047
16084GR016	24	2302.	2353.	111898	0941
16084GR017	24	2353.	2404.	111898	0944
16084GR038	24	2353.	2403.	111898	1049
16084GR039	24	2402.	2452.	111898	1052
16084GR018	24	2404.	2456.	111898	0946
16084GR031	24	2451.	2502.	111898	1028
16084GR019	24	2452.	2503.	111898	0949
16084GR020	24	2502.	2552.	111898	0953
16084GR040	24	2502.	2553.	111898	1055
16084GR021	24	2601.	2654.	111898	0956
16084GR041	24	2602.	2658.	111898	1058
16084GR032	24	2700.	2758.	111898	1031
16084GR022	24	2704.	2761.	111898	0959
16084GR023	24	2798.	2859.	111898	1002
16084GR042	24	2799.	2862.	111898	1102
16084GR033	24	2905.	2966.	111898	1034
16084GR024	24	2907.	2969.	111898	1005

SOURCE: 16085 CONFIG 4

C04:SCARF TRT INL W/TRT LIP,TRT FFCC,KEEL-MICS,ICD,AFT WALLS;NO PT PRB

*** SORTED BY N1C ***

RECORD ID	No. of ANGLES	N1CORR	N1OBS	DATE	TIME
16085GR001	24	0.	0.	111898	1316
16085GR042	24	0.	0.	111898	1619
16085GR043	24	0.	0.	111898	1624
16085GR003	24	588.	602.	111898	1323
16085GR024	24	1512.	1548.	111898	1431
16085GR004	24	1515.	1549.	111898	1328
16085GR005	24	1603.	1640.	111898	1331
16085GR025	24	1608.	1646.	111898	1434
16085GR026	24	1705.	1744.	111898	1437
16085GR006	24	1706.	1746.	111898	1335
16085GR027	24	1751.	1792.	111898	1440
16085GR007	24	1757.	1799.	111898	1338
16085GR008	24	1805.	1847.	111898	1341
16085GR028	24	1805.	1848.	111898	1442
16085GR009	24	1850.	1894.	111898	1344
16085GR029	24	1854.	1899.	111898	1446
16085GR002	24	1861.	1904.	111898	1320
16085GR030	24	1899.	1945.	111898	1448
16085GR010	24	1906.	1952.	111898	1347
16085GR011	24	2005.	2053.	111898	1350
16085GR012	24	2101.	2150.	111898	1353
16085GR031	24	2202.	2257.	111898	1452
16085GR013	24	2203.	2257.	111898	1356
16085GR014	24	2252.	2306.	111898	1359
16085GR032	24	2255.	2311.	111898	1455
16085GR033	24	2304.	2357.	111898	1500
16085GR015	24	2305.	2358.	111898	1403
16085GR016	24	2352.	2404.	111898	1406
16085GR034	24	2352.	2405.	111898	1503
16085GR035	24	2401.	2456.	111898	1506
16085GR017	24	2402.	2455.	111898	1408
16085GR018	24	2451.	2505.	111898	1411
16085GR036	24	2453.	2510.	111898	1509
16085GR019	24	2504.	2561.	111898	1415
16085GR037	24	2505.	2562.	111898	1512
16085GR020	24	2601.	2662.	111898	1418
16085GR038	24	2603.	2663.	111898	1515
16085GR039	24	2701.	2763.	111898	1519
16085GR021	24	2703.	2767.	111898	1421
16085GR022	24	2802.	2870.	111898	1424
16085GR040	24	2804.	2869.	111898	1522
16085GR023	24	2901.	2972.	111898	1427
16085GR041	24	2906.	2973.	111898	1528

SOURCE: 16086 CONFIG 5

C05:SCARF TRT INLET,R1 FFCC, KEEL-MICS,ICD,AFT WALLS;NO PT PROBE

*** SORTED BY N1C ***

RECORD ID	No. of ANGLES	N1CORR	N1OBS	DATE	TIME
16086GR001	24	0.	0.	111998	1837
16086GR002	24	0.	0.	111998	1841
16086GR039	24	0.	0.	111998	2203
16086GR040	24	0.	0.	111998	2207
16086GR003	24	573.	586.	111998	1904
16086GR004	24	1557.	1584.	111998	1909
16086GR024	24	1557.	1584.	111998	2016
16086GR005	24	1602.	1630.	111998	1913
16086GR034	24	1611.	1636.	111998	2056
16086GR035	24	1703.	1730.	111998	2058
16086GR006	24	1704.	1734.	111998	1916
16086GR007	24	1752.	1782.	111998	1920
16086GR025	24	1753.	1782.	111998	2019
16086GR026	24	1802.	1832.	111998	2023
16086GR008	24	1803.	1834.	111998	1923
16086GR009	24	1851.	1884.	111998	1927
16086GR027	24	1854.	1884.	111998	2027
16086GR010	24	1900.	1933.	111998	1930
16086GR036	24	1904.	1934.	111998	2103
16086GR011	24	2000.	2034.	111998	1933
16086GR012	24	2106.	2142.	111998	1936
16086GR028	24	2204.	2240.	111998	2031
16086GR013	24	2204.	2242.	111998	1939
16086GR014	24	2252.	2291.	111998	1943
16086GR037	24	2255.	2290.	111998	2108
16086GR015	24	2305.	2345.	111998	1946
16086GR038	24	2307.	2343.	111998	2112
16086GR016	24	2354.	2394.	111998	1949
16086GR017	24	2401.	2443.	111998	1952
16086GR029	24	2404.	2444.	111998	2035
16086GR030	24	2450.	2490.	111998	2038
16086GR018	24	2455.	2497.	111998	1955
16086GR019	24	2501.	2544.	111998	1958
16086GR031	24	2502.	2542.	111998	2041
16086GR020	24	2601.	2646.	111998	2002
16086GR032	24	2700.	2744.	111998	2045
16086GR021	24	2702.	2748.	111998	2005
16086GR022	24	2800.	2848.	111998	2008
16086GR033	24	2900.	2946.	111998	2050
16086GR023	24	2900.	2949.	111998	2011

SOURCE: 16087 CONFIG 6
CO6:SCARF TRT INLET,R2 FFCC, KEEL-MICS,ICD,AFT WALLS;NO PT PROBE
*** SORTED BY N1C ***

RECORD ID	No. of ANGLES	N1CORR	N1OBS	DATE	TIME
16087GR001	24	0.	0.	112098	0800
16087GR002	24	0.	0.	112098	0802
16087GR042	24	0.	0.	112098	1355
16087GR043	24	0.	0.	112098	1359
16087GR003	24	565.	576.	112098	1044
16087GR024	24	1554.	1588.	112098	1148
16087GR004	24	1557.	1589.	112098	1047
16087GR025	24	1602.	1639.	112098	1151
16087GR005	24	1608.	1640.	112098	1050
16087GR026	24	1700.	1739.	112098	1154
16087GR006	24	1704.	1740.	112098	1053
16087GR027	24	1750.	1789.	112098	1156
16087GR007	24	1754.	1791.	112098	1056
16087GR008	24	1802.	1841.	112098	1059
16087GR028	24	1802.	1841.	112098	1159
16087GR009	24	1851.	1892.	112098	1102
16087GR029	24	1852.	1892.	112098	1203
16087GR030	24	1902.	1942.	112098	1206
16087GR010	24	1903.	1942.	112098	1105
16087GR011	24	2002.	2044.	112098	1107
16087GR012	24	2100.	2145.	112098	1110
16087GR013	24	2200.	2248.	112098	1114
16087GR031	24	2203.	2252.	112098	1209
16087GR032	24	2251.	2303.	112098	1213
16087GR014	24	2254.	2303.	112098	1117
16087GR015	24	2302.	2353.	112098	1120
16087GR033	24	2302.	2356.	112098	1215
16087GR034	24	2353.	2408.	112098	1219
16087GR016	24	2354.	2404.	112098	1123
16087GR035	24	2400.	2456.	112098	1222
16087GR017	24	2401.	2452.	112098	1125
16087GR018	24	2450.	2502.	112098	1129
16087GR036	24	2453.	2509.	112098	1224
16087GR019	24	2501.	2557.	112098	1132
16087GR037	24	2501.	2558.	112098	1228
16087GR038	24	2603.	2661.	112098	1231
16087GR020	24	2605.	2662.	112098	1135
16087GR039	24	2699.	2762.	112098	1234
16087GR021	24	2703.	2763.	112098	1138
16087GR022	24	2802.	2863.	112098	1141
16087GR040	24	2803.	2869.	112098	1237
16087GR023	24	2905.	2972.	112098	1144
16087GR041	24	2907.	2972.	112098	1239

SOURCE: 16088 CONFIG 7

C7:SCARF TRT INL,R2 8-3" HW SPL FFCC,KEEL TO MICS,ICD,AFT WALLS,NO PT PBE

*** SORTED BY N1C ***

RECORD ID	No. of ANGLES	N1CORR	N1OBS	DATE	TIME
16088GR001	24	0.	0.	112098	1652
16088GR002	24	0.	0.	112098	1656
16088GR003	24	0.	0.	112098	1711
16088GR043	24	0.	0.	112098	2116
16088GR044	24	0.	0.	112098	2129
16088GR004	24	569.	579.	112098	1734
16088GR005	24	1554.	1583.	112098	1740
16088GR025	24	1557.	1584.	112098	1851
16088GR006	24	1599.	1628.	112098	1743
16088GR026	24	1602.	1629.	112098	1854
16088GR007	24	1704.	1736.	112098	1746
16088GR027	24	1707.	1735.	112098	1858
16088GR028	24	1751.	1780.	112098	1903
16088GR008	24	1759.	1791.	112098	1749
16088GR009	24	1803.	1836.	112098	1752
16088GR029	24	1803.	1834.	112098	1906
16088GR030	24	1854.	1885.	112098	1912
16088GR010	24	1856.	1890.	112098	1756
16088GR031	24	1902.	1934.	112098	1915
16088GR011	24	1903.	1938.	112098	1759
16088GR012	24	2001.	2038.	112098	1801
16088GR013	24	2102.	2140.	112098	1805
16088GR032	24	2203.	2239.	112098	1919
16088GR014	24	2206.	2246.	112098	1808
16088GR015	24	2251.	2292.	112098	1811
16088GR033	24	2253.	2290.	112098	1922
16088GR016	24	2301.	2342.	112098	1814
16088GR034	24	2303.	2341.	112098	1926
16088GR017	24	2351.	2394.	112098	1816
16088GR040	24	2354.	2392.	112098	1947
16088GR018	24	2401.	2444.	112098	1819
16088GR035	24	2402.	2441.	112098	1929
16088GR036	24	2451.	2490.	112098	1932
16088GR019	24	2452.	2495.	112098	1823
16088GR037	24	2501.	2541.	112098	1935
16088GR020	24	2503.	2547.	112098	1827
16088GR021	24	2601.	2647.	112098	1831
16088GR041	24	2607.	2648.	112098	1951
16088GR022	24	2700.	2747.	112098	1836
16088GR038	24	2700.	2744.	112098	1939
16088GR023	24	2802.	2850.	112098	1839
16088GR042	24	2803.	2847.	112098	1955
16088GR024	24	2900.	2950.	112098	1845
16088GR039	24	2903.	2949.	112098	1943

SOURCE: 16089 CONFIG 8
C8:SCARF TRT INL,R2 3-3" HW SPL FFCC,KEEL TO MICS,ICD,AFT WALLS,NO PT PBE
*** SORTED BY N1C ***

RECORD ID	No. of ANGLES	N1CORR	N1OBS	DATE	TIME
16089GR001	24	0.	0.	112198	0906
16089GR044	24	0.	0.	112198	1159
16089GR045	24	0.	0.	112198	1201
16089GR046	24	0.	0.	112198	1205
16089GR003	24	1.	1.	112198	0918
16089GR002	24	1.	1.	112198	0909
16089GR004	24	565.	575.	112198	0930
16089GR005	24	1545.	1575.	112198	0933
16089GR025	24	1551.	1584.	112198	1035
16089GR006	24	1601.	1632.	112198	0936
16089GR026	24	1607.	1641.	112198	1037
16089GR027	24	1700.	1737.	112198	1040
16089GR007	24	1702.	1735.	112198	0939
16089GR028	24	1752.	1790.	112198	1043
16089GR008	24	1752.	1786.	112198	0942
16089GR029	24	1799.	1838.	112198	1046
16089GR009	24	1804.	1840.	112198	0946
16089GR030	24	1854.	1894.	112198	1050
16089GR010	24	1857.	1893.	112198	0949
16089GR031	24	1902.	1943.	112198	1053
16089GR011	24	1903.	1941.	112198	0952
16089GR012	24	2003.	2042.	112198	0955
16089GR013	24	2100.	2142.	112198	0957
16089GR014	24	2199.	2243.	112198	1001
16089GR032	24	2201.	2249.	112198	1057
16089GR033	24	2202.	2250.	112198	1101
16089GR015	24	2252.	2298.	112198	1004
16089GR034	24	2253.	2302.	112198	1105
16089GR016	24	2303.	2350.	112198	1007
16089GR035	24	2304.	2355.	112198	1108
16089GR017	24	2352.	2400.	112198	1010
16089GR036	24	2353.	2406.	112198	1110
16089GR037	24	2401.	2455.	112198	1113
16089GR018	24	2403.	2452.	112198	1013
16089GR038	24	2453.	2508.	112198	1116
16089GR019	24	2453.	2504.	112198	1016
16089GR020	24	2501.	2553.	112198	1019
16089GR039	24	2502.	2558.	112198	1120
16089GR040	24	2604.	2661.	112198	1122
16089GR021	24	2605.	2660.	112198	1022
16089GR041	24	2700.	2761.	112198	1125
16089GR022	24	2703.	2759.	112198	1024
16089GR042	24	2802.	2865.	112198	1128
16089GR023	24	2802.	2860.	112198	1027
16089GR043	24	2903.	2969.	112198	1132
16089GR024	24	2903.	2965.	112198	1030

SOURCE: 16090 CONFIG 9
C9:SCARF TRT INL,R2,3-1.25" HW SPL FFCC,KEEL-MICS,ICD,AFT WALLS,NO PT PBE
*** SORTED BY N1C ***

RECORD ID	No. of ANGLES	N1CORR	N1OBS	DATE	TIME
16090GR002	24	0.	0.	112198	1337
16090GR003	24	0.	0.	112198	1341
16090GR043	24	0.	0.	112198	2200
16090GR044	24	0.	0.	112198	2205
16090GR004	24	562.	576.	112198	1351
16090GR005	24	1541.	1579.	112198	1355
16090GR025	24	1546.	1582.	112198	1454
16090GR026	24	1602.	1639.	112198	1457
16090GR006	24	1605.	1644.	112198	1358
16090GR007	24	1702.	1743.	112198	1400
16090GR027	24	1702.	1742.	112198	1500
16090GR008	24	1751.	1795.	112198	1403
16090GR028	24	1754.	1796.	112198	1503
16090GR009	24	1804.	1849.	112198	1406
16090GR029	24	1807.	1850.	112198	1506
16090GR010	24	1851.	1898.	112198	1409
16090GR030	24	1854.	1900.	112198	1509
16090GR011	24	1901.	1949.	112198	1412
16090GR031	24	1901.	1949.	112198	1512
16090GR012	24	2003.	2053.	112198	1415
16090GR013	24	2104.	2156.	112198	1418
16090GR014	24	2201.	2255.	112198	1420
16090GR032	24	2205.	2261.	112198	1515
16090GR033	24	2253.	2309.	112198	1518
16090GR015	24	2257.	2311.	112198	1423
16090GR016	24	2301.	2356.	112198	1426
16090GR034	24	2302.	2360.	112198	1521
16090GR017	24	2349.	2406.	112198	1429
16090GR035	24	2353.	2411.	112198	1523
16090GR018	24	2399.	2457.	112198	1431
16090GR036	24	2403.	2462.	112198	1526
16090GR019	24	2453.	2513.	112198	1434
16090GR037	24	2457.	2516.	112198	1530
16090GR020	24	2500.	2562.	112198	1437
16090GR038	24	2502.	2562.	112198	1533
16090GR039	24	2601.	2662.	112198	1535
16090GR021	24	2605.	2669.	112198	1440
16090GR040	24	2702.	2764.	112198	1539
16090GR022	24	2703.	2770.	112198	1443
16090GR041	24	2801.	2865.	112198	1542
16090GR023	24	2804.	2872.	112198	1447
16090GR024	24	2904.	2972.	112198	1450
16090GR042	24	2907.	2973.	112198	1544

SOURCE: 16091 CONFIG

C11:SCARF TRT INL,R2,3-0.625" HW SPL FFCC,KEEL-MICS,ICD,AFT WALLS,NO PT PB

*** SORTED BY N1C ***

RECORD ID	No. of ANGLES	N1CORR	N1OBS	DATE	TIME
16091GR001	24	0.	0.	112198	1751
16091GR002	24	0.	0.	112198	1755
16091GR003	24	0.	0.	112198	1759
16091GR043	24	0.	0.	112198	2132
16091GR044	24	0.	0.	112198	2136
16091GR004	24	555.	564.	112198	1808
16091GR005	24	1547.	1574.	112198	1811
16091GR030	24	1548.	1572.	112198	1931
16091GR031	24	1607.	1631.	112198	1934
16091GR006	24	1611.	1639.	112198	1814
16091GR007	24	1703.	1733.	112198	1817
16091GR032	24	1707.	1733.	112198	1936
16091GR033	24	1749.	1777.	112198	1940
16091GR008	24	1754.	1783.	112198	1820
16091GR009	24	1801.	1832.	112198	1823
16091GR014	24	1803.	1833.	112198	1843
16091GR019	24	1852.	1883.	112198	1900
16091GR034	24	1852.	1881.	112198	1943
16091GR020	24	1901.	1932.	112198	1903
16091GR035	24	1903.	1933.	112198	1946
16091GR021	24	2007.	2040.	112198	1906
16091GR022	24	2105.	2139.	112198	1908
16091GR015	24	2201.	2237.	112198	1846
16091GR010	24	2203.	2240.	112198	1826
16091GR023	24	2252.	2288.	112198	1911
16091GR036	24	2256.	2291.	112198	1950
16091GR037	24	2303.	2338.	112198	1952
16091GR024	24	2305.	2341.	112198	1914
16091GR038	24	2351.	2386.	112198	1955
16091GR025	24	2352.	2389.	112198	1916
16091GR026	24	2401.	2438.	112198	1919
16091GR039	24	2401.	2438.	112198	1957
16091GR016	24	2450.	2490.	112198	1849
16091GR011	24	2455.	2497.	112198	1830
16091GR040	24	2500.	2538.	112198	2000
16091GR027	24	2504.	2544.	112198	1921
16091GR041	24	2601.	2640.	112198	2003
16091GR028	24	2604.	2645.	112198	1924
16091GR012	24	2702.	2749.	112198	1835
16091GR017	24	2704.	2749.	112198	1853
16091GR029	24	2801.	2845.	112198	1927
16091GR042	24	2803.	2844.	112198	2006
16091GR013	24	2902.	2951.	112198	1838
16091GR018	24	2902.	2949.	112198	1856

SOURCE: 16092 CONFIG 10
C10:SCRF TRT INL,R2 3-1.25"+6"HW FFCC,KEEL-MICS,ICD,AFT WALL,NO PT PRB
*** SORTED BY N1C ***

RECORD ID	No. of ANGLES	N1CORR	N1OBS	DATE	TIME
16092GR001	24	0.	0.	112298	0654
16092GR002	24	0.	0.	112298	0733
16092GR003	24	0.	0.	112298	0727
16092GR044	24	0.	0.	112298	1358
16092GR045	24	0.	0.	112298	1404
16092GR043	24	568.	580.	112298	1350
16092GR005	24	1549.	1582.	112298	1126
16092GR025	24	1551.	1586.	112298	1231
16092GR026	24	1602.	1638.	112298	1234
16092GR006	24	1602.	1636.	112298	1129
16092GR007	24	1702.	1738.	112298	1133
16092GR027	24	1706.	1744.	112298	1237
16092GR008	24	1750.	1788.	112298	1136
16092GR028	24	1752.	1791.	112298	1244
16092GR009	24	1803.	1842.	112298	1139
16092GR029	24	1805.	1846.	112298	1247
16092GR030	24	1852.	1894.	112298	1253
16092GR010	24	1852.	1891.	112298	1142
16092GR031	24	1902.	1946.	112298	1256
16092GR011	24	1902.	1944.	112298	1145
16092GR012	24	2002.	2048.	112298	1148
16092GR013	24	2104.	2152.	112298	1152
16092GR014	24	2202.	2251.	112298	1156
16092GR032	24	2203.	2253.	112298	1301
16092GR015	24	2250.	2298.	112298	1159
16092GR033	24	2251.	2301.	112298	1304
16092GR016	24	2301.	2351.	112298	1203
16092GR034	24	2302.	2354.	112298	1306
16092GR035	24	2353.	2406.	112298	1309
16092GR017	24	2356.	2405.	112298	1206
16092GR018	24	2400.	2454.	112298	1209
16092GR036	24	2401.	2456.	112298	1312
16092GR019	24	2450.	2506.	112298	1212
16092GR037	24	2452.	2509.	112298	1315
16092GR038	24	2501.	2558.	112298	1319
16092GR020	24	2501.	2556.	112298	1215
16092GR021	24	2603.	2660.	112298	1218
16092GR039	24	2604.	2663.	112298	1323
16092GR040	24	2701.	2763.	112298	1326
16092GR022	24	2702.	2761.	112298	1221
16092GR023	24	2800.	2864.	112298	1224
16092GR041	24	2802.	2864.	112298	1332
16092GR024	24	2902.	2968.	112298	1227
16092GR042	24	2905.	2970.	112298	1334

SOURCE: 16093 CONFIG 6A
C06:SCARF TRT INL,w/TRIPS,FFCC R2,KEEL-MICS,ICD,AFT WALLS;NO PT
*** SORTED BY N1C ***

RECORD ID	No. of ANGLES	N1CORR	N1OBS	DATE	TIME
16093GR001	24	0.	0.	112398	0906
16093GR002	24	0.	0.	112398	0909
16093GR024	24	0.	0.	112398	1405
16093GR025	24	0.	0.	112398	1411
16093GR003	24	558.	570.	112398	1227
16093GR004	24	1551.	1586.	112398	1230
16093GR005	24	1606.	1641.	112398	1233
16093GR006	24	1702.	1738.	112398	1236
16093GR007	24	1756.	1794.	112398	1239
16093GR008	24	1802.	1840.	112398	1242
16093GR009	24	1851.	1888.	112398	1245
16093GR010	24	1903.	1940.	112398	1248
16093GR011	24	2000.	2040.	112398	1251
16093GR012	24	2103.	2146.	112398	1254
16093GR013	24	2201.	2246.	112398	1258
16093GR014	24	2252.	2298.	112398	1300
16093GR015	24	2302.	2349.	112398	1303
16093GR016	24	2350.	2399.	112398	1306
16093GR017	24	2398.	2450.	112398	1309
16093GR018	24	2450.	2503.	112398	1312
16093GR019	24	2501.	2556.	112398	1316
16093GR020	24	2604.	2659.	112398	1319
16093GR021	24	2702.	2762.	112398	1321
16093GR022	24	2801.	2860.	112398	1324
16093GR023	24	2904.	2964.	112398	1327

SOURCE: 16094 CONFIG 10A
C10A:SCRF INL W/TRIPS,R2 3-1.25"+6"HW FFCC,KEEL-MICS,ICD,AFTWALL,NO PT
*** SORTED BY N1C ***

RECORD ID	No. of ANGLES	N1CORR	N1OBS	DATE	TIME
16094GR001	24	0.	0.	112398	1610
16094GR002	24	0.	0.	112398	1613
16094GR003	24	0.	0.	112498	1227
16094GR044	24	0.	0.	112498	1210
16094GR045	24	0.	0.	112498	1213
16094GR046	24	0.	0.	112498	1216
16094GR004	24	587.	596.	112498	1256
16094GR005	24	1546.	1568.	112498	1300
16094GR025	24	1550.	1574.	112498	1103
16094GR026	24	1602.	1627.	112498	1106
16094GR006	24	1607.	1631.	112498	1005
16094GR027	24	1701.	1728.	112498	1109
16094GR007	24	1702.	1727.	112498	1008
16094GR028	24	1749.	1777.	112498	1112
16094GR008	24	1753.	1780.	112498	1011
16094GR009	24	1801.	1828.	112498	1014
16094GR029	24	1802.	1831.	112498	1114
16094GR030	24	1849.	1881.	112498	1117
16094GR010	24	1851.	1880.	112498	1018
16094GR031	24	1903.	1935.	112498	1120
16094GR011	24	1903.	1931.	112498	1021
16094GR012	24	2004.	2034.	112498	1024
16094GR043	24	2100.	2139.	112498	1207
16094GR013	24	2104.	2135.	112498	1027
16094GR014	24	2203.	2237.	112498	1029
16094GR032	24	2203.	2240.	112498	1123
16094GR033	24	2251.	2291.	112498	1126
16094GR015	24	2254.	2288.	112498	1033
16094GR016	24	2301.	2336.	112498	1035
16094GR034	24	2301.	2342.	112498	1129
16094GR017	24	2352.	2387.	112498	1038
16094GR035	24	2353.	2394.	112498	1132
16094GR036	24	2400.	2442.	112498	1134
16094GR018	24	2401.	2437.	112498	1041
16094GR019	24	2452.	2489.	112498	1044
16094GR037	24	2453.	2496.	112498	1137
16094GR020	24	2503.	2542.	112498	1047
16094GR038	24	2503.	2546.	112498	1140
16094GR039	24	2599.	2644.	112498	1143
16094GR021	24	2600.	2640.	112498	1049
16094GR022	24	2701.	2742.	112498	1052
16094GR040	24	2701.	2749.	112498	1146
16094GR023	24	2802.	2845.	112498	1056
16094GR041	24	2802.	2852.	112498	1149
16094GR042	24	2901.	2955.	112498	1152
16094GR024	24	2906.	2952.	112498	1059

END OF PHASE 1A TEST CONFIGURATIONS AND ENGINE X841-10A

START OF PHASE 1B TEST CONFIGURATIONS AND ENGINE X841-12
SOURCE: 16101 CONFIG P3
P3-BOM ROT INLET/BM,TRT F&A FC,BMTs,KULITES,ICD,NO PT2 PROBE
*** SORTED BY N1C ***

RECORD ID	No. of ANGLES	N1CORR	N1OBS	DATE	TIME
16101GR001	22	0.	0.	060999	1445
16101GR002	22	0.	0.	060999	1447
16101GR003	22	589.	605.	060999	1522
16101GR004	22	1616.	1659.	060999	1526
16101GR016	22	1702.	1736.	060999	2117
16101GR005	22	1709.	1753.	060999	1531
16101GR015	22	1805.	1841.	060999	2114
16101GR006	22	1809.	1855.	060999	1535
16101GR007	22	1902.	1950.	060999	1538
16101GR008	22	2008.	2059.	060999	1542
16101GR009	22	2208.	2263.	060999	1546
16101GR010	22	2303.	2348.	060999	2058
16101GR011	22	2405.	2452.	060999	2101
16101GR012	22	2451.	2498.	060999	2104
16101GR013	22	2603.	2653.	060999	2107
16101GR014	22	2805.	2859.	060999	2110

SOURCE: 16102 CONFIG P3
P3-BOM ROT INLET/BM,TRT F&A FC,BMTs,KULITES,NO FLOOR ICD,NO PT2 PROBE
*** SORTED BY N1C ***

RECORD ID	No. of ANGLES	N1CORR	N1OBS	DATE	TIME
16102GR001	22	0.	0.	061099	0921
16102GR002	22	0.	0.	061099	0932
16102GR003	22	0.	0.	061199	0919
16102GR004	22	587.	604.	061199	1232
16102GR019	22	1619.	1660.	061199	1344
16102GR005	22	1627.	1672.	061199	1236
16102GR006	22	1701.	1747.	061199	1239
16102GR007	22	1800.	1851.	061199	1242
16102GR008	22	1904.	1958.	061199	1245
16102GR009	22	2003.	2060.	061199	1248
16102GR010	22	2202.	2262.	061199	1251
16102GR011	22	2300.	2364.	061199	1254
16102GR012	22	2401.	2470.	061199	1257
16102GR013	22	2451.	2521.	061199	1300
16102GR015	22	2502.	2573.	061199	1319
16102GR014	22	2603.	2679.	061199	1305
16102GR016	22	2703.	2778.	061199	1323
16102GR018	22	2802.	2874.	061199	1334
16102GR017	22	2805.	2879.	061199	1325

SOURCE: 16103 CONFIG S1

S1-SCARF ROT INLET,TRT-F&A FCC,BMTs,KULITES,NO FLOOR ICD,NO PT2 PROBE

*** SORTED BY N1C ***

RECORD ID	No. of ANGLES	N1CORR	N1OBS	DATE	TIME
16103GR001	22	0.	0.	061599	1006
16103GR002	22	0.	0.	061599	1013
16103GR003	22	0.	0.	061599	1042
16103GR004	22	0.	0.	061599	1048
16103GR005	22	586.	602.	061599	1323
16103GR021	22	1624.	1667.	061599	1432
16103GR006	22	1625.	1666.	061599	1328
16103GR007	22	1704.	1744.	061599	1331
16103GR008	22	1804.	1846.	061599	1334
16103GR022	22	1804.	1852.	061599	1438
16103GR009	22	1903.	1947.	061599	1337
16103GR010	22	2001.	2047.	061599	1341
16103GR023	22	2001.	2055.	061599	1442
16103GR011	22	2203.	2253.	061599	1344
16103GR024	22	2203.	2262.	061599	1445
16103GR012	22	2306.	2359.	061599	1347
16103GR013	22	2400.	2455.	061599	1350
16103GR025	22	2451.	2518.	061599	1449
16103GR014	22	2454.	2511.	061599	1353
16103GR015	22	2504.	2562.	061599	1356
16103GR016	22	2600.	2662.	061599	1400
16103GR019	22	2601.	2668.	061599	1423
16103GR017	22	2702.	2772.	061599	1414
16103GR020	22	2799.	2874.	061599	1426
16103GR018	22	2803.	2876.	061599	1418

SOURCE: 16104 CONFIG S3

S3-Scarf ROT inlet,Trt F&A FC,BMTs,kulites,ICD no flr,no pt2,flo viz

*** SORTED BY N1C ***

RECORD ID	No. of ANGLES	N1CORR	N1OBS	DATE	TIME
16104GR001	22	0.	0.	061599	2202
16104GR006	22	209.	213.	061699	1007
16104GR002	22	586.	597.	061599	2234
16104GR011	22	1616.	1656.	061699	1211
16104GR007	22	1623.	1662.	061699	1017
16104GR003	22	1623.	1653.	061599	2241
16104GR008	22	2001.	2051.	061699	1022
16104GR012	22	2001.	2054.	061699	1215
16104GR004	22	2002.	2038.	061599	2246
16104GR014	22	2401.	2462.	061699	1221
16104GR005	22	2404.	2447.	061599	2250
16104GR009	22	2407.	2466.	061699	1025
16104GR010	22	2800.	2869.	061699	1029
16104GR013	22	2808.	2880.	061699	1218

SOURCE: 16105 CONFIG S13A
S13A-Scarf ROT HW BOT 90deg diff+lip,TRT-FCC,BMTs,kulites,ICD no gp,no Pt2
*** SORTED BY N1C ***

RECORD ID	No. of ANGLES	N1CORR	N1OBS	DATE	TIME
16105GR001	22	0.	0.	061799	1148
16105GR002	22	0.	0.	061799	1154
16105GR003	22	0.	0.	061799	1203
16105GR004	22	587.	602.	061799	1229
16105GR018	22	1622.	1662.	061799	1350
16105GR005	22	1623.	1665.	061799	1232
16105GR006	22	1704.	1748.	061799	1235
16105GR007	22	1802.	1848.	061799	1238
16105GR019	22	1806.	1852.	061799	1353
16105GR008	22	1904.	1954.	061799	1241
16105GR020	22	2000.	2050.	061799	1356
16105GR009	22	2001.	2047.	061799	1323
16105GR021	22	2200.	2255.	061799	1400
16105GR010	22	2203.	2252.	061799	1326
16105GR011	22	2303.	2353.	061799	1329
16105GR012	22	2406.	2460.	061799	1332
16105GR013	22	2452.	2508.	061799	1334
16105GR022	22	2453.	2517.	061799	1404
16105GR014	22	2502.	2560.	061799	1337
16105GR015	22	2603.	2664.	061799	1340
16105GR016	22	2699.	2766.	061799	1343
16105GR017	22	2807.	2875.	061799	1345

SOURCE: 16106 CONFIG S15A-1
S15A-1 Scarf ROT 3" circ HW fwd of "A" flg, Trt FCC, BMT&KUL, ICD, no pb
*** SORTED BY N1C ***

RECORD ID	No. of ANGLES	N1CORR	N1OBS	DATE	TIME
16106GR001	22	0.	0.	061899	0845
16106GR002	22	0.	0.	061899	0852
16106GR003	22	0.	0.	062199	0741
16106GR004	22	0.	0.	062199	0745
16106GR005	22	0.	0.	062199	0924
16106GR006	22	585.	597.	062199	0933
16106GR007	22	1626.	1662.	062199	0939
16106GR020	22	1626.	1662.	062199	1018
16106GR008	22	1706.	1744.	062199	0942
16106GR009	22	1801.	1841.	062199	0945
16106GR021	22	1801.	1842.	062199	1021
16106GR010	22	1901.	1943.	062199	0948
16106GR022	22	1998.	2044.	062199	1024
16106GR011	22	2003.	2049.	062199	0950
16106GR023	22	2169.	2219.	062199	1027
16106GR012	22	2201.	2252.	062199	0953
16106GR027	22	2201.	2253.	062199	1041
16106GR013	22	2302.	2355.	062199	0956
16106GR014	22	2404.	2459.	062199	0959
16106GR024	22	2449.	2506.	062199	1030
16106GR015	22	2453.	2509.	062199	1001
16106GR016	22	2500.	2558.	062199	1004
16106GR025	22	2600.	2661.	062199	1033
16106GR017	22	2602.	2660.	062199	1007
16106GR018	22	2704.	2763.	062199	1010
16106GR019	22	2802.	2863.	062199	1012
16106GR026	22	2805.	2871.	062199	1037

SOURCE: 16107 CONFIG S15A-3
S15A-3 Scarf ROT 3-3"x 6" HW strips fwd of "A" Trt FCC,BMT&KUL, ICD, no pb
*** SORTED BY N1C ***

RECORD ID	No. of ANGLES	N1CORR	N1OBS	DATE	TIME
16107GR001	22	0.	0.	062199	1347
16107GR002	22	0.	0.	062199	1354
16107GR003	22	0.	0.	062199	1357
16107GR004	22	584.	600.	062199	1437
16107GR005	22	1623.	1670.	062199	1443
16107GR006	22	1703.	1750.	062199	1446
16107GR007	22	1804.	1852.	062199	1448
16107GR008	22	1905.	1957.	062199	1451
16107GR009	22	2005.	2060.	062199	1454
16107GR010	22	2199.	2263.	062199	1457
16107GR011	22	2300.	2368.	062199	1500
16107GR012	22	2401.	2470.	062199	1503
16107GR013	22	2452.	2522.	062199	1505
16107GR017	22	2452.	2521.	062199	1518
16107GR014	22	2501.	2574.	062199	1508
16107GR015	22	2605.	2677.	062199	1512
16107GR016	22	2703.	2778.	062199	1514

SOURCE: 16108 CONFIG S15A-4
S15A-4 Scarf ROT,HW Bott 90 deg Throat&Lip,TRT FCC, BMT&KUL, ICD, no pb
*** SORTED BY N1C ***

RECORD ID	No. of ANGLES	N1CORR	N1OBS	DATE	TIME
16108GR001	22	0.	0.	062199	2246
16108GR002	22	0.	0.	062199	2249
16108GR024	22	0.	0.	062299	0139
16108GR025	22	0.	0.	062299	0142
16108GR003	22	587.	596.	062199	2354
16108GR005	22	1615.	1639.	062299	0007
16108GR017	22	1627.	1653.	062299	0045
16108GR004	22	1696.	1722.	062299	0002
16108GR006	22	1803.	1831.	062299	0010
16108GR018	22	1806.	1835.	062299	0048
16108GR007	22	1901.	1930.	062299	0013
16108GR008	22	1999.	2030.	062299	0016
16108GR019	22	2000.	2031.	062299	0051
16108GR020	22	2202.	2237.	062299	0054
16108GR009	22	2204.	2239.	062299	0020
16108GR010	22	2304.	2340.	062299	0023
16108GR011	22	2399.	2436.	062299	0026
16108GR012	22	2451.	2489.	062299	0028
16108GR021	22	2451.	2489.	062299	0059
16108GR013	22	2503.	2542.	062299	0031
16108GR022	22	2600.	2640.	062299	0102
16108GR014	22	2605.	2646.	062299	0034
16108GR015	22	2713.	2755.	062299	0037
16108GR016	22	2801.	2845.	062299	0041
16108GR023	22	2806.	2849.	062299	0105

SOURCE: 16109 CONFIG S16

S16-Scarf TRT,keel dwn ,TRT FCC, BMTs,Kulites,ICD no gp, no PT2 probe

*** SORTED BY N1C ***

RECORD ID	No. of ANGLES	N1CORR	N1OBS	DATE	TIME
16109GR001	24	0.	0.	062299	0920
16109GR002	24	0.	0.	062299	0926
16109GR003	24	0.	0.	062299	0932
16109GR004	24	0.	0.	062399	0712
16109GR005	24	0.	0.	062399	0902
16109GR006	24	585.	599.	062399	0958
16109GR020	24	1623.	1664.	062399	1046
16109GR007	24	1625.	1664.	062399	1004
16109GR008	24	1702.	1743.	062399	1007
16109GR009	24	1799.	1841.	062399	1010
16109GR021	24	1803.	1849.	062399	1049
16109GR027	24	1804.	1858.	062399	1351
16109GR010	24	1909.	1956.	062399	1013
16109GR011	24	2000.	2050.	062399	1016
16109GR022	24	2002.	2053.	062399	1053
16109GR023	24	2201.	2257.	062399	1056
16109GR012	24	2203.	2256.	062399	1019
16109GR028	24	2208.	2275.	062399	1354
16109GR013	24	2299.	2354.	062399	1022
16109GR014	24	2405.	2463.	062399	1025
16109GR015	24	2449.	2510.	062399	1028
16109GR024	24	2454.	2518.	062399	1059
16109GR029	24	2457.	2525.	062399	1357
16109GR016	24	2500.	2563.	062399	1030
16109GR017	24	2601.	2668.	062399	1033
16109GR025	24	2602.	2668.	062399	1102
16109GR030	24	2603.	2673.	062399	1400
16109GR018	24	2701.	2771.	062399	1036
16109GR019	24	2799.	2871.	062399	1041
16109GR026	24	2803.	2873.	062399	1105

SOURCE: 16119 CONFIG S16A

S16-Scarf TRT,keel dwn ,TRT FCC, BMTs,Kulites,ICD -12",no GP,no PT2 Pb

*** SORTED BY N1C ***

RECORD ID	No. of ANGLES	N1CORR	N1OBS	DATE	TIME
16110GR001	24	0.	0.	062399	1208
16110GR002	24	586.	602.	062399	1217
16110GR003	24	1623.	1667.	062399	1222
16110GR004	24	1803.	1853.	062399	1225
16110GR005	24	2001.	2056.	062399	1228
16110GR006	24	2202.	2262.	062399	1232
16110GR007	24	2455.	2523.	062399	1235
16110GR008	24	2605.	2678.	062399	1238
16110GR009	24	2801.	2880.	062399	1241

SOURCE: 16111 CONFIG S16B

S16-Scarf TRT,keel dwn ,TRT FCC, BMTs,Kulites,ICD +12",no GP,no PT2 Pb

*** SORTED BY N1C ***

RECORD ID	No. of ANGLES	N1CORR	N1OBS	DATE	TIME
16111GR001	24	0.	0.	062399	1546
16111GR002	24	0.	0.	062399	1551
16111GR011	24	0.	0.	062399	1744
16111GR012	24	0.	0.	062399	1748
16111GR003	24	587.	601.	062399	1644
16111GR004	24	1616.	1655.	062399	1648
16111GR005	24	1802.	1846.	062399	1651
16111GR006	24	2001.	2050.	062399	1655
16111GR007	24	2201.	2256.	062399	1658
16111GR008	24	2452.	2512.	062399	1701
16111GR009	24	2601.	2664.	062399	1704
16111GR010	24	2802.	2869.	062399	1707

SOURCE: 16112 CONFIG S13A-1

S13A-1 Scarf Rot HW bot 90 deg diff, TRT LIP&FCC, BMTs,ICD no GP,no PT2 Pb

*** SORTED BY N1C ***

RECORD ID	No. of ANGLES	N1CORR	N1OBS	DATE	TIME
16112GR001	24	0.	0.	062499	1850
16112GR002	24	0.	0.	062499	1853
16112GR024	24	0.	0.	062499	2327
16112GR003	24	588.	598.	062499	2148
16112GR017	24	1624.	1652.	062499	2234
16112GR004	24	1624.	1651.	062499	2151
16112GR005	24	1703.	1732.	062499	2154
16112GR018	24	1803.	1835.	062499	2237
16112GR006	24	1803.	1834.	062499	2157
16112GR007	24	1904.	1937.	062499	2201
16112GR019	24	2002.	2038.	062499	2240
16112GR008	24	2004.	2038.	062499	2204
16112GR020	24	2201.	2241.	062499	2244
16112GR009	24	2201.	2239.	062499	2207
16112GR010	24	2301.	2341.	062499	2210
16112GR011	24	2403.	2445.	062499	2213
16112GR012	24	2453.	2496.	062499	2216
16112GR021	24	2455.	2498.	062499	2247
16112GR013	24	2505.	2549.	062499	2219
16112GR022	24	2604.	2649.	062499	2251
16112GR014	24	2605.	2651.	062499	2222
16112GR015	24	2702.	2750.	062499	2225
16112GR016	24	2802.	2851.	062499	2228
16112GR023	24	2804.	2854.	062499	2254

SOURCE: 16113 CONFIG S17
S17-Scarf Rot, TRT Inlet+FCC, BMT's, ICD no GP, no walls, PT2 Probe in
*** SORTED BY N1C ***

RECORD ID	No. of ANGLES	N1CORR	N1OBS	DATE	TIME
16113GR001	32	0.	0.	062599	0947
16113GR002	32	0.	0.	062599	1112
16113GR003	32	0.	0.	062599	1115
16113GR004	32	584.	599.	062599	1247
16113GR005	32	1618.	1661.	062599	1252
16113GR018	32	1620.	1658.	062599	1348
16113GR006	32	1702.	1747.	062599	1256
16113GR019	32	1800.	1842.	062599	1352
16113GR007	32	1801.	1850.	062599	1300
16113GR008	32	1903.	1955.	062599	1304
16113GR009	32	2002.	2057.	062599	1308
16113GR020	32	2004.	2047.	062599	1356
16113GR010	32	2204.	2264.	062599	1312
16113GR011	32	2307.	2369.	062599	1316
16113GR012	32	2401.	2466.	062599	1320
16113GR013	32	2451.	2520.	062599	1323
16113GR021	32	2453.	2503.	062599	1400
16113GR014	32	2502.	2570.	062599	1328
16113GR015	32	2601.	2671.	062599	1332
16113GR016	32	2709.	2773.	062599	1336
16113GR017	32	2801.	2867.	062599	1343
16113GR022	32	2809.	2864.	062599	1404

References

1. Dougherty, R. P., "Nacelle Acoustic Design by Ray Tracing in Three Dimensions", AIAA 96-1773, 2nd AIAA /CEAS Aeroacoustics Conference, May 6-8, 1996/State College, PA.
2. Dougherty, R. P. and Stoker, R. W. "Sidelobe Suppression for Phased Array Aeroacoustic Measurements," AIAA/CEAS 98-2242
3. J. M. Tyler and T. G. Sofrin, "Axial Flow Compressor Noise," SAE Trans. v. 70, pp. 309-332, 1962
4. Ganz, Joppa, Patten, and Scharpf, "Boeing 18-Inch Fan Rig Broadband Noise Test," Boeing Commercial Airplane Group, Seattle, WA, NASA/CR—1998-208704.

REPORT DOCUMENTATION PAGE					*Form Approved* *OMB No. 0704-0188*
The public reporting burden for this collection of information is estimated to average 1 hour per response, including the time for reviewing instructions, searching existing data sources, gathering and maintaining the data needed, and completing and reviewing the collection of information. Send comments regarding this burden estimate or any other aspect of this collection of information, including suggestions for reducing this burden, to Department of Defense, Washington Headquarters Services, Directorate for Information Operations and Reports (0704-0188), 1215 Jefferson Davis Highway, Suite 1204, Arlington, VA 22202-4302. Respondents should be aware that notwithstanding any other provision of law, no person shall be subject to any penalty for failing to comply with a collection of information if it does not display a currently valid OMB control number. PLEASE DO NOT RETURN YOUR FORM TO THE ABOVE ADDRESS.					
1. REPORT DATE *(DD-MM-YYYY)* 01-02-2014		**2. REPORT TYPE** Final Contractor Report		**3. DATES COVERED** *(From - To)*	
4. TITLE AND SUBTITLE Pratt & Whitney/Boeing Engine Validation of Noise Reduction Concepts Final Report for NASA Contract NAS3-97144, Phase 1				**5a. CONTRACT NUMBER** NAS3-97144	
				5b. GRANT NUMBER	
				5c. PROGRAM ELEMENT NUMBER	
6. AUTHOR(S) Mathews, Douglas, C.; Bock, Larry, A.; Bielak, Gerald, W.; Dougherty, R., P.; Premo, John, W.; Scharpf, Dan, F.; Yu, Jia				**5d. PROJECT NUMBER**	
				5e. TASK NUMBER	
				5f. WORK UNIT NUMBER WBS 473452.02.03.07.06.01.02	
7. PERFORMING ORGANIZATION NAME(S) AND ADDRESS(ES) United Technologies Corporation, Pratt & Whitney 400 Main Street East Hartford, Connecticut 06108				**8. PERFORMING ORGANIZATION REPORT NUMBER** E-18783	
9. SPONSORING/MONITORING AGENCY NAME(S) AND ADDRESS(ES) National Aeronautics and Space Administration Washington, DC 20546-0001				**10. SPONSORING/MONITOR'S ACRONYM(S)** NASA	
				11. SPONSORING/MONITORING REPORT NUMBER NASA/CR-2014-218088	
12. DISTRIBUTION/AVAILABILITY STATEMENT Unclassified-Unlimited Subject Categories: 02 and 71 Available electronically at http://www.sti.nasa.gov This publication is available from the NASA Center for AeroSpace Information, 443-757-5802					
13. SUPPLEMENTARY NOTES					
14. ABSTRACT This report presents results of the work completed in Phase 1 of the Engine Validation of Noise Reduction Concepts (EVNRC) contract. The purpose of the program was to validate, through engine testing, advanced noise reduction concepts aimed at reducing engine noise up to 6 EPNdB and improving nacelle suppression by 50 percent relative to 1992 technology. Phase 2 of the program is currently near completion and upon its conclusion will be summarized in a separate report.					
15. SUBJECT TERMS Fans; Noise; Inlet aerodynamics					
16. SECURITY CLASSIFICATION OF:			**17. LIMITATION OF ABSTRACT**	**18. NUMBER OF PAGES**	**19a. NAME OF RESPONSIBLE PERSON** STI Help Desk (email:help@sti.nasa.gov)
a. REPORT U	**b. ABSTRACT** U	**c. THIS PAGE** U	UU	150	**19b. TELEPHONE NUMBER** *(include area code)* 443-757-5802

Standard Form 298 (Rev. 8-98)
Prescribed by ANSI Std. Z39-18